Lawrence Berkeley Laboratory
UNIVERSITY OF CALIFORNIA

Materials & Molecular
Research Division

THE CHEMISTRY OF HO_2NO_2 AND THE PHOTOCHEMISTRY OF THE HO_x-NO_x-CO_x SYSTEM

David Littlejohn
(Ph.D. thesis)

August 1980

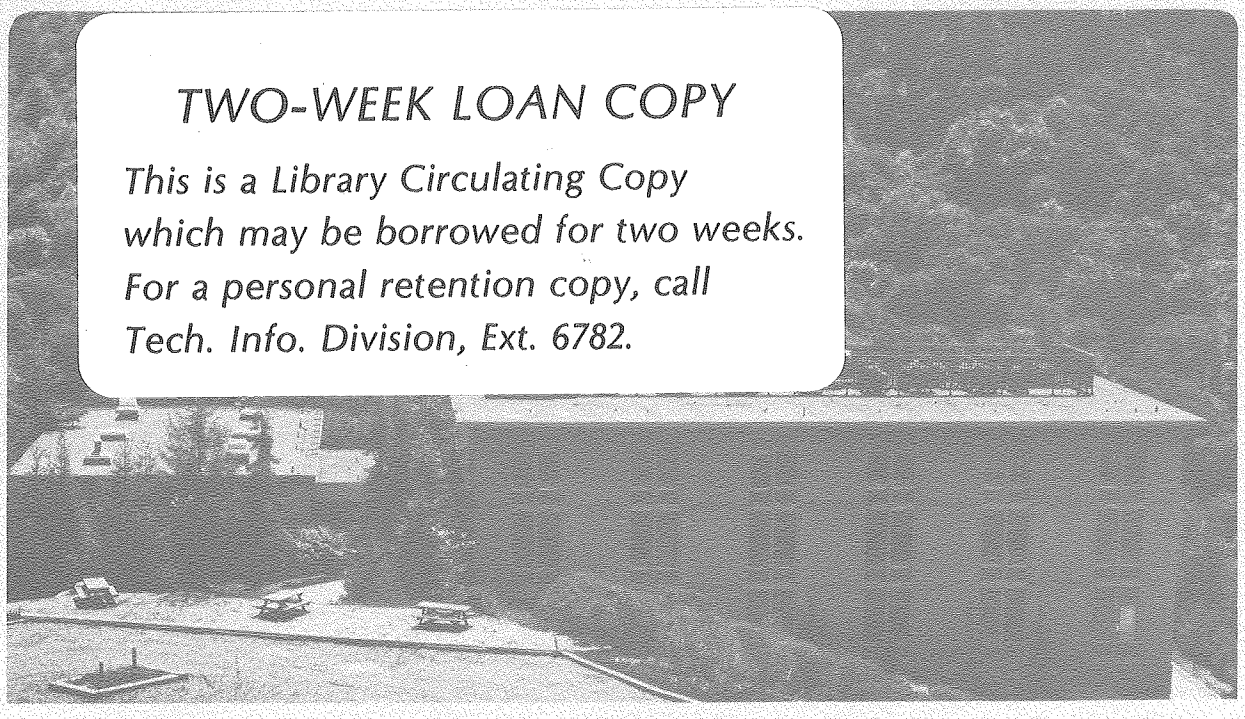

Prepared for the U.S. Department of Energy under Contract W-7405-ENG-48

DISCLAIMER

LBL-11480

THE CHEMISTRY OF HO_2NO_2 AND THE PHOTOCHEMISTRY OF THE HO_x-NO_x-CO_x SYSTEM

David Littlejohn

Materials and Molecular Research Division
Lawrence Berkeley Laboratory

and
Department of Chemistry
University of California
Berkeley, California 94720

This work was supported by the U.S. Department of Energy
under Contract No. W-7405-ENG-48.

THE CHEMISTRY OF HO_2NO_2 AND THE PHOTOCHEMISTRY OF THE HO_x - NO_x - CO_x SYSTEM

David Littlejohn

TABLE OF CONTENTS

I. Introduction 1

A. Peroxynitric Acid 2

B. Alternate Methods of Producing HNO_4 9

C. The Reaction of HNO_4 with OH 12

D. Ozone in the Troposphere 15

II. Experimental 23

A. Methods 23

1. Expansions 23

2. Static Cell Photolysis 25

3. Flowing Photolysis 26

4. Numerical Simulation of Chemical Systems 29

B. Apparatus 30

1. Reaction Cell and Temperature Control 30

2. Optical System 32

3. Detectors 34

4. Electronics 36

5. Photolytic Light Sources 39

C. Gases and Flow System 45

III. Absorption Cross Sections 51

A. Infrared Cross Sections 51

B. Visible Cross Sections 77

C. Ultraviolet Cross Sections 79

IV. The Reaction of N_2O_5 + H_2O_2 84

A. Experimental Procedures and Data 84

1. Reactant Decomposition and Flow-in 84

2. Expansion Methodology 90

3. Investigation of Complicating Factors in the H_2O_2 - N_2O_5 System 92

4. Products and Reactant Concentration Dependence on H_2O_2 + N_2O_5 99

B. Results and Discussion 132

1. Other Reactions in the H_2O_2 - N_2O_5 System 132

2. Analysis of the Reaction of N_2O_5 with H_2O_2 . . . 138

V. The Reaction of OH + HNO_4 158

A. Experimental Procedures and Data 158

1. Reaction system for the Investigation of OH + HNO_4 158

2. Experimental Technique 164

3. Actinometry 168

B. Results and Discussion 170

VI. The Photochemistry of the HO_x - NO_x - CO_x System 196

A. Experimental Procedures and Data 196

B. Results and Discussion 205

Acknowledgments 214

Appendix A: Photomultiplier Tube Gating 215

Appendix B: Pressure Broadening of Rotational Lines in Infrared Spectra 218

Appendix C: Reaction Sets for Numerical Modeling of Chemical Systems 223

Bibliography 232

THE CHEMISTRY OF HO_2NO_2 AND THE PHOTOCHEMISTRY AND KINETICS OF THE HO_x - NO_x - CO_x SYSTEM

David Littlejohn

Materials and Molecular Research Division
Lawrence Berkeley Laboratory and Department of Chemistry
University of California, Berkeley, California 94720

ABSTRACT

The objectives of this work were: (1) to investigate formation and destruction reactions of peroxynitric acid, HO_2NO_2 and (2) to study the photochemistry and kinetics of the HO_x - NO_x - CO_x system were also studied. Investigations were done using infrared spectroscopy to observe the behavior of species involved with the reactions of interest.

Several techniques were used, including expansion of reactants into an evacuated cell, static cell decays under constant illumination, and periodic photolysis of flow systems. Infrared absorption cross sections were obtained for CO, CO_2, NO, NO_2, N_2O_5, HNO_3, H_2O_2, and H_2O. The spectroscopic measurements were used to derive kinetic information on the systems under study.

The reaction of H_2O_2 with N_2O_5 has previously been studied only in the liquid phase.[6,7] This study investigated the reaction of gaseous H_2O_2 and N_2O_5 in the temperature range of 253 K to 283 K and a pressure range of 10 torr to 80 torr. The reaction occurred primarily heterogeneously in the apparatus in which it was studied. The upper limit for the bimolecular reaction giving the products

$$H_2O_2 + N_2O_5 \xrightarrow{a} HNO_4 + HNO_3$$

was determined to be $k_a < 1 \times 10^{-18} cm^3$ molecule^{-1} second^{-1}.

The reaction of H_2O_2 with two other species was also examined.

$$H_2O_2 + NO \xrightarrow{b} \text{products}$$

$$H_2O_2 + HNO_3 \xrightarrow{c} \text{products}$$

Both reactions proceed by primarily heterogeneous pathways and appear to be fairly slow in the temperature range of 263 K to 283 K. The upper limit for the bimolecular rate constant for both reactions is $<1 \times 10^{-19}$ cm^3 molecule^{-1} second^{-1}.

The decomposition products of HNO_4, HO_2 and NO_2, may react by two pathways

$$HO_2 + NO_2 + M \underset{-d}{\overset{d}{\rightleftharpoons}} HNO_4 + M$$

$$HO_2 + NO_2 \xrightarrow{e} HONO + O_2$$

This study found the ratio $k_e/k_d < 0.05$ at 263 K and 30 torr. Using the equation for k_d given by Graham et al.,[18] an upper limit for $k_e < 5 \times 10^{-14}$ cm^3 molecule^{-1} second^{-1} was obtained.

The products of the reaction of OH with HNO_4 were determined to be

$$OH + HNO_4 \xrightarrow{f} H_2O + NO_2 + O_2$$

and the rate constant for the reaction was found to be $k_f = 2.9 \pm 1.0 \times 10^{-12}$ cm^3 $molecule^{-1}$ $second^{-1}$ over the temperature range of 263 K to 283 K.

The decay profiles of species in the static cell photolysis of NO_2, H_2O_2 and CO in 0.1 and 1.0 atmosphere of O_2 were observed and compared with numerical simulations.

The appearance of O_3 after the initiation of photolysis of the system was observed. A chemical reaction cycle has been proposed as a source of O_3 in the troposphere;[54,111]

$$\begin{aligned}
&OH + CO \rightarrow H + CO_2 \\
&H + O_2 \xrightarrow{M} HO_2 \\
&HO_2 + NO \rightarrow OH + NO_2 \\
&NO_2 + h\nu \rightarrow NO + O \\
&O + O_2 \rightarrow O_3 \\
\text{net:}\quad &\overline{CO + 2O_2 \rightarrow CO_2 + O_3}
\end{aligned}$$

Numerical simulations indicate that this cycle was not responsible for the generation of the ozone observed.

I. INTRODUCTION

In the past few decades, there has been growing interest and concern regarding chemical processes in the atmosphere. Initially, this interest was limited to chemistry in the troposphere,[1] but more recently interest has spread to the stratosphere as well.[2] In the atmosphere, the chemistry of peroxynitric acid is presently of particular interest. The chemistry associated with its formation and decomposition is still not completely understood. One currently known method of formation of peroxynitric acid is[3,4]

$$HO_2 + NO_2 \overset{M}{\rightarrow} HNO_4. \qquad (1)$$

$$HNO_4 \overset{M}{\rightarrow} HO_2 + NO_2 \qquad (-1)$$

The reverse reaction is responsible for its destruction. A reaction that may compete with (1) for consumption of HO_2 and NO_2 is

$$HO_2 + NO_2 \rightarrow HONO + O_2 \ . \qquad (2)$$

Other reactions may also be responsible for the formation and decomposition of peroxynitric acid. One reaction of particular importance is

$$OH + HNO_4 \rightarrow \text{products} \ . \qquad (3)$$

Work has been done to investigate the formation and destruction processes of peroxynitric acid.

In the troposphere, it has been noted recently[5] that there is an apparent hemispheric asymmetry in the global distribution of the measured concentration of ozone. Non-chemical mechanisms for creating this asymmetry have been investigated previously and appear not to be responsible for the hemisphere variation of the ozone concentration. Research was performed to study a possible chemical mechanism that could account for the observed asymmetry.

One of the objectives of this research was to study the formation and destruction reactions of HNO_4, particularly formation by the gas phase reaction of H_2O_2 and N_2O_5, and destruction by attack of OH radical. Another objective was to investigate the photochemistry and kinetics of the HO_x-NO_x-CO_x system by observing the response of species to photolytic light in a mixture of H_2O_2, NO_2, CO and O_2.

A. Peroxynitric Acid

Initial investigations of the chemistry associated with HO_2NO_2 began shortly after the turn of the century. Early investigations of its formation and behavior in solution were done by D'Ans and Friederich,[6] and somewhat later by Schwarz.[7] They investigated the reactions of H_2O_2 and N_2O_5 and H_2O_2 with HNO_3 at low temperatures. The first reaction was reported to be very vigorous. The reaction product (presumably HNO_4) is very unstable and explosively decomposes at 243K. HNO_4 was found to be stable in room temperature aqueous solutions at concentrations between 20 and 70 percent.

In recent years, a resurgence in interest in HNO_4 occurred when the possibility of its existence in the atmosphere was postulated. The radicals HO_2 and NO_2 are very important in the chemical balance of trace species in both the troposphere and the stratosphere. Initially it was believed that they only reacted in a radical disproportionation reaction[8,9]

$$HO_2 + NO_2 \rightarrow HONO + O_2 \qquad (2)$$

It was noted by Simonaitis and Heicklen[10] that HNO_4 could exist in equilibrium with HO_2 and NO_2

$$HO_2 + NO_2 \overset{M}{\rightarrow} HNO_4 \qquad (1,-1)$$

Their measurements indicated a lifetime of HNO_4 on the order of 50 seconds at room temperature.

Niki et al.[3] were the first to determine the infrared absorption of HNO_4 with a Fourier transform infrared spectrometer in a mixture of Cl_2, H_2 and NO_2 photolyzed by black lamps. The absorption spectrum was confirmed by Hanst and Gay,[11] who used a mixture of Cl_2, NO_2 and H_2CO in a similar system to that used by Niki.

Levine et al.[12] investigated the kinetics of $HO_2 + NO_2$ reactions in a mixture of HONO, CO, NO_2 and NO in synthetic air at 700 torr pressure. Along with reactions (1) and (2), they studied

$$HO_2 + NO \rightarrow HO + NO_2 \qquad (4)$$

They obtained values for the ratios of the three reactions. Their results indicated that $k_2/k_1 \approx 0.7 \pm 0.4$, $k_2/k_4 \approx 0.043 \pm 0.02$ and k_1/k_4 0.058 ± 0.02. They suggested that HNO_4 may be important in the chemistry of polluted air.

Simonaitis and Heicklen[13] photolyzed a mixture of N_2O, H_2, O_2, NO and NO_2 at 213.9 nm and reported that (1) was the only reaction of HO_2 and NO_2 that was observed. They obtained a value of 6×10^{17} exp $(-26{,}000$ mole^{-1} cal/RT) sec^{-1} for the unimolecular decomposition of HNO_4.

Graham, Winer and Pitts[4] prepared HNO_4 with relatively low amounts of impurities and investigated the unimolecular decomposition of HNO_4 as a function of temperature. HNO_4 was mixed with excess NO, which scavenges HO_2 by reaction (3). They obtained a value of $k_{-1} = 1.4 \times 10^{14}$ exp$(-2{,}700 \pm 500/RT)$sec^{-1}. From this they calculated thermal decomposition lifetimes of HNO_4 at one atmosphere total pressure of 12 sec at 298 K, 5 min at 273 K and 1 month 220 K. They reported the ratio of $k_2/k_1 < 0.001$.

Baldwin *et al.*[14] estimated the entropy of HNO_4 to be 71.6 eu. This value was obtained by correcting the measured value of the entropy for $MeONO_2$ for internal rotation. This estimate was then used to calculate a high pressure A factor of $\log_{10}A = 15.9$ sec^{-1} for reaction (-1). They estimated an activation energy for reaction (-1) to be in the range of 23-25 kcal/mole from modeling smog chamber experiments of n-butane photo-oxidation.

Jesson et al. obtained ultraviolet absorption cross sections of HNO_4 in an aqueous solution at wavelengths between 300 and 360 nm. These values, along with measured rate constants for reactions (1) and (4), and estimates of the rate constants for

$$HNO_4 + Cl \rightarrow HCl + O_2 + NO_2 \quad (5)$$

$$HNO_4 + O \rightarrow OH + O_2 + NO_2 \quad (6)$$

$$HNO_4 + OH \rightarrow H_2O + O_2 + NO_2 \quad (7)$$

were used in a one-dimensional numerical model of atmospheric chemistry and transport to estimate the effect of HNO_4 on the atmosphere. They concluded that maximum concentrations of 1 to 3 ppb could exist in the stratosphere, but that more information on the kinetics and photochemistry of HNO_4 were needed.

Howard[16] used laser magnetic resonance to directly study the reaction of $HO_2 + NO_2$ in the pressure range of 0.5 to 3 torr. His measurements indicated $k_2/k_1 < 0.15$. He determined the M gas dependence of the reaction for M = He, N_2, O_2 and NO_2 at 300 K.

Baldwin and Golden[17] used more recent results and RRKM theory to predict a revised value of logio of the high pressure A factor = 16.4 sec^{-1} at 300 K for reaction (-1).

Graham, Winer and Pitts[18] investigated the pressure and temperature dependence of the unimolecular decomposition of HNO_4. They obtained a

rate constant for reaction (-1) in the second-order regime of 5.2×10^{-6} $\exp(-19900 \pm 500/RT)$ cm^3 $molec^{-1}$ sec^{-1} for N_2 pressures up to ~7 torr. For 278 K, the limiting first-order high pressure value of reaction (-1) was estimated to be ~0.018 sec^{-1}. They obtained a $K_{equil} = k_{-1}/k_1$ of 8.1×10^{10} molec cm^{-3} using their results with those obtained by Howard. They developed empirical expressions for the rate constants of reactions (1) and (-1).

$$k_1,N_2 = 7.3\times10^{-33}\exp(2000/RT) \times [M]/(1+4.86\times10^{-12}[M]^{0.61}) \text{ cm}^3\text{molec}^{-1}\text{sec}^{-1}$$

$$k_{-1},N_2 = 5.2 \times 10^{-6}\exp(-19900/RT) \times [M]/(1+4.86\times10^{-12}[M]^{0.61})\text{sec}^{-1}$$

The relative M gas efficiencies from their results are $[N_2] = 1$ and $[O_2] = 0.83 \pm 0.12$.

Uselman et. al.[19] made another investigation of the kinetics of the unimolecular decomposition of HNO_4 in a mixture of Cl_2, H_2 and NO_2 in synthetic air at 700 torr total pressure. From their measurements of K_{equil} for reactions (1) and (-1) over the temperature range of 293.3 to 301.4 K, they obtained values of $\Delta H^\circ = 23.8 \pm 2.7$ kcal/mole and $\Delta S^\circ = 40.5 \pm 8.8$ eu for reaction (-1). Using the entropy estimate of Baldwin et al.[14], they estimate $\Delta H^\circ_{f_{298}}(HNO_4) \approx -10.8$ kcal/mole.

More recently, Graham, Winer and Pitts[20] have determined infrared and ultraviolet cross-sections for HNO_4. From their ultraviolet cross sections and the solar flux intensities of Leighton,[1] they obtain a HNO_4 lifetime of about 3 hours in the troposphere. Molina and Molina[21]

have obtained UV cross sections of HNO_4 that are considerably lower than those obtained by Graham et al. at longer wavelengths. From their values, they obtain a HNO_4 lifetime in the lower atmosphere of ~30 hours. Cox and Patrick[22] have made measurements of HNO_4 UV cross sections that are somewhat higher than the measurements made by others. A comparison of the measured UV cross sections for HNO_4 is shown in Fig. 1.

Cox and Patrick[22] also studied the kinetics of formation of HNO_4 from $HO_2 + NO_2$ in a modulation system. They obtain values of $k_{-1} = 1.5 \pm 0.5 \times 10^{-12}$ $cm^3 molec^{-1} sec^{-1}$ for the second-order limit and $k_{-1} = 2.5 \pm 0.5 \times 10^{-31}$ cm^6 $molec^{-2} sec^{-1}$ in the third-order limit. They derive a value for the unimolecular decomposition of HNO_4 of $k_1 = 1.2 + 1.0/-0.6 \times 10^{15} \exp(-21900 \pm 340/RT) sec^{-1}$. From this they obtain an entropy for HNO_4 of $S^\circ = 76.2$ eu, with the assumption that the activation energy for formation is zero.

Barker et al.[23] have investigated the reaction of several species with HNO_4. The products of the reactions were not determined. The reactions studied and the rate constants obtained are as follows:

$$O + HNO_4 \rightarrow \text{products} \quad k_7 = 7.5 \pm 3.4 \times 10^{12} \exp(-2600 \pm 130/T) cm^3 molec^{-1} sec^{-1} \quad (6)$$

$$OH + HNO_4 \rightarrow \text{products} \quad k_8 \leq 3.5 \times 10^{-12} cm^3 molec^{-1} sec^{-1} \text{ for } T = 275\text{-}297 \text{ K} \quad (3)$$

$$O_3 + HNO_4 \rightarrow \text{products} \quad k_9 \leq 5 \times 10^{-20} cm^3 molec^{-1} sec^{-1} \quad T = 278 \text{ K} \quad (7)$$

$$H + HNO_4 \rightarrow \text{products} \quad k \approx 2.7 \pm 0.4 \times 10^{-14} cm^3 molec^{-1} sec^{-1} \quad T > 250 \text{ K} \quad (8)$$

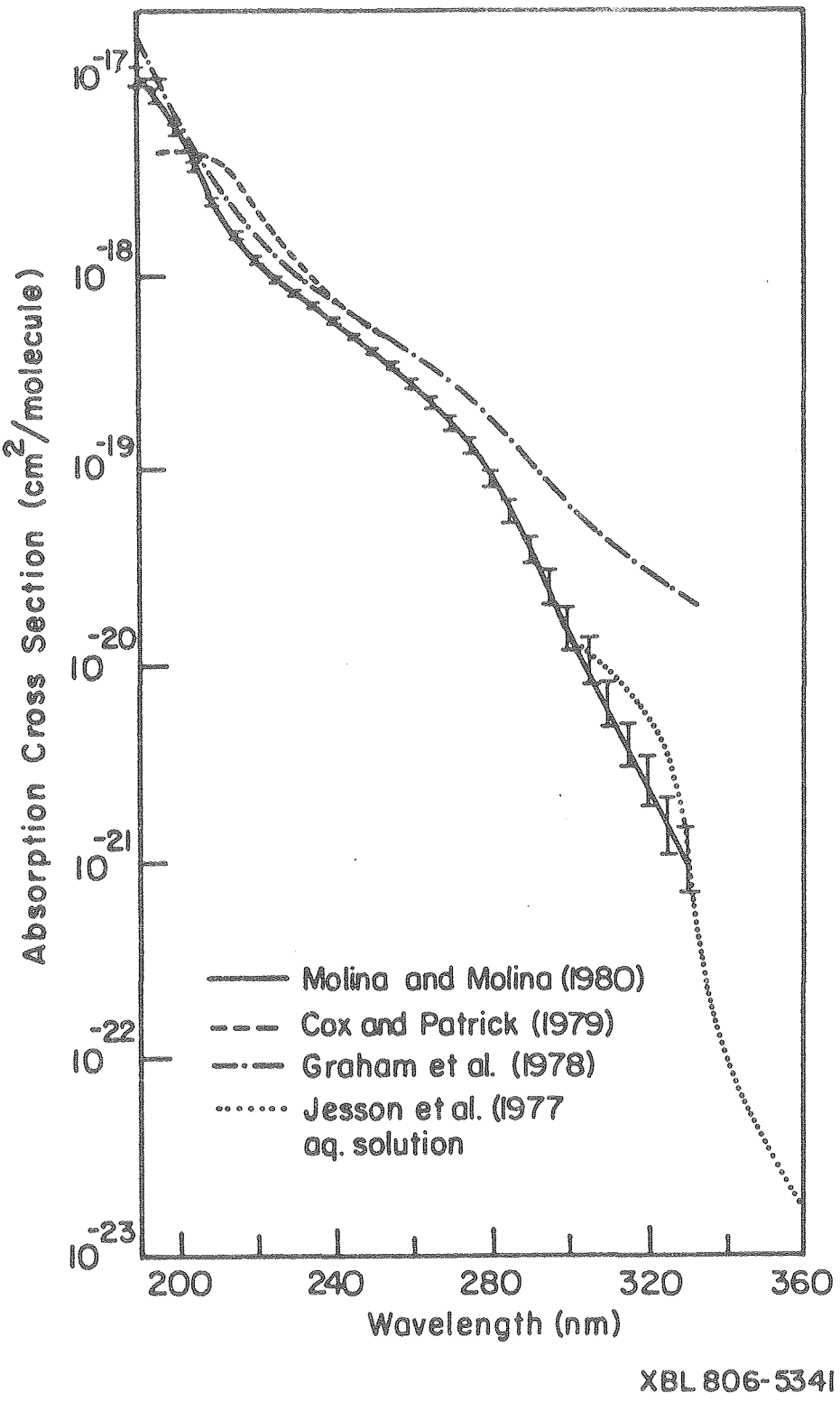

Fig. 1. UV absorption spectrum of HNO_4

Graham et al.[18] obtain an upper limit of ~3 x 10^{-12} $cm^3 molec^{-1} sec^{-1}$ for k_8, which does not disagree with these results. Table 1 summarizes the literature values for the HO_2-NO_2-HNO_4 system.

Further work needs to be done to better understand the chemical behavior of HNO_4. Part of the present research was done to provide more information on this system.

B. Alternate Methods of Producing HNO_4

To date, all studies have considered formation of HNO_4 in the gas phase only by reaction (1). In solution, several methods of preparation exist. D'Ans and Freiderich[6] and Schwarz[7] prepared aqueous solutions of HNO_4 by reacting HNO_3 with H_2O_2. They also prepared HNO_4 by the reaction of N_2O_5 with H_2O_2 at low temperatures. Since then, Barker and coworkers[2] have devised other techniques, as well as using the ones established by earlier workers. The three techniques they have used are:

1) Slowly adding 0.9g of 90 percent H_2O_2 to 2g of 70 percent HNO_3 at 0°C,

2) Very slowly adding 0.4g NO_2BF_4 powder to 2g of 90 percent H_2O_2 at 0°C with vigorous stirring,

3) Slowly adding 0.2g NO_2BF_4 powder to 0.1g of 90 percent H_2O_2 in 1g CH_3CN (acetonitrile) at 0°C.

It should be noted here that NO_2BF_4 is hygroscopic and preparations utilizing this compound should be done in an atmosphere free of water vapor.

It was decided to investigate the possibility of forming HNO_4 by reacting H_2O_2 with N_2O_5 and HNO_3 in the gas phase. Two other reactions that should be considered in analyzing the results of the above reactions

TABLE 1

$$HO_2 + NO_2 \xrightarrow{M} HNO_4 \quad (1)$$

$$HNO_4 \rightarrow HO + NO \quad (-1)$$

$$HO_2 + NO_2 \rightarrow HONO + O_2 \quad (2)$$

Reference	k_1	k_{-1}	k_2	k_2/k_1
24	----	----	~ 3×10^{-17}	---
25	1.97×10^{-31}	----	---	---
12	----	----	---	0.7 ± 0.4
16	$1.0 \pm 0.25 \times 10^{-31}$ (M = He) $2.1 \pm 0.52 \times 10^{-31}$ ($M = N_2$) $1.5 \pm 0.38 \times 10^{-31}$ ($M = O_2$) $6.6 \pm 3.0 \times 10^{-31}$ ($M = NO_2$)	----	$< 3 \times 10^{-15}$	< 0.15
4	----	$1.4 \times 10^{14} \exp(-20700/RT)$	---	< 0.001
13	----	$6 \times 10^{17} \exp(-26000/RT)$	---	(small)
18	$7.3 \times 10^{33} \exp(2000/RT) \times [M]_{eff}$ $[M]_{eff} = \left\lvert \frac{[M]}{(1+4.86\times10^{-12} \times [M]^{0.61})} \right\rvert$	$5.2 \times 10^{-6} \exp(-9900/RT) \times [M]_{eff}$ rel. eff.: $N_2 = 1.0$ $O_2 = 0.83 \pm 0.2$	$< 5 \times 10^{-16}$	---
22	$1.5 \pm 0.5 \times 10^{-12}$ (2nd order limit) $2.5 \pm 0.5 \times 10^{-31}$ (3rd order limit)	----	---	

are those of H_2O_2 with NO_2 and N_2O_5 with H_2O. Some of the possible products of these reactions and the enthalphies of reaction are listed below.

$$H_2O_2 + N_2O_5 \rightarrow HNO_3 + HONO + O_2 \qquad \Delta H = -21.5 \text{ kcal/mole}$$
$$\rightarrow HNO_3 + HNO_4 \qquad -13.2 \text{ " "}$$
$$\rightarrow HNO_3 + HO_2 + NO_2 \qquad + 6.0 \text{ " "} \qquad (9)$$
$$\rightarrow H_2O + NO_3 + NO_3 \qquad + 6.1 \text{ " "}$$

$$H_2O_2 + HNO_3 \rightarrow H_2O + HONO + O_2 \qquad \Delta H = -12.0 \text{ " "}$$
$$\rightarrow H_2O + HNO_4 \qquad - 3.7 \text{ " "} \qquad (10)$$

$$H_2O_2 + NO_2 \rightarrow NO_3 + NO_3 + H_2O \qquad \Delta H = -16.1 \text{ " "}$$
$$\rightarrow HNO_3 + OH \qquad 1.7 \text{ " "} \qquad (11a)$$

$$H_2O_2 + 2NO_2 \rightarrow HNO_3 + HNO_3 \qquad \Delta H = -47.8 \text{ " "} \qquad (11b)$$

$$H_2O_2 + N_2O_4 \rightarrow HNO_3 + HNO_3 \qquad \Delta H = -34.2 \text{ " "} \qquad (11c)$$

$$N_2O_5 + H_2O \rightarrow HNO_3 + HNO_3 \qquad \Delta H = - 9.5 \text{ " "} \qquad (12)$$

The enthalphy of formation for HNO_4 was that determined by Uselman et al.[19] which is uncertain by several kcal/mole.

These reactions are of potential importance in tropospheric and stratospheric chemistry. This research is directed toward determining values of the rate constants and products for these reactions.

C. The Reaction of HNO_4 with OH

The reaction of OH with HNO_4 is of considerable potential importance in atmospheric chemistry. The atmospheric lifetimes of a number of HO_x and NO_x species could be influenced by this reaction. It provides an alternate mechanism for the OH and HO_2 by the following reactions.

$$HO_2 + NO_2 \xrightarrow{M} HNO_4 \qquad (1)$$

$$OH + HNO_4 \rightarrow H_2O + NO_2 + O_2 \qquad (3)$$

$$\text{net: } OH + HO_2 \rightarrow H_2O + O_2 \qquad (13)$$

If reaction (3) is fast, it could significantly affect the lifetimes of OH, HO_2 and HNO_4 in the atmosphere.

No definite experimental values for this reaction have been published. In a review of atmospherically important reaction rate constants, Baulch. et al.[26] assume the reaction occurs by hydrogen atom abstraction. Considering the rate constant for OH + HNO_3, they suggest a value of 1×10^{-13} cm^3 $molecule^{-1}$ $second^{-1}$ for the reaction, with the uncertainty of at least an order of magnitude.

Graham et al. suggest an approximate upper limit of $3 \times 10^{-12} cm^3$ $molecule^{-1}$ $second^{-1}$ for the rate constant of OH + HNO_4. They arrived at this value from observing the concentrations of various species during

the unimolecular decomposition of HNO_4 in the presence of NO with and without added n-butane. The n-butane is an effective scavenger of OH by the reaction:

$$n - C_4H_{10} + OH \rightarrow \text{products}, \; k = 2.5E10^{-12} cm^3 molec^{-1} sec^{-1}. \qquad (14)$$

The OH is produced by the reaction

$$NO + HO_2 \rightarrow HO + NO_2 \; . \qquad (15)$$

They observed no detectable change in the unimolecular decomposition rate of HNO_4 when n-butane was added. A significant reduction of HNO_3 formed by the reaction

$$OH + NO_2 \xrightarrow{M} HNO_3 \qquad (16)$$

was observed.

Barker et al.[23] investigated the reaction of OH with HNO_4 using a flow tube-mass spectrometer system. OH radicals were produced by the reaction

$$H + NO_2 \rightarrow OH + NO. \qquad (17)$$

HNO_4 was produced by reacting NO_2BF_4 with H_2O_2 and the evolved vapor was flowed into the flow tube. HNO_4 was monitored using the m/e = 46 peak in

the mass spectrometer and OH was monitored by resonance fluorescence. Their experiments were done with HNO_4 concentration in excess of the OH concentration, so that pseudo-first order kinetics occurred. The experimental condition that was varied was either the time the reactants were allowed to mix before sampling or the concentration of one of the reactants. Varying the mixing time gave a value of 3.7×10^{-12} cm^3 $molecule^{-1}$ $second^{-1}$ for the rate constant of reaction (3). Varying the concentration of HNO_4 with a flow tube temperature of 298K gave a value of 3.3×10^{-12} cm^3 $molecule^{-1}$ $second^{-1}$ for (3). Similar experiments at 275K gave values of either 3.4×10^{-12} or 5.4×10^{-13} cm^3 $molecule^{-1}$ $second^{-1}$ for (3). The apparent rate constant would alternate between the two values at 275K. Their attempts to eliminate the variation in the rate constant at 275K were unsuccessful. They speculate that the observed rate is the sum of homogeneous and heterogeneous rates and that the slower value of the rate constant observed is likely to be near to the value of the homogeneous component. They conclude, however, that their experimental results indicate an upper limit for the rate constant of reaction (3) of $k_3 \leq 3.5 \times 10^{-12} cm^3$ $molecule^{-1}$ $second^{-1}$.

The values for the bimolecular rate constants for hydrogen abstraction vary widely, ranging from less than 10^{-14} cm^3 $molecule^{-1}$ $second^{-1}$ to greater than 10^{-11} cm^3 $molecule^{-1}$ $second^{-1}$. The best reaction models for reaction (3) would be reactions of OH with peroxy compounds. The reactions of OH with H_2O_2 has a rate constant[27] of 1.6×10^{-12} cm^3 $molecule^{-1}$ $second^{-1}$ and the reaction of OH with HO_2 has a rate

constant of about 3.5×10^{-11} cm^3 $molecule^{-1}$ $second^{-1}$. The reactions of OH with other oxyacids of nitrogen are

$$OH + HONO \rightarrow H_2O + NO_2 \qquad k = 6.6 \times 10^{-12} cm^3 \text{ molecule}^{-1} \text{second}^{-1} \quad (18)$$

$$OH + HNO_3 \rightarrow H_2O + NO_3 \qquad k = 8.5 \times 10^{-14} \text{ " } \quad \text{ " } \quad \text{ " } \quad (19)$$

Since HNO_4 is less stable than HNO_3 and the H atom to be abstracted is part of a peroxy group, it would be expected that the rate constant for $OH + HNO_4$ to be somewhat faster than the reaction rate constant for $OH + HNO_3$. It would be expected to be considerably slower than the reaction of $OH + HO_2$. Thus, the expected range for the rate constant 10^{-11} to 10^{-13} cm^3 $molecule^{-1}$ $second^{-1}$ is fairly wide. Since rate constants at the extremes of this range will have greatly differing effects on atmospheric chemistry, the experimental determination of the value for this reaction is needed to generate better models of the chemistry of the atmosphere.

D. Ozone in the Troposphere

The concentration of ozone in the troposphere is of interest for a variety of reasons. Reactions of ozone with a number of trace species in the troposphere are important in determining their lifetimes, as well as that of ozone. Its concentration is important in modeling the chemistry of the troposphere.

Knowledge of background levels of ozone in "clean air" is needed as a reference for studying the effect of anthropogenic pollutants in the atmosphere. In addition, it is important in understanding the transport mechanisms in the troposphere and the processes that exchange air between the stratosphere and the troposphere.

For over a decade, there has been considerable controversy over the role of ozone in tropospheric chemistry and photochemistry, as well as the relative importance of ozone sources and sinks.[28-56] Much of the controversy was centered on whether ozone was an inert species in the trososphere that originated in the stratosphere, or if it was photochemically active in the troposphere. Many of the early studies were hampered by uncertainty in potentially important rate constants and uncertainty and variability of atmospheric measurements of important trace species. Local variations in trace species' concentrations made it difficult to determine mean values of the concentrations.

The traditional view was that ozone diffused down from the stratosphere into the troposphere. Ozone is produced in the stratosphere by photolysis of molecular oxygen, generating oxygen atoms which eventually react with other oxygen molecules to generate ozone.

$$\begin{aligned} O_2 + h\nu &\rightarrow O(^3P) + O(^3P) \quad 175\ nm < \lambda < 242\ nm \\ O_2 + h\nu &\rightarrow O(^3P) + O(^1D) \quad 133\ nm < \lambda < 175\ nm \\ O(^1D) &\xrightarrow{M} O(^3P) \\ O(^3P) + O_2 &\xrightarrow{M} O_3 \end{aligned} \tag{20}$$

Because of the large column of O_2 above it, essentially no ultraviolet sunlight with wavelengths shorter than 200 nm is transmitted to the troposphere. Hence, there is no ozone production in the troposphere by the mechanism that operates in the stratosphere. The concentration of ozone reaches a maximum at 18 to 25 km. This appears to support the concept that the source for tropospheric ozone is the stratosphere and the major sink is destruction at the earth's surface.

A photochemical alternative to this was proposed whereby ozone was generated by cycles such as

$$\begin{aligned} 2NO + O_2 &\rightarrow 2NO_2 \\ 2(NO_2 + h\nu &\rightarrow NO + O) \\ 2(O + O_2 + M &\rightarrow O_3 + M) \\ \text{net:} \quad 3O_2 + 2h\nu &\rightarrow 2O_3 \quad . \end{aligned}$$

Destruction of ozone could occur by cycles such as

$$\begin{aligned} NO + O_3 &\rightarrow NO_2 + O_2 \\ O_3 + h\nu &\rightarrow O_2 + O \\ NO_2 + O &\rightarrow NO + 3O_2 \\ \text{net:} \quad 2O_3 + h\nu &+ 3O_2 \quad . \end{aligned}$$

This is discussed in more detail by Johnston and Podolske[12].

This alternative suggested that transport from the stratosphere and destruction at the earths surface were not the major source and sink for tropospheric ozone.

Hemispheric asymmetries in experimental measurements of ozone, CO and CH_4 have been noted.[55] It is difficult to explain the ozone asymmetry by purely meteorological effects, suggesting photochemistry may influence ozone concentrations.

It now appears that stratosphere-troposphere air exchange, transport, and photochemistry are all important in determining ozone concentration in the troposphere. Any model that attempts to duplicate the behavior of ozone should include both photochemistry and transport mechanisms. Considerable uncertainty still exists in both these areas, however.

The most recent models[53,54] of the tropospheric behavior of ozone indicate a significant fraction of the tropospheric ozone originating from the stratosphere is photochemically destroyed by

$$\begin{aligned} & O_3 + h\nu \rightarrow O_2 + O(^1D) \qquad \lambda < 320 \text{ nm} \\ & O(^1D) + H_2O \rightarrow OH + OH \\ \text{net:} \quad & O_3 + H_2O \rightarrow O_2 + OH + OH \end{aligned} \tag{23}$$

Other chemical sinks exist, such as

$$\begin{aligned} & NO_2 + O_3 \rightarrow NO_3 + O_2 \\ & NO_2 + NO_3 \rightarrow NO + NO_2 + O_2 \\ & NO + O_3 \rightarrow NO_2 + O_2 \\ \text{net:} \quad & O_3 + O_3 \rightarrow O_2 + O_2 + O_2 \end{aligned} \tag{24}$$

and

$$\begin{aligned} HO_2 + O_3 &\rightarrow OH + O_2 + O_2 \\ OH + O_3 &\rightarrow HO_2 + O_2 \\ \text{net:}\quad O_3 + O_3 &\rightarrow O_2 + O_2 + O_2 \quad , \end{aligned} \tag{25}$$

but these are considered less important than the photochemical sink of reaction set (23).

Two series of reactions involving the oxidation of CO and CH_4 have been proposed as mechanisms for the production of ozone.[51] These reaction schemes are catalytic in the sense that they regenerate intermediates consumed in the reactions. The CO oxidation system is

$$\begin{aligned} CO + OH &\rightarrow CO_2 + H \\ H + O_2 &\xrightarrow{M} HO_2 \\ HO_2 + NO &\rightarrow NO_2 + OH \\ NO_2 + h\nu &\rightarrow NO + O \\ O + O_2 &\xrightarrow{M} O_3 \\ \text{net:}\quad CO + 2O_2 &\rightarrow CO_2 + O_3 \end{aligned} \tag{26}$$

The CH_4 oxidation scheme is similar but somewhat more complicated.

$$CH_4 + OH \rightarrow H_2O + CH_3$$

$$CH_3 + O_2 \rightarrow CH_3O_2$$

$$CH_3O_2 + NO \rightarrow CH_3O + NO_2$$

$$NO_2 + h\nu \rightarrow NO + O$$

$$O + O_2 \xrightarrow{M} O_3$$

$$CH_3O + O_2 \rightarrow H_2CO + HO_2$$

$$HO_2 + NO \rightarrow NO_2 + OH$$

$$NO_2 + h\nu \rightarrow NO + O$$

$$O + O_2 \xrightarrow{M} O_3$$

$$H_2CO + h\nu \rightarrow CO + H_2$$

net: $CH_4 + 4O_2 \rightarrow H_2O + CO + H_2 + 2O_3$

Similar systems can be devised for higher hydrocarbons, although the number of reactions increases considerably. For these systems to be of importance in the troposphere, each of the reactions involving an intermediate must be the dominant mechanism for consumption of that intermediate. If it is only a minor process, then the chain will terminate and it will not be important in ozone generation. In the case of the simpler CO oxidation system, Fishman et al.[56] and Johnston and Podolske[112] point out that if reaction (4) is slow, a reaction system to destroy ozone can occur.

$$\begin{aligned} OH + OH &\rightarrow H + CO_2 \\ H + O_2 &\rightarrow HO_2 + M \\ HO_2 + O_3 &\rightarrow O_2 + O_2 + OH \\ \text{net:}\quad CO + O_3 &\rightarrow CO_2 + O_2 \end{aligned} \tag{28}$$

For this system, the reactions in (26) are generally regarded as the major pathways for the intermediates involved. The critical reaction in this system is reaction (4). It competes with

$$HO_2 + O_3 \rightarrow O_2 + O_2 + OH \tag{29}$$

and

$$HO_2 + HO_2 \rightarrow H_2O_2 + O_2 \tag{30}$$

for the HO_2 radical. A recent measurement of the rate constant for reaction (4) by Howard and Evenson[57] indicates it is fast compared to (29) and (30). The other factor in the competion between reactions is the atmospheric concentrations of NO, O_3 and HO_2. There is still considerable uncertainty in the NO and HO_2 profiles in the atmosphere.[58] It does appear that there is sufficient NO present to make reaction (4) the dominant pathway for HO_2 in some regions of the troposphere, and consequently the CO oxidation cycle is important as a source of tropospheric O_3.

The oxidation cycles for methane and higher hydrocarbons are more complicated and many of the reactions have not been thoroughly investigated. The validity of the concept that this system can generate ozone in the troposphere cannot be confirmed without more laboratory investigations of the kinetics and more atmospheric measurements.

With the low atmospheric concentrations of the species involved in these cycles, observation of ozone generation in the atmosphere is extremely difficult. It is a large-scale, low-level effect. Long term, simultaneous observations of CO, NO, NO_2 and O_3 are needed. Careful laboratory investigations of the photochemistry and kinetics in systems where ozone generating cycles may occur are needed. It is to this end that part of the present research is directed.

CHAPTER II. EXPERIMENTAL

A. Methods

Different techniques were utilized for each of the experimental studies that were done in this research. However, all techniques are based on determining concentrations of various species by conventional infrared absorption spectroscopy. A folloiwng section will discuss the methods involved in determining infrared cross-sections.

1. Expansions

To investigate the kinetics and reaction products of the following reactions

$$\begin{aligned} N_2O_5 + H_2O_2 &\rightarrow \text{products} \\ HNO_3 + H_2O_2 &\rightarrow \text{products} \\ NO_2 + H_2O_2 &\rightarrow \text{products} \\ NO_2 + H_2O &\rightarrow \text{products} \\ N_2O_5 + H_2O &\rightarrow \text{products}, \end{aligned} \tag{31}$$

a technique is needed in which one can quantitatively observe the conversion of reactants into products. For this research, this was satisfied by expanding the reactants into the cell from two bulbs, each containing one reactant. Following expansion into the cell, the decay of reactants and the buildup of intermediates and products can be observed.

The possible products of these reactions were outlined in the previous section. In the case of the reaction of N_2O_5 with H_2O_2, two of the product sets, those of $HNO_4 + HNO_3$ and $HO_2 + NO_2 + HNO_3$, can give similar results because of the equilibrium between HNO_4 and $HO_2 + NO_2$. The actual products can be determined in this situation by the addition of nitric oxide to the reactants and carrier gas. At low temperatures, the equilibrium between HNO_4 and $HO_2 + NO_2$ is slow. Consequently, if the products are $HO_2 + NO_2 + HNO_3$, the added NO can scavenge most of the HO_2 by reaction (4) before it reacts with NO_2 to produce HNO_4. If the products are $HNO_4 + HNO_3$, the HNO_4 will decompose slowly, so that it will exist in significant amounts during the observation period. In all other cases, the reaction products can be determined by their characteristic infrared absorptions.

Kinetic information can be derived from the rate of decay of reactants or rate of buildup of products. In most cases, the rate of flow-in of the reactants will have to be taken into consideration. The flow-in of an inert specie will follow the behavior

$$\frac{[x]_t}{[x]} = (1 - e^{-t/t_o}) \qquad (32)$$

where t_o is a time constant characteristic of the flow system used, and $[x]$ is the ultimate concentration of x.

Several heterogeneous reactions must be taken into consideration when H_2O_2, N_2O_5 and HNO_4 are present.[59-62] These include

$$
\begin{aligned}
H_2O + N_2O_5 &\rightarrow HNO_3 + HNO_3 \\
H_2O_2 &\rightarrow H_2O + 1/2\ O_2 \\
HNO_4 &\rightarrow \text{products} \\
H_2O + 2NO_2 &\rightarrow HNO_3 + HONO \\
H_2O_2 + 2NO_2 &\rightarrow HNO_3 + HNO_3\ .
\end{aligned}
\tag{33}
$$

In certain situations, these reactions can be dominant loss processes for the species involved.

2. Static Cell Photolysis

The study of the CO oxidation cycle listed in equation (26) was conducted by flowing the reactants H_2O_2, NO_2 and CO in O_2 carrier gas into the cell. After concentrations of these compounds reached steady-state, the flow was stopped. To initiate the cycle, the photolytic lamps, with output in the near ultraviolet region of the spectrum, were activated and maintained at a constant illumination level. The ultraviolet light photolyzed NO_2 and H_2O_2 to generate the absent intermediates in the CO oxidation cycle.

$$
\begin{aligned}
NO_2 + h\nu &\rightarrow NO + O(^3P) \\
H_2O_2 + h\nu &\rightarrow OH + OH
\end{aligned}
\tag{34}
$$

In order to adequately characterize the kinetics of the reaction system, the behavior of a number of species had to be observed. Since the apparatus was a conventional infrared spectrometer system, each species had to be observed separately. One set of operating conditions was maintained until all species of interest had been observed.

For the low pressure investigations, a similar procedure was used. Once steady state flow conditions were achieved, the cell was rapidly pumped down to the desired pressure. The photolytic lamps were turned on and data were collected on the species under observation. As before, the procedure was repeated until all species had been observed.

In this system, the possible occurrence of several heterogeneous reactions should be noted. Three that have been mentioned previously are

$$\begin{aligned} H_2O_2 &\rightarrow H_2O + \tfrac{1}{2} O_2 \\ N_2O_5 + H_2O &\rightarrow HNO_3 + HNO_3 \\ H_2O_2 + 2NO_2 &\rightarrow HNO_3 + HNO_3 \ . \end{aligned} \qquad (35)$$

The first and last reactions represent a significant loss mechanism for H_2O_2. The last reaction may be responsible for the presence of HNO_3 in the absence of photolytic light.

Because of the complexity of this system, meaningful analytic rate expressions are difficult or impossible to generate. There are over 15 species of significance present during photolysis. To adequately describe the photochemistry and kinetics of the system, a set of over 60 reactions is needed. To accurately analyze a reaction set this size, numerical techniques are needed. Solutions for the chemical behavior of all species of interest can be generated in this manner.

3. Flowing Photolysis

An investigation of the reaction of OH with HNO_4 was performed by flowing N_2O_5 and H_2O_2 in N_2 carrier gas into the cell to generate HNO_4.

Black lamps were used as the photolytic light source. The lamps were turned on and off periodically at a very low frequency. This induced a concentration fluctuation in species affected by photolysis or by the photolytic products. NO_2 is present as the decomposition product of N_2O_5 and HNO_4. With black lamps as the photolytic light source, NO_2 is the only species that has a significant photolysis rate in the system,

$$NO_2 + h\nu \rightarrow NO + O(^3P) \qquad (36)$$

The O atoms are likely to react with NO_2 to produce more NO,

$$NO_2 + O \rightarrow NO + O_2 \qquad (37)$$

The NO can then react with HO_2 generated by HNO_4 decomposition to produce OH,

$$HNO_4 \rightarrow HO_2 + NO_2 \qquad (-1)$$

$$NO + HO_2 \rightarrow OH + NO_2 \qquad (4)$$

Thus, the OH concentration variation will be closely coupled to the lamp flashing rate. There will be competition among the following reactions for the consumption of OH

$$OH + NO_2 \xrightarrow{M} HNO_3 \quad (16)$$

$$OH + HNO_4 \rightarrow \text{products} \quad (3)$$

$$OH + HNO_3 \rightarrow H_2O + NO_3 \quad (19)$$

$$OH + H_2O_2 \rightarrow H_2O + HO_2 \; . \quad (38)$$

The relative rates of these reactions can be determined by observing the behavior of various species associated with these reactions. Since the rate constant for reactions (16), (19) and (38) are known, the rate constant for reaction (3) can be obtained by comparing it to one of the known reactions.

As with the other systems studied in this investigation, the ocurrence of heterogeneous reactions is a possibility that must be considered. However, most heterogeneous reactions should not be affected by the photolytic light. The occurrence of these reactions should have an insignificant effect on the concentration variations created by the photolytic light, and they should not have to be considered in the analysis.

The results obtained from the experiments can be analyzed by using them in an analytical expression that adequately describes the kinetics of the system. They can also be compared with computer simulations of the kinetics and photochemistry to determine how well the known reactions describe the chemical system.

4. Numerical Simulation of Chemical Systems

Since the chemical systems being investigated are complex in terms of both the number of reactions and the number of species, exact analytical expressions often cannot be developed. To be able to predict the behavior of a complex chemical system, numerical techniques must be utilized. The set of chemical reactions that are important in determining the behavior of the system can be written as a system of ordinary differential equations. Generally, the ordinary differential equations will have widely varying time constants, and consequently are known as "stiff" systems.[63] Conventional numerical integration techniques have a tendency to exhibit instability and inaccuracy when used on stiff systems. Recently, several techniques for solving stiff systems have been developed. They are available as computer subroutines to provide a basis for a program to predict the time dependent behavior of a chemical system. One of the most powerful techniques devised to analyze stiff systems is that developed by C. W. Gear.[64] A version that has been modified by Hindmarsh[65] is the basis for the CHEMK chemical kinetics program[66] used in this research.

To simulate the expansion experiments, the flow-in rates of the reactants, and the reactions and reaction rate constants considered to be of importance are used as inputs into the program. Estimated rate constants are used where rate constants have not been established for reactions. The first order or second order equivalent rate constants are used to simulate heterogeneous reactions where necessary.

The output from the program provides a time dependent profile of all of the species involved in the reactions, as well as periodic rate information. This can be compared with experimentally determined profiles to gain an understanding of the chemical behavior of the system.

Simulations of the static cell photolysis experiments were done by inputting the initial concentrations of the reactants, the set of reactions and rates needed to describe the system, and the light intensity. The photodecomposition rates of various species in the system were determined by either experimental observation of the decay of the isolated specie in the presence of the photolytic light, or by the calculation of the "j" value, which is the product of light intensity, cross section and quantum yield integrated over the wavelength region of interest.

Comparison of the experimental profiles with the numerical predictions can give insight into the chemistry of the system and assist in the selection of experimental conditions that wll be the most informative.

B. Apparatus

1. Reaction Cell and Temperature Control

The reaction cell used in these investigations consists of a quartz cylinder 28.0 cm inside diameter (28.9 cm outside diameter) by 102.0 cm long, whose ends are enclosed in nickel-plated stainless steel end caps. The cell is sealed by double silicone o-rings at each end of the cylinder. The end caps are maintained at a fixed separation by four Kovar

beams. Three mirrors and mounted in the end caps in a White cell configuration with a base pathlength of 1 meter. The optical pathlength of the cel may be varied externally by a fine adjustment screw. Usable path lengths vary from 4 to 32 meters. The volume of the cell is 63.0 liters, as determined by expansions from bulbs with calibrated volumes. This provides a surface to volume ratio of 0.175 cm^{-1}, when the surface of the mirror mounts is included.

The entire apparatus and optical system is mounted on a Newport Research Corporation vibration damping table. The cell framework is isolated from the metal surface of the table by nylon pads and 5 cm thick high density closed cell neoprene foam. Thermal isolation from the laboratory environment is provided by 20 cm of rigid polyurethane foam backed by 5 cm of aluminum foil backed fiberglass on all sides and on top of the cell.

Cooling within the insulating box is provided by a finned radiator mounted above the cell framework. Coolant is circulated through the radiator continuously. For temperatures above 280 K, pressurized chilled water is used as a coolant. For lower temperatures, methanol chilled by a Neslab LT9 low temperature refrigerator is flowed through an elevated 22 liter accumulator and into the radiator above the cell. Methanol flow is maintained by a combination of siphoning action and gravity.

Temperature control is maintained by resistive heating wire wrapped around the radiator. The current through the wire is regulated by a proportional temperature controller utilizing a precision thermistor as a temperature sensing element. A 50 liter/second muffin fan actively

circulates the air around the cell for even temperature distribution. The temperature distribution inside the insulating box is monitored by a conventional alcohol thermometer as well as four iron-constantan thermocouples. Three of these are distributed around the cell, while the fourth is placed in a sealed stainless steel tube which extends 30 cm into the cell. The maximum temperature differential indicated within the insulating box is 0.5 K.

A schematic diagram of the apparatus is indicated in Fig. 2. The reaction cell can be pumped out by a large capacity mechanical roughing pump for high pressures, or a liquid nitrogen trapped oil diffusion pump for low pressures. The cell can be evacuated to less than 10^{-3} torr.

2. Optical System

All optics external to the cell are enclosed within a plexigas housing. The housing and the monochromator are purged with a steady flow of dry nitrogen to minimize absorption of infrared light by water vapor and carbon dioxide. The light sources used are an Infrared Industries regulated 2mm by 12 mm cylindrical Nernst glower for work in the infrared domain and a General Electric No. 1142 tungsten bulb with a current regulated power supply for work in the visible domain. Selection of the light source is done by a mirror. The Nerst glower is operated at 1700K, as measured by an optical pyrometer. The tungsten bulb was operated at 12.6v and 1.44A. Light from either source is chopped at 400 Hz by American Time Products tuning fork choppers driven by regulated power supplies. The light is then directed on a collection mirror which

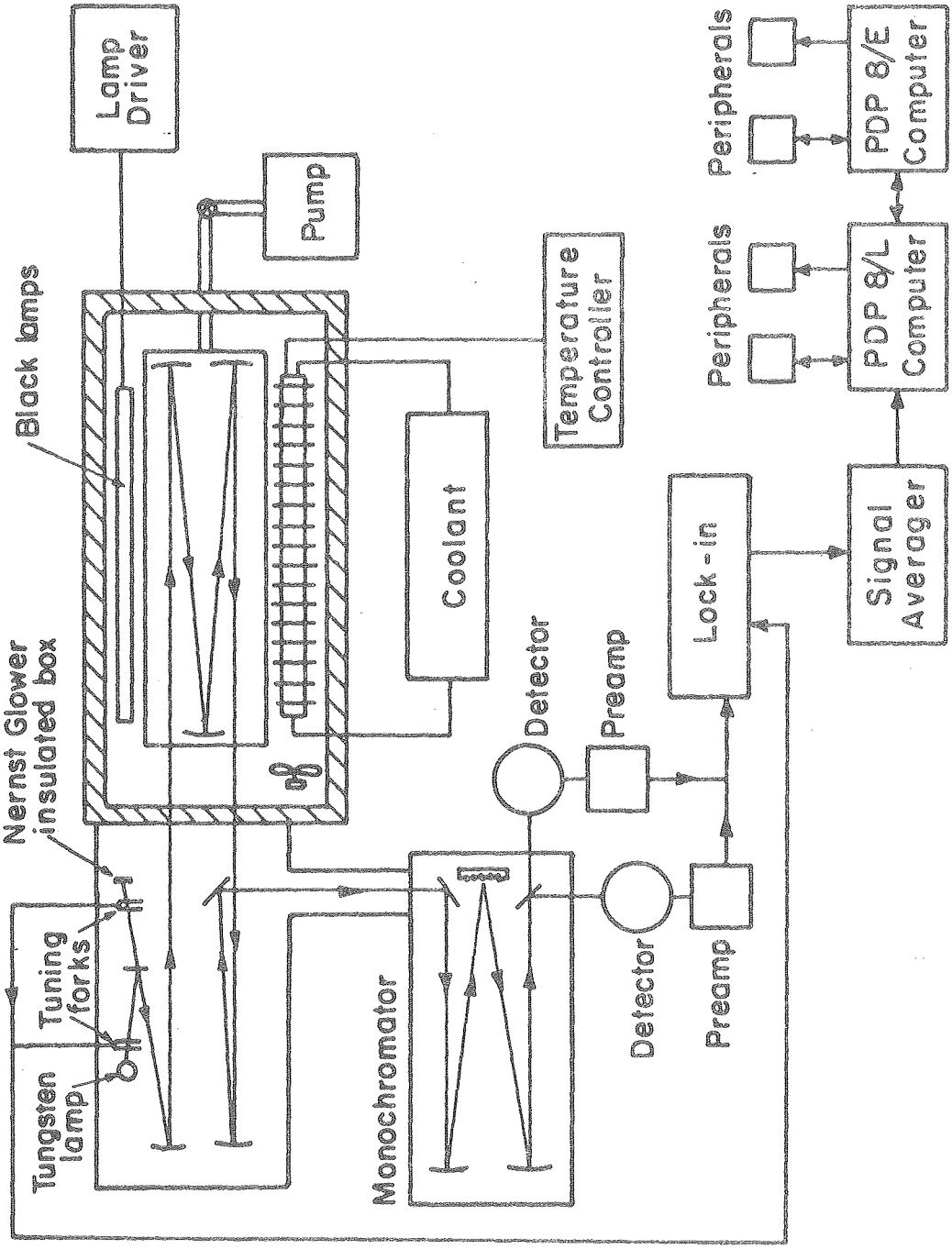

Fig. 2. Schematic diagram of apparatus used in experiments

focuses the light through the entrance windows and into the cell. There are two windows for both the entrance and exit light paths. The outer window is KBr and is sealed to one end of a Pyrex tube. The inner window and the other end of the tube are mounted in one of the cell end caps with silicone o-rings. The Pyrex tube contains a packet of dessicant and is evacuated to prevent damage to the windows by water vapor and to reduce thermal conduction from the cooled end cap during low temperature experiments. The inner windows were CaF_2 for early experiments and BaF_2 for more recent experiments. The light exiting the cell is focused by another collection mirror onto the entrance slit of the monochromator.

The internal mirrors are coated with gold over a chromium undercoat. This was followed by a 2000 Å MgF_2 overcoat to prevent coating degradation by chemical attack, particularly from H_2O_2. Thinner overcoats on gold or aluminum were found to be susceptible to chemical attack. The optical system is designed to underfill the internal mirros and the second collection mirror and overfill the monochromator entrance slit to minimize vibration induced light fluctuations. The McPherson one meter monochromator can be used with 75 line/mm, 150 line/mm, 300 line/mm and 600 line/mm gratings with 12 μm, 6 μm, 3.5 μm and 1.6 μm blaze wavelengths, respectively.

3. Detectors

A variety of detectors were available for use in this work. They are listed in Table 2 with typical bias voltages used and their useful

Table 2

Detectors

Detector	Bias	Wavelength Range
RCA 1P28B S-5 photomultiplier tube	-700 to -1250v	200 to 700 nm
RCA 4832 GaAs photomultiplier tube	-500 to -1200v	200 to 900 nm
EG and G SGD-100A Si photodiode	-50 to -100v	400 to 1200 nm
Rofin 7460 Ge photodiode	0 to -15v	600 to 1900 nm
SBRC ATO PbS detector	+300 to +400v	1 to 3.5 μm
SBRC ITO PbS detector[1]	+300 to +400v	1 to 4.0 μm
SBRC InSb photovoltaic detector[2]	0V	2 to 5.5 μm
SBRC HgCdTe photoconductive detector[2]	+1v	4 to 15 μm
SBRC Ge:Cu photoconductive detector[3]	+135v	4 to 30 μm

Notes

1. Operated at dry ice temperature.
2. Operated at liquid nitrogen temperature.
3. Operated at liquid helium temperature.

wavelength ranges. Much of the work was done using the HgCdTe detector. The housing of this detector allows it to be used with either the McPherson monochromator, or a circular variable filter (CVF), which acts as a low resolution monochromator. The housing is illustrated in Fig. 3. The CVF consists of two germanium half discs which support a thin dielectric film whose thickness increases radially around the disc. The wavelength transmitted by the CVF varies linearly with angle around it. One half disc covers the wavelength range of 3.1 to 6.2 μm and has a peak transmission of 25 to 45 percent. The other half disc covers the wavelength range of 6.0 to 12.1 μm and has a peak transmittance of greater than 40 percent. The CVF is positioned by a 200 step/revolution stepping motor driven by a controller that determines the direction of rotation and the stepping rate. The transmission curve of the CVF at one position and at positions two steps adjacent to it are shown in Fig. 4. The CVF has a resolution of about 1 percent. Because of the spectral overlap problems that existed in the experiments that were done, the CVF was unsuitable for use as a monochromator and was not used.

4. Electronics

A variety of preamplifiers were used in these experiments. The Ge:Cu infrared detector signal was amplified by an op amp preamplifier which has been discussed elsewhere.[67] A Princeton Applied Research Corporation CR-4A low noise amplifier with selectable gain and bandwidth was used in conjunction with the HgCdTe infrared detector. The power

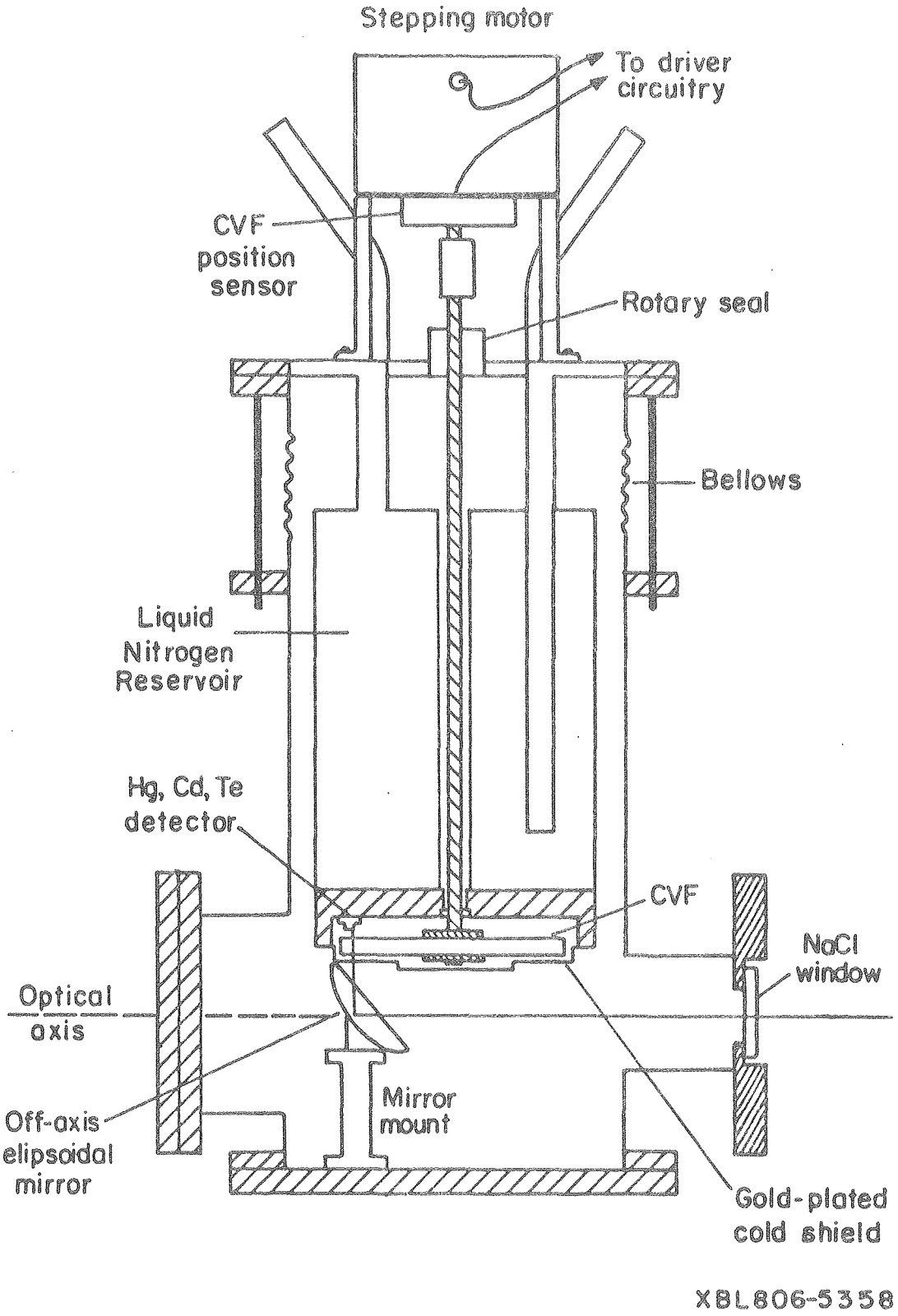

Fig. 3. Infrared detector and CVF housing

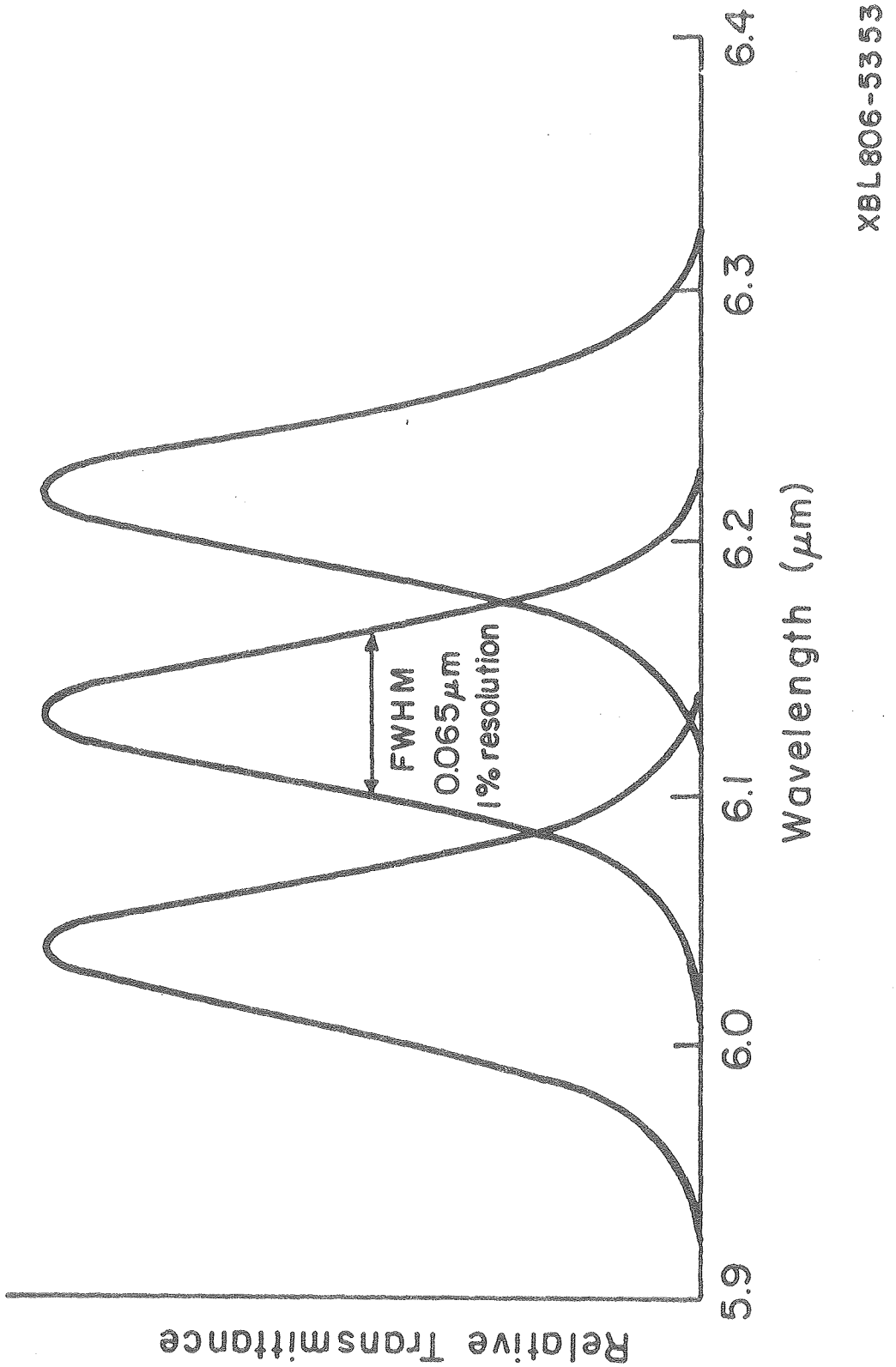

XBL806-5353

Fig. 4. CVF transmission of three positions separated by two steps

supply of the amplifier was modified to improve stability and reduce the 60 Hz ripple. The InSb detector was used with an A210 matched preamplifier from Santa Barbara Research Corporation. The photomultiplier tubes were used with a FET input op amp shown in Fig. 5.

Signals from the preamplifiers mentioned above and signals from the PbS (both ATO and ITO), Si and Ge detector were fed into a Princeton Applied Research Corporation Model 124 lock-in amplifier with a Model 116 low noise, high impedance differential reamplifier. The lock-in amplifier amplifies and rectifies the 400 Hz signal and provides a dc voltage output whose level is proportional to the light intensity incident on the detector.

The dc signal from the lock-in amplifier is monitored with a digital voltmeter and recorded with a Fabritek 1074 hardwired signal averager. The analog signal is fed through a RC filter and is digitized by a 12 bit ADC. The digitized signal is stored at selectable intervals as 18 bit words in quadrants of the 4k of memory available. The data can be manipulated using a PDP 8/ℓ computer which is interfaced to the Fabritek. The data can be stored on paper tape or be transferred to a PDP 8/e computer via an interprocesser buffer for storage on magnetic tape. Signals can be displayed on an oscilloscope or be plotted on a X-Y recorder.

5. Photolytic Light Sources

Two types of photolysis lamps were utilized in these investigations. 30 watt General Electric G30T8 low pressure mercury germicidal

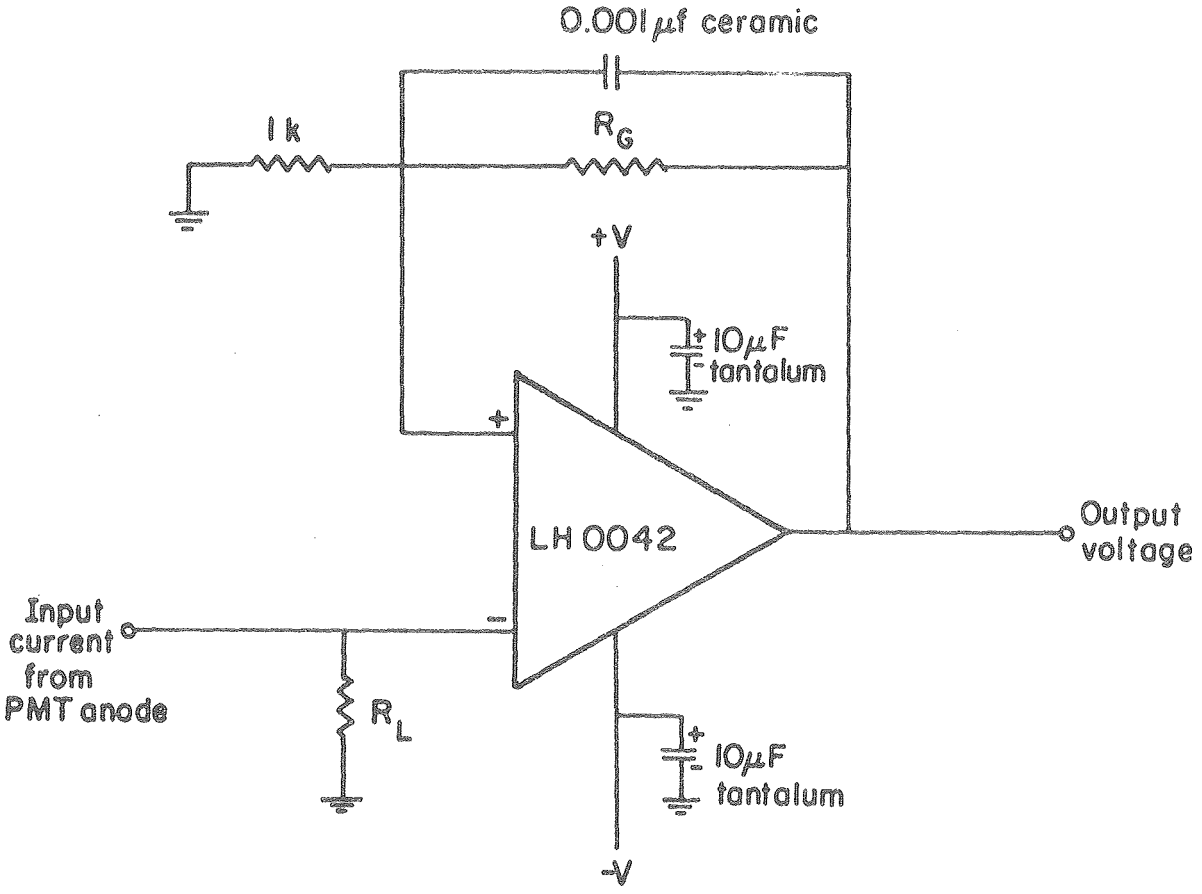

Notes:

	4832	1P28
+V	+10v	+15v
-V	-10v	-15v
R_L	1.21M	100k
R_G	40k	switchable between 10k and 100k

All resistors 1% metal film

XBL806-5359

Fig. 5. Schematic diagram of PMT preamplifier circuit

lamps were used to provided photolytic light consisting of ultraviolet mercury emission lines. 30 watt General Electric G30T8-BL black lamps provided broadband ultraviolet light in the near ultraviolet region. Four lamps are located symmetrically around the axis of the cell at a distance of 8 cm from the exterior cell surface. Sheets of Alzak high reflectivity aluminum surround the cell on three sides to increase uniformity of the light distribution. Six volt transformers are used to heat the lamp electrodes to a red glow to assist in turning the lamps on. Further assistance is provided by a Tesla coil discharge applied to wires connected to the center of the lamps.

The lamps can be powered by either of two lamp driver systems. One is a 700 volt regulated power supply utilizing "brute force" techniques to regulate the lamp current with large ballast resistors. The power supply can switch the lamps on and off electronically in response to a low frequency reference square wave.

The other lamp driver uses more sophisticated methods to control the current to the lamps. The power dissipated by the lamps is easily controllable and the lamp's output can be modulated in a variety of waveforms about a dc level. The schematic diagram of this lamp driver is illustrated in Fig. 6. The lamps can be driven at current levels from 0.04 to 0.7A per lamp and the lamp current can be modulated up to 90 percent.

Lamp output is monitored with a EG and G UV100B ultraviolet enhanced silicon photodiode. Since a silicon photodiode is most sensitive to visible and near infrared radiation, the radiation it receives must be

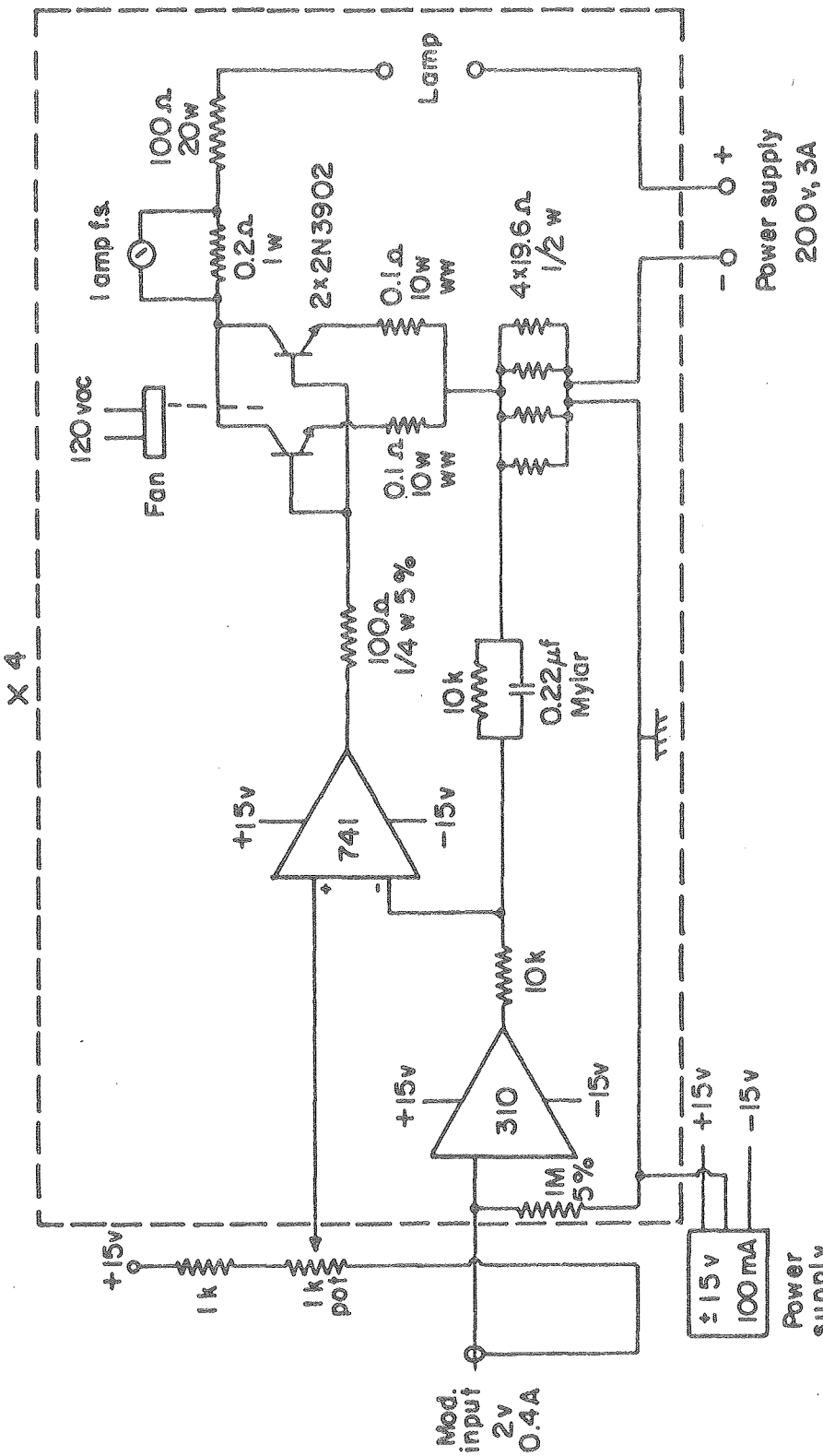

Fig. 6. Schematic diagram of lamp driver circuit

filtered. A 254 nm interference filter with 12 percent peak transmittance and 15 nm FWHM bandwidth is used in conjunction with the germicidal lamps. A Schott UG-5 glass filter, which has broadband transmission between 300 and 400 nm, is used with the black lamps. The current from the photodiode is fed into a LH0042 op amp acting as a photodiode follower with feedback resistance switchable between 100 kΩ and 1MΩ. The knee frequency of the amplifier response is well above that of the lamp modulation system. The maximum photodiode current generated with this system is within its linear response region. The output voltage is monitored on a digital voltmeter and recorded on a X-Y recorder. The photodiode is located inside the temperature-controlled box and its output increases approximately 7 percent from 300 to 250K.

Spectral distribution of the emission from the photolytic lamps was determined by directing the light from the lamps through an American Time Products 400 Hz tuning fork chopper into a McPherson Model 218 0.3 meter monochromator with a RCA 1P28B photomultiplier tube. The amplified 400 Hz signal from the PMT was rectified by the PAR Model 124 lock-in amplifier and recorded in the Fabritek. The emission in the 290 to 460 nm region of the black lamps is shown in Fig. 7. The spectrum has been approximately corrected for variation of PMT response and variation of grating efficiency with wavelength. The mercury emission lines superimposed on the broadband emission of the phosphor can be seen in the figure. The 577 - 579 nm lines and the 546 nm line are present, but are not shown in the spectrum. Their intensity is comparable to that of the 436 nm line.

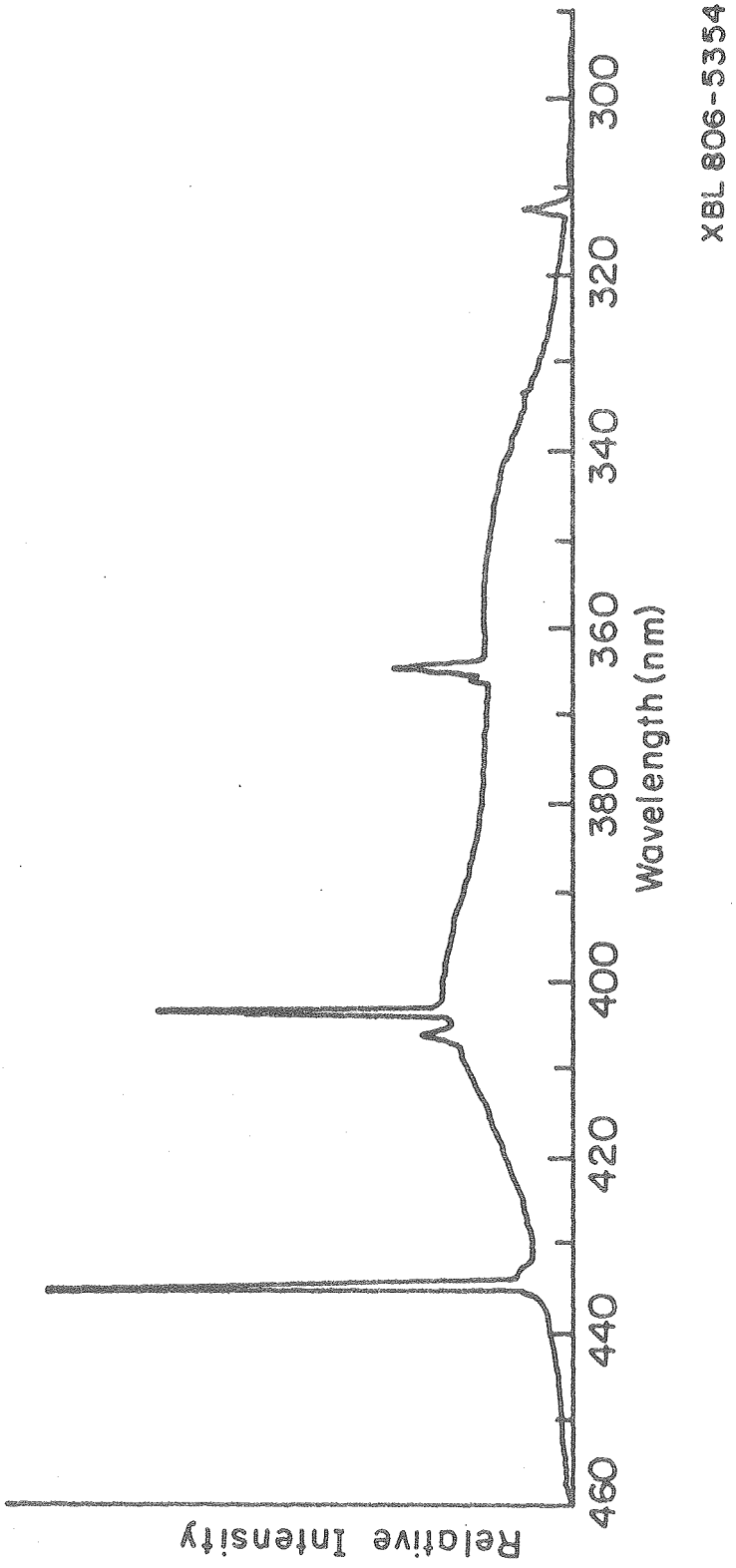

Fig. 7. Output of black lamps in the visible and near UV region

The G30T8 germicidal lamps were fitted with cylindrical gaseous chlorine filters. These consist of a sealed double-wall concentric quartz jacket filled with an atmosphere of chlorine. The lamps were inserted inside the filters. The chlorine ultraviolet absorption spectrum[6] is such that it selectively absorbs light in the 300 to 400 nm region. This allows near ultraviolet mercury lines to be attenuated with relatively little effect on the 254 nm line, and the longer wavelength mercury lines are only weakly apparent. The spectral distribution is in good agreement with that given by the manufacturer.[69]

C. Gases and Flow System

The carrier gases used in these studies were supplied by the Lawrence Berkeley Laboratory. High dry grade nitrogen was flowed through a Matheson moisture and particulate filter and through a column containing P_2O_5 before use. High dry grade oxygen was passed through a column containing copper turnings at 700K and a column of 5 percent palladium on an alumina substrate at 600K to convert hydrocarbon impurities to CO_2 and H_2O. The flow as then passed through ascarite and P_2O_5 columns to remove the CO_2 and H_2O, respectively. The oxygen is then flowed through a silica gel packed U-tube maintained at 196K with a dry ice-isopropanol bath for further drying. The gas supplier gives the following specifications for maximum impurity concentrations:

	High Dry Nitrogen	High Dry Oxygen
N_2	99.999 percent min.	500 ppm
O_2	1.5 ppm	99.5 percent min.
H_2O	1.5 ppm	1.5 ppm
CO_2	---	10 ppm
AR	5 ppm	400 ppm

Carbon monoxide from Matheson Company of 99.9 percent purity was passed through a silica gel trap maintained at 142K with a liquid nitrogen n-pentane slush bath for purification. An impurity, apparently a metal carbonyl, stained the silica gel a light brown color after extended use.

Carbon dioxide of 99.9 percent purity from Pacific Oxygen Company was checked for impurities using infrared spectroscopy. None were found in concentrations that would significantly affect results. The gas was used only for making cross section determinations of CO_2.

Distilled water of 99.9 percent purity was degassed and vacuum distilled, discarding the initial and final fractions. It was then used without further purification. Hydrogen peroxide of 98 percent purity was obtained from the Becco Chemical Division of FMC Corporation and used without further purification. The major impurity was H_2O.

Nitric oxide of 99.0 percent purity from the Matheson Company was passed through a silica gel trap maintained at 196K by a dry ice-isopropanol slush bath. The major impurity was NO_2, which was trapped as N_2O_3. It was then used without further purification.

Nitrogen dioxide of 99.5 percent purity from the Matheson Company was collected at 196K and purified by vacuum distillation and stored under an atmosphere of oxygen to oxidize any remaining NO to NO_2. The oxygen was then pumped off and two further vacuum transfers were done. The remaining white solid was stored at 196K.

Preparation of dinitrogen pentoxide was performed by the technique of Schott and Davidson.[70] Oxygen coming from the purification line was divided into two flows. One flow was directed into an Ozone Research and Equipment Company ozonator, which generated a flow of approximately 5 percent ozone in oxygen. The other stream passed through a regulating needle valve and flowmeter and was bubbled through a bulb with liquid NO_2 and N_2O_4 which was maintained at 274K. The two flows were recombined, where NO_2 and O_3 react to form N_2O_5. The heat of reaction heats the tubing just beyond the mixing region to about 305K. The flow carrying NO_2 is regulated so there is an excess of ozone in the mixing region, indicated by the oxidation of natural rubber. The flow passes through a previously evacuated Pyrex saturator. The saturator is cooled to 196K in a dry ice-isopropanol slush bath after the mix has flowed through it for about 15 minutes. This is to allow HNO_3 formed by the contact of N_2O_5 with the interior walls of the saturator to be transported out of the vessel.

N_2O_5 is collected until all the NO_2 in the bubbler has been consumed. Residual O_2 and O_3 are then pumped off the needle-shaped white crystals in the saturator. The N_2O_5 is then stored at 196K. Less than 1 percent NO_2 is present in the N_2O_5, as determined by

infrared absorption. HNO_3 is present at levels of about 10-15 percent. It is apparently formed by a heterogeneous reaction of N_2O_5 with water on the interior surfaces of the gas handling system. The system was not designed to to bakeable; so, the total removal of water was not possible.

The gas handling manifold was constructed of Pyrex. All stopcocks on the system were Kontes high vacuum stopcocks with teflon bores and Viton o-rings, which were greased with small amounts of Apiezon Type N grease. Gas lines to the manifold were connected with stainless steel Ultra-Torr fittings or stainless steel Swagelock fittings with teflon ferrules. A liquid nitrogen trapped glass oil diffusion pump was used to evacuate the system.

Hastings thermocouple vacuum gauges were used to monitor the pressure on the low side of the diffusion pumps. For measuring pressures in the 0-100 torr range, a MKS Instruments Baratron Model 220-246-100 capacitance manometer was used. For higher pressure measurements, a Texas Instruments Model 145 quartz Bourdon precision pressure gauge and a MKS Instruments Baratron Model 310 BHS-100 capacitance manometer were used. Comparison of pressure readings on the three instruments showed excellent agreement.

The flow rates of gases used during the flow experiments were monitored with either Fisher and Porter Corporation or Manostat Company flowmeters. The flowmeters were calibrated by timing the period needed for a gas flowing through a flowmeter to fill a calibrated volume.

In some flow experiments, gases are flowed into the cell through two Pyrex disperser tubes. Each tube has fine holes on alternate sides at 2.5 cm intervals along its length. The diameter of the holes is such that the pressure drop across the holes is large compared to the pressure drop along the tube. These tubes create turbulent mixing within the cell and provide an even distribution of gases. The gases are exhausted through a port in one end of the cell.

Other flow experiments were done by mixing the gases prior to entry into the cell and flowing them in through one disperser tube. The gases were exhausted through the other disperser tube.

In the flow experiments involving NO_2, H_2O_2 and CO, the carrier gas was split into two flows. One flow passed through a regulating needle valve and a flowmeter and then was bubbled through liquid NO_2 and N_2O_4 before going into the cell. Another flow of carrier gas was passed through a regulating valve and a flowmeter before going through a temperature regulated saturator containing H_2O_2. A flow of CO passed through a regulating needle valve and a flowmeter and was mixed with the other flows. When a more dilute mixture of reactants was desired, a third flow of pure carrier gas was added and monitored with a flowmeter. The pressure drop across the cell and the flow system was dependent on flow rate. It was generally less than five torr at one atmosphere total pressure.

In the flowing photolysis experiments, the flow of nitrogen carrier gas was split into three streams. All three flows passed through regulating valves and flowmeters. Two of the flows passed through tempera-

ture controlled saturators containing either H_2O_2 or N_2O_5. These flows were mixed with the third flow and directed into the cell though one of the disperser tubes. At the flow rates used in these experiments, the pressure drop was about 7 torr across the flow system and the cell.

In the expansion experiments, the reactants were jetted into the evacuated cell from pressurized bulbs. Each bulb was connected to one of the disperser tubes, preventing mixing of the reactants outside of the cell. Each bulb was filled with the desired pressure of the reactant and then filled with carrier gas. The total pressure in the bulbs was controlled so that the pressure-volume products of the two bulbs were equal. The stopcocks sealing the bulbs from the cell were opened simultaneously, so that both reactants would enter the cell at the same time.

The flow behavior of the gases can be described by

$$\text{fraction of gas in cell at time } t = (1 - \exp(-t/t_o)) \qquad (39)$$

where t_o is a time constant characteristic of a particular expansion system. The time constant for the system used in these experiments was about 4.3 seconds.

III. ABSORPTION CROSS SECTIONS

A. Infrared Cross Sections

The experimental apparatus described previously was employed as a single beam spectrometer to determine absorption cross sections. The regulated Nernst glower proved to be a very stable source of infrared radiation. Very little change was observed in its output over the course of several hours, and any change was generally fairly constant throughout the spectral region of interest.

Absorption cross sections were determined by recording $I_0(\lambda)$ and then recording $I(\lambda)$. The cross section, σ, was determined by calculating σ as

$$\sigma(\lambda) = \ln(I_0(\lambda)/I(\lambda))/n\ell \qquad (40)$$

where n is the concentration in molecules/cm^3 and ℓ is the optical pathlength in cm. If necessary, baselines of the absorption spectra were adjusted linearly to zero in spectral regions where no absorption occurred.

All absorption cross sections determined in this study were measured with the 150 line/mm grating and with 2 mm entrance and exit slits on the monochromator. The resulting resolution was 0.013 μm in first order (4–12 μm) and 0.0065 μm in second order (2.4–4 μm). Spectra were obtained by scanning the monochromator at 0.16 μm/minute for all species except H_2O_2 and O_3, which were done at 0.40 μm/minute. The signals were

digitized and recorded at 0.4 second intervals and with a 0.4 second time constant. In all cases the spectral region scanned during one time constant was less than or equal to 0.1 times the resolution determined by the slits. The optical path length used in all measurements was 800 cm. The faster scan rates were used for H_2O_2 and O_3 because of their significant heterogeneous decay rates.

The wide range of conditions involved in these experiments necessitated the measurement of absorption cross sections as a function of total pressure, temperature, and concentration of the absorbing specie. Measurements were made at temperatures of 263K, 293K and 313K, and at pressure of 0.1 and 1 atmosphere. Many species displayed a marked absorption dependence on all three variables, presumably due to broadening of rotational lines. This is addressed in more detail in Appendix B.

The Beers law formulation of

$$OD = \sigma n \ell \tag{41}$$

where OD is the optical density and σ is the cross section at the wavelength of interest was modified to accommodate the species that exhibited a dependence on concentration. It was rewritten as

$$n = OD^{\alpha}/\sigma\ell \quad \text{or} \quad n = OD^{\alpha}10^{\beta} \tag{42}$$

where α is the correction factor for non-Beers law behavior. In the measurements made in these studies, α ranged from 1 to more than 2.

This expression was further modified into

$$n = 10^{(\alpha \log(OD) + \beta)} \tag{43}$$

where $\beta = -\log(\sigma \ell)$, for computer analysis of decay curves. The α and β coefficients for each species observed are tabulated in Table 3, for the three temperatures and two pressures used in these studies. The one exception to this formulation is the cross section for NO_2 at 6.258 μm. The cross sections determined by Connell[67] were in good agreement with those determined in this investigation, and were used in the same formulation.

Another factor that had been taken into consideration was that of spectral overlap. In conditions where there are a number of species present, a number of absorption bands may overlap and cannot be used for concentration determinations without deconvolution. Fig. 8 schematically illustrates the absorption bands and their approximate strengths. This figure is not necessarily complete and the locations and strengths are only approximate. Overlap problems are particularly severe with the nitrogen oxides and oxyacids of nitrogen. Spectral regions to monitor concentrations of species were chosen where little or no overlap problems existed.

Cross sections for NO_2 at 3.428 μm were measured by expanding a measured pressure of purified NO_2 from a 1081 cm^3 bulb into the

TABLE 3

Infrared Cross Sections

$n = OD^{\alpha}\ 10^{\beta}$ (n - molecules/cm^3, OD - optical density)

Compound	Pressure	T = 263K γ(μm)	α	β	T = 293K γ(μm)	α	β	T = 313K γ(μm)	α	β
NO_2	1 atm	3.428	1.09±0.02	16.26±0.01	3.428	1.16±0.02	16.29±01.01	3.428	1.04±0.03	16.27±0.02
	0.1 atm		1.39±0.04	16.60±0.03		1.40±0.04	16.59>0.03		1.42>0.05	16.64>0.03
CO_2	1 atm	4.238	1.28±0.05	15.15±0.02	4.238	1.20±0.02	15.19±0.01	4.239	1.39±0.03	15.15±0.01
	0.1 atm		1.04±0.05	16.01±0.04		1.48±0.03	16.13±0.02		1.64±0.05	16.22±0.05
CO	1 atm	4.609	1.50±0.02	16.74±0.01	4.610	1.58±0.03	16.91±0.02	4.607	1.54±0.04	16.83±0.01
	0.1 atm		1.70±0.04	17.77±0.03		1.17±0.03	17.97±0.03		1.76±0.04	17.88±0.03
NO	1 atm	5.242	1.65±0.02	16.93±0.01	5.246	1.48±0.02	17.12±0.01	5.242	1.56±0.02	17.06±0.01
	0.1 atm		1.84±0.002	17.92±0.01		1.56±0.05	18.12±0.04		1.81±0.03	18.12±0.02
H_2O	1 atm	6.634	1.27±0.10	16.60±0.07	6.634	1.40±0.04	16.75±0.01	6.634	1.55±0.07	16.46±0.02
	0.1 atm		1.52±0.10	17.58±0.08		1.32±0.06	17.51±0.05		1.43±0.07	17.31±0.05
HNO_4	note 1	7.158	1.0	15.32	7.158	1.0	15.32	7.158	1.0	15.32
		12.315	1.0	15.35	12.315	1.0	15.35	12.315	1.0	15.35
HNO_3	note 1	7.400	1.0	15.83	7.400	1.0	15.83	7.400	1.0	15.83
		8.264	1.0	16.62	8.264	1.0	16.62	8.264	1.0	16.62
N_2O_5	note 1	7.400	1.0	16.03	7.400	1.0	16.03	7.400	1.0	16.03
		7.960	1.0	15.04	7.960	1.0	15.04	7.960	1.0	15.04
		8.040	1.0	14.82	8.040	1.0	14.82	8.040	1.0	14.82
H_2O_2	1 atm	7.896	1.38±0.20	15.43±0.10	7.896	2.8±0.10	16.18±0.03	7.896	1.49±0.10	15.51±0.05
	0.1 atm		2.30±0.20	16.90±0.10		2.82±0.20	16.90±0.10		2.14±0.20	16.84±0.08
	1 atm	8.040	1.44±0.20	15.61±0.10	8.040	2.15±0.10	16.28±0.03	8.040	1.44±0.10	15.58±0.03
	0.1 atm		2.10±0.20	16.90±0.10		2.23±0.20	16.66±0.10		2.08±0.20	16.93±0.10
	1 atm	8.264	1.06±0.10	16.47±0.10	8.264	1.98±0.10	17.67±0.10	8.264	1.26±0.04	16.51±0.07
	0.1 atm		1.06±0.20	17.10±0.30		1.85±0.20	17.67±0.30		1.27±0.20	17.01±0.30
O_3	1 atm	9.476	1.03±0.04	15.47±0.03	9.478	1.10±0.04	15.48±0.02	9.476	1.05±0.003	15.17±0.01
	0.1 atm		1.13±0.05	15.64±0.04		1.06±0.05	15.57±0.04		1.13±0.10	15.39±0.05
NO_2	1 atm	6.258	$\sigma = (1.04-0.1\ OD) \times 10^{-18}$		6.258	$\sigma = (1.00-0.1\ OD) \times 10^{-18}$				
	note 2		cm^2/molecule			cm^2/molecule				

Note 1: There was no change in cross section with pressure or concentration

Note 2: The change in cross section with concentration was not fitted to the α, β format.

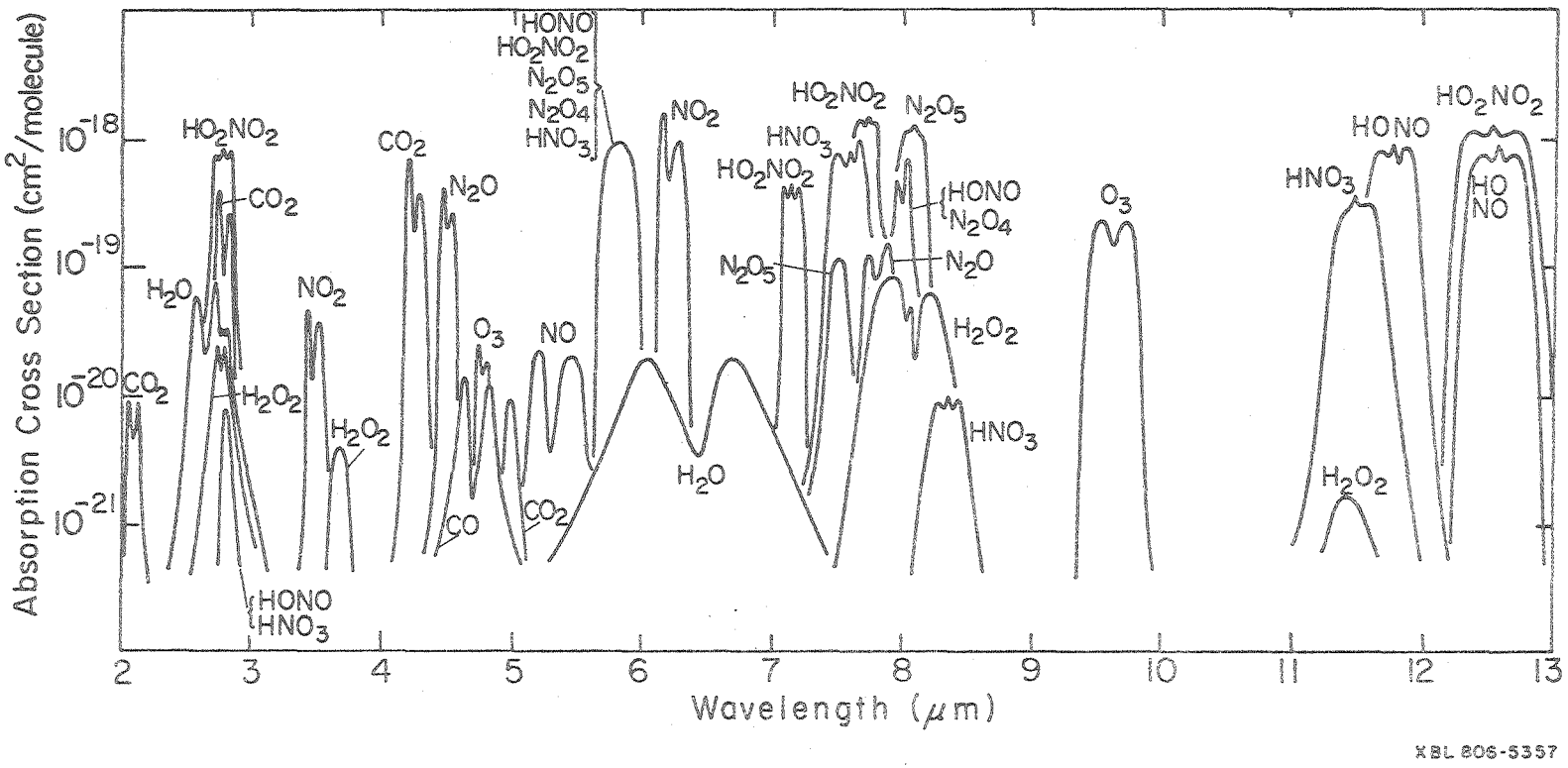

Fig. 8. Infrared absorptions of species involved in these studies.

evacuated cell, and then filling the cell to 0.1 or 1 atmosphere total pressure with nitrogen. Low pressures were measured with the MKS Baratron and higher pressures were measured with the TI Bourdon gauge. Corrections were made for the dimerization of NO_2 into N_2O_4, using the results of Verhoek and Daniels,[71] when determining NO_2 concentrations in the bulb and in the cell. NO_2 illustrated a significant cross section dependence on concentration as well as pressure and temperature. The NO_2 absorption at 3.428 μm was free of interference from absorptions by other species. A representative absorption spectrum at 0.1 and 1 atmosphere total pressure is shown in Fig. 9, which was taken at 313K.

The NO_2 cross sections of 6.258 μm were obtained in a similar manner. Measurements were made at 1 atmosphere total pressure only. The wavelength at which NO_2 is monitored occurs at an absorption minimum between the P and R branches of a H_2O absorption. At one atmosphere, the absorption cross section of H_2O is less than 10^{-3} times that of the NO_2 cross section. In most cases, H_2O will have an insignificant effect on the optical density obtained at this wavelength. A typical absorption spectrum is shown in Fig. 10.

CO_2 cross section determinations were made at 4.238 μm at 263K and 293K, and at 4.239 μm at 313K. Mixtures of CO_2 and N_2 were prepared in a 1081 cm^3 bulb in ratios of 1:50 to 1:100. Fractions of these mixtures were expanded into the evacuated cell, and nitrogen was added to the desired pressure. Because of the large cross section of CO_2, the double dilution method was used to obtain reasonable optical

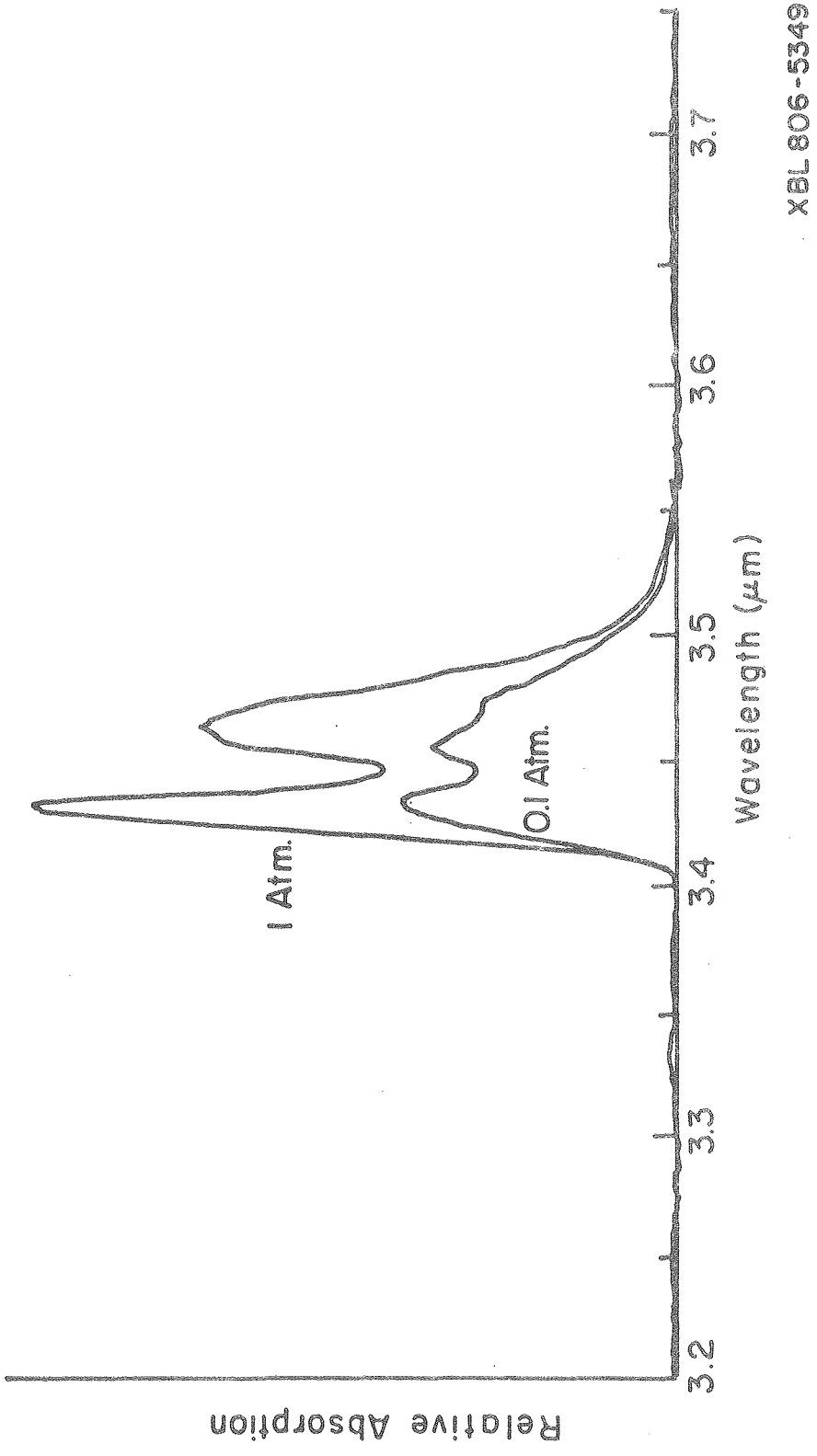

Fig. 9. NO_2: spectrum at 0.1 and 1.0 atmosphere pressure

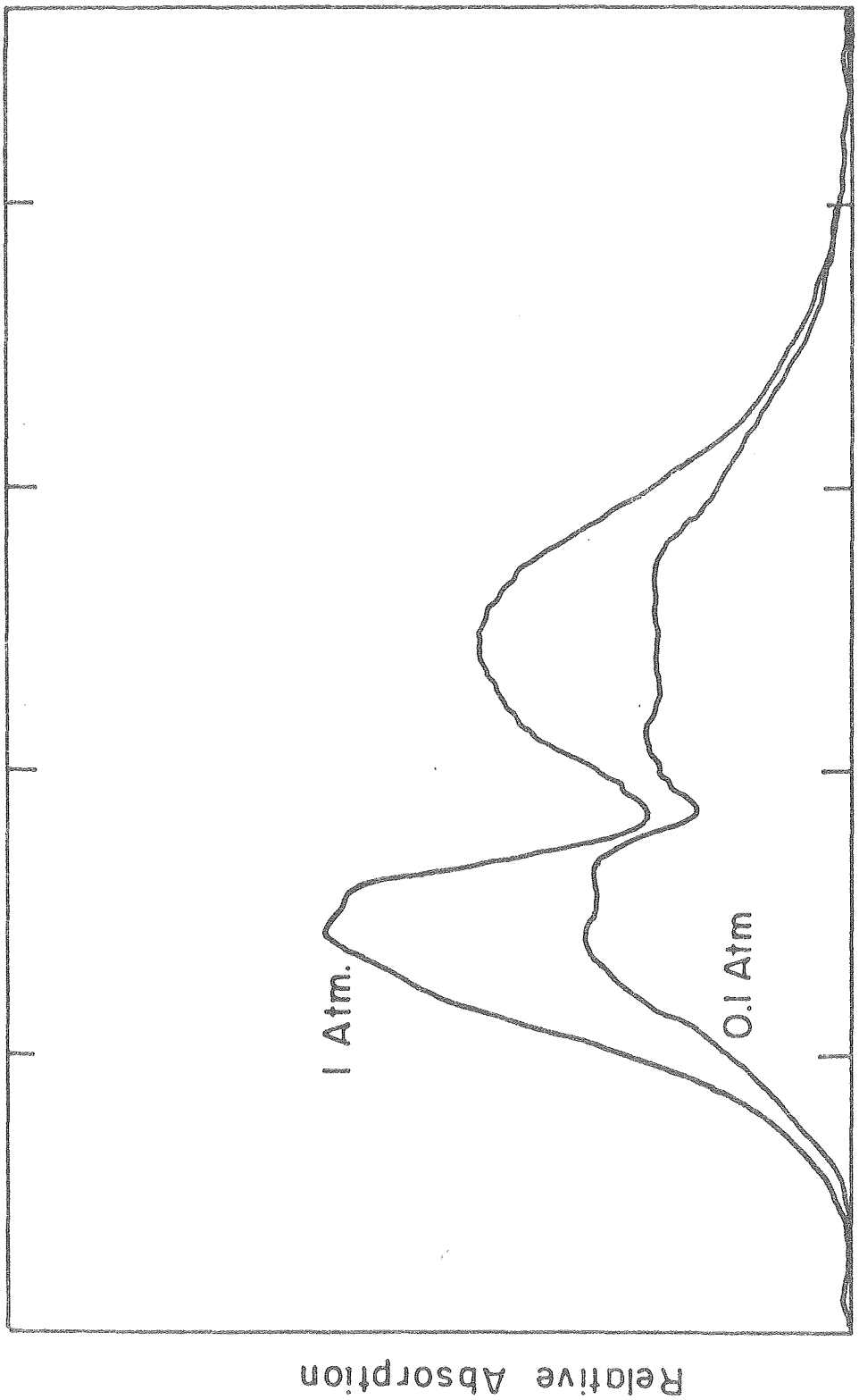

Fig. 10. NO_2 absorption spectrum at 0.1 and 1.0 atmosphere pressure XBL809-5869

densities for the cross section deteminations. Fig. 11 illustrates a typical absorption spectrum of CO_2 at 313K for 0.1 and 1 atmosphere total pressure.

Cross section for CO were measured at 4.609 μm at 263K, 4.610 μm at 292K, and 4.607 μm at 313K. The rotational lines in the absorption band were partially resolved and the monitoring wavelength was shifted to match the largest peak. Purified samples of CO were expanded into the evacuated cell. Expanded pressures were measured with the MKS Baratron gauge, and nitrogen was added to either 0.1 or 1 atmosphere total pressure. The CO absorption band at 313K is shown in Fig. 12 for 0.1 and 1 atmosphere.

NO cross sections were obtained at 5.242 μm for 263K and 313K and at 5.246 μm for 293K. The methods used in their determination were similar to those used to determine the CO cross sections. Care had to be taken to avoid the presence of O_2 which would oxidize the NO to NO_2 and give abnormally high apparent cross sections. The rotational lines of NO were partially resolved, as indicated in Fig. 13, which illustrates the absorption band at 0.1 and 1 atmosphere total pressure at a temperature of 313K. The irregularities of the long wavelength end of the spectrum are due to the roll-off of the detector spectral response.

The NO_2, CO_2, CO and NO cross section determinations were done largely with the InSb detector. All other cross section measurements were done at longer wavelengths. The HgCdTe detector was used for these measurements. H_2O has a broad infrared absorption that extends from below 5 μm to above 8 μm. The pattern of rotational lines is complex,

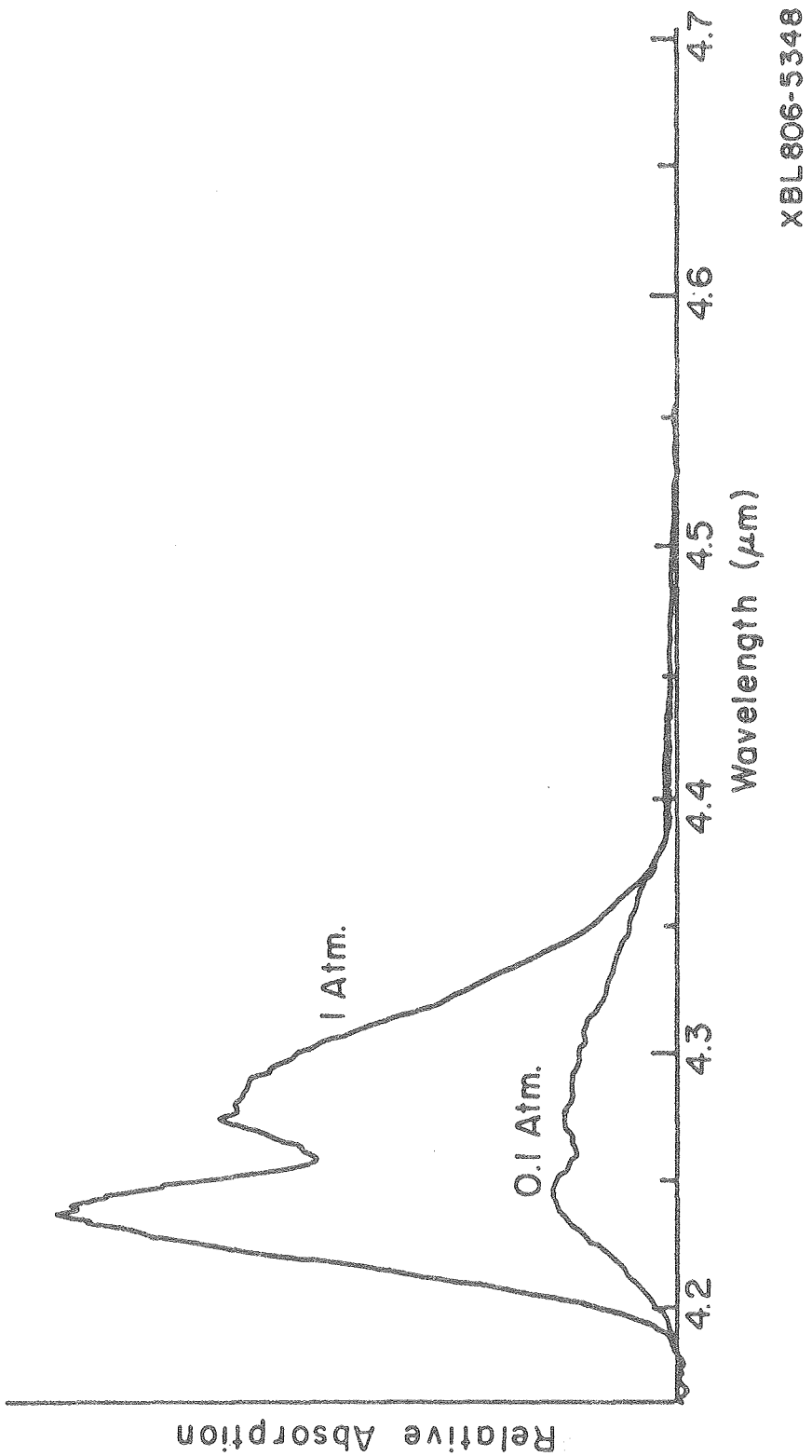

Fig. 11. CO_2 spectrum at 0.1 and 1.0 atmosphere pressure

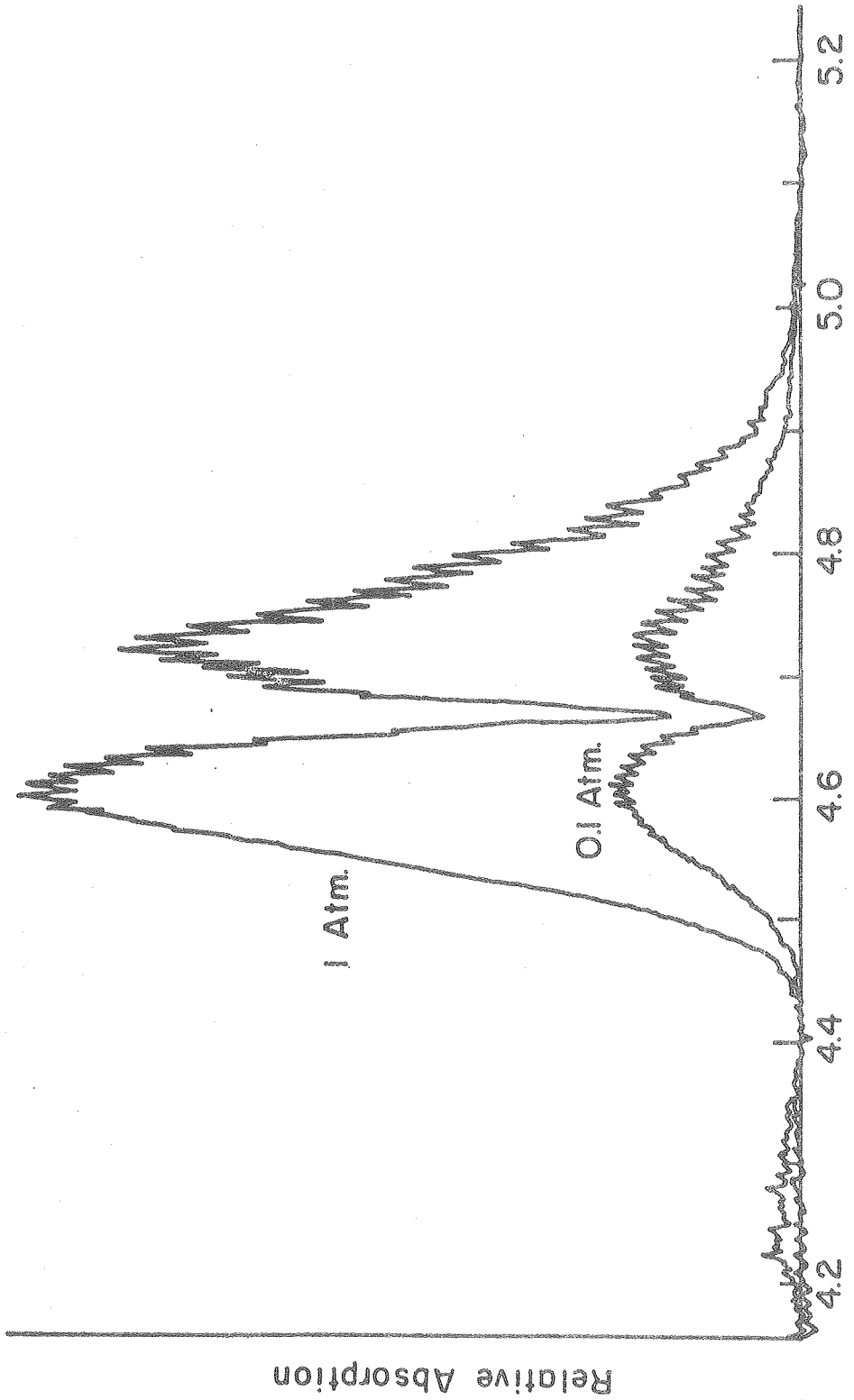

Fig. 12. Absoprtion spectrum of CO at 0.1 and 1.0 atmosphere pressure

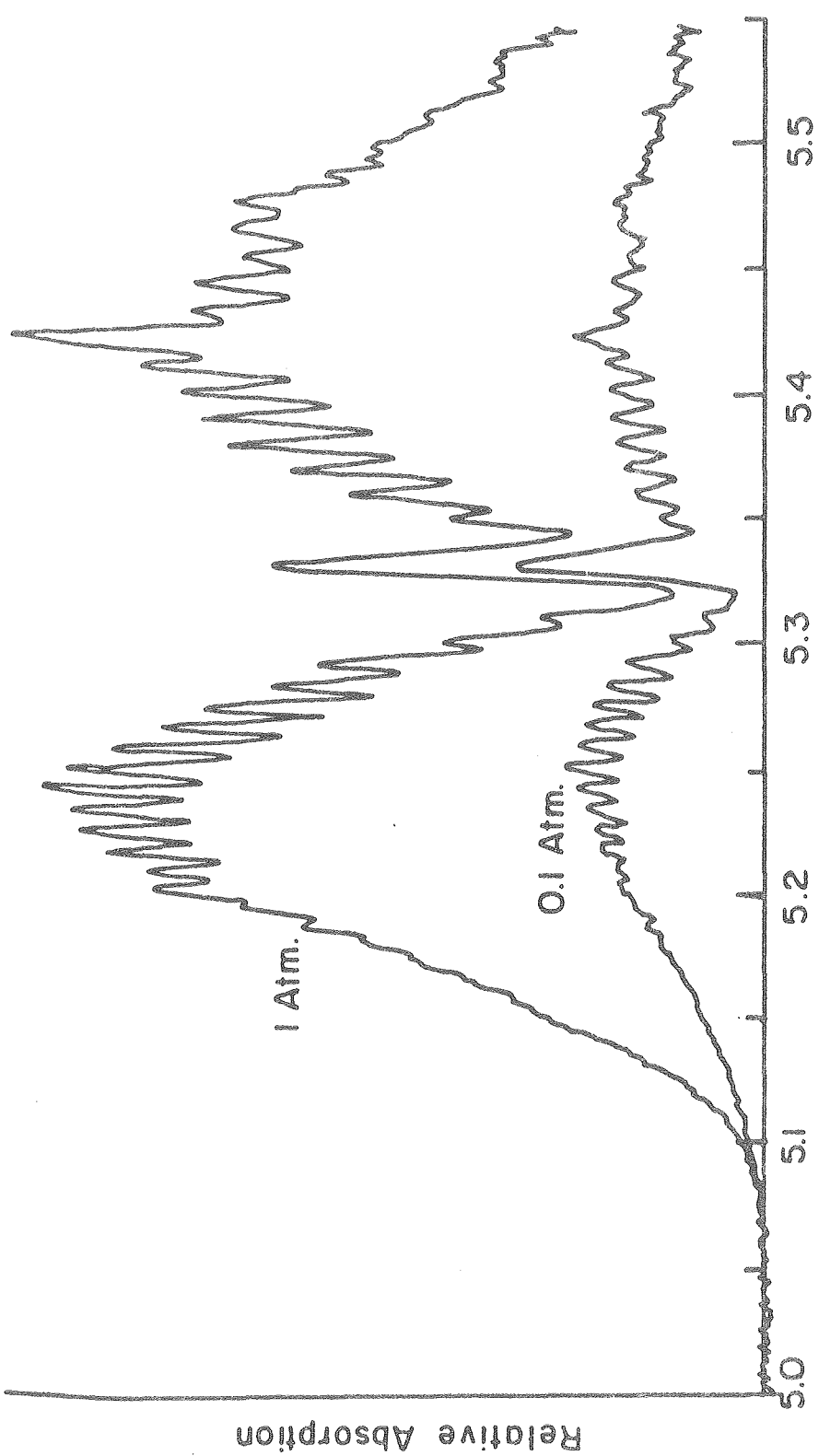

XBL806-5346

Fig. 13. Absorption spectrum of NO at 0.1 and 1.0 atmosphere pressure

but the lines are widely spaced. The line at 6.634 μm was used for cross section determinations at all temperatures. It is one of the strongest lines in the spectrum at the resolution used for these measurements. It was necessary to make baseline correction at a considerably different wavelength from that used for the cross section determination because of the broad absorption. To do this a reference measurement was made and the monochromator was then rapidly slewed to the absorbing region, where standard measurements were done. For the measurements, purified H_2O in liquid form was evaporated directly into the evacuated cell to the desired pressure. At 263K, the H_2O pressure had to be maintained below two torr to prevent condensation within the cell. At higher temperatures, this was not a problem. The restriction of low H_2O pressures at 263K made accurate determination of the α and β factors difficult. A spectrum of H_2O in the region of measurement at 313K is shown in Fig. 14 at 0.1 and 1 atmosphere total ressure.

Because H_2O_2 and O_3 exhibit heterogeneous decomposition at the temperature range in which these experiments were done, the techniques previously used were not useful in determining their cross sections. Previous cross section measurements had been done by Giguere[72] with H_2O_2 and by McCaa and Shaw[73] with O_3, but these were not applicable to these studies. It is difficult to make concentration determinations from pressure measurements because it is unknown what fraction of the pressure of the gas expanded into the cell is due to the decomposition products.

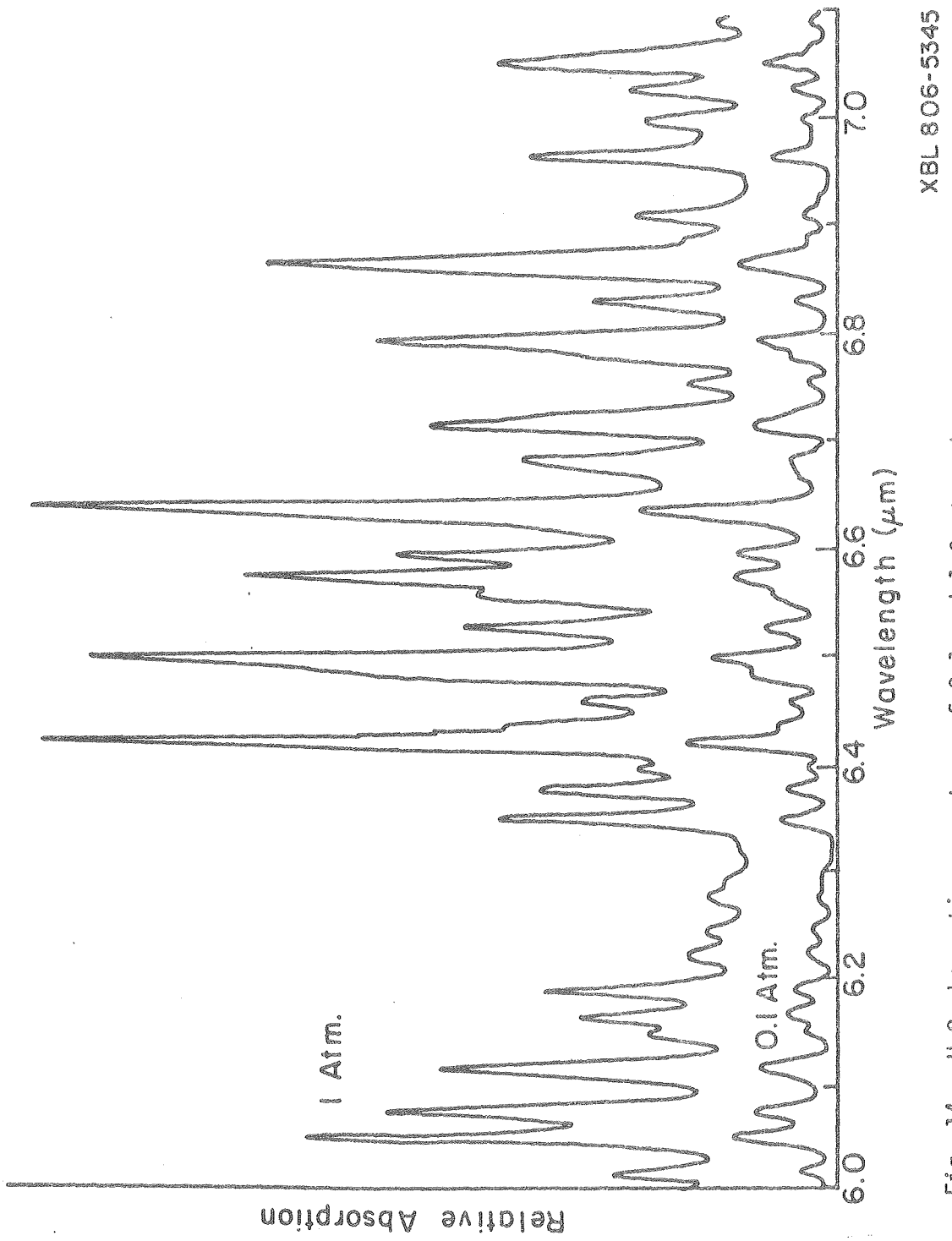

Fig. 14. H_2O absorption spectrum of 0.1 and 1.0 atmosphere pressure

Since the ultraviolet cross sections of H_2O_2[21,74,75] and O_3[76,77] are well known, it was decided to utilize them in concentration determination for the infrared cross section measurements. The measurements were done using a flow system in which the compound to be measured and the carrier gas were flowed in the disperser tubes of the cell and out the exhaust port at the end of the cell. The flow out of the cell was directed through a 98 cm long, 2.5 cm diamter Pyrex tube with 2 mm thick CaF_2 windows. Light from a deuterium lamp was chopped at 400 Hz by a tuning fork chopper and then focused through the cell with an off-axis spherical mirror of 21 cm focal length. The light passing through the cell was directed into a McPherson 218 0.3 meter monochromator with a 2400 line/mm grating. The dispersed light was detected by a 1P28 photomultiplier tube operating at -800 volts. The output signal was amplified and fed into a lock-in amplifier constructed by the Chemistry Department electronics shop. The output from the lock-in amplifier was directed to a digital voltmeter and a recorder for monitoring. The system is shown in Fig. 15.

The flow into the monitoring cell can be quickly switched between the flow out of the cell and the flow of pure carrier gas. This allowed rapid sequential determination of I and I_o to determine the concentration of the absorbing species. The regulated deuterium lamp exhibits good short term stability and some slow long term drift. H_2O_2 was monitored at 200 nm, near the short wavelength limit of the operating system. Nitrogen was used as a carrier gas since oxygen has a significant absorption at this wavelength. O_3 was monitored at 300 nm, which

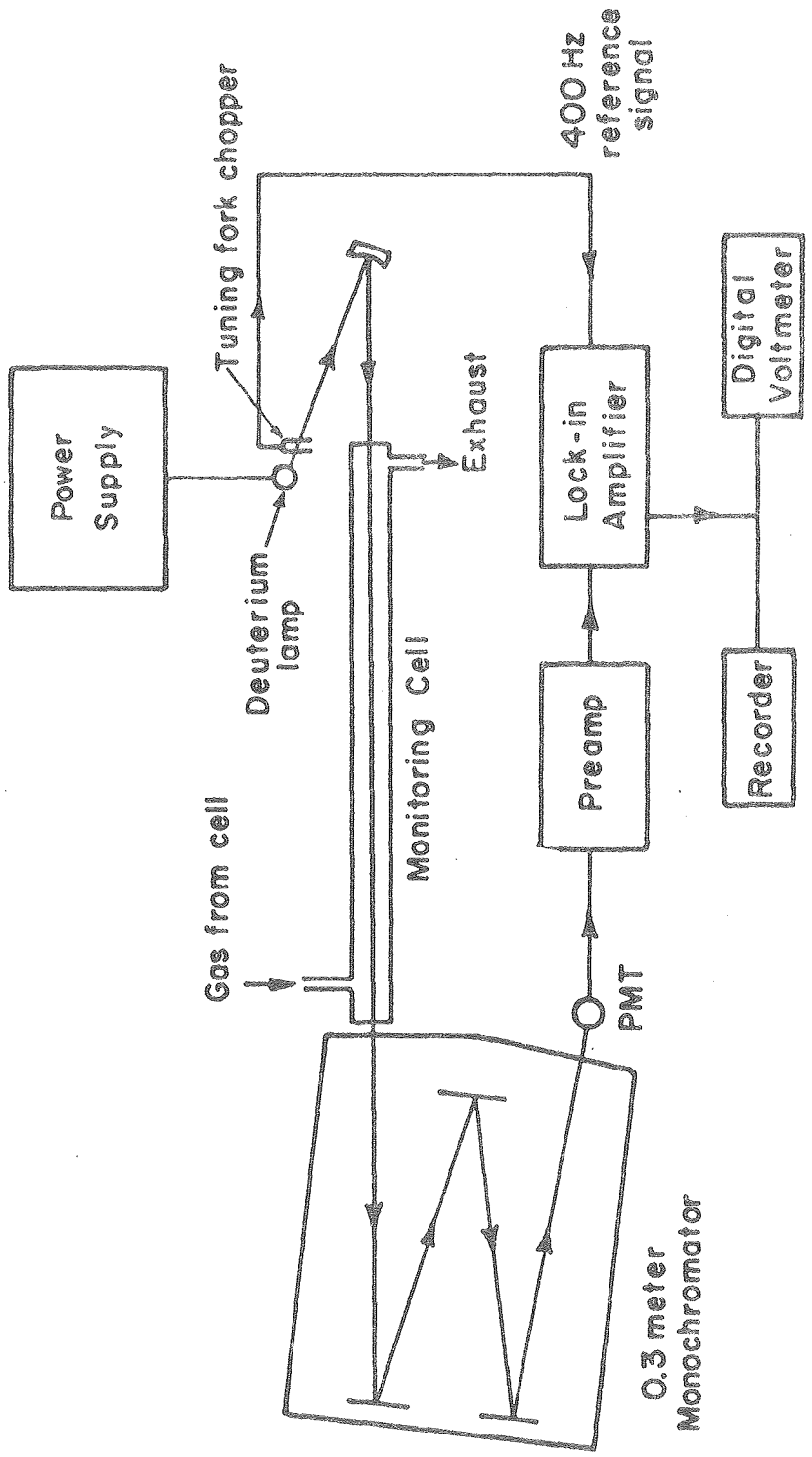

Fig. 15 Ultraviolet monitor used for determining H_2O_2 and O_3 concentrations

allowed use of oxygen as a carrier gas. The large ozone absorption cross section at shorter wavelengths caused excessively high light absorption at the concentrations of interest.

This system provided real-time detection of H_2O_2 and O_3 and was simple to use. It is considered highly superior to titration techniques in this application.

To determine H_2O_2 infrared absorption cross sections, nitrogen carrier gas was flowed through a temperature-controlled saturator containing H_2O_2. The flow passed through the cell and through the UV monitor. Concentration determinations were made before and after each run. For low pressure measurements, a concentration measurement was made and the cell was quickly pumped down to the desired pressure and an infrared scan was done. The H_2O_2 decomposition was then monitored and used to correct the low pressure measurement. A spectrum of H_2O_2 at 313K and 1 atmosphere pressure is shown in Fig. 16. Two peaks due to H_2O, a decomposition product, can be seen at the short wavelength end of the spectrum. Cross section measurements were made at the Q branch (at 7.896 μm) and on the P branch (at 8.040 and 8.264 μm) to minimize interference by H_2O lines. Accurate low pressure measurements were difficult to obtain because of the low vapor pressure of H_2O_2, particularly at low temperatures.

O_3 cross section measurements were performed by passing an ozone-oxygen flow from the ozonator into the cell and the UV monitor. Ozone concentration was controlled by regulating the power of the discharge in the ozonator. For lower levels of ozone than were obtainable directly

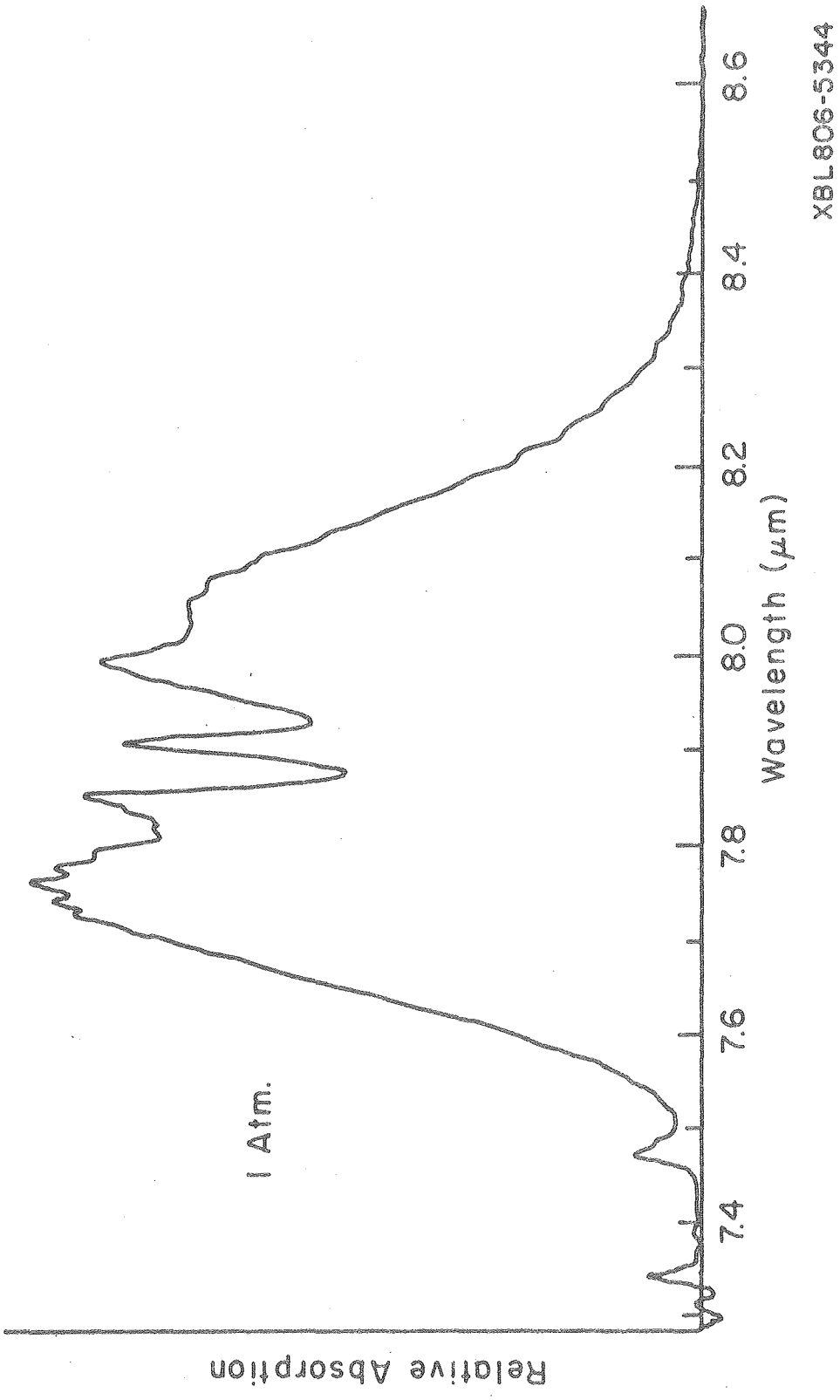

Fig. 16 H_2O_2 absorption spectrum at 1.0 atmosphere pressure

from the ozonator, the ozone-oxygen mixture was diluted with more oxygen. The concentration was determined before and after each infrared scan at 1 atmosphere. The technique used for low pressure H_2O_2 cross section measurements was also used for low pressure O_3 cross section measurements. It was found that the O_3 decomposition was slow enough that corrections were not needed. Early measurements were made with CaF_2 windows on the cell, which have an absorption cutoff near 10 μm. Hence, cross section determinations were made on the R branch. Fig. 17 illustrates the O_3 absorption band at 313K and 1 atmosphere total pressure.

The cross sections for N_2O_5 and HNO_3 have been previously determined by Connell,[67] Graham,[78] and Harker,[79] using systems similar to the one used in these experiments. To confirm these measurements, the technique similar to that of Connell was used.

N_2O_5 was flowed into a 3.06 liter bulb and then purified oxygen carrier gas was added to the desired pressure. This mixture was expanded into the vacuated cell and the absorbing region was scanned. Cross sections obtained by Graham[78] were used to determine the amount of HNO_3 present and the concentration of N_2O_5 was obtained. The N_2O_5 absorption cross sections are shown in Fig. 18 for 263K and 16 torr total pressure and are in good agreement with the previously determined values of Connell, Graham and Harker. The N_2O_5 cross section appears to be independent of pressure for < 10 torr to 1 atmosphere total pressure and independent of concentration from < 1×10^{14} molecules/cm^3 to > 2×10^{15} molecules/cm^3.

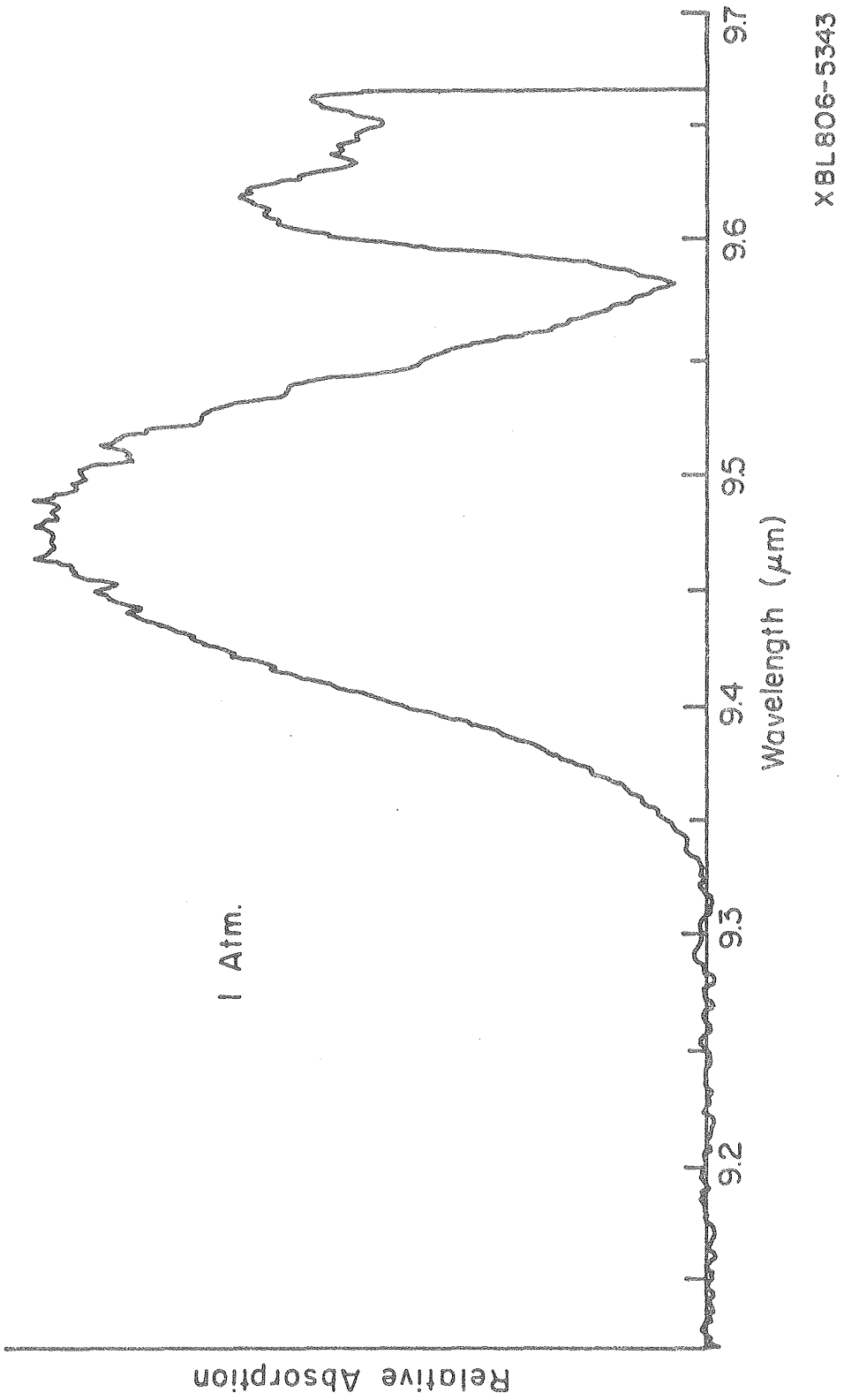

Fig. 17 O_3 absorption spectrum at 1.0 atmosphere pressure

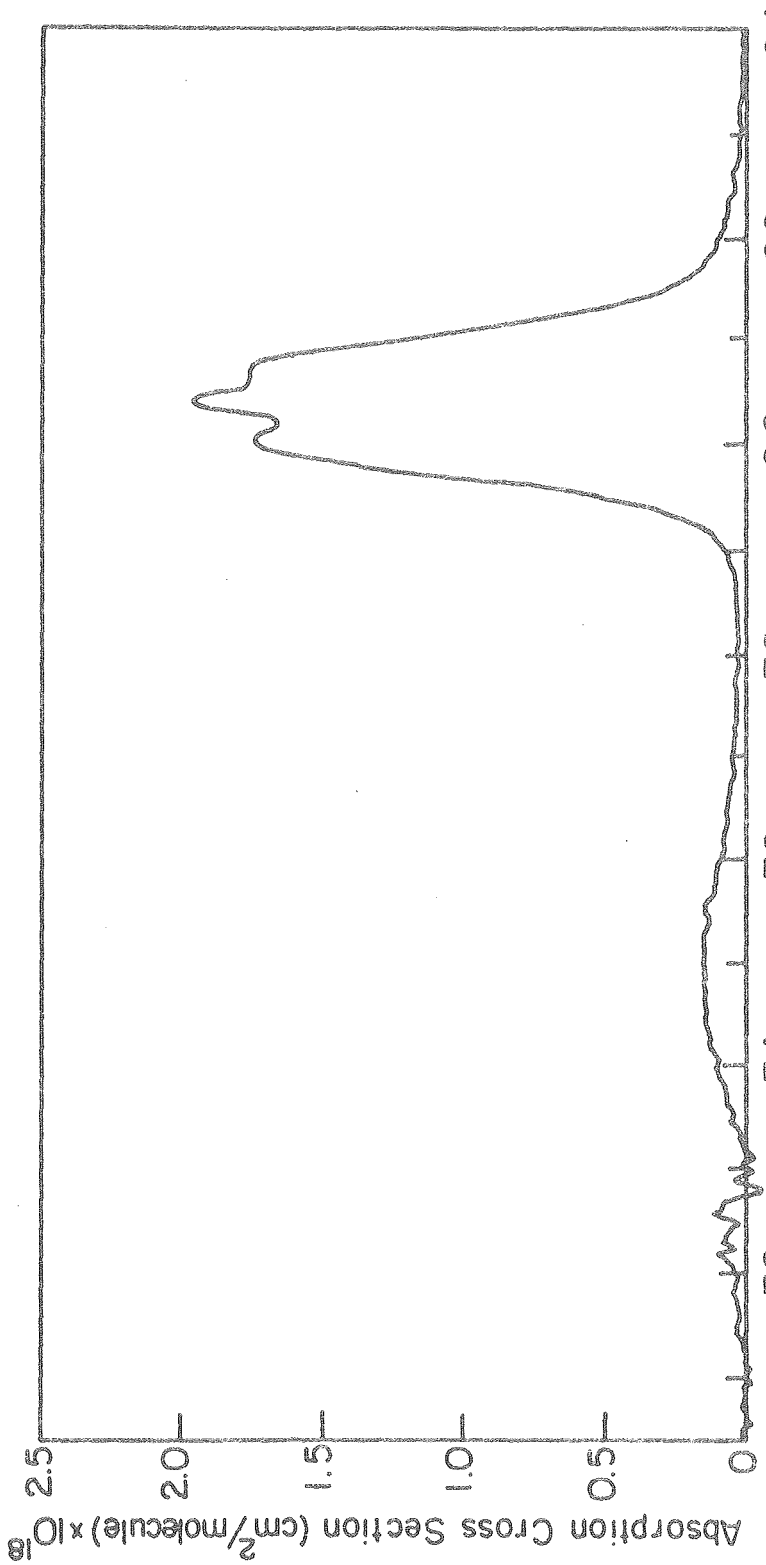

XBL 806-5339

Fig. 18 N_2O_5 absorption spectrum

HNO_3 cross sections were checked by filling a 3.06 liter bulb with N_2O_5 to the desired pressure and then adding excess H_2O vapor. Carrier gas was then added to the bulb and the mixture was expanded into cell. The absorbing region was scanned and the cross section determined from the initial pressure of N_2O_5 used. This technique produced somewhat variable HNO_3 concentrations after expansion due to the tendancy of HNO_3 to adhere to cell surfaces and to the heterogeneous nature of the conversion of N_2O_5 to HNO_3. The results, while somewhat uncertain, are in agreement with those obtained by Connell,[67], Graham[78] and Harker.[79]. Fig. 19 shows the HNO_3 absorption band at 273K and 39 torr total pressure.

Absolute cross sections for HNO_4 were not determined. The values determined by Graham et al.[20] using a Fourier transform spectrometer were used in these studies. A comparison of the relative peak heights of the Q branches determined in these studies was in good agreement with the published values. An R branch of HNO_4 used by Graham et al.[20] was used in monitoring HNO_4 in these experiments because the cross section is independent of pressure, temperature, concentration, and resolution effects over a fairly wide range. There is also freedom from overlapping absorptions in this region. A cross section of 5.6×10^{-19} cm^3/molecule at 12.315 μm was used. Fig. 20 illustrates the HNO_4 absorptions in the 7 to 8.5 μm region after other absorptions due to HNO_3 and H_2O_2 have been subtracted. The 7.2 to 7.4 μm region is somewhat noisy due to a dip in reflectivity of the mirrors in this region. Fig. 21 shows the longer wavelength HNO_4 absorption, which

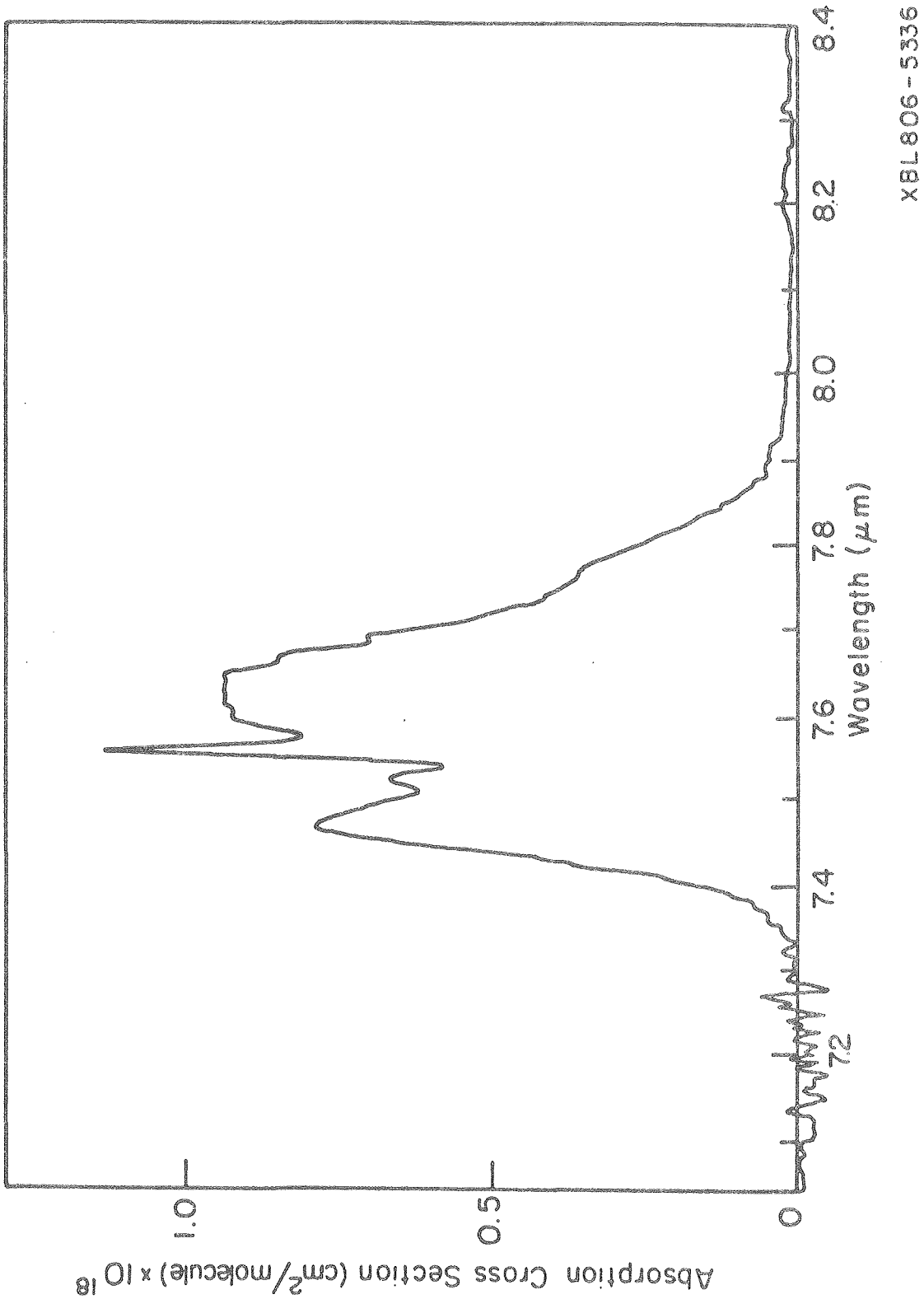

XBL806-5336

Fig. 19 HNO_3 absorption spectrum

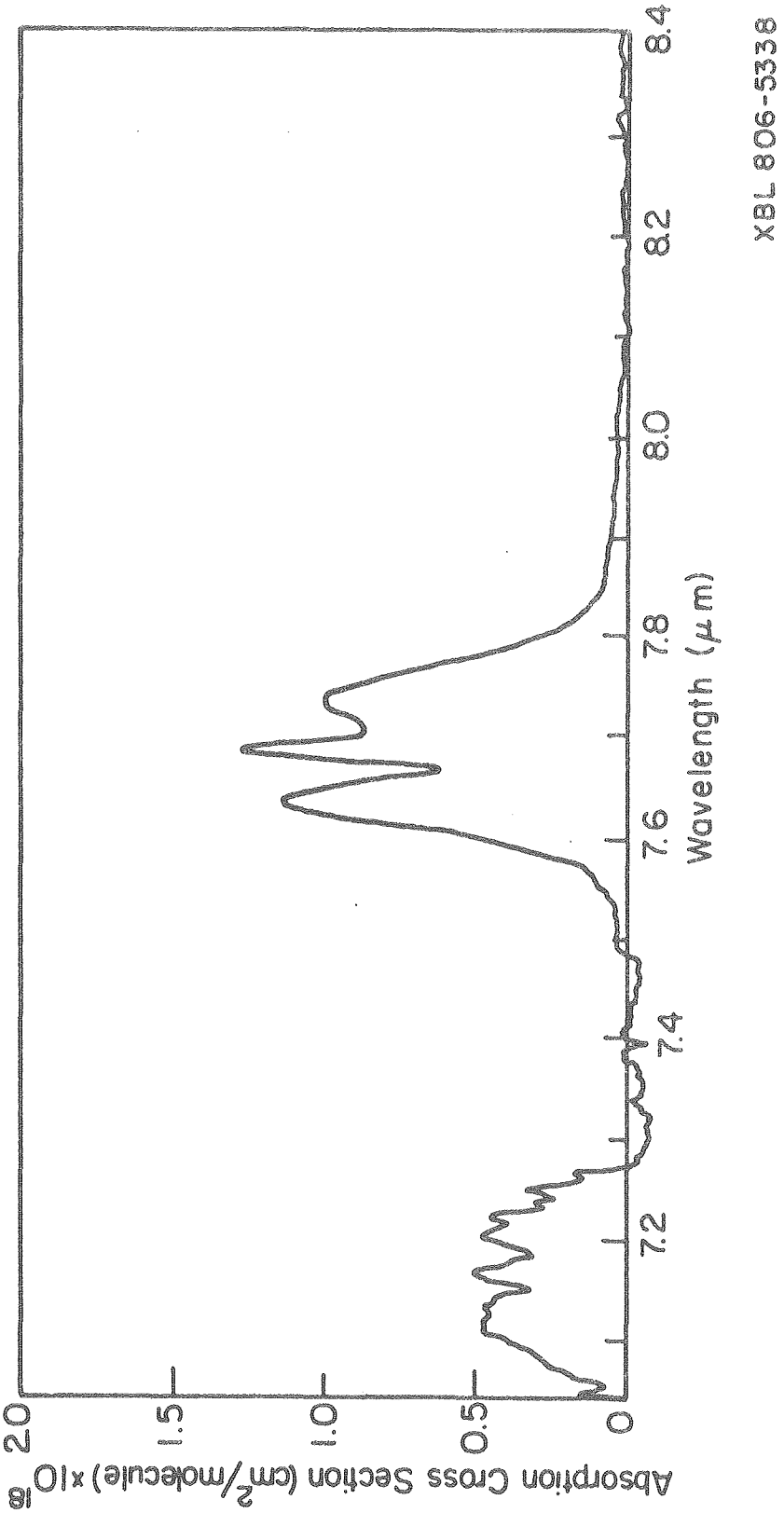

XBL 806-5338

Fig. 20. HNO_4 absorption spectrum at 1.0 atmosphere pressure

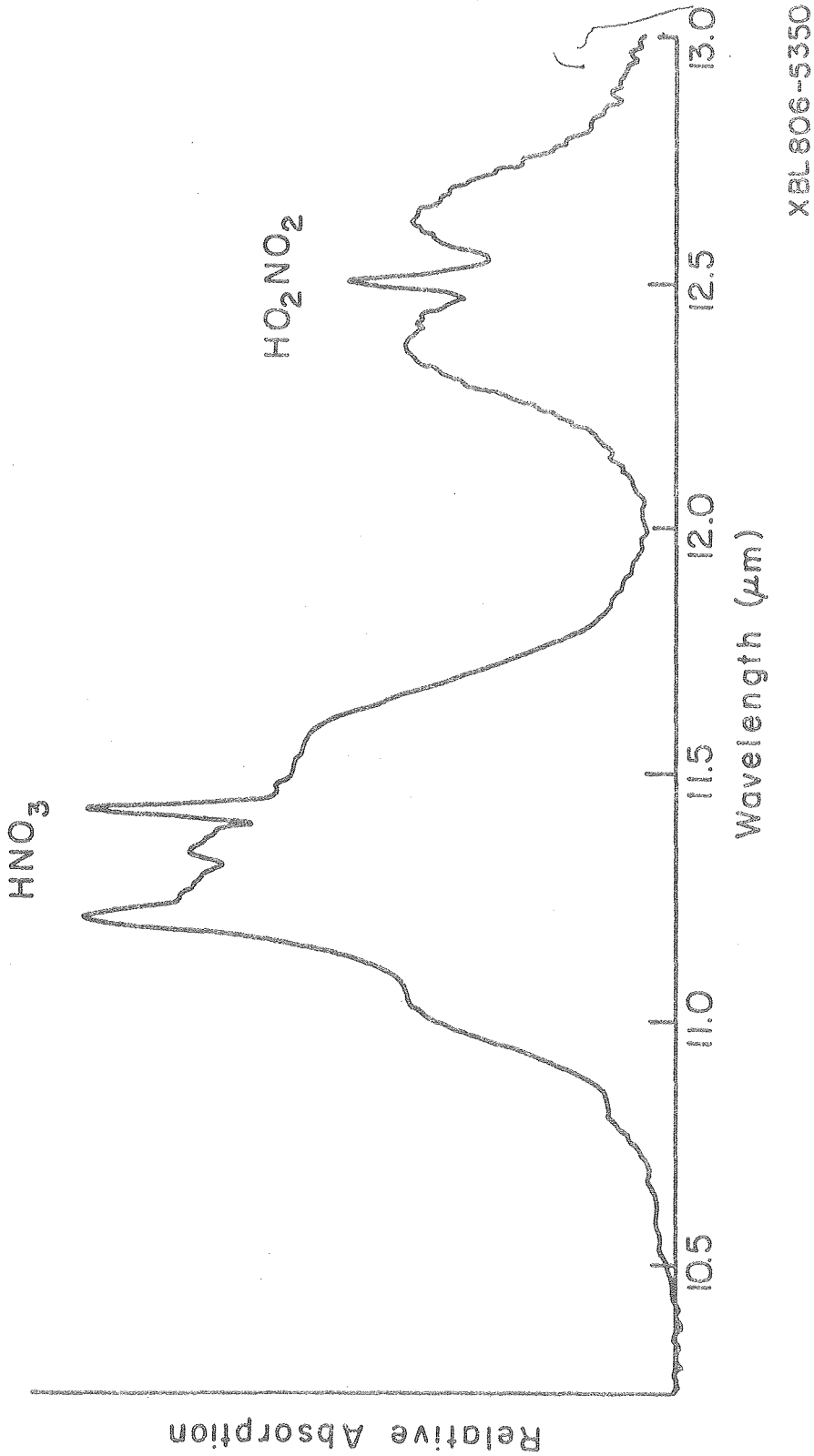

Fig. 21. Absorption spectrum of HNO_3 and HNO_4

includes the R branch used in monitoring concentrations. The 11.0 to 11.5 μm HNO_3 absorption is also illustrated on this figure. The HNO_3 concentration is roughly twice that of HNO_4.

The cross sections for HONO used for this work were obtained from published sources.[80,81,82] HONO has two isomeric structures, that of cis-HONO and trans-HONO. The trans form is about 0.5 kcal/mole more stable than the cis form, and the barrier to internal rotation is about 12 kcal/mole. The cis form has a strong absorption in the 11 to 12 μm region and the trans form absorbs at slightly longer wavelengths in the 12 to 13 μm region. The Q branches are at 11.72 μm and at 12.61 μm. While somewhat uncertain, the absorption cross sections appear to be approximately $1.0 \times 10^{-18} cm^2$/molecule for both Q branches at 298K. The pressure, temperature and resolution dependence of the cross sections at these wavelengths is not known.

It was noticed in the determination of infrared cross sections that Q branches of absorptions tend to exhibit markedly different characteristics than the P and R branches. The P and R branches of an absorption generally exhibited similar response to temperature, pressure and resolution variations. In many cases, the Q branch response would be markedly different from that of the P and R branch response. For this reason, P and R branch absorptions were often chosen for monitoring concentrations over Q branch absorptions.

B. Visible Cross Sections

NO_2, NO_3 and O_3 have absorption bands in the visible region of the spectrum. In photolysis experiments, visible light from the black lamps, particularly the 546 nm mercury line, can photolyze or excite these species. Visible photolysis of NO_3 is particularly important, since no ultraviolet absorptions are known. The visible absorptions are also potentially useful for monitoring concentrations of these species in chemical systems.

Of these three components, NO_3 and O_3 are photolyzed throughout most of the visible region. The absorption cross sections for these molecules determined by Graham[78] are shown in Fig. 22. The thermodynamic cutoff for photolytic production of NO_2 and $O(^3P)$ is 580 nm. The primary quantum yield for production of NO_2 and $O(^3P)$ at wavelengths shorter than 580 nm is about 0.85 and the quantum yield for the production of NO and O_2 is about 0.15[78,113]. NO_2 has a thermodynamic cutoff for photolytic production of NO and $O(^3P)$ at 398 nm. However, a small pressure-dependent quantum yield for production of $O(^3P)$ atoms extends to 440 nm[83].

Since the absorption bands of the three compounds overlap, it would be difficult to monitor a particular species when the others are present. The NO_3 absorption b and appears to end around 710 nm. The absorption bands of NO_2 and O_3 which extend into the near infrared were investi-ated as possible concentration monitoring regions.

Ozone was prepared by flowing a purified oxygen stream through the ozonator. The flow containing oxygen and ozone was passed through the

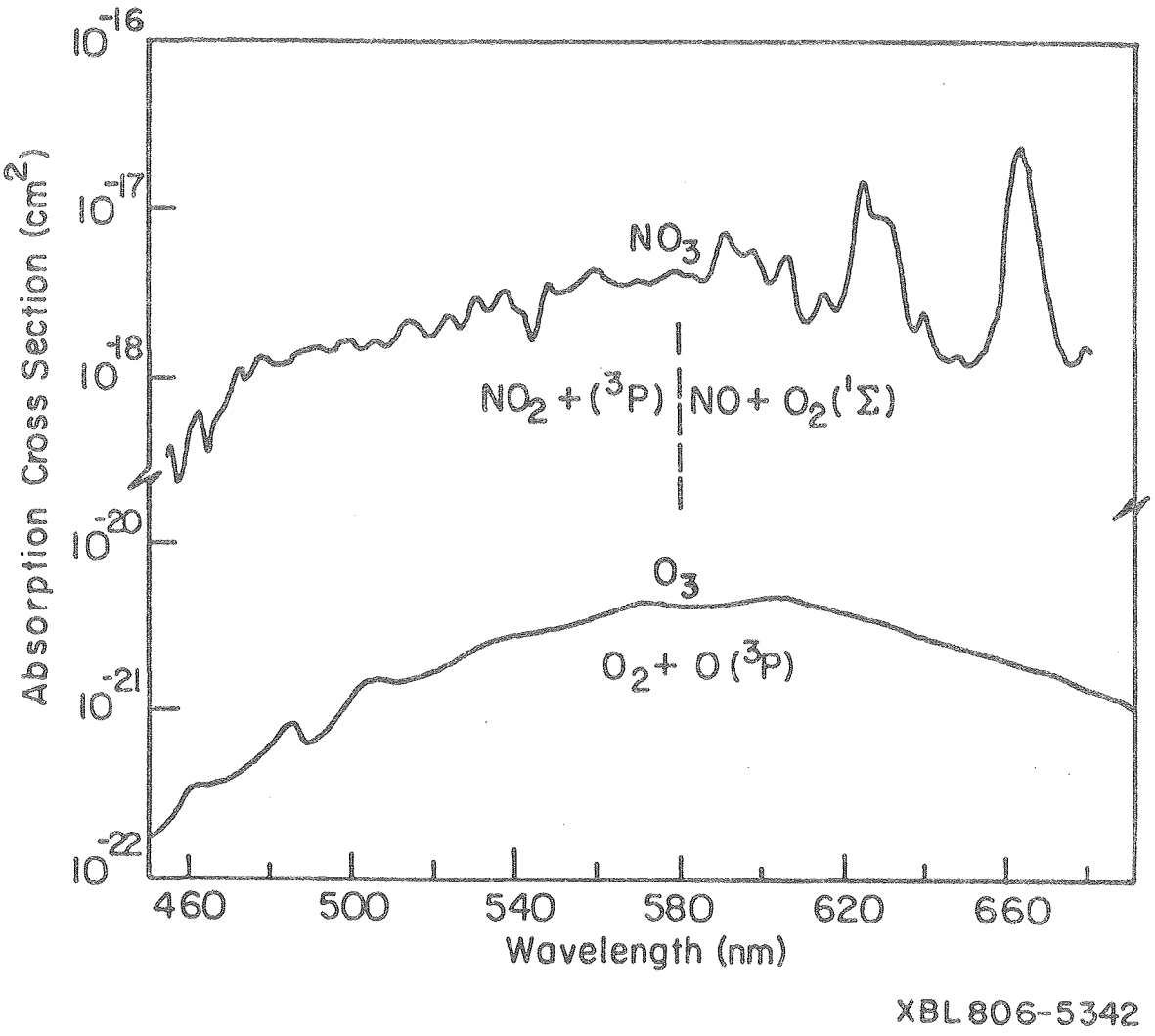

Fig. 22. Visible absorption bands of NO_3 and O_3

cell at one atmosphere total pressure. When the ozone concentration inside the cell had stabilized, scans were made from 500 to 900 nm, using a IP28 PMT and a silicon photodiode. Ozone cross section determinations by Graham[78] 574.7 and 602.5 nm were used to calibrate the absorption curve. The spectrum obtained is shown in Fig. 23. The absorption appears to terminate at about 840 nm.

NO_2 spectra were obtained by filling the cell with purified NO_2 to the desired pressure and scanning the region of interest with a RCA 4832 PMT and silicon photodiode. The spectra were found to be independent of pressure from 10 torr to 1 atmosphere at the resolution at which the spectra were taken. The spectra obtained are illustrated in Fig. 24. The left-hand spectrum was obtained with the PMT and the right-hand spec- spectrum was obtained with the silicon photodiode. The spectra are in good qualitative agreement with those of Gillispie and Khan,[84] who provide a theoretical interpretation of the structure.

C. Ultraviolet Cross Sections

Ultraviolet absorption cross sections are needed in the interpretation of the photolysis experiments. Since the cross sections for the molecules of interest are generally well-known, there was no attempt made to obtain new values. The spectra for NO_2[78], N_2O_5[85,86], O_3[76,77], HNO_3[78,87] and H_2O_2[74,75] are shown in Fig. 25. The spectrum of HNO_4 was shown previously in Fig. 1.

The cross sections were used to obtain j-values by numerically integrating the cross section - lamp emission product over wavelength at

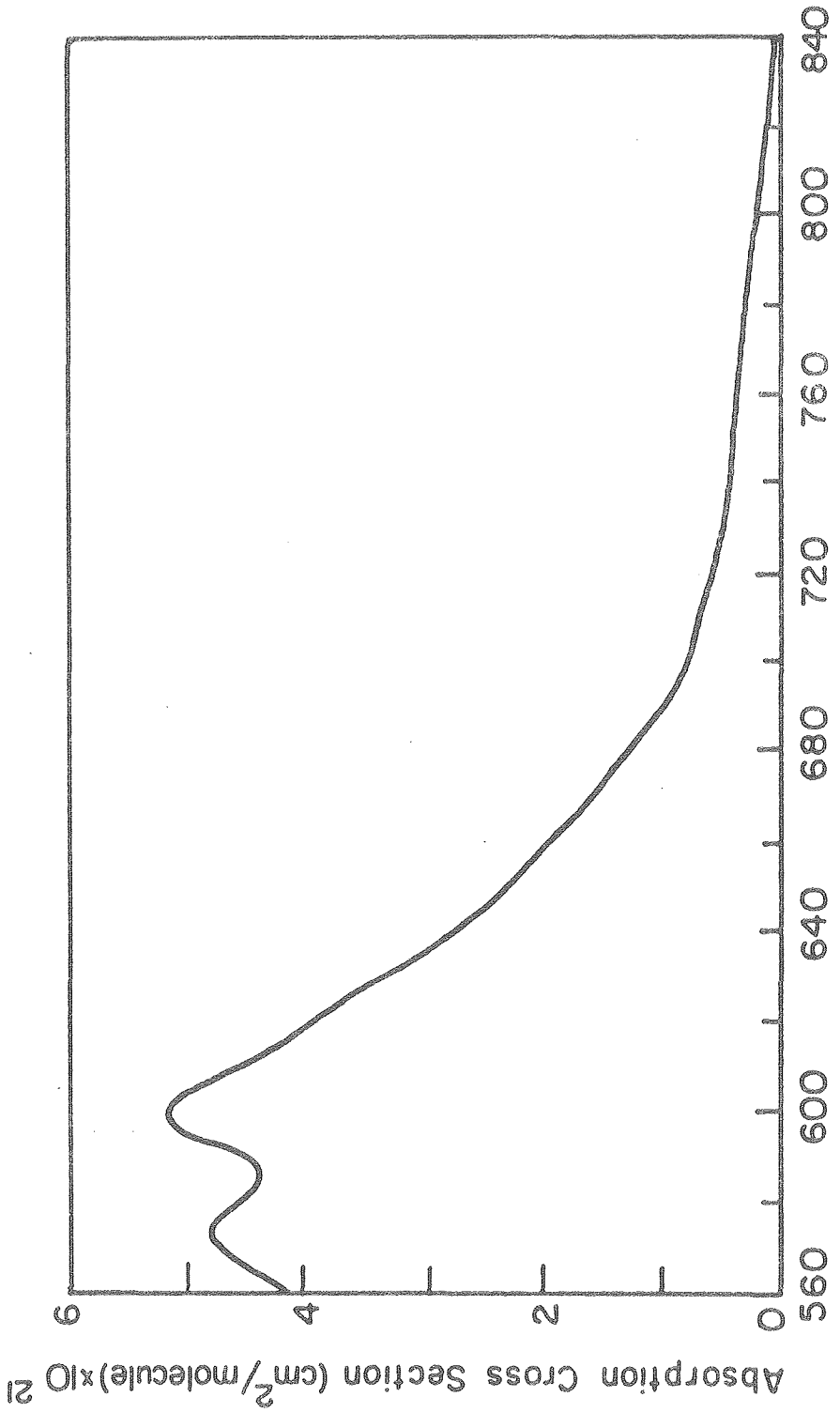

XBL806-5337

Fig. 23. Absorption spectrum of O_3 in the visible and near-infrared region

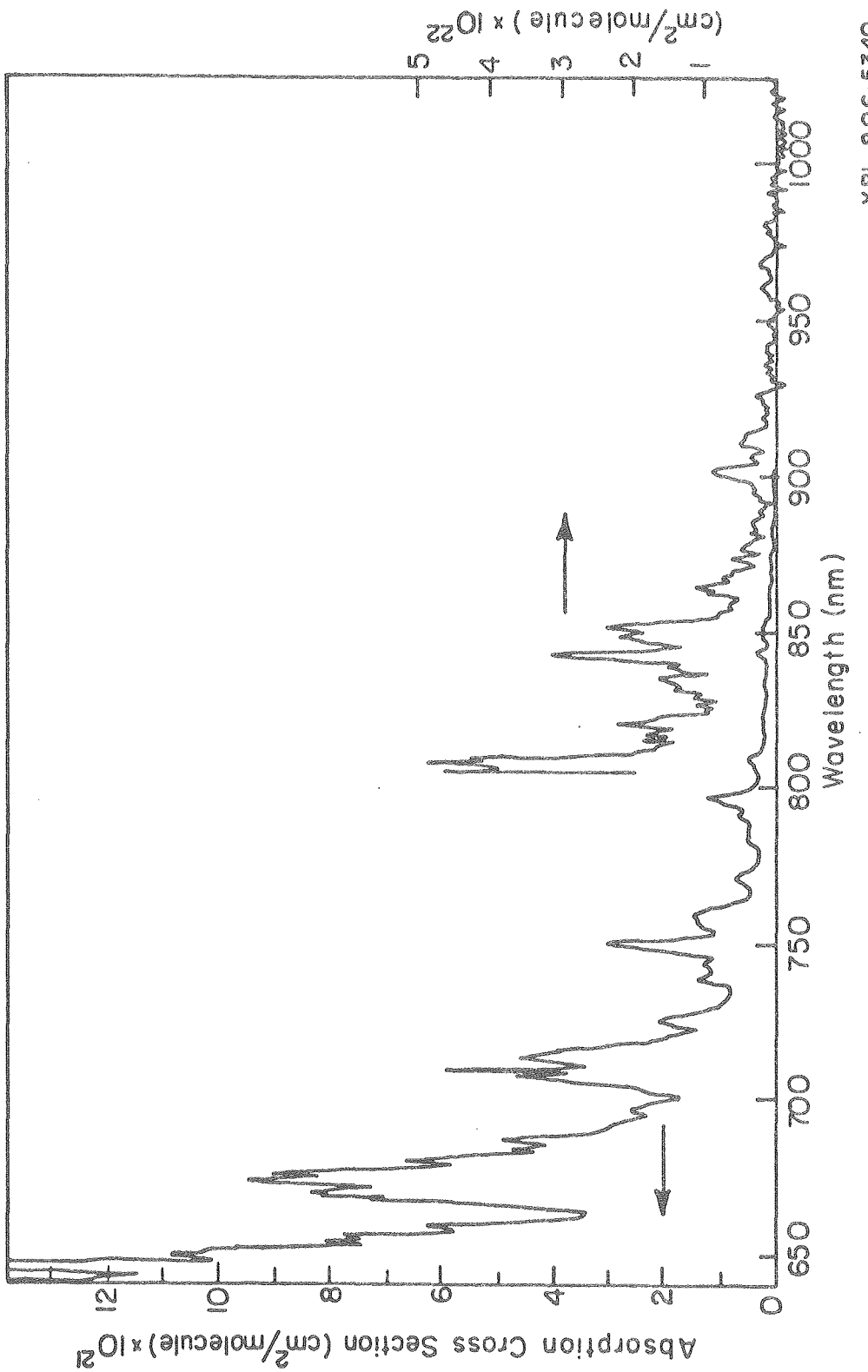

Fig. 24 Absorption spectrum of NO_2 in the near infrared region

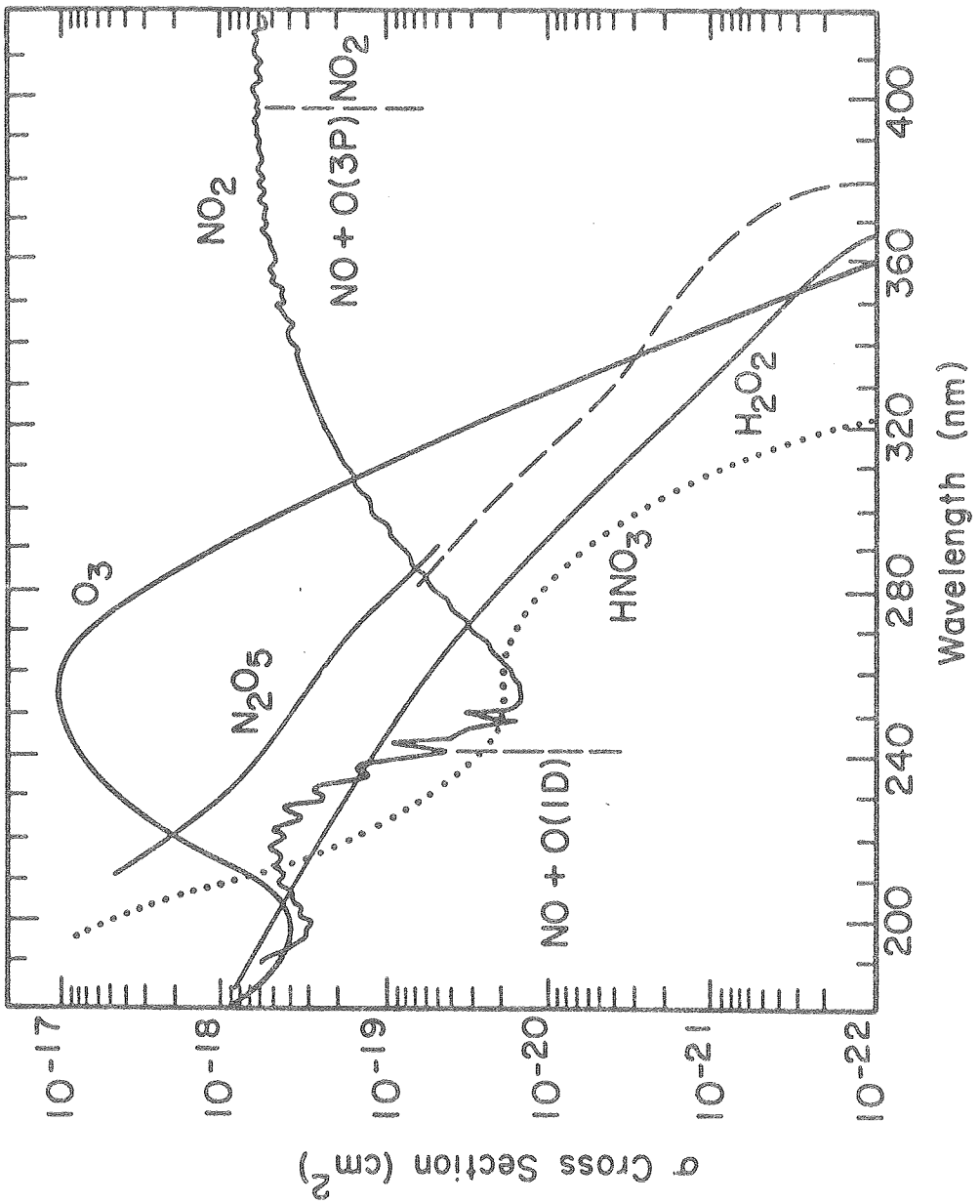

Fig. 25. UV absorption spectra of NO_2, O_3, N_2O_5, H_2O_2 and HNO_3

1 nm intervals. The spectrum of HONO was omitted for the sake of clarity. Cox and Derwent[88] report it to have diffuse bands between 310 and 380 nm and a strong broad absorption centered about 215 nm. With the exception of HNO_4, the photolysis products have been determined for these compounds. Since HNO_4 does not exist in large concentrations in the static photolysis system, the photolysis products were not of importance. In the flowing photolysis system, the overlap between the black lamp output and the HNO_4 absorption spectrum was small, so the photolysis rate was small and not important.

CHAPTER IV. THE REACTION OF N_2O_5 + H_2O_2

A. Experimental Procedures and Data

1. Reactant Decomposition and Flow-in

The experiments were performed by expanding the reactants and the carrier gas from two bulbs into the evacuated cell. Prior to expansion a bulb was filled to the desired pressure with a reactant, and purified carrier gas was then added. There are separate lines connecting the bulbs to the disperser tubes in the cell; so, the reactants did not mix until they flowed into the cell. This was done to prevent the occurrence of any reaction between the reactants before flowing into the cell. A previous worker, Peter Connell, has shown that the turbulent jetting of the reactants from disperser tubes in the cell provides adequate mixing of the reactants by comparison of this technique with a method where the reactants were mixed prior to expansion into the cell.

A 3.06 liter Pyrex bulb was used for holding N_2O_5, HNO_3 and NO_2 when they were used as reactants. A 5.33 liter Pyrex bulb was used for holding H_2O_2 and H_2O when they were used as reactants. The carrier gas pressure in each bulb was adjusted so the pressure-volume product of the two bulbs were approximately the same. The stopcocks on the bulbs were opened simultaneously, allowing the reactants and the carrier gas to enter the cell at the same time. The temperature of the bulbs and the Pyrex lines connecting them to the cell was 295 ± 2K.

The reactants H_2O_2 and N_2O_5 were stored in evacuated, temperature controlled Pyrex containers prior to use. The H_2O_2 was stored in an ethylene glycol bath at 295K. Although significant heterogeneous decomposition occurred by the process

$$H_2O_2 \xrightarrow{\text{surface}} H_2O + \frac{1}{2} O_2 \qquad (44)$$

at this temperature, lower temperatures did not provide sufficient H_2O_2 vapor pressure for these experiments. Prior to filling the 5.33 liter bulb with H_2O_2, the saturator was pumped on to remove the decomposition products, both of which have much higher vapor pressures than H_2O_2 at 295K.[89,90]

The N_2O_5 saturator was kept at 273K in an ice-water bath. Decomposition by the processes

$$\begin{aligned} N_2O_5 &\rightarrow NO_2 + NO_3 \\ NO_2 + NO_3 &\rightarrow NO + NO_2 + O_2 \\ NO + NO_3 &\rightarrow NO_2 + NO_2 \end{aligned} \qquad (45)$$

occurred more rapidly at higher temperatures. HNO_3 was present with N_2O_5 due to its formation in the process of preparing N_2O_5. The ratio of vapor pressure of HNO_3 to the vapor pressure of N_2O_5 is lower at higher temperatures. The temperature used was a compromise between minimizing N_2O_5 decomposition and minimizing the fraction of HNO_3 present. The N_2O_5 saturator was pumped on periodically to

remove the NO_2 and O_2 decomposition products. In between series of experiments, the N_2O_5 container was stored in a dry ice-isopropanol slush bath.

The vapor pressure[91] of H_2O_2, H_2O, N_2O_5, NO_2 and HNO_3 are tabulated in Table 4 at various temperatures of interest.

To minimize the heterogeneous decomposition of the reactants, the walls of the bulbs used in the expansions were conditioned by exposing them to the reactants for an extended period before experiments were done. After sufficient exposure to N_2O_5, heterogeneous production of HNO_3 in the 3.06 liter bulb was insignificant. The decomposition by the series of reactions in (45) was determined by observing the pressure increase in the 3.06 liter bulb and the manifold to which it was attached using the Baratron pressure gauge. The net reaction for decomposition is

$$N_2O_5 \rightarrow 2NO_2 + \frac{1}{2} O_2 \quad . \tag{46}$$

Thus the change in pressure will be proportional to 1.5 times the amount of N_2O_5 decomposed. The rate of decomposition was found to be approximately 15 percent/hour, less than the decomposition rate of H_2O_2. Therefore, the 3.06 liter bulb was filled before the 5.33 liter bulb. Since the N_2O_5 was in the bulb for less than ten minutes, the amount of decomposition was considered unimportant.

Although H_2O_2 decomposition in the 5.33 liter bulb remained significant after conditioning, it appeared to be fairly reproducible.

Table 4

Vapor Pressures of Compounds Used in Expansion Experiments[91]

Temperature (K)	Vapor Pressures (torr)				
	H_2O_2	H_2O	N_2O_5	HNO_3	NO_2
293K	1.52	17.5	284	46.8	560
283K	0.76	9.2	124	27.0	317
273K	0.76	4.6	50.7	14.9	172
263K	0.16	1.95	19.4	7.9	88.8
253K	0.07	0.78	6.9	4.0	43.6
196K	—	—	—	0.02	0.05

(from CRC Handbook of Chemistry and Physics, 1970-71)

The pressure increase due to H_2O_2 decomposition was monitored in the same manner that the N_2O_5 decomposition was monitored. The decomposition reaction indicates that the change in pressure will be proportional to 0.5 times the amount of H_2O_2 decomposed. The experimentally determined decay profile is shown in Fig. 26. The error bars indicate the maximum variation observed in the decays. Since the rate of decomposition was fairly reproducible on short time scales, the expansion of the reactants into the cell was always done four minutes after filling the bulb with H_2O_2.

The concentrations of the reactants in the bulbs at the time of expansion must be known to analyze the kinetic results. From the ratio of the vapor pressures of N_2O_5 and HNO_3, it is expected that HNO_3 should be about 23 percent of the total amount of gas in the bulb. This is in good agreement with infrared absorption measurements made immediately following expansion of N_2O_5 into the cell. This technique gave values of 20-25 percent HNO_3.

The relative amounts of H_2O_2 and H_2O in the 5.33 liter bulb at the time of expansion were determined from the rate of H_2O_2 decomposition obtained by pressure measurements. This could not be confirmed by infrared measurements because of the continued heterogeneous decomposition of H_2O_2 in the cell. The initial fraction of H_2O_2 in the bulb was determined by assuming that the pressure increase observed one hour after the addition of H_2O_2 to the bulb represented complete decomposition of H_2O_2. From this value and the observed rate of decomposition (Fig. 26), it was determined that 40 ± 5 per cent of the gas admitted to the bulb was H_2O_2 at the time of expansion.

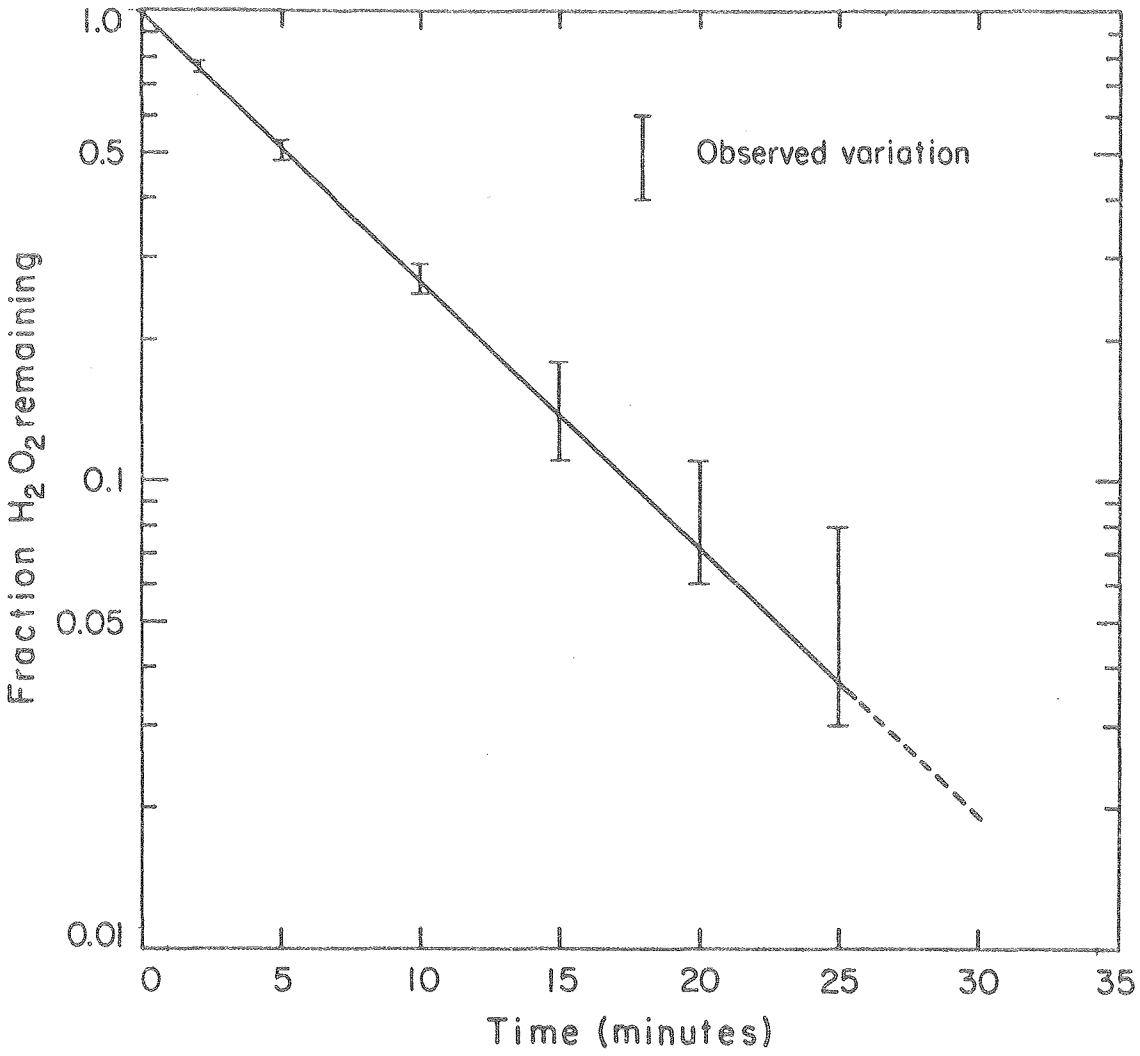

Fig. 26 Rate of H_2O_2 decomposition in bulb used in expansion experiments

When H_2O and NO_2 were used as reactants, they were prepared in the same manner as that for the cross section measurements. NO_2 was corrected for N_2O_4, both in the bulb and in the cell. When HNO_3 was used as a reactant, it was prepared by the heterogeneous reaction of N_2O_5 with excess H_2O. No N_2O_5 was observed in spectra obtained of the expanded mixture. The concentration of HNO_3 obtained is somewhat uncertain due to the tendency of HNO_3 to adhere to wall surfaces.

2. Expansion methodology

The rate at which the reactants and carrier gas flow into the cell must be known accurately to interpret the kinetics that occur when the reactants initially mix. The fraction of the gas that has flowed into the cell at a time t after expansion is equal to $(1 - \exp(-t/t_o))$, where t_o is the time constant for the flow system, determined by the conductance of the tubing connecting the bulbs of the cell. The time constant was determined by connecting the Baratron pressure gauge to a port on the cell and feeding the gauge output into the Fabritek signal averager. The bulbs were filled with carrier gas and expanded into the cell. A typical output trace is shown in Fig. 27a (upper curve).

The accuracy of this technique was checked by monitoring the buildup of N_2O_5 in the cell by infrared absorption. The bulbs were filled with N_2O_5 and O_2 carrier gas and expanded into the evacuated cell. A typical profile is shown in Fig. 27b (lower curve). The time constant obtained in this manner was in good agreement with that obtained by the first method. The average value obtained was $t_o = 4.3 \pm 0.3$ seconds.

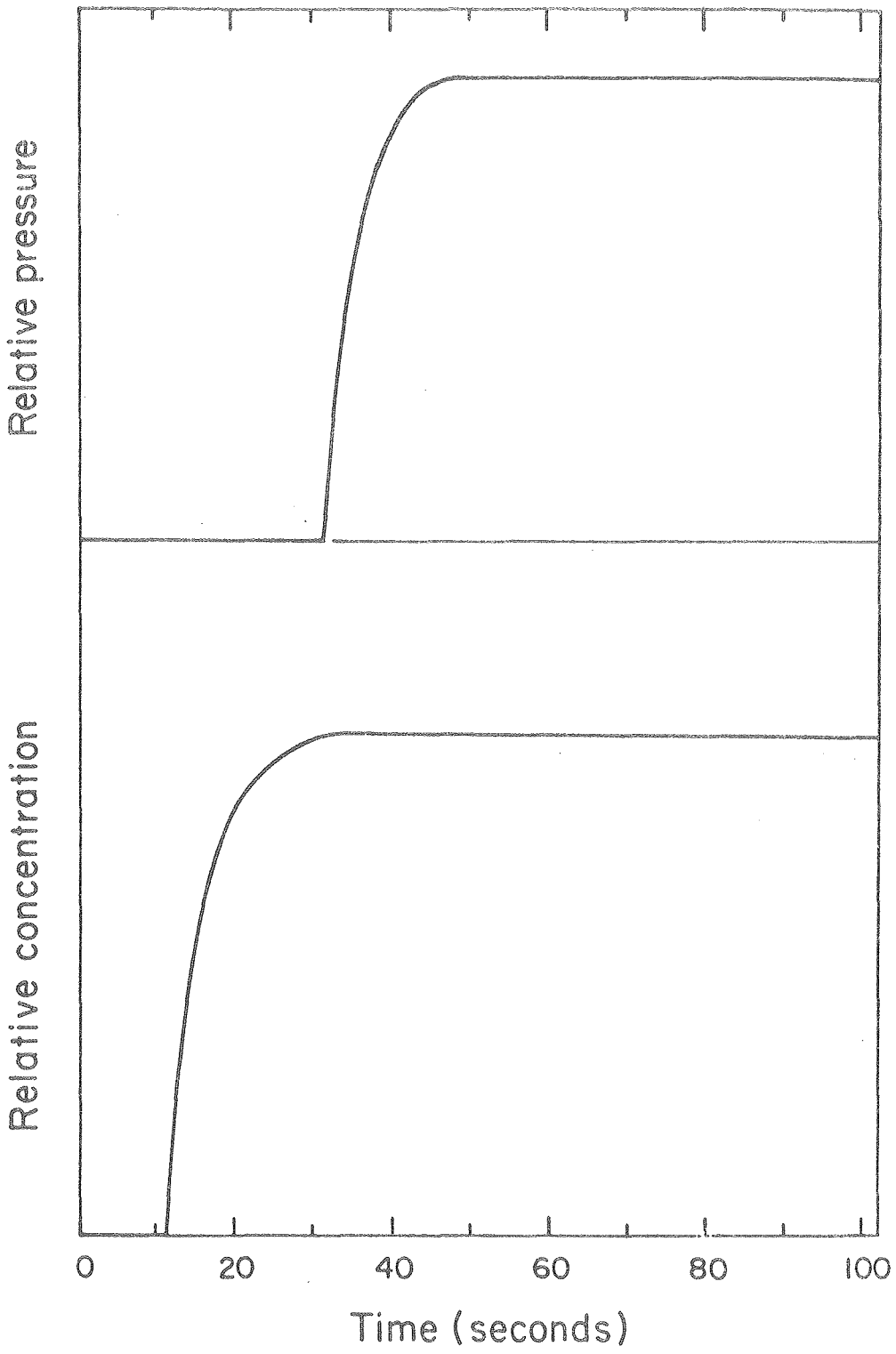

XBL 807-1413

Fig. 27. Rate of expansion of gases into cell
Upper - pressure measurement
Lower - absorption measurement

Kinetic information for a reaction system can be obtained by observing the decay of reactants and build-up of products following expansion of the reactants into the cell. The design of the apparatus allows only one wavelength to be monitored at a time. In order to observe all the species of interest in a reaction system, a number of expansions had to be performed under similar conditions. It was found that the concentrations of the reactants and the pressure of the carrier gas in the bulbs were reproducible to ± 5 percent.

In addition to monitoring one wavelength during an expansion, scans were made following an expansion to detect any new absorptions. Expansions and scans were done at a number of pressures and temperatures to observe the effects of these variables on the reaction system. The concentrations of the reactants were varied to determine their effect on the reaction kinetics.

3. Investigation of Complicating Factors in the H_2O_2-N_2O_5 System

Some of the complicating factors in these investigations were the heterogeneous decompositions of N_2O_5 into HNO_3 and H_2O_2 into H_2O and O_2. Being heterogeneous, there were some variations in these rates from run to run. Also, the tendency of HNO_3 to adhere to surfaces, particularly at low temperatures, makes it difficult to obtain quantitative information on its production or destruction.

The species monitored in the expansion experiments and the wavelengths used to monitor them are listed below.

NO_2	3.428 μm	
NO	5.249 μm	
H_2O	6.634 μm	
HNO_4	7.158 μm	(47)
HNO_3	7.400 μm	
N_2O_5	7.960 μm	
HNO_4	12.315 μm	

The wavelength at which NO_2 is monitored is free of interfering absorptions, as are the wavelengths for NO and H_2O. The 7.158 μm absorption of HNO_4 does not overlap with absorption bands of other species in the system, but is located at a reflection minimum of the mirrors in the cell. This wavelength was used to monitor HNO_4 in initial experiments when CaF_2 windows on the cell prevented use of wavelengths longer than 10 μm. 7.400 μm was used to observe HNO_3 to avoid overlap problems with HNO_4. The cross section at this wavelength is low enough that excessively high optical densities are not incurred at high HNO_3 concentrations. The optical density at this wavelength was corrected for the weak absorption due to N_2O_5. N_2O_5 was observed at 7.960 μm to avoid overlap problems with HNO_3 and to obtain a reasonable cross section. H_2O_2 does absorb weakly here, but the optical density obtained was not corrected since the contribution was generally less than 5 percent.

H_2O_2 could not be successfully monitored by infrared absorption in this system. The strongest absorptions were overlapped by one or more absorption bands of other species which had considerably larger cross sections than H_2O_2. The only band free of interfering absorptions was at 3.8 μm, which had a cross section of less than 10^{-21} cm^2 $molecule^{-1}$ under the conditions of the experiments. This is too small to be of use in these experiments.

A slight shift in baseline would occasionally occur with the pressure increase caused by the expansion of gases into the cell. A wavelength free of any absorptions near the monitoring wavelength was used as a reference to correct for this shift, if it occurred.

Both of the reactants heterogeneously decompose after expansion into the cell. The approximate rates of the reactions were needed to analyze the experimental observations. The decomposition rate of H_2O_2 in the cell was determined at all temperatures of 263K, 273K and 283K by expanding H_2O_2 and O_2 carrier gas into the cell. The H_2O_2 decay was observed at 8.040 μm. The first order decay rate ranged between 2 x 10^{-3} and 2 x $10^{-4}$$sec^{-1}$, depending on cell conditioning. The rates appeared to increase with a decrease in temperature, presumably due to the greater tendency of H_2O_2 to adhere to cell surfaces at low temperatures.

The decomposition of N_2O_5 is regarded as being primarily heterogeneous. Morris and Niki[59] reported a first order decay rate of 6-8 x 10^{-4} sec^{-1} with a 67 liter Pyrex cell. Connell[67] reported a variation in first order rate of 1 x 10^{-3} to 7 x 10^{-5} sec^{-1} with the cell used in these experiments. The values obtained under the condi-

tions used for these experiments ranged from about 5×10^{-4} sec^{-1} to less than 1×10^{-4} sec^{-1} after the cell was well conditioned. The presence of H_2O_2 deconditioned the cell walls, and the larger value is the best estimate for the decomposition rate that occurred during experiments.

The reaction of N_2O_5 with H_2O must be taken into consideration, since H_2O is present in significant quantities with H_2O_2. Morris and Niki[59] investigated this reaction and reported that it occurs both heterogeneously and in the gas phase. They gave an upper limit of 1.3×10^{-20} cm^3/ molecule-second for the homogeneous rate constant.

This reaction was investigated by expanding H_2O and N_2O_5 into the cell and observing the decay of N_2O_5. Fig. 28 illustrates a semilog plot of four N_2O_5 profiles in the presence of excess H_2O. The decays of N_2O_5 should obey pseudo-first order kinetics under these conditions. The initial concentrations of the reactants and the approximate first order decay rate for N_2O_5 are listed below.

Run	$[N_2O_5]$	$[H_2O]$	$k(sec^{-1})$
A	5.6×10^{14}	1.7×10^{16}	7.6×10^{-3}
B	7.3×10^{14}	9.7×10^{15}	5.0×10^{-3}
C	7.3×10^{14}	9.5×10^{15}	5.0×10^{-3}
D	8.8×10^{14}	5.5×10^{15}	6.0×10^{-3}

D'Ans and Friederick[6] and Schwarz[7] used the reaction of H_2O_2 with HNO_3 in solution to generate HNO_4. This reaction system was investigated by expanding HNO_3 and H_2O_2 into the evacuated cell. H_2O_2 was monitored at 8.040 μm, where there is a minimum in the HNO_3 absorption

Fig. 28. Decay profiles of N_2O_5 in the presence of H_2O

Curve A: $[N_2O_5] = 5.6 \times 10^{14}$ molecules/cm^3

$[H_2O] = 1.7 \times 10^{15}$ " "

Curve B: $[N_2O_5] = 7.3 \times 10^{14}$ " "

$[H_2O] = 9.7 \times 10^{15}$ " "

Curve C: $[N_2O_5] = 7.3 \times 10^{14}$ " "

$[H_2O] = 9.5 \times 10^{15}$ " "

Curve D: $[N_2O_5] = 8.8 \times 10^{14}$ " "

$[H_2O] = 5.5 \times 10^{15}$ " "

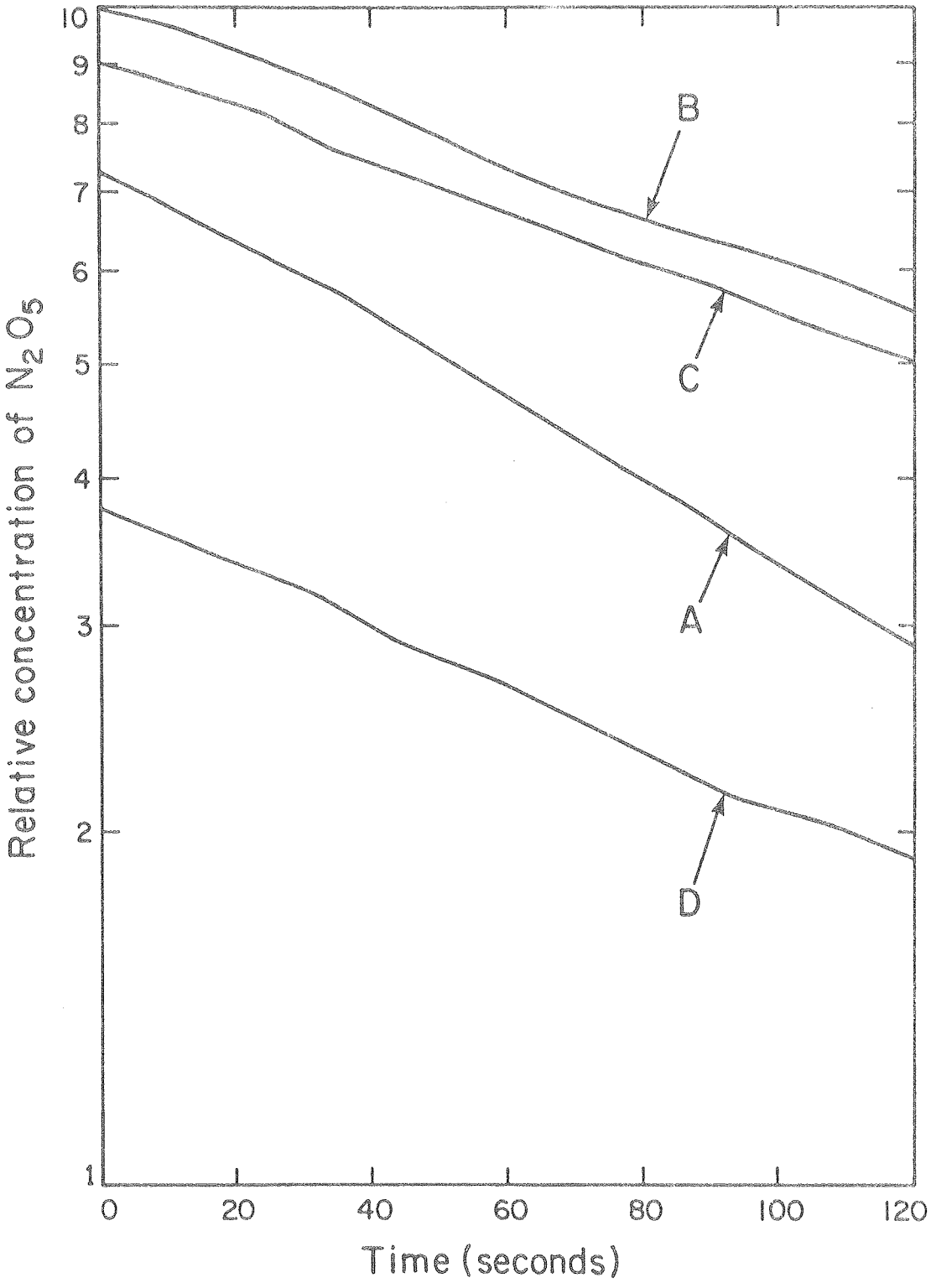
Relative concentration of N_2O_5
10
9
8
7
6
5
4
3
2
1
0
20
40
60
80
100
120
Time (seconds)
A
B
C
D
XBL807-1411

Fig. 28

bands. The H_2O_2 decay rates were within the range of those obtained with H_2O_2 alone. The HNO_3 first order decay rates were 1 to 5 x 10^{-4} second^{-1}, and were less than or equal to the observed H_2O_2 decay rate. When a series of expansions were done in succession, the decay rate for HNO_3 decreased with each run. There were no detectable absorptions by HNO_4 or HONO, which are possible products of the reaction of HNO_3 with H_2O_2.

The reaction of NO_2 with H_2O and H_2O_2 should be considered since NO_2 will be formed by the decomposition of N_2O_5. Kaiser and Wu[92] and McKinnon et al.[60] have investigated the reaction of NO_2 with H_2O,

$$2NO_2 + H_2O \rightarrow HNO_3 + HONO \qquad (48)$$

The gas phase rate constants given by refs. 60 and 92 are $k_f \approx 1 \times 10^{-37}$ cm^6/molecule^2-second and $k_r \approx 1.5 \times 10^{-17}$cm^3/molecule-second. The reaction apparently proceeds more rapidly heterogeneously. The reaction of H_2O_2 with NO_2 can proceed in a similar fashion

$$2NO_2 + H_2O_2 \rightarrow 2HNO_3 \quad . \qquad (49)$$

Gray et al.[62] investigated the reaction of NO_2 with H_2O_2 and concluded it was primarily heterogeneous. The reaction was investigated by expanding H_2O_2 and NO_2 into the cell. The H_2O_2 decay rates were within the limits obtained with H_2O_2 alone. There was no decay of NO_2 observed within the limits of experimental uncertainty. Scans

taken 200 seconds after expansion indicated the presence of approximately 1×10^{14} molecules/cm^3 of HNO_3 and $< 5 \times 10^{13}$ molecules/cm^3 of HONO.

When HNO_4 is formed in a chemical system, a major loss mechanism is that of heterogeneous decomposition. To obtain approximate values for this mode of decay, HNO_4 was synthesized by the techniques developed by Barker et al.[23] so that its decay could be observed without large concentrations of other species present. The gases evolved from the mixture were flowed into the cell to determine the concentration of HNO_4 obtainable. However, no HNO_4 was detected. It appears that all the HNO_4 in the flow decomposed on the tubing walls before entering the cell. The HNO_4 heterogeneous decomposition rates used in this study were obtained from its decay in the presence of significant concentrations of other species, which introduced some uncertainty to the value.

4. Products and Reactant Concentration Dependence of H_2O_2+N_2O_5

N_2O_5 and H_2O_2 were expanded with O_2 carrier gas into the evacuated cell, as described previously. The decay of N_2O_5 was more rapid than the decay that occurred in the N_2O_5-H_2O system. Scans were made after expansion to determine which species were present.

Fig. 29 illustrates a typical scan obtained following the expansion of H_2O_2 and N_2O_5. The scan was taken 200 seconds after expansion with a cell temperature of 263K. The noise in the spectrum between 7.2 and 7.3 μm is due the reflection minimum in the cell mirrors. The 7.0-7.3 μm absorption band is due to HNO_4. HNO_3 and HNO_4 absorptions

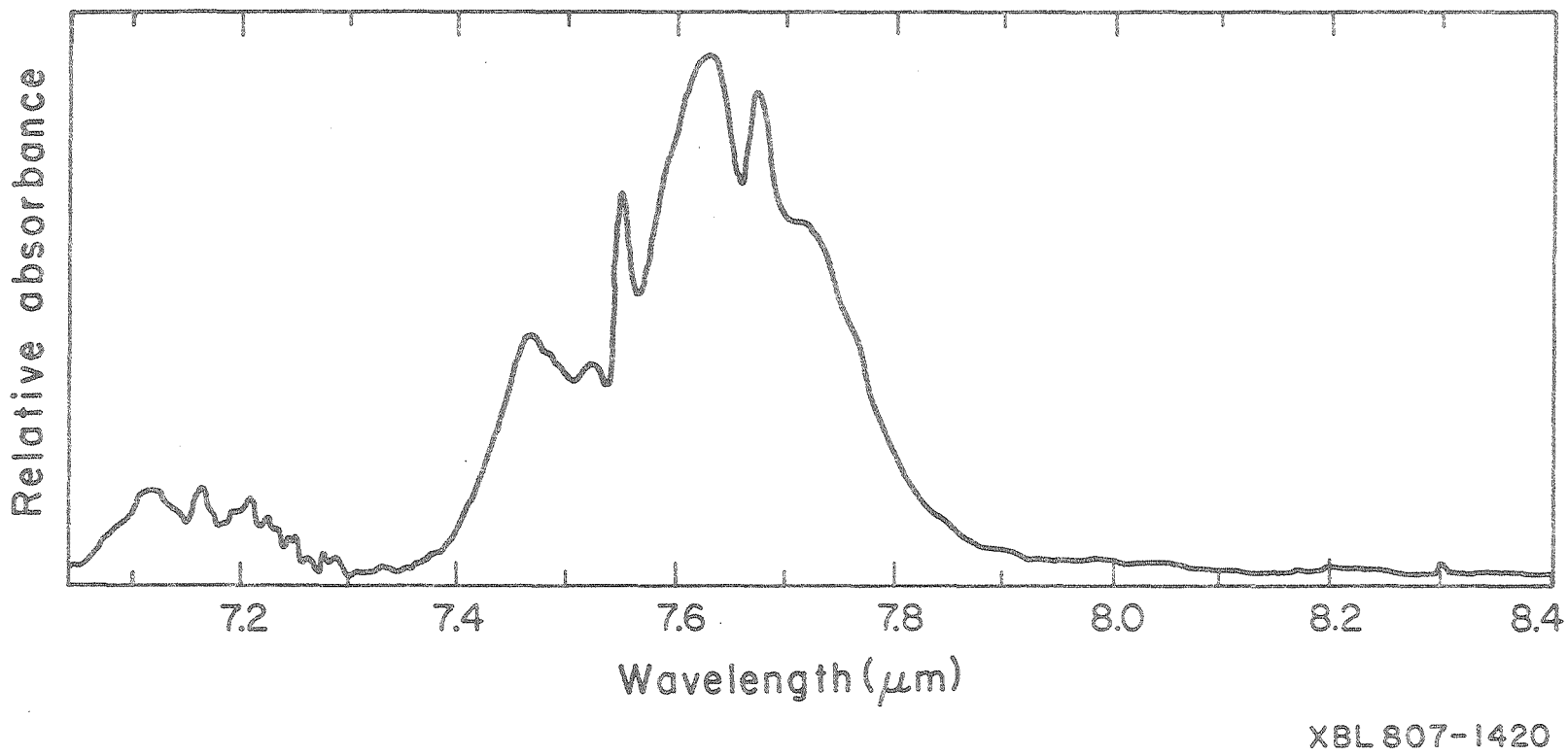

Fig. 29. Absorption spectrum of products of the reaction of H_2O_2 with N_2O_5

overlap in the 7.4 to 7.8 μm region. Subtracting absorptions due to HNO_3, N_2O_5 and H_2O_2 from this figure yielded the spectrum shown in Fig. 19. No absorption due to HONO was observed.

Initial work was done with CaF_2 windows on the cell, which limited infrared transmission to wavelengths shorter than 10 μm. These were replaced with BaF_2 windows to allow observation of the HNO_4 band between 12 and 13 μm (Fig. 20). This absorption is free of interference by other species and has a larger cross section than the 7.1 to 7.3 μm band. No HONO was observed in this region.

The presence of HNO_4 indicated the products of the reaction of H_2O_2 with N_2O_5 with one of the following sets.

$$\begin{aligned} H_2O_2 + N_2O_5 &\rightarrow HNO_4 + HNO_3 \\ &\rightarrow HO_2 + NO_2 + HNO_3 \end{aligned} \qquad (50)$$

HO_2 and NO_2 can quickly combine to form HNO_4. To discriminate between the product sets, a small amount of NO was added to the cell prior to expansion.

NO scavenges HO_2 by reaction (4), the rate of which is more than an order of magnitude faster than the rate for reaction (1) given by Graham et al.[18] If the primary products of H_2O_2 and N_2O_5 are HNO_3, HO_2 and NO_2, the HNO_4 concentration will exist at observable levels when NO is present. If HNO_4 is formed directly, the HO_2 formed by HNO_4 decomposition will react with NO. This will reduce the HNO_4 concentration somewhat, but the concentration will still be observable.

Approximately 0.3 torr of NO was added to the cell prior to the expansion of H_2O_2 and N_2O_5. Such a low pressure does not significantly interfere with the expansion of gases. The process was repeated three times so that the profiles of HNO_4, HNO_3 and N_2O_5 could be observed. The profiles are tabulated in Table 5. The profiles without NO are listed in Table 6.

The dependence of HNO_4 concentration on each of the reactants was determined by independently varying the concentrations of N_2O_5 and H_2O_2. These expansions were done at a cell temperature of 263K, and at final pressures of 33 and 66 torr. The HNO_4 profiles are shown in Figs. 30-33. For the runs in Fig. 30, the initial H_2O_2 concentration was held constant at 1.8×10^{15} molecules/cm^3 while the N_2O_5 concentration was varied from 3.6×10^{15} molecules/cm^3 (curve A) to 2.1×10^{14} molecules/cm^3 (curve G). Similarly, in Fig. 31, the initial H_2O_2 concentration was 1.8×10^{15} molecules/cm^3 and the initial N_2O_5 concentration was varied from 8.9×10^{15} molecules/cm^3 (curve A) to 8.7×10^{14} molecules/cm^3 (curve E).

The runs shown in Fig. 32 were done with an initial N_2O_5 concentration of 1.3×10^{15} molecules/cm^3 and the H_2O_2 concentration was varied from 1.8×10^{15} molecules/cm^3 (curve A) to 2.1×10^{14} molecules/cm^3 (curve F). The N_2O_5 concentration was 4.1×10^{15} molecules/cm^3 for the runs shown in Fig. 33, and the H_2O_2 concentration was again varied from 1.8×10^{15} molecules/cm^3 (curve A) to 2.1×10^{14} molecules/cm^3 (curve E).

TABLE 5

Temp. = 273K	Pres. = 71 torr		
Time	Concentration (Molecules/cm^3)		
(Seconds)	$[HO_2NO_2]$	$[N_2O_5]$	$[HNO_3]$
0	---	---	---
10	2.9E14	3.9E15	4.3E14
20	4.7E14	4.1E15	7.1E14
30	5.8E14	3.8E15	1.3E15
40	6.1E14	3.6E15	1.3E15
50	6.6E14	3.5E15	1.4E15
60	6.8E14	3.4E15	1.4E15
70	7.0E14	3.2E15	1.6E15
80	7.3E14	3.1E15	1.8E15
90	7.3E14	3.0E15	1.9E15
100	7.3E14	2.9E15	2.0E15
110	7.4E14	2.8E15	1.9E15
120	7.3E14	2.7E15	2.1E15
130	7.3E14	2.7E15	2.1E15
140	7.2E14	2.6E15	2.3E15
150	7.1E14	2.6E15	2.4E15
160	6.9E14	2.5E15	2.3E15
170	6.8E14	2.4E15	2.5E15

TABLE 6

Temp. = 273K		Pres. = 71 torr	
Time		Concentration (Molecules/cm^3)	
(Seconds)	$[HO_2NO_2]$	$[N_2O_5]$	$[HNO_3]$
0	---	---	---
10	5.7E14	3.7E15	6.4E14
20	7.8E14	3.8E15	1.2E15
30	9.4E14	3.6E15	1.7E15
40	1.0E15	3.5E15	1.7E15
50	1.0E15	3.3E15	1.9E15
60	1.1E15	3.2E15	2.0E15
70	1.1E15	3.1E15	2.2E15
80	1.2E15	3.0E15	2.3E15
90	1.2E15	2.9E15	2.4E15
100	1.2E15	2.8E15	2.7E15
110	1.2E15	2.8E15	2.7E15
120	1.2E15	2.7E15	2.7E15
130	1.2E15	2.7E15	2.8E15
140	1.2E15	2.6E15	3.0E15
150	1.2E15	2.6E15	2.9E15
160	1.2E15	2.5E15	3.0E15
170	1.2E15	2.5E15	3.0E15

Fig. 30 HNO_4 profiles following expansion of N_2O_5 and H_2O_2
$[H_2O_2] = 1.8 \times 10^{15}$

Curve A: $[N_2O_5] = 3.6 \times 10^{15}$ molecules/cm^3
Curve B: $[N_2O_5] = 2.5 \times 10^{15}$ " "
Curve C: $[N_2O_5] = 1.5 \times 10^{15}$ " "
Curve D: $[N_2O_5] = 1.1 \times 10^{15}$ " "
Curve E: $[N_2O_5] = 8.0 \times 10^{14}$ " "
Curve F: $[N_2O_5] = 4.0 \times 10^{14}$ " "
Curve G: $[N_2O_5] = 2.1 \times 10^{14}$ " "

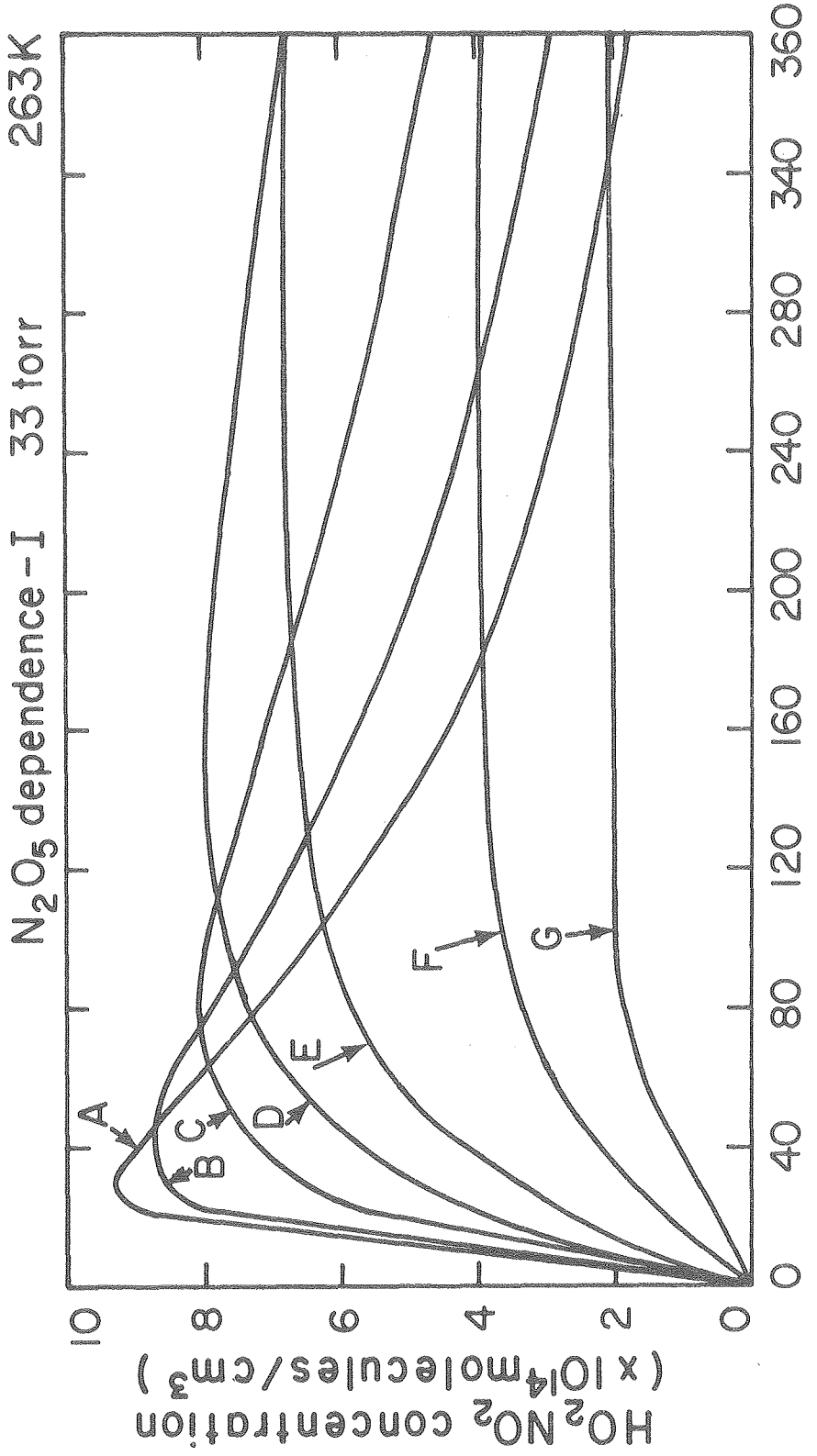

XBL807-1416

Fig. 30

Fig. 31 HNO_4 profiles following expansion of N_2O_5 and H_2O_2

$[H_2O_2] = 1.8 \times 10^{15}$ molecules/cm^3 for all curves

Curve A: $[N_2O_5] = 8.9 \times 10^{15}$ molecules/cm^3

Curve B: $[N_2O_5] = 5.6 \times 10^{15}$ " "

Curve C: $[N_2O_5] = 3.6 \times 10^{15}$ " "

Curve D: $[N_2O_5] = 1.8 \times 10^{15}$ " "

Curve E: $[N_2O_5] = 8.7 \times 10^{14}$ " "

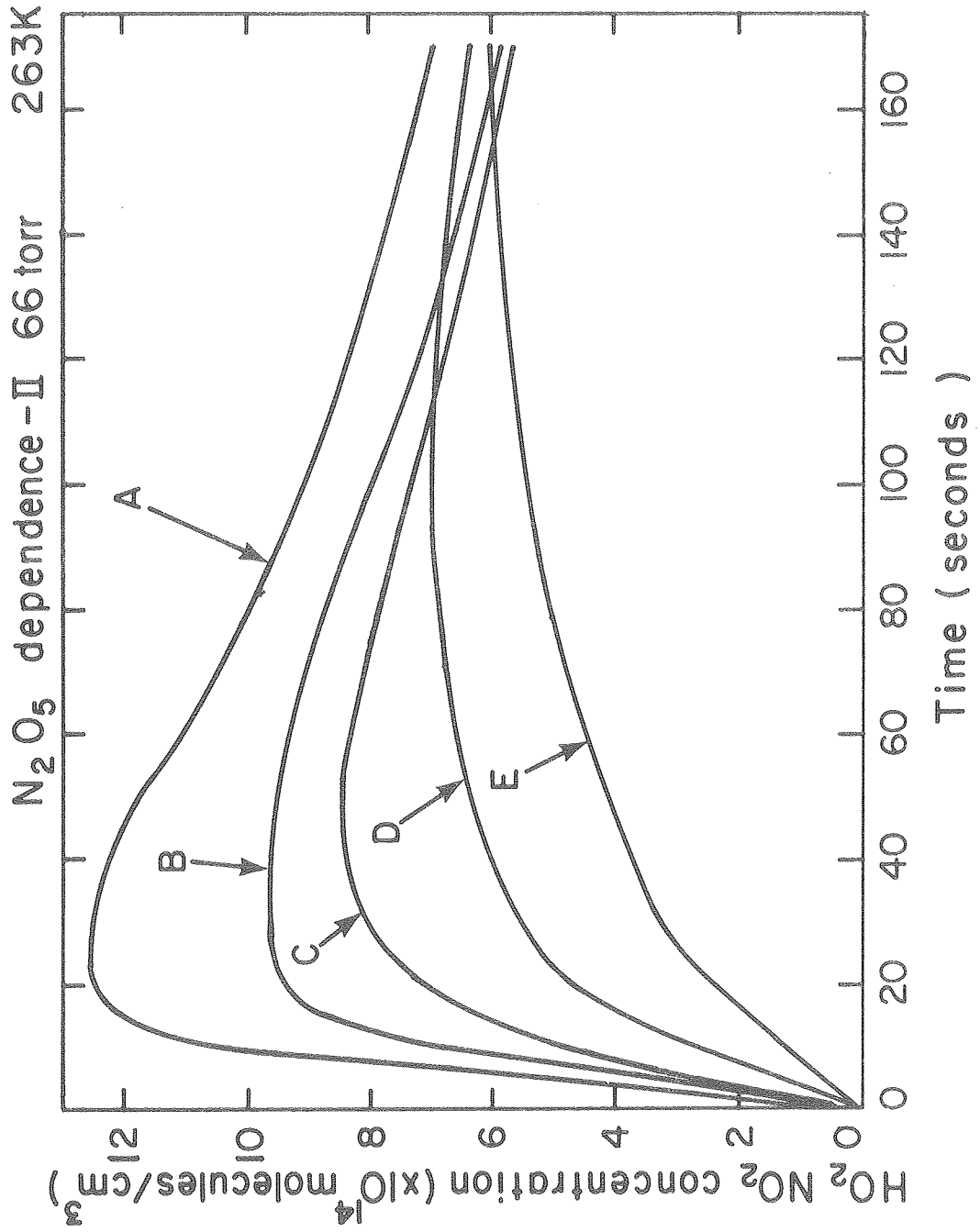

XBL 807-1426

Fig. 31

Fig. 32 HNO_4 profiles following expansion of N_2O_5 and H_2O_2. $[N_2O_5] = 1.3 \times 10^{15}$ molecules/cm^3 for all curves.

Curve A: $[H_2O_2] = 1.8 \times 10^{15}$ molecules/cm^3

Curve B: $[H_2O_2] = 1.3 \times 10^{15}$ " "

Curve C: $[H_2O_2] = 9.5 \times 10^{14}$ " "

Curve D: $[H_2O_2] = 6.9 \times 10^{14}$ " "

Curve E: $[H_2O_2] = 3.3 \times 10^{14}$ " "

Curve F: $[H_2O_2] = 2.1 \times 10^{14}$ " "

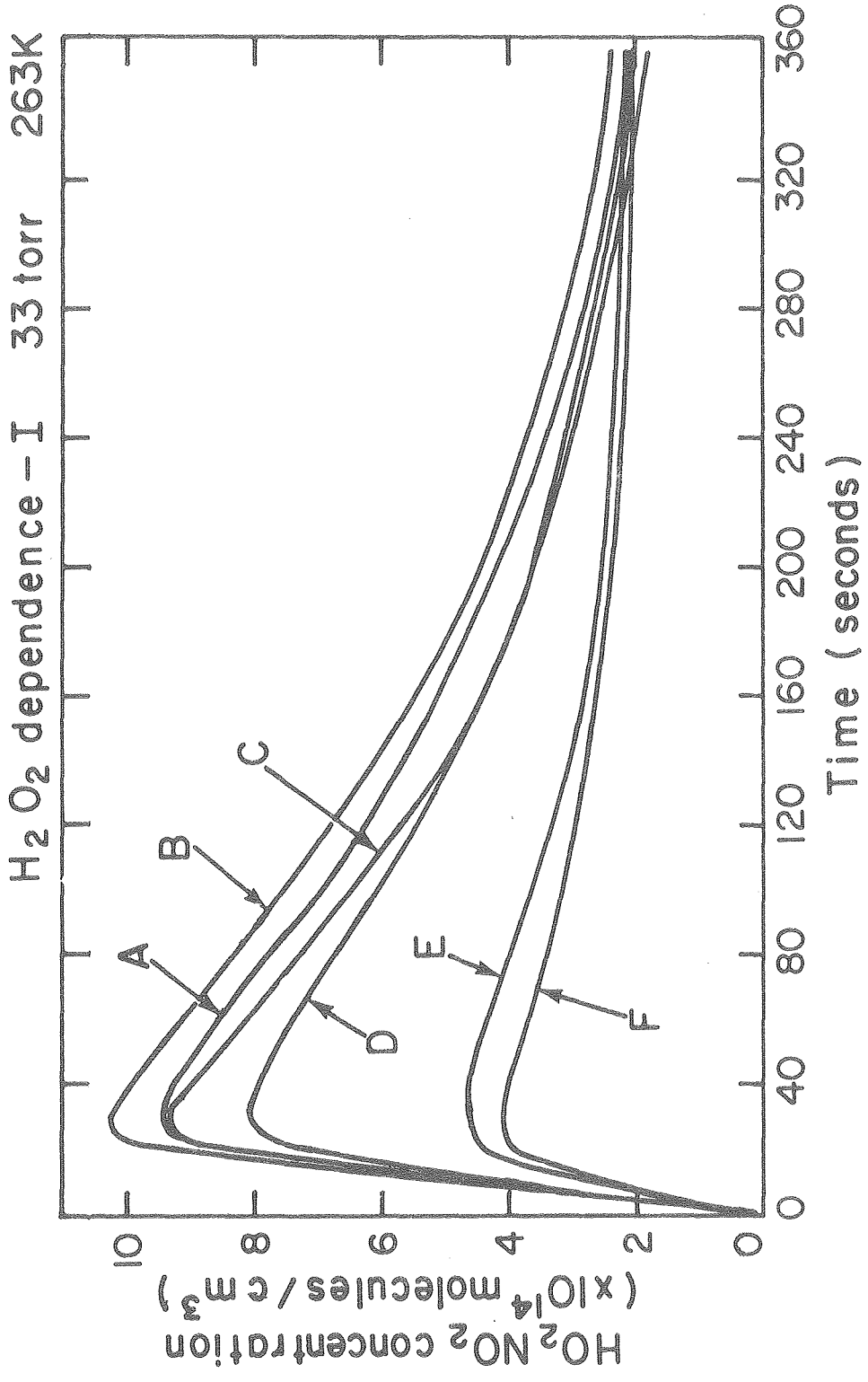

XBL807-1423

Fig. 32

Fig. 33 HNO_4 profiles following expansion of N_2O_5 and H_2O_2
$[N_2O_5] = 4.1 \times 10^{15}$ molecules/cm^3 for all curves

Curve A: $[H_2O_2] = 1.8 \times 10^{15}$ molecules/cm^3

Curve B: $[H_2O_2] = 1.0 \times 10^{15}$ " "

Curve C: $[H_2O_2] = 6.3 \times 10^{14}$ " "

Curve D: $[H_2O_2] = 3.6 \times 10^{14}$ " "

Curve E: $[H_2O_2] = 2.1 \times 10^{14}$ " "

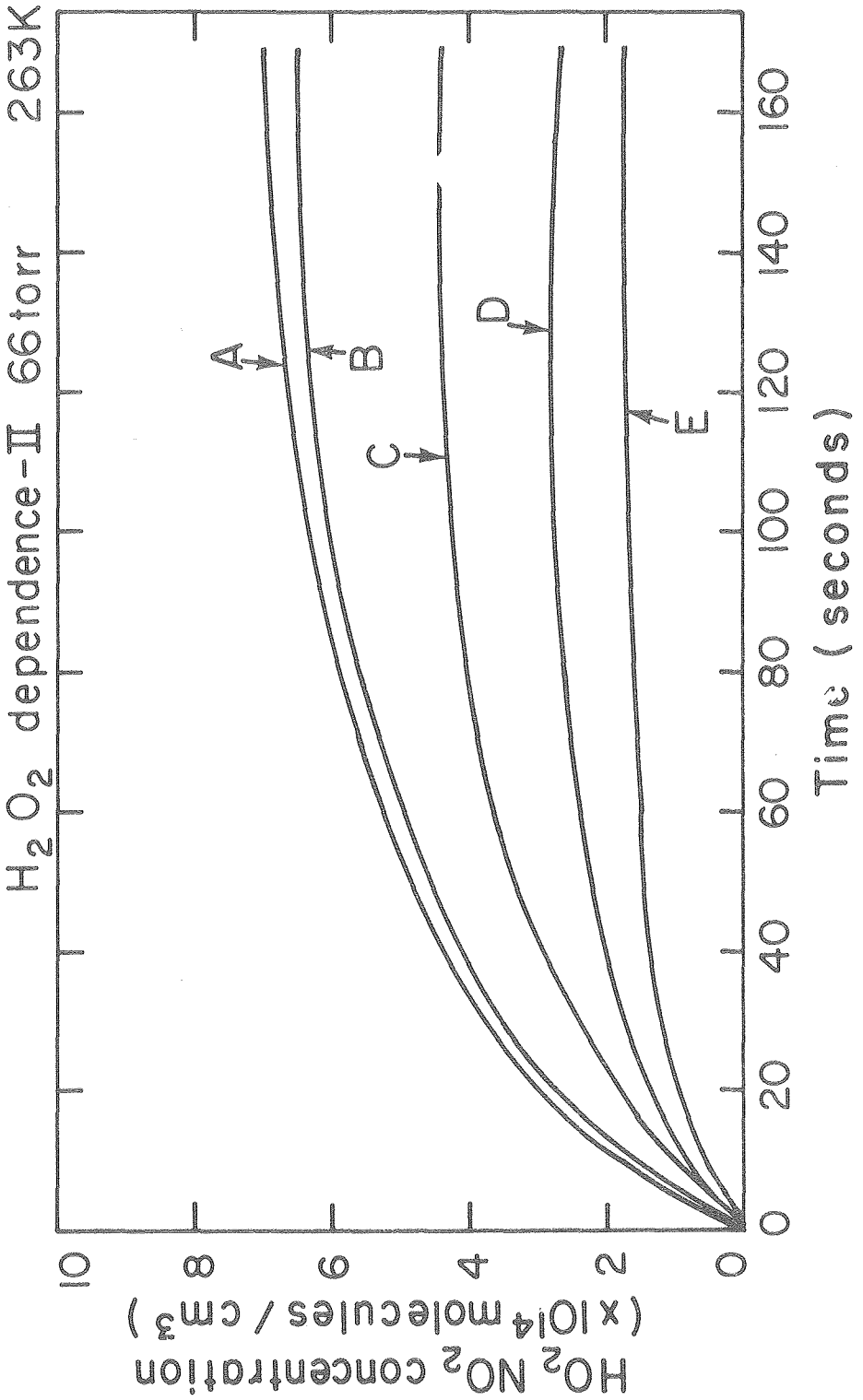

XBL807-1429

Fig. 33

The effects of temperature and pressure on the product profile were investigated. Expansions were done with a cell temperature of 253 K, 263 K, 273 K and 283 K. In most cases, the concentration profiles of HNO_4, N_2O_5, HNO_3 and NO_2 were observed. In some cases, H_2O was also observed. The cross sections of NO_2 and H_2O at temperatures where they had not been determined were obtained by interpolating from the 293 K and 263 K values. Since NO_2 was generally present in low concentrations and the 0.1 atmosphere cross section is small, there is considerable uncertainty in the concentration. H_2O was present in fairly large concentrations, but the low cross section made it difficult to obtain accurate values of its concentration.

HNO_4 was the only species monitored during the expansions done at 253 K. The expanded pressures of H_2O_2 approached 70 percent of the extrapolated H_2O_2 vapor pressure at 253 K. It was noted that HNO_4 was generated by expansion of N_2O_5 alone into the evacuated cell when the preceding expansion contained H_2O_2. Apparently, H_2O_2 exhibits a strong tendency to adsorb to surfaces under these conditions, or else a significant amount of condensation occurs. The H_2O_2 could be removed by pumping on the cell for several hours or by adding N_2O_5 to react with it. The HNO_4 profiles obtained are illustrated in Fig. 34. The initial H_2O_2 and N_2O_5 concentrations for each curve are listed below in units of molecules/cm^3.

Fig. 34 HNO_4 profiles following expansion of N_2O_5 and H_2O_2 at 253 K
$[H_2O_2] = 1.8 \times 10^{15}$ molecules/cm^3 for all curves

Curve A: $[N_2O_5] = 3.5 \times 10^{14}$ molecules/cm^3

Curve B: $[N_2O_5] = 2.9 \times 10^{14}$ " "

Curve C: $[N_2O_5] = 5.6 \times 10^{14}$ " "

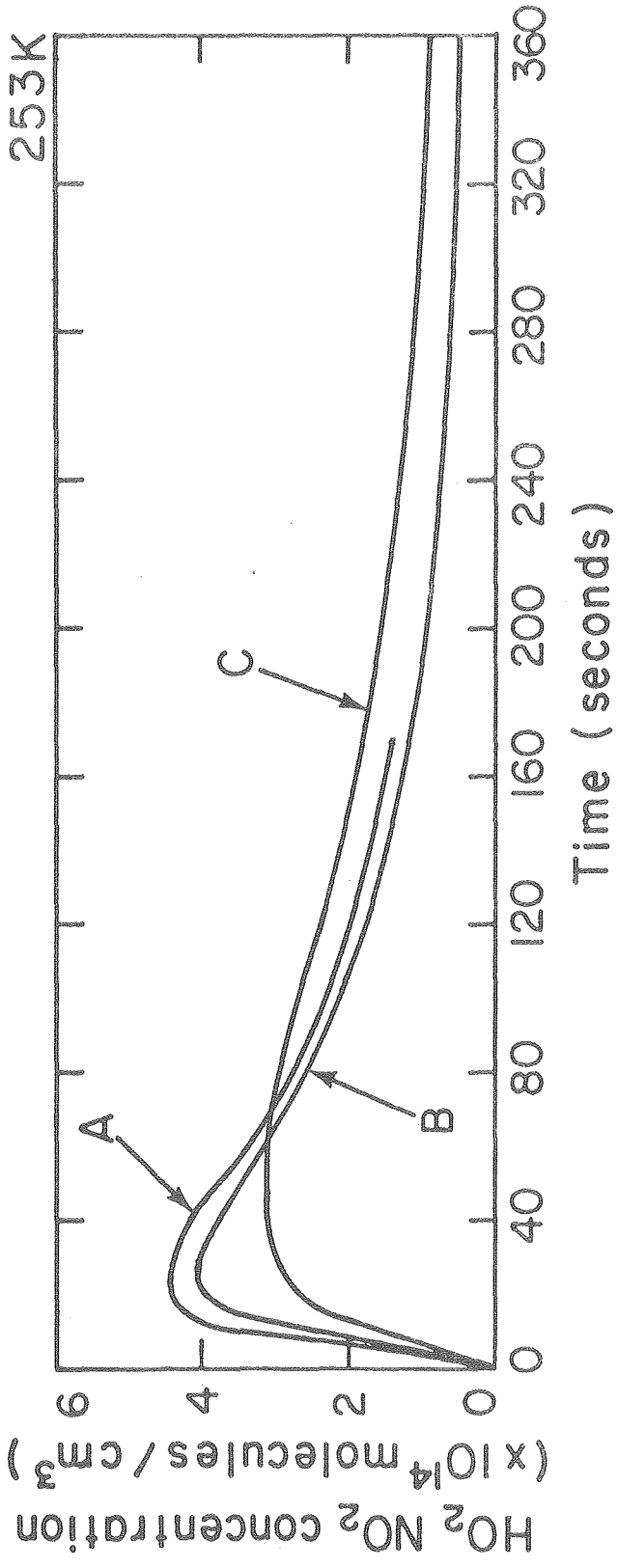

XBL807-1417

Fig. 34

Curve A $[H_2O_2] = 1.8 \times 10^{15}$ $[N_2O_5] = 3.5 \times 10^{14}$

Curve B $= 1.8 \times 10^{15}$ $= 2.9 \times 10^{14}$

Curve C $= 1.8 \times 10^{15}$ $= 5.6 \times 10^{14}$

The expanded pressure was 33 torr for these runs.

The problem of H_2O_2 adhering to the cell surfaces was not observed at 263K or higher temperatures. Sample runs at 263K, 273K, and 283K are illustrated in Figs. 35-37 and tabulated in Tables 7-9, respectively. The initial H_2O_2 and N_2O_5 concentrations for these expansions are as follows, in units of molecules/cm^3:

263K $[H_2O_2] = 1.8 \times 10^{15}$ $[N_2O_5] = 9.3 \times 10^{14}$

273K $= 1.8 \times 10^{15}$ 5.6×10^{14}

283K $= 1.8 \times 10^{15}$ 5.6×10^{14}

Runs were done at each temperature under several sets of conditions, to obtain a good understanding of the kinetics.

The pressure dependence of the HNO_4 profiles was examined under two different initial concentrations of N_2O_5 and H_2O_2. The HNO_4 profiles are illustrated in Figs. 38 and 39 and tabulated in Tables 10 and 11. The initial concentrations of H_2O_2 and in molecules/cm^3 are listed below.

Fig. 35 Concentration profiles of HNO_3, HNO_4, N_2O_5 and NO_2 following expansion of N_2O_5 and H_2O_2 at 263 K

$[N_2O_5] = 9.3 \times 10^{14}$ molecules/cm^3

$[H_2O_2] = 1.8 \times 10^{15}$ " "

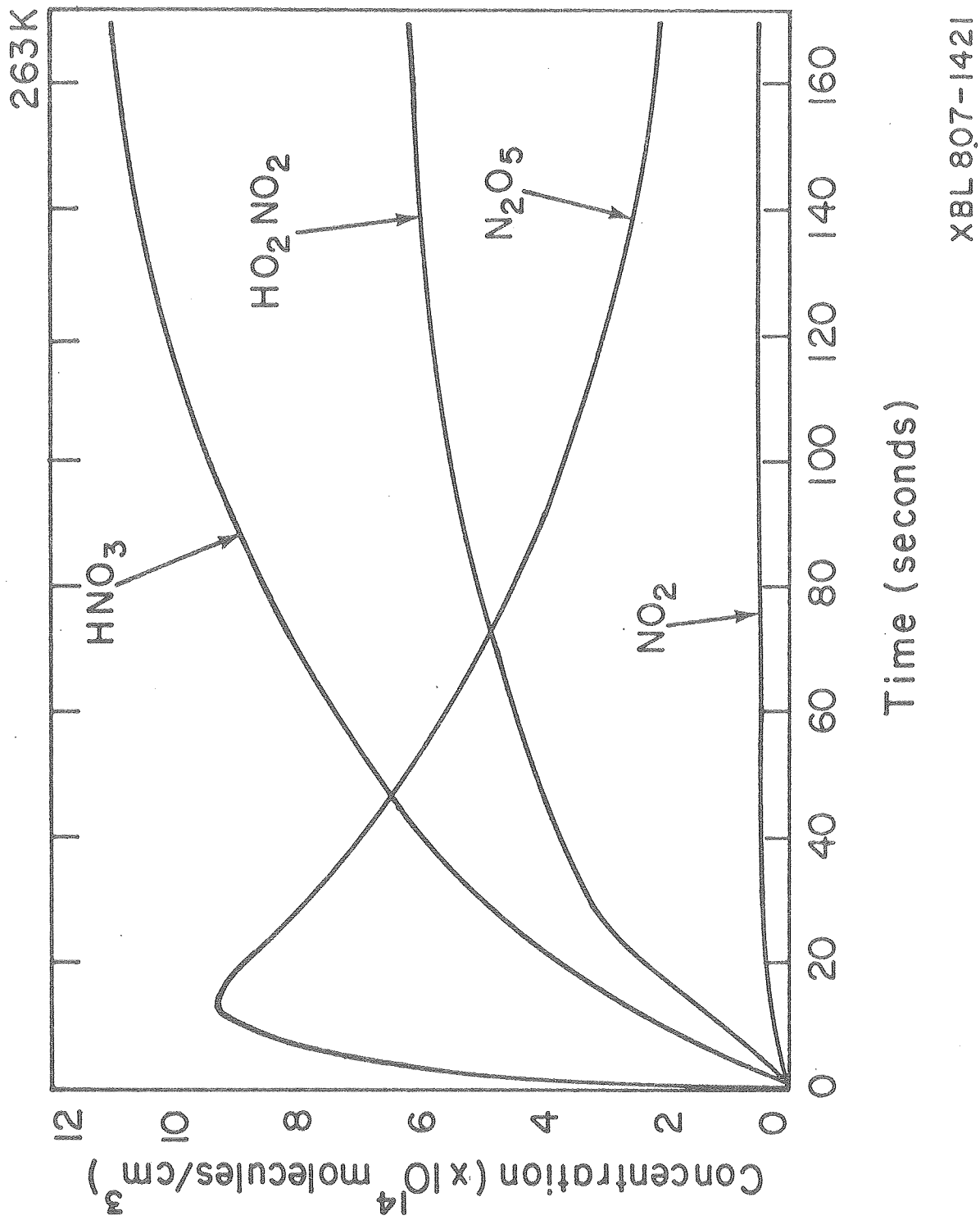

XBL807-1421

Fig. 35

Fig. 36 Concentration profiles of HNO_3, HNO_4, N_2O_5, NO_2 and H_2O following expansion of N_2O_5 and H_2O_2 at 273 K

$[N_2O_5] = 5.6 \times 10^{14}$ molecules/cm^3

$[H_2O_2] = 1.8 \times 10^{15}$ " "

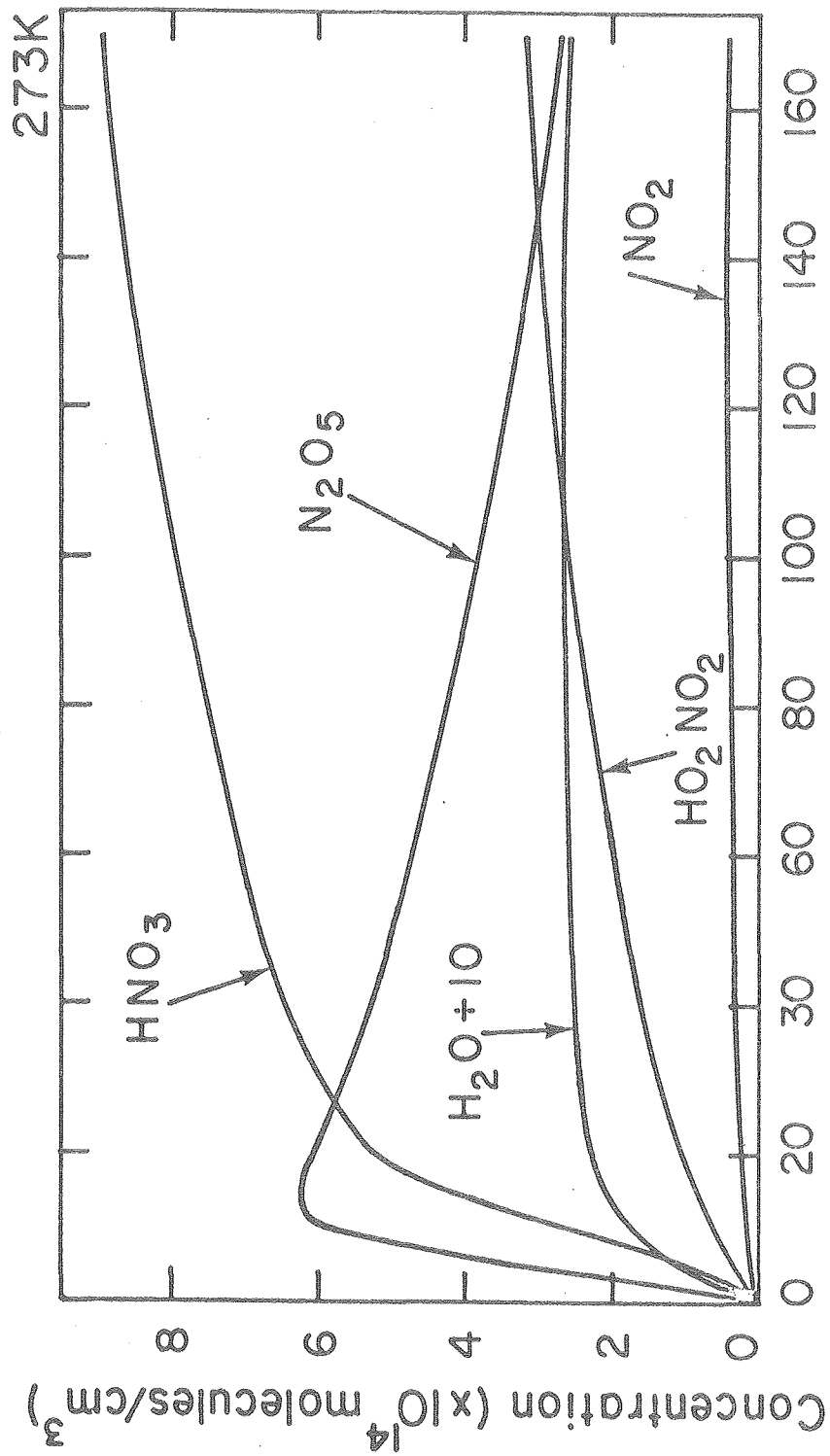

XBL 807-1428

Fig. 36

Fig. 37 Concentration profiles of HNO_3, HNO_4, N_2O_5, NO_2 and H_2O following expansion of N_2O_5 and H_2O_2 at 283 K

$[N_2O_5] = 5.6 \times 10^{14}$ molecules/cm^3

$[H_2O_2] = 1.8 \times 10^{14}$ " "

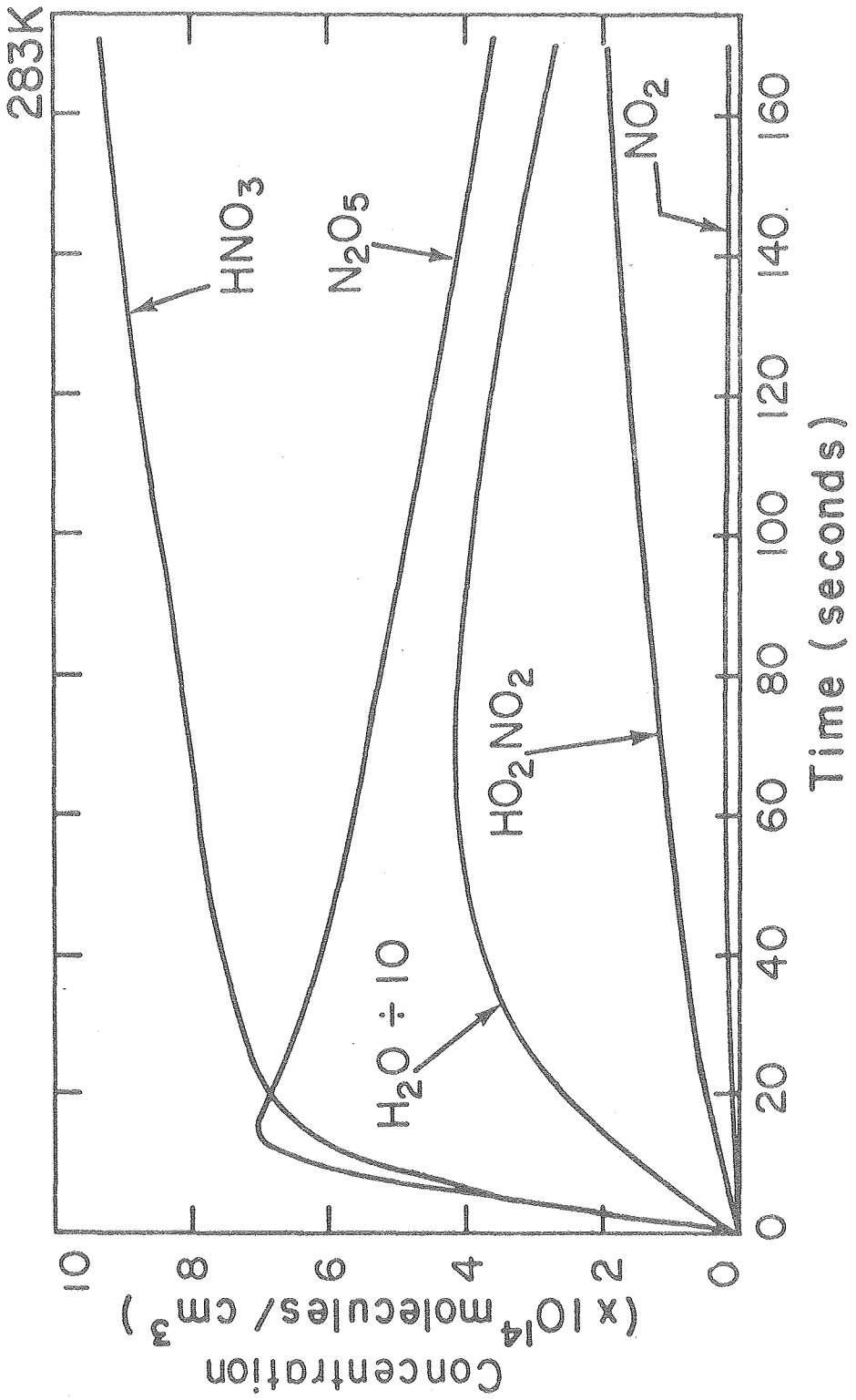

XBL 807-1419

Fig. 37

TABLE 7

Temp. = 263K Pres. = 68 torr

Time (Seconds)	Concentration (Molecules/cm^3)			
	$[HO_2NO_2]$	$[N_2O_5]$	$[HNO_3]$	$[NO_2]$
0	---	---	---	---
10	1.3E14	8.9E14	1.4E14	4.0E13
20	2.5E14	8.9E14	3.7E14	4.0E13
30	3.4E14	7.6E14	5.5E14	9.5E13
40	3.8E14	6.9E14	6.3E14	2.5E13
50	4.1E14	6.4E14	6.6E14	3.2E13
60	4.4E14	5.6E14	7.4E14	5.7E13
70	4.8E14	5.0E14	7.7E14	1.8E13
80	5.1E14	4.5E14	8.8E14	2.5E13
90	5.3E14	4.1E14	8.9E14	4.0E13
100	5.5E14	3.7E14	9.5E14	9.5E13
110	5.7E14	3.4E14	9.6E14	3.2E13
120	5.7E14	3.1E14	1.0E15	3.2E13
130	5.8E14	2.8E14	1.0E15	6.6E13
140	5.9E14	2.6E14	1.1E15	5.7E13
150	6.0E14	2.4E14	1.1E15	3.2E13
160	6.0E14	2.2E14	1.1E15	3.2E13
170	6.1E14	2.1E14	1.1E15	8.5E13

TABLE 8

Temp. = 273K Pres. = 73 torr

Time (Seconds)	Concentration (Molecules/cm^3)				
	$[HO_2NO_2]$	$[N_2O_5]$	$[HNO_3]$	$[NO_2]$	$[H_2O]$
0	---	---	---	---	---
10	6.7E13	5.8E14	2.6E14	1.0E13	1.7E15
20	1.1E14	5.9E14	5.5E14	1.2E13	2.3E15
30	1.3E14	5.4E14	5.6E14	2.4E13	2.4E15
40	1.5E14	5.2E14	6.4E14	5.4E13	2.2E15
50	1.7E14	5.0E14	7.3E14	7.2E13	2.4E15
60	1.8E14	4.8E14	5.7E14	4.6E13	2.5E15
70	2.0E14	4.45E14	7.0E14	1.7E13	2.5E15
80	2.2E14	4.2E14	6.1E14	2.4E13	2.6E15
90	2.4E14	4.0E14	7.6E14	3.8E13	2.5E15
100	2.5E14	3.8E14	8.2E14	3.8E13	2.5E15
110	2.7E14	3.6E14	8.1E14	2.4E13	2.4E15
120	2.7E14	3.4E14	7.9E14	2.4E13	2.5E15
130	2.9E14	3.2E14	8.4E14	2.4E13	2.6E15
140	2.9E14	3.1E14	8.4E14	5.4E13	2.5E15
150	3.0E14	2.9E14	8.8E14	1.7E13	2.5E15
160	3.0E14	2.8E14	8.7E14	2.4E13	2.6E15
170	3.1E14	2.7E14	8.6E14	1.7E13	2.5E15

TABLE 9

Temp. = 283K Pres. = 75 torr

Time (Seconds)	Concentration (Molecules/cm^3)				
	$[HO_2NO_2]$	$[N_2O_5]$	$[HNO_3]$	$[NO_2]$	$[H_2O]$
0	---	---	---	---	---
10	2.5E13	6.3E14	5.4E14	6.5E12	9.7E15
20	5.1E13	6.8E14	6.9E14	6.5E12	2.9E15
30	7.1E13	6.4E14	7.7E14	3.0E13	4.2E15
40	8.7E13	6.1E14	7.4E14	3.0E13	3.6E15
50	9.2E13	5.9E14	7.8E14	3.0E13	3.9E15
60	1.1E14	5.7E14	7.7E14	1.1E13	4.2E15
70	1.2E14	5.5E14	7.8E14	1.1E13	4.2E15
80	1.3E14	5.3E14	8.0E14	1.5E13	4.2E15
90	1.4E14	5.0E14	8.4E14	1.7E13	4.2E15
100	1.5E14	4.9E14	8.8E14	3.7E13	3.9E15
110	1.5E14	4.7E14	8.7E14	2.3E13	3.9E15
120	1.7E14	4.5E14	8.6E14	1.1E13	3.9E15
130	1.8E14	4.3E14	8.8E14	1.1E13	2.9E15
140	1.8E14	4.1E14	8.7E14	6.5E12	2.9E15
150	1.9E14	4.0E14	9.2E14	1.1E13	2.9E15
160	1.9E14	3.8E14	9.1E14	6.5E12	2.3E15
170	2.0E14	3.7E14	9.4E14	1.5E13	2.3E15

Fig. 38 HNO_4 profiles following the expansion of H_2O_2 and N_2O_5 at different pressures

$[N_2O_5] = 1.1 \times 10^{15}$ molecules/cm^3

$[H_2O_2] = 2.1 \times 10^{14}$ " "

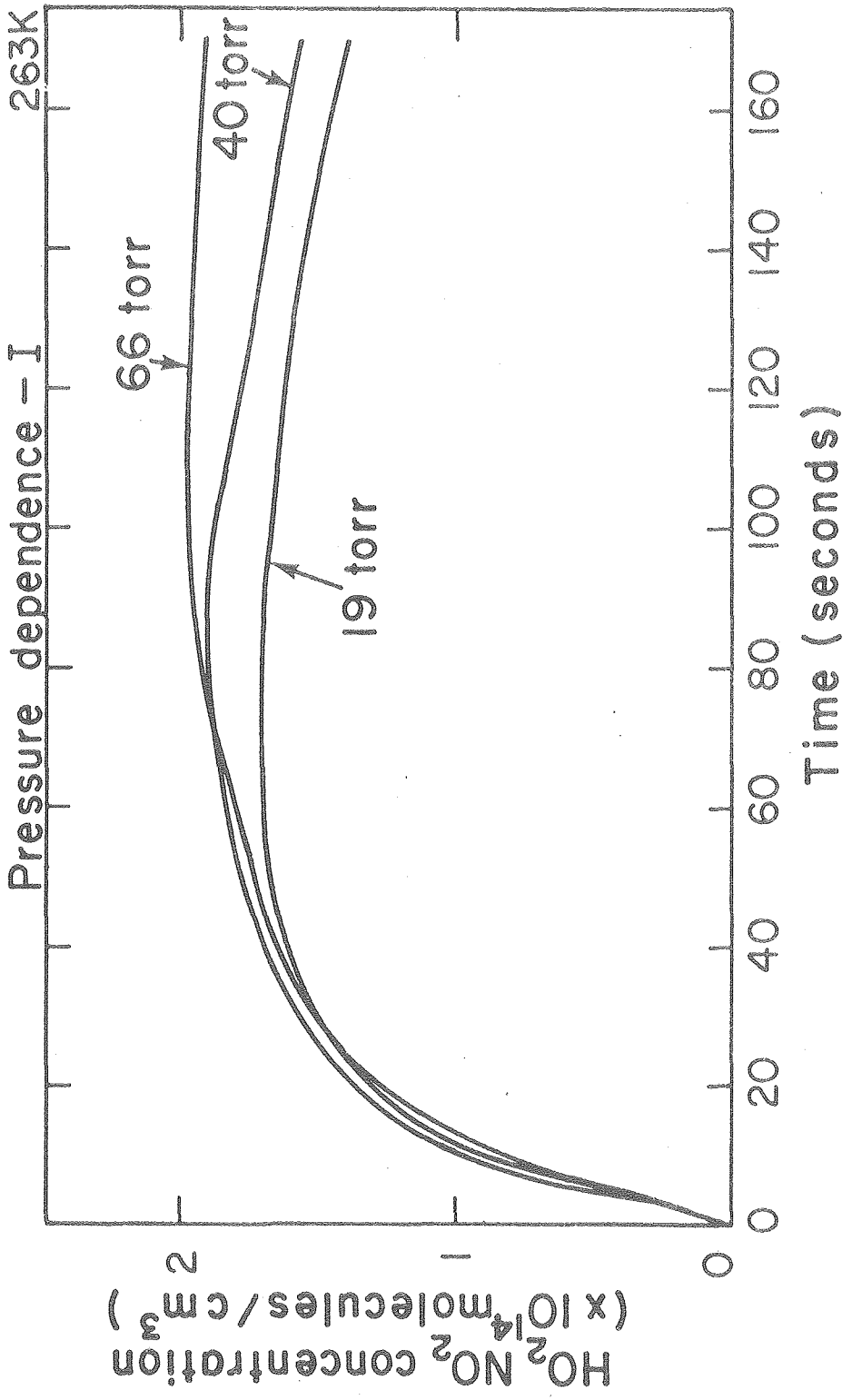

XBL807-1425

Fig. 38

Fig. 39 HNO_4 profiles following the expansion of H_2O_2 and N_2O_5 at different pressures

$[N_2O_5] = 3.5 \times 10^{15}$ molecules/cm^3

$[H_2O_2] = 1.8 \times 10^{15}$ " "

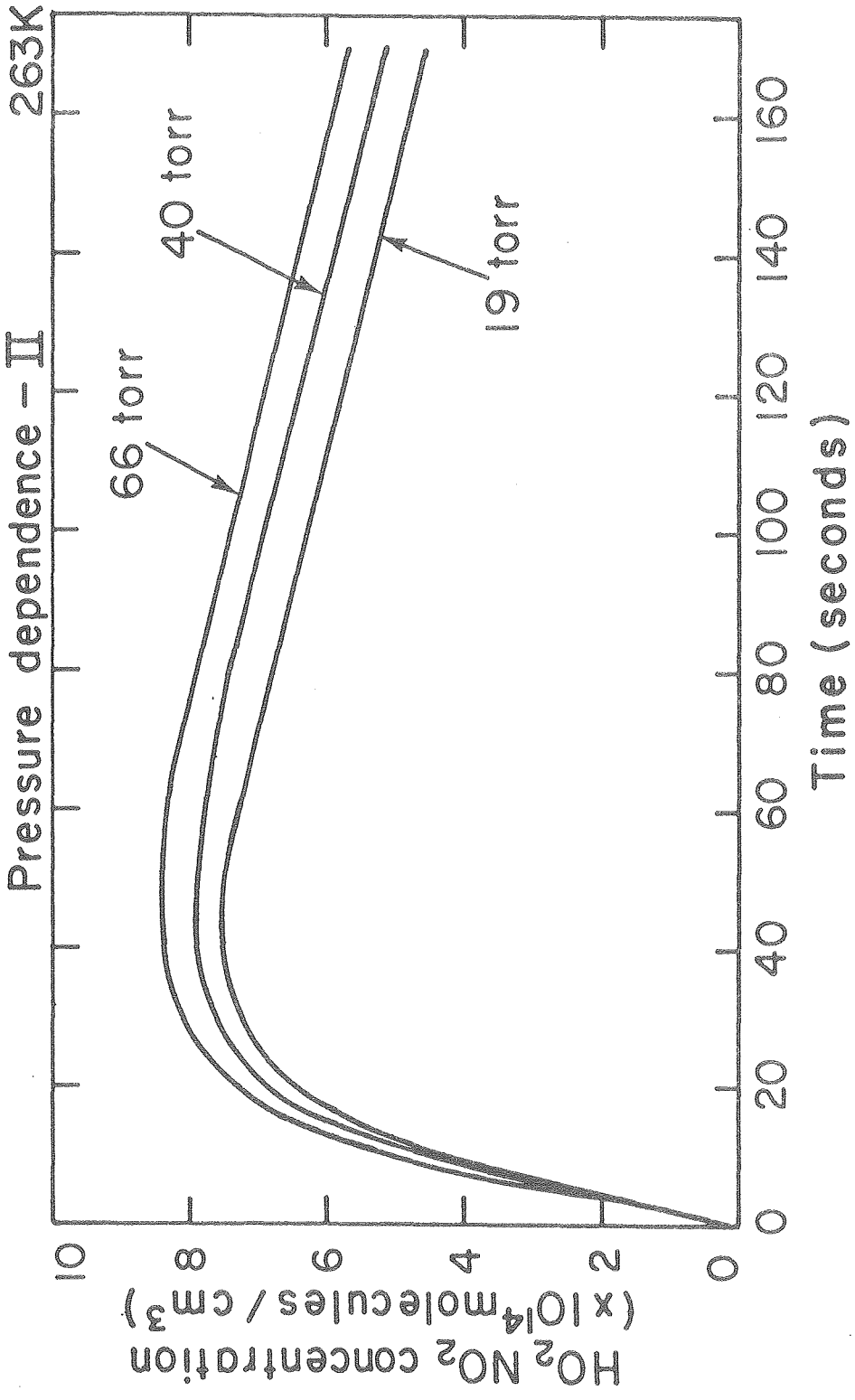

XBL 807-1424

Fig. 39

TABLE 10

Temp. = 263K — Pressure Dependence – I

Time (Seconds)	Concentration (Molecules/cm^3) $[HO_2NO_2]$	$[HO_2NO_2]$	$[HO_2NO_2]$
0	—	—	—
10	9.6E13	1.0E14	8.9E13
20	1.1E14	1.3E14	1.3E14
30	1.4E14	1.6E14	1.5E14
40	1.6E14	1.7E14	1.6E14
50	1.7E14	1.7E14	1.7E14
60	1.7E14	1.8E14	1.7E14
70	1.7E14	1.8E14	1.6E14
80	1.9E14	1.9E14	1.7E14
90	1.9E14	1.9E14	1.7E14
100	2.0E14	1.9E44	1.7E14
110	1.9E14	1.8E14	1.6E14
120	1.9E14	1.8E14	1.6E14
130	2.0E14	1.7E14	1.6E14
140	1.9E14	1.7E14	1.6E14
150	1.9E14	1.7E14	1.5E14
160	1.9E14	1.6E14	1.5E14
170	1.9E14	1.6E14	1.4E14
Pres	66 torr	40 torr	19 torr

TABLE 11

Temp. = 263K — Pressure Dependence – II

Time (Seconds)	Concentration (Molecules/cm^3) $[HO_2NO_2]$	$[HO_2NO_2]$	$[HO_2NO_2]$
0	---	---	---
10	5.0E14	4.6E14	4.2E14
20	7.3E14	6.9E14	6.4E14
30	8.1E14	7.6E14	7.2E14
40	8.3E14	7.8E14	7.5E14
50	8.5E14	7.9E14	7.5E14
60	8.2E14	7.8E14	7.2E14
70	8.0E14	7.6E14	7.0E14
80	7.9E14	7.5E14	6.8E14
90	7.6E14	7.2E14	6.6E14
100	7.4E14	6.9E14	6.2E14
110	7.1E14	6.6E14	6.0E14
120	6.8E14	6.4E14	5.7E14
130	6.6E14	6.2E14	5.5E14
140	6.3E14	5.9E14	5.3E14
150	6.2E44	5.6E14	5.0E14
160	5.9E14	5.5E14	4.8E14
170	5.7E14	5.3E14	4.6E14
Pres	66 torr	40 torr	19 torr

Run I $[H_2O_2] = 2.1 \times 10^{14}$ $[N_2O_5] = 1.1 \times 10^{15}$

Run II $= 1.8 \times 10^{15}$ $= 3.5 \times 10^{15}$

Both runs were done at 263K.

The effect of cell volume and surface-to-volume ratio were investigated by inserting sealed Pyrex tubing into the cell. Thirty-two 0.9 cm diameter tubes 85 cm long were loosely stacked in the cell and kept separated by Pyrex rods. This added 7600 cm^2 surface area, increasing the surface area of the cell by 70 percent. The surface-to-volume ratio of the cell was increased to 0.303 cm^{-1}.

Expansions were done immediately preceding and following the insertion of the tubes to observe the effect of added surface. The expansions were done with a cell temperature of 283K. Three HNO_4 profiles are shown in Fig. 40. Curve A was obtained without the extra surface, and curves B and C were obtained after the extra surface had been added. The initial concentrations were 1.8×10^{15} molecules/cm^3 for H_2O_2 and 2.7×10^{15} molecules/cm^3 for N_2O_5 in all three runs.

B. Results and Discussion

1. Other Reactions in the N_2O_5-H_2O_2 System

The presence of contaminants and decomposition products in the samples of H_2O_2 and N_2O_5 mixed together in these experiments complicate the kinetics of the system. The contaminating species can react with H_2O_2 or N_2O_5 and make the reaction between them

Fig. 40 HNO_4 profiles following expansion of H_2O_2 and N_2O_5

Curve A - cell in standard configuration

Curves B, C- cell with additional surface area

$[N_2O_5] = 2.7 \times 10^{15}$ molecules/cm^3

$[H_2O_2] = 1.8 \times 10^{15}$ " "

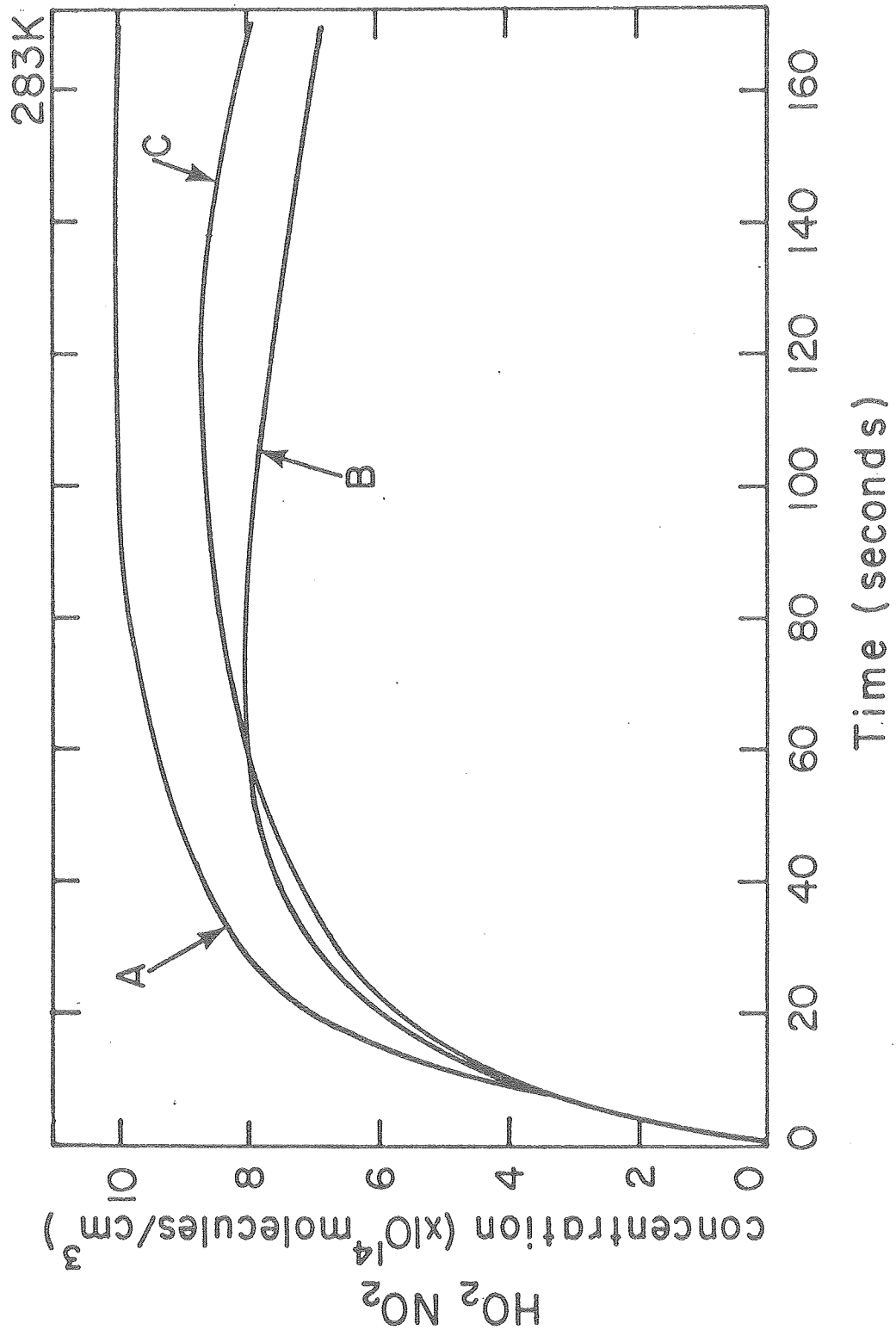

XBL807-1427

Fig. 40

difficult to observe. The major contaminants are H_2O and HNO_3, as well as some NO_2.

Reactions involving these species, as well as the heterogeneous decomposition of the reactants in the cell, were investigated to determine their effect on the kinetics.

The reaction of H_2O with N_2O_5 has been investigated by Morris and Niki.[59] It was investigated in this system to see whether it occurred primarily homogeneously or heterogeneously. Typical curves of N_2O_5 decay in the presence of H_2O at 263K are shown in Fig. 28. The curves exhibit some curvature, which is more pronounced at longer time scales. The average slopes of the lines did not correlate well with either of the initial reactant concentrations or with the product of the concentrations. It was concluded that the reaction is primarily heterogeneous in this system. This conclusion is in agreement with other studies.[93] However, a significant amount of N_2O_5 is lost in this manner.

The possibility of a reaction between H_2O_2 and HNO_3 was investigated. The H_2O_2 decomposition rate was the same as that of H_2O_2 alone. The HNO_3 disappearance rate decreased with succeeding runs, suggesting a heterogeneous process was occurring. There was an absence of absorption by any of the likely products of the reaction of H_2O_2 with HNO_3 in scans taken following their expansion.

HNO_3 exhibits a tendency to absorb or adhere to a surface, and this could explain the disappearance of HNO_3. Morris and Niki[59]

noted a slow, long term loss of HNO_3 from the gas phase with an estimated first order loss rate of ~10^{-4} second^{-1}. The values obtained in this system, which has a similar surface-to-volume ratio to that of ref. 59, were in the range of 0.8 to 5 x 10^{-4} second^{-1}. From these results, it appears that the reaction between H_2O_2 and HNO_3 in the gas phase is very small, if it occurs at all. The upper limit for the rate constant for this reaction was determined to be ~1 x 10^{-19} cm^3/molecule-second.

NO_2 will be formed in the H_2O_2-N_2O_5 system by the decomposition of N_2O_5 and HNO_4. H_2O will be formed by the decomposition of H_2O_2. The reaction between H_2O and NO_2 has been investigated by refs. 60 and 92. The concentrations of HNO_3 and HONO observed after the expansion of H_2O_2 and NO_2 into the cell were well in excess of the amounts that would be produced by the gas phase reaction of NO_2 and H_2O if the values for the rate constant in ref. 60 are correct.

HONO exists in cis and trans forms only the trans absorption was monitored following the expansion of H_2O_2 and NO_2. From the equilibrium constants given by Altshuller,[94] the cis form should be present in somewhat lower concentrations than the trans form, indicating a total HONO concentration of ~5-7 x 10^{13} molecules/cm^3, somewhat less than that of the HNO_3 observed. At the time of expansion, H_2O was present at levels approximately 50 percent higher than H_2O_2 due to the decomposition of H_2O_2 in the bulb prior to expansion. The majority of the HONO was apparently formed heterogeneously by

$$H_2O + 2NO_2 \rightarrow HONO + HNO_3 \quad . \tag{51}$$

An equilibrium exists between HONO and H_2O, NO_2 and NO,

$$2HONO \rightleftarrows H_2O + NO_2 + NO \quad . \tag{52}$$

If HONO was present at levels of ~7 x 10^{13} molecules/cm^3, NO would exist at levels of ~1 x 10^{15} molecules/cm^3 if the system was in equilibrium. While the absorption band of NO was not monitored, the conversion of this much NO_2 into NO would have been observed when NO_2 was monitored. HONO was apparently not equilibrated with the products in (52) at the time of observation.

Since HNO_3 tends to adhere to the cell walls, the amount of HNO_3 generated was presumably present in larger concentrations than observed and was present in excess of the HONO concentration. The difference could be due to loss of HONO through the equilibrium process into H_2O, NO_2 and NO.[95] Alternatively, some HNO_3 could have been produced by the reaction of H_2O_2 with NO_2 or N_2O_4. The N_2O_4 concentration was about 1 percent of the NO_2 concentration in the runs where this was investigated. In either case, the reaction is slow and is not important in the system under study. The upper limit for the rate constant for the reaction of H_2O_2 with NO_2 in the gas phase is < 1 x 10^{-19} cm^3/molecule-second. No information was obtained on whether the reaction occurred by a heterogeneous pathway.

Kaiser and Wu[92] investigated the possibility of a reaction of HNO_3 with NO_2 and H_2O and did not observed any noticeable reaction. Consequently, these reactions were not investigated in this system.

2. Analysis of the reaction of N_2O_5 with H_2O_2 Scans taken after the expansion of H_2O_2 and N_2O_5 into the cell indicated the presence of HNO_4 and the absence, within detectable limits, of HONO. The detection limit for HONO is less than 3×10^{13} molecules/cm^3. HNO_4 could be formed directly by the reaction of N_2O_5 with H_2O_2 or indirectly from the recombination of HO_2 and NO_2. Tests were made to determine the reaction product set by adding ~0.3 torr of NO to the cell prior to the expansion of the reactants. NO scavenges HO_2 by reaction (4), which is more rapid than the reaction of HO_2 with NO_2 to form HNO_4 under the experimental conditions of 0.1 atmosphere pressure and 273K.

If the products of the reaction of H_2O_2 and N_2O_5 were HO_2 + NO_2 + HNO_3, the HNO_4 concentration would not rise to detectable limits. If the products were HNO_4 and HNO_3, HNO_4 would be present at levels somewhat reduced from that without NO. This is due to loss of HNO_4 by dissociation into NO_2 and HO_2, which would react with NO. The experimental observations were in good agreement with those predicted for the reaction products of HNO_4 and HNO_3. This product set was > 90 percent of all product channels.

If the reaction occurs in the gas phase, it may proceed though an complex re-arrangement because of the geometry of the molecules.

Electron diffraction studies[96] of N_2O_5 indicated a central angle of 95 ± 3° and an O-N-O angle of the end nitro groups of 134 ± 9°. The central N-O distance of 1.46Å and the end N-O distance of 1.21Å were obtained. H_2O_2 has C_2 symmetry and an H-O-O angle of 102°. The O-O distance is 1.48Å and the O-H distance is 0.98Å[72]. The rearrangement of these molecules into HNO_3 and HNO_4 would be fairly complex.

The rate expression for the HNO_4 buildup and decay in the cell will be:

$$\frac{d[HNO_4]}{dt} = k_7[H_2O_2][N_2O_5]-k_8[HNO_4]+k_9[HO_2][NO_2]-k_{21}[HNO_4] \qquad (53)$$

using the numbering system in Appendix C. The concentrations of H_2O_2 and N_2O_5 during expansion will be described by the flow-in equation

$$[x] = [x]_o\ (1-\exp(-t/t_o)) \qquad (32)$$

where $[x]_o$ is the final concentration in the cell if species x is inert. The value for t_o is 4.3 seconds for the expansion system used. For approximately ten seconds following the start of expansion, this equation is adequate for describing the flow-in of the reactants $[H_2O_2]$ and $[N_2O_5]$ can be determined from the reactant concentrations in the bulbs at the time of expansion. Also the reactions affecting HNO_4 other than (7) will be small and

$$\frac{d[HNO_4]}{dt} = k_7[H_2O_2]\ \ [N_2O_5]\ \ (1-\exp(-\ t/4.3))^2 \qquad (54)$$

The build-up of HNO_4 can be obtained by integrating the above equation

$$[HNO_4]_t \approx k_7[H_2O_2]\,[N_2O_5]\,\cdot$$

$$[t+8.6\,\exp(-t/4.3) - 2.15\,\exp(-2t/4.3) - 6.45] \qquad (55)$$

The bimolecular rate constant for reaction (7) can be obtained by the HNO_4 build-up and the concentrations of the reactants in the bulbs.

The effect of independent variation of reactant concentrations on the HNO_4 profile observed can be determined from the results used to generate Figs. 30-33. The ratios of the N_2O_5 and H_2O_2 initial concentrations, along with the ratios of the HNO_4 concentrations at 20 and 40 seconds after expansion and at maximum, relative to the minimum values are listed in Table 12. The ratios for the HNO_4 concentrations are generally less than those of the reactants because of reactions which compete with reaction (7). A low value of $[HNO_4]$ obtained in run G of Fig. 30 is probably the cause of the t = 20 second $[HNO_4]$ ratios being higher than the $[N_2O_5]$ ratios.

The time of occurrence of the maximum HNO_4 concentration is usually longer than 40 seconds. It can be seen from Table 12 that the $[HNO_4]$ ratios approach the ratios of $[N_2O_5]$ as the time of observation approaches the time of expansion. From Table 12, it is apparent that $[HNO_4]$ ratios approach the $[H_2O_2]$ ratios as time increases following expansion.

TABLE 12

From Fig. 30

Run	$[N_2O_5]_{t=0}$	$[HNO_4]_{t=20sec}$	$[HNO_4]_{t=40sec}$	$[HNO_4]_{max}$
A/G	16.9	19.5	8.2	4.7
B/G	11.9	17.4	7.9	4.4
C/G	6.9	11.9	6.5	4.1
D/G	5.0	9.1	5.3	4.0
E/G	3.8	6.0	3.8	3.4
F/G	1.9	2.8	2.2	2.0
G/G	1.0	1.0	1.0	1.0

From Fig. 31

Run	$[N_2O_5]_{t=0}$	$[HNO_4]_{t=20sec}$	$[HNO_4]_{t=40sec}$	$[HNO_4]_{max}$
A/E	10.3	5.0	3.2	2.1
B/E	6.5	3.8	2.5	1.6
C/E	4.2	2.9	2.2	1.4
D/E	2.1	1.9	1.6	1.2
E/E	1.0	1.0	1.0	1.0

From Fig. 32

Run	$[N_2O_5]_{t=0}$	$[HNO_4]_{t=20sec}$	$[HNO_4]_{t=40sec}$	$[HNO_4]_{max}$
A/F	8.8	2.2	2.3	2.3
B/F	6.5	2.3	2.5	2.5
C/F	4.6	2.1	2.3	2.3
D/F	3.4	1.9	2.0	2.0
E/F	1.6	1.1	1.2	1.2
F/F	1.0	1.0	1.0	1.0

From Fig. 33

Run	$[N_2O_5]_{t=0}$	$[HNO_4]_{t=20sec}$	$[HNO_4]_{t=40sec}$	$[HNO_4]_{max}$
A/E	8.8	3.2	3.4	3.9
B/E	5.0	3.1	3.2	3.6
C/E	3.0	2.1	2.2	2.4
D/E	1.9	1.6	1.6	1.6
E/E	1.0	1.0	1.0	1.0

Computer simulations were done of the HNO_4 dependence on reactants using a simplified version of the reaction scheme shown in Appendix C. Reactions 2, 3, 6, 7, 20, 21 and 22 were used. These simulations indicated that the $[HNO_4]$ ratios should approach the ratios of either reactant at times near to the time of expansion. This disagrees with what was observed when the H_2O_2 variation was tested.

The experimentally observed effects of pressure on the HNO_4 profiles were shown in the previous section. The most apparent effect is that the final HNO_4 concentration is larger at higher pressures. The total pressure of the system will affect the rate constants for unimolecular decomposition of N_2O_5 and HNO_4, but will not affect the equilibrium of these species with their decomposition products. The pressure will also affect the rate of diffusion to the walls, where heterogeneous reactions may occur. The pressure dependence of the heterogeneous decomposition of N_2O_5, H_2O_2 and HNO_4 is unknown. The time for a molecule to diffuse a given distance at 19 torr will be about one-third of the diffusion time at 66 torr.

Computer simulations were made of the effect of pressure on the reaction system using the complete set of reactions in Appendix C. The only significant effect of pressure in the simulation was a ~ 25 percent decrease in the concentration of NO_2 as the pressure doubled from 34 to 68 torr at 263 K. This suggests the effects observed are due to heterogeneous processes.

The experimental profiles of the spectra observed at 263 K, 273 K and 283 K were simulated using the CHEMK chemical kinetics program and

the reaction set in Appendix C. The rate constant for reaction (7) was varied to provide the best fit with the experimental data. There was some difficulty in obtained a good fit because of the variability of the heterogeneous decomposition rates of N_2O_5, H_2O_2 and HNO_4. Typical simulation profiles along with the experimental profiles are shown in Figs. 41-43 for cell temperatures of 263K, 273K and 283K, respectively. The upper curves are those obtained from the computer simulations. The most prominent disagreement between experimental and simulated curves occurred with H_2O and NO_2. The experimental curves of these compounds were the most uncertain because of the weak absorption by these species. The experimental NO_2 profiles indicate that some NO_2 was present with the N_2O_5 at the time of expansion. The build-up of NO_2 occurs largely in the first 20 seconds after expansion. The rate of change during later periods is much lower. This factor was not included in the simulations. There was some variation in the best rate constant for reaction (7) to fit the experimental data at each temperature, and the rate constants tended to be higher at lower temperatures. This is in contradiction to what would be expected for a gas phase bimolecular reaction. The rate constants used for simulations in Figs. 41-43 were 0.8, 1.0 and 0.3 x $10^{-17}cm^3$/molecule-second, respectively.

Another unusual feature found was that the calculated HNO_4 concentration generally would initially be lower than the experimental values. The initial observed build-up HNO_4 for several runs is shown in Fig. 44. The temperatures and $[H_2O_2]$ $[N_2O_5]$ product corresponding to the curves are listed below.

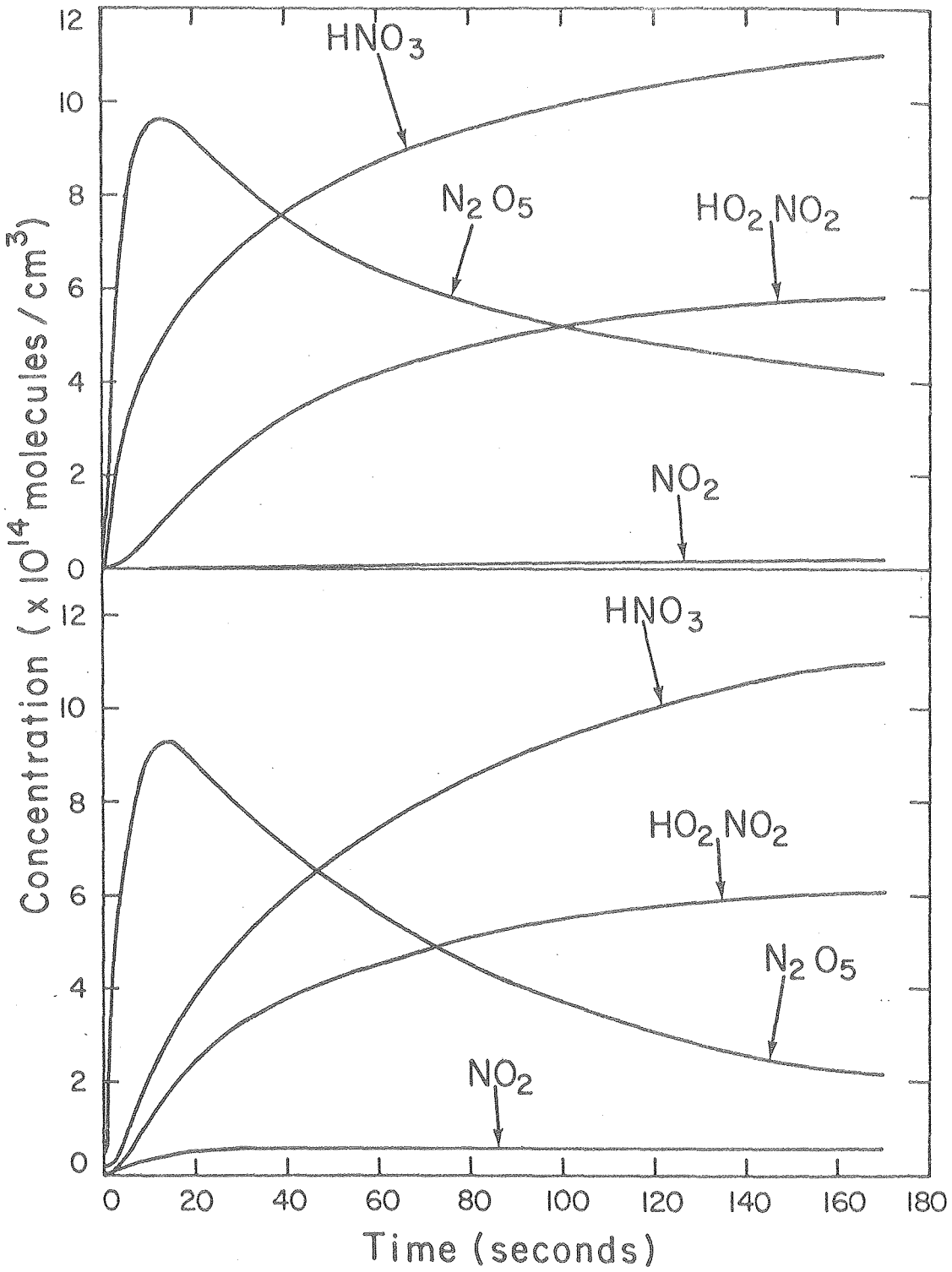

XBL 807-1409

Fig. 41 Simulated (upper) and experimental (lower) profiles of a 263 K expansion

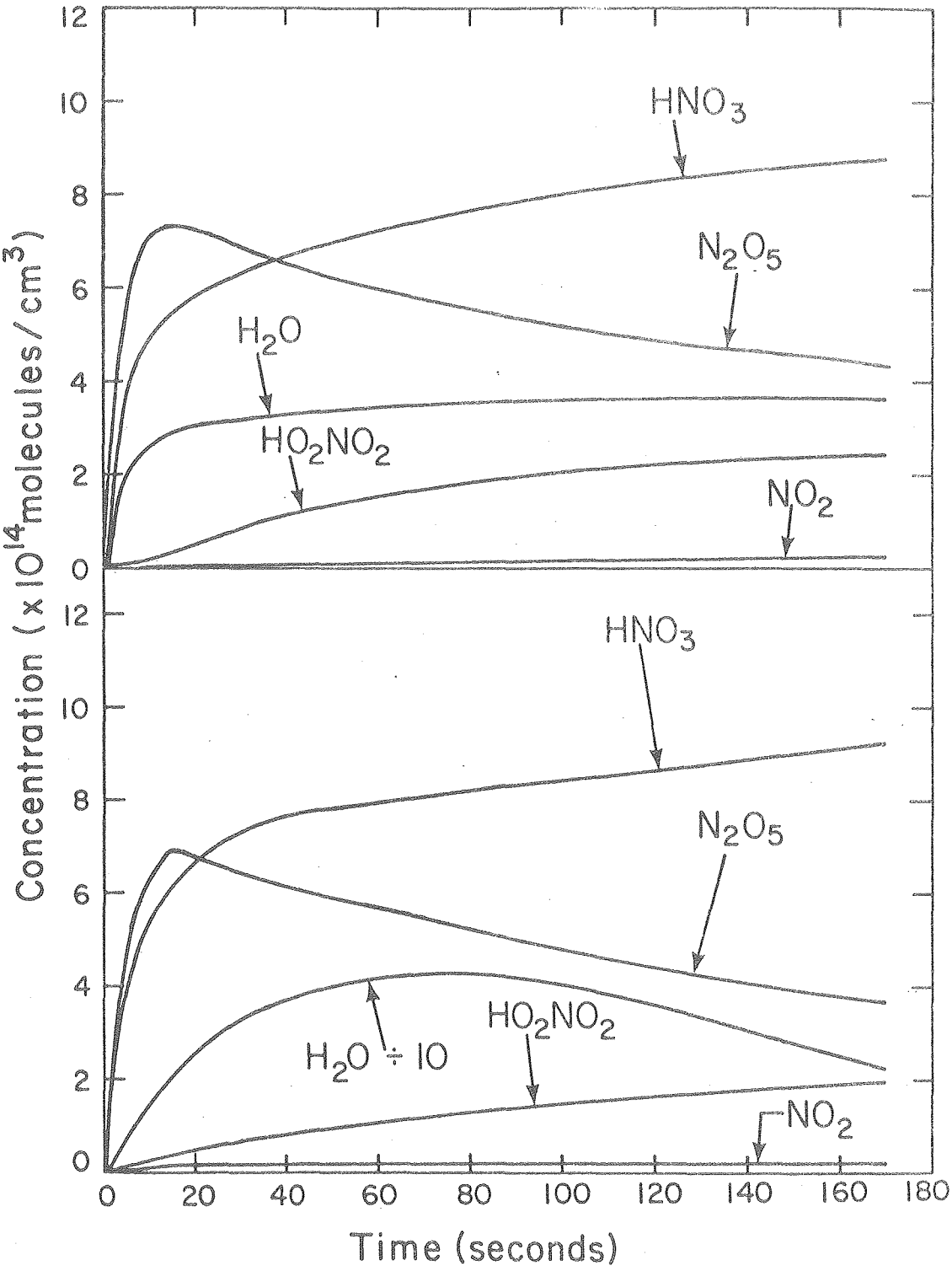

XBL807-1412

Fig. 42 Simulated (upper) and experimental (lower) profiles of a 273 K expansion

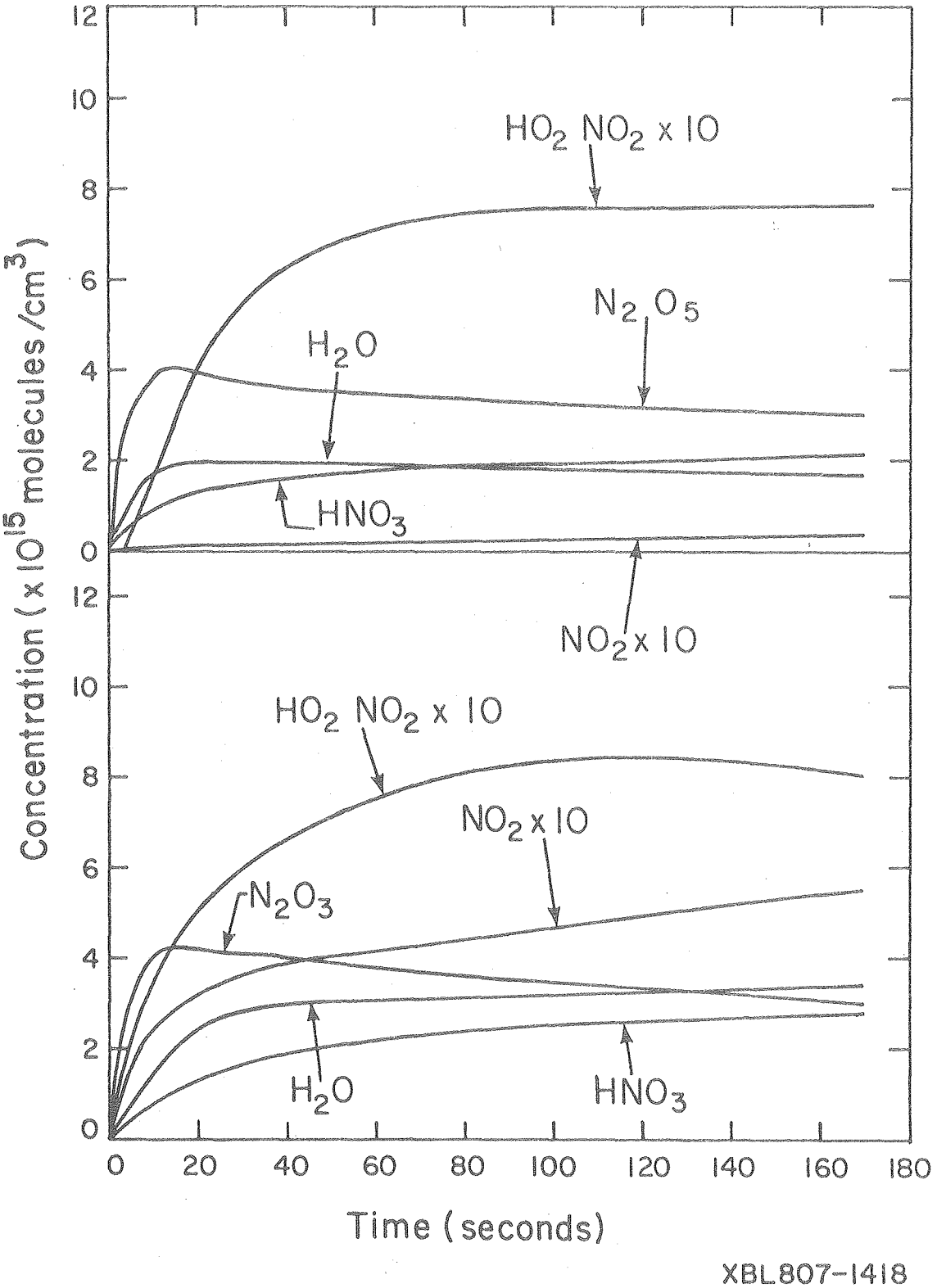

Fig. 43 Simulated (upper) and experimental (lower) profiles of a 283 K expansion

Fig. 44 HNO_4 profiles immediately following expansion of H_2O_2 and N_2O_5 into the cell

Curve	Temperature	$[N_2O_5] \times [H_2O_2]$
A	263 K	7.4×10^{30} molecules^2/cm^6
B	263 K	2.2×10^{30} " "
C	273 K	3.2×10^{30} " "
D	273 K	7.4×10^{30} " "
E	273 K	1.1×10^{30} " "
F	273 K	4.1×10^{30} " "
G	283 K	7.4×10^{30} " "
H	283 K	1.1×10^{30} " "

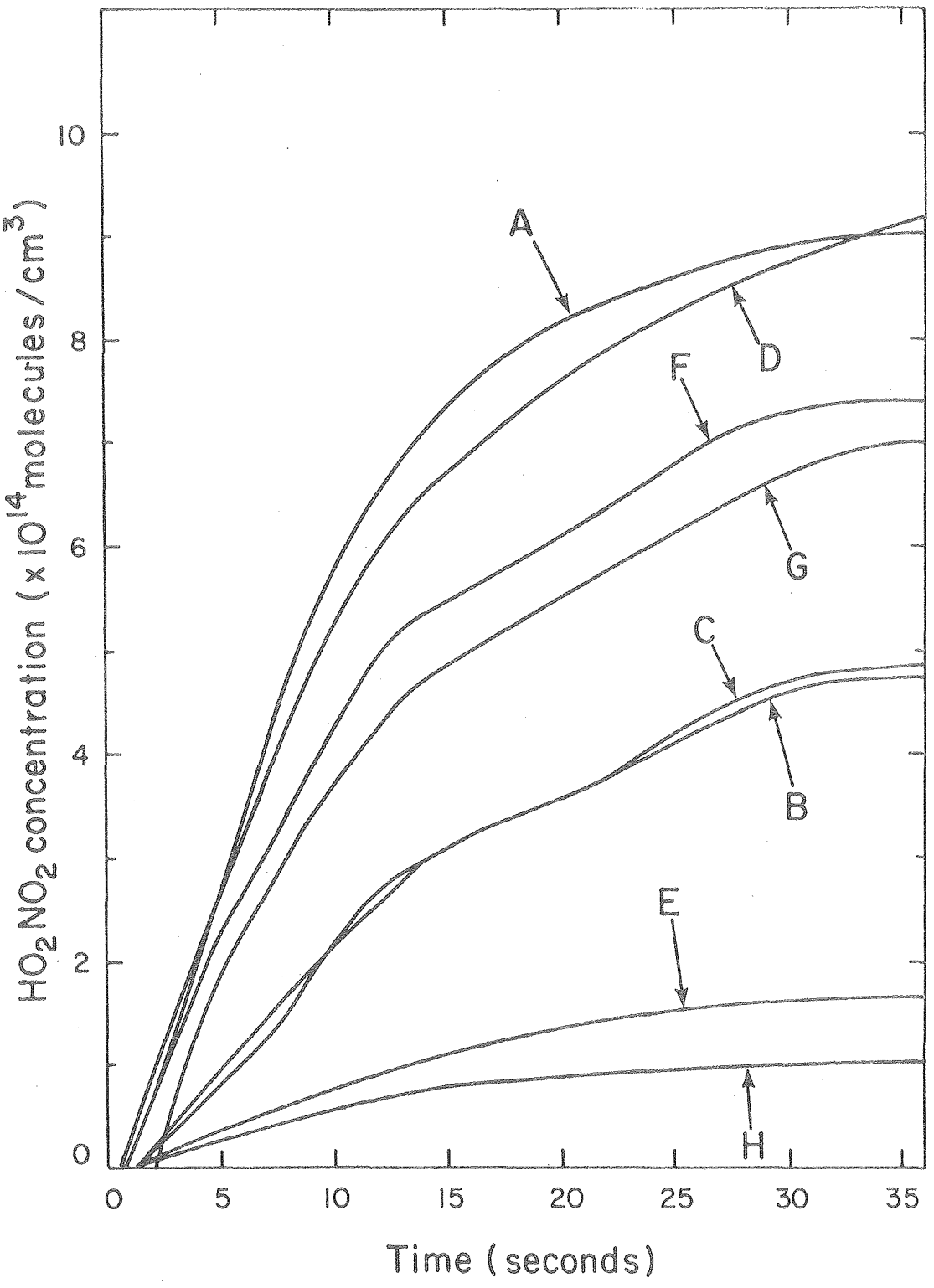

XBL 807-1410

Fig. 44

A	263K	7.4×10^{30}	$molecules^2/cm^6$
B	263K	2.2×10^{30}	" "
C	273K	3.2×10^{30}	" "
D	273K	7.4×10^{30}	" "
E	273K	1.1×10^{30}	" "
F	273K	4.1×10^{30}	" "
G	283K	7.4×10^{30}	" "
H	283K	1.1×10^{30}	" "

Many of the curves exhibit a marked change in slope between 10 and 15 seconds. From equation (55), the HNO_4 concentration at a given time will depend on the rate constant and the product $[H_2O_2]\,[N_2O_5]$. From the curves and the values of $[H_2O_2]\,[N_2O_5]$ listed, the unusual temperature dependence can be seen.

The HNO_4 profiles obtained from computer simulation, equation (55) and experiment are compared in Fig. 45. Curve A is experimentally obtained. Curves C and E are calculated from equation (55) using $k_7 = 5 \times 10^{-18}$ and 1×10^{-17} cm^3/molecule-second, respectively. Curves B and D are from computer simulation using $k_7 = 5 \times 10^{-18}$ and 1×10^{-17} cm^3/molecule-second, respectively. Curve F is the build up of the total gas concentration in the cell divided by 3500. The curves obtained by computer simulation and equation (55) are in good agreement during the period initially following expansion. The other reactions involving HNO_4 become importaant after several seconds and cause the deviation between the curves.

Fig. 45 Calculated and observed concentration profiles following expansion

Curve A - HNO_4, experimental

Curve B - HNO_4, computer simulation

$k_7 = 5 \times 10^{-18}$ cm^3/molecule-second

Curve C - HNO_4, calculated from eqn. (55)

$k_7 = 1 \times 10^{-17}$ cm^3/molecule-second

Curve D - HNO_4, computer simulation

$k_7 = 5 \times 10^{-18}$ cm^3/molecule-second

Curve E - HNO_4, calculated from eq. (55)

$k_7 = 1 \times 10^{-17}$ cm^3/molecule-second

Curve F - total pressure divided by 3500, experimental

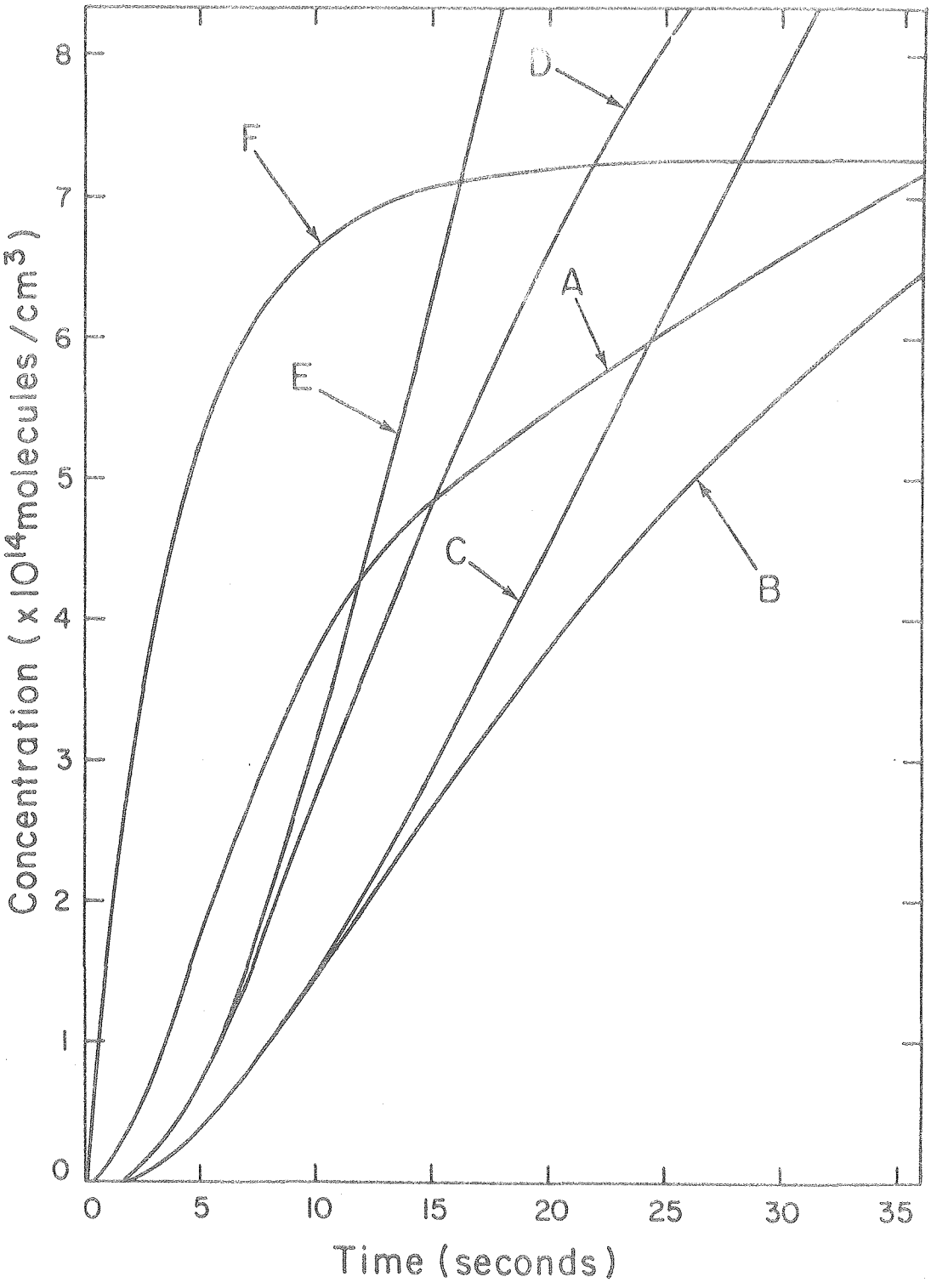

XBL807-1414

Fig. 45

The experimental curve is in poor agreement with all of the calculated curves. It is unlikely that the observed behavior is due to the reactants not cooling until several seconds after expansion. The process of expansion should provide significant cooling and the gases should be adequately prechilled by the lines before mixing. It is also unlikely that heterogeneous decomposition is responsible for the lack of agreement. The computer simulation includes a first order decomposition of HNO_4 ($k = 1 \times 10^{-3}$ second^{-1}) which is used to simulate a heterogeneous decomposition. The rate would have to be much larger to be responsible for the observed behavior. Such a large rate is inconsistent with the behavior of HNO_4 at longer time periods. An estimate of the heterogeneous rate constant can be obtained from the experiments in which NO was present with the reactants. The difference in HNO_4 concentrations in the expansion with and without NO is due to the decomposition of HNO_4 into HO_2 and NO_2. The HO_2 reacts with NO and cannot reform HNO_4. The unimolecular decomposition accounts for part of the loss and the rest is due to heterogeneous decomposition. From computer simulations of these expansions, it is estimated that the HNO_4 heterogeneous rate is 5×10^{-3} second^{-1} or less. This is in the same range as that observed for H_2O_2 and N_2O_5.

It is unlikely that the observed behavior of the HNO_4 build-up is due to HNO_4 reacting with another species in the system. The species present were substantially the same as those present in systems used by other workers who observed no anomalous behavior.

The observed concentrations of HNO_4 following expansion of H_2O_2 and N_2O_5 was used to obtain a value for the rate constant for reaction (7) using equation (55). The results are listed in Table 13 for the runs listed in Tables 7-9 for one to fifteen seconds after expansion. For times shorter than ~10 seconds, there should be < 10 percent error in the calculated rate constant due to complicating reactions. All of the HNO_4 profiles exhibit a decrease in apparent rate constant of reaction (7) with time. The range of rate constants calculated varies widely and does not exhibit any trend with temperature. This type of behavior is highly unlikely in a gas phase bimolecular reaction.

The possibility of reaction (7) occurring by a heterogeneous pathway was investigated by observing the decay of N_2O_5 after expansion into the cell with H_2O_2. Semilog plots of the decay of N_2O_5 are shown in Fig. 46. The solid lines are experimental observations and the dashed line was obtained from a computer simulation. The N_2O_5 concentration was several times lower than that of H_2O_2 in all observations shown. Curvature occurred in the simulated result because N_2O_5 is involved in a number of reactions. The experimental decays exhibit variable decay behavior that is indicative of a heterogeneous reaction. The reaction of N_2O_5 with H_2O_2 is its major loss mechanism.

TABLE 13

263K (Table 7) $[H_2O_2][N_2O_5] = 2.0 \times 10^{30}$ molecules^2/cm^6

Time (seconds)	$[HNO_4]$molecules/cm^3	k_9(eff)cm^3/molecule-second
1	---	---
3	3.0×10^{13}	5.1×10^{-17}
5	7.2×10^{13}	3.5×10^{-17}
7	1.2×10^{14}	2.8×10^{-17}
9	1.7×10^{14}	2.4×10^{-17}
11	2.2×10^{14}	2.1×10^{-17}
13	2.6×10^{14}	1.9×10^{-17}
15	2.8×10^{14}	1.6×10^{-17}

273K (Table 7) $[H_2O_2][N_2O_5] = 1.15 \times 10^{30}$molecules^2/cm^6

Time (seconds)	$[HNO_4]$molecules/cm^3	k_9(eff)cm^3/molecule-second
1	---	---
3	1.9×10^{13}	5.7×10^{-17}
5	3.8×10^{13}	3.2×10^{-17}
7	5.4×10^{13}	2.2×10^{-17}
9	7.2×10^{13}	1.7×10^{-17}
11	8.6×10^{13}	1.4×10^{-17}
13	9.2×10^{13}	1.2×10^{-17}
15	1.1×10^{14}	1.1×10^{-17}

273K (Table 7) $[H_2O_2][N_2O_5] = 1.1 \times 10^{30}$ molecules^2/cm^6

Time (seconds)	$[HNO_4]$molecules/cm^3	k_9(eff)cm^3/molecule-second
1	4.5×10^{12}	2.7×10^{-16}
3	2.0×10^{13}	6.1×10^{-17}
5	2.8×10^{13}	2.5×10^{-17}
7	4.3×10^{13}	1.8×10^{-17}
9	4.4×10^{13}	1.1×10^{-17}
11	6.0×10^{13}	1.0×10^{-17}
13	7.3×10^{13}	9.5×10^{-18}
15	7.1×10^{13}	7.4×10^{-18}

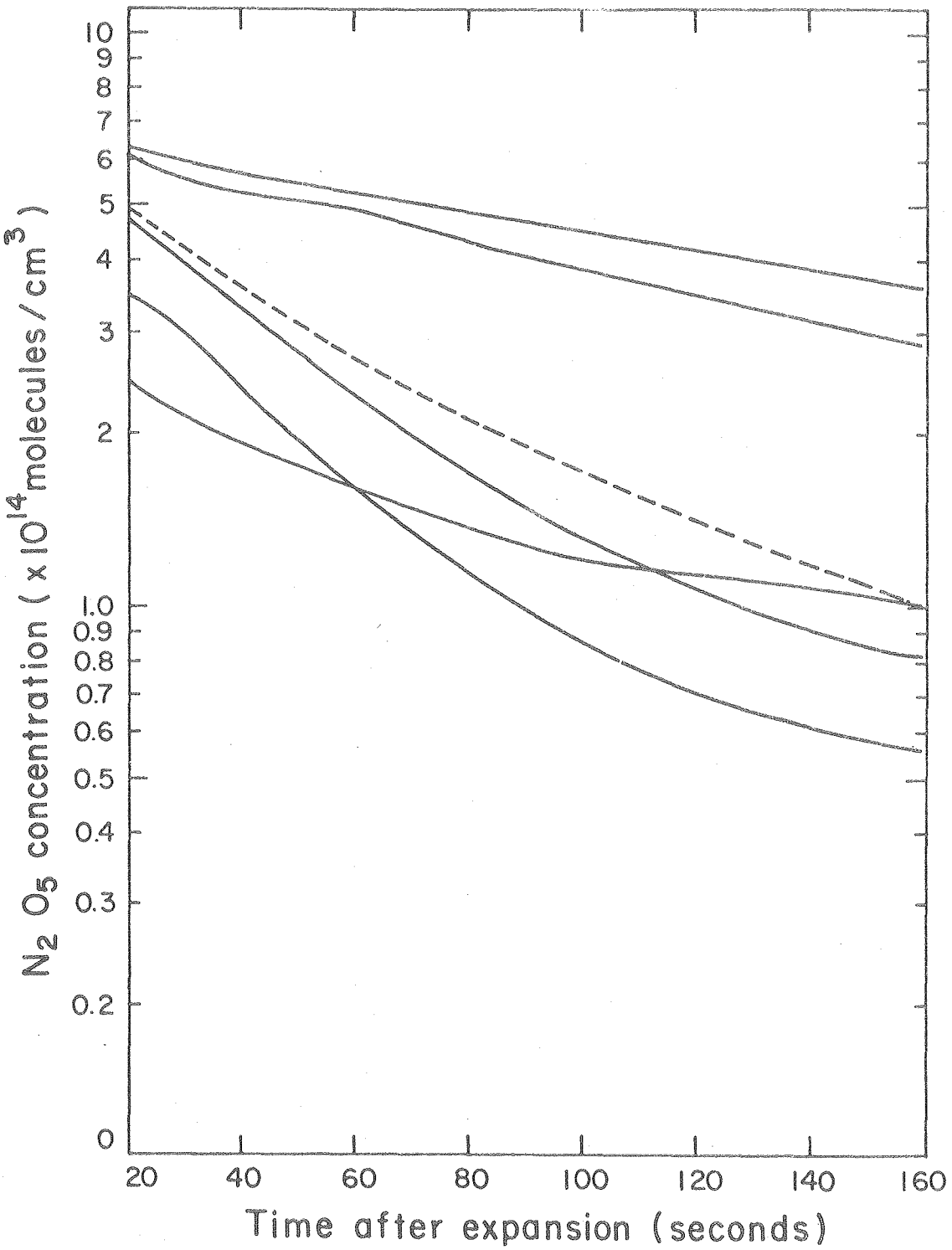

XBL807-1415

Fig. 46 Experimental and simulated N_2O_5 profiles after expansion

The data taken with the additional surface in the cell were somewhat noisy but indicate that the HNO_4 decay rate is larger when more surface is present. The increased surface did not increase the apparent rate of reaction (7) suggesting that the reaction may be occurring primarily on the metal end caps. An alternative explanation is that there is increased heterogeneous decomposition of the reactants, preventing an increase in the products of reaction (7).

The results of the investigation of the reaction of H_2O_2 and N_2O_5 indicate the reaction forms primarily HNO_3 and HNO_4 as reaction products. The reaction is predominantly heterogeneous in the reaction system used to study it. The evidence for this comes from the reactant concentration effects, the temperature and pressure dependence and the characteristics of the initial build-up of HNO_4. The unusual behavior of the HNO_4 dependence on H_2O_2 concentration is not what would be expected from a homogeneous reaction. The increasing apparent rate constant with decreasing temperature also suggests a heterogeneous mechanism. The H_2O_2 heterogeneous decay exhibits an increase in rate at lower temperatures. Both reactions could be related to the tendency of H_2O_2 to adhere to surfaces at low temperatures. The appearance of HNO_4 when N_2O_5 was expanded into an evacuated cell previously exposed to H_2O_2 at 253K supports this contention.

The variable behavior of the initial build-up of HNO_4 and the variability of the N_2O_5 decay in the presence of excess H_2O_2 also indicate the occurrence of a heterogeneous process. The results of expansions with extra surface in the cell does not disagree with this.

With the exception of the production of HNO_4, the chemistry of the H_2O_2-N_2O_5 system was adequately modeled by computer simulation, indicating the kinetics of the system are reasonably well-known.

Some further information that can be obtained from these studies is related to the relative rates of reactions (1) and (2). The HNO_4 formed by the reaction of H_2O_2 and N_2O_5 will undergo unimolecular, and possibly heterogeneous, decomposition to form HO_2 and NO_2. These species can react to form either of the products in (1) or (2).

Levine et al.[12] obtained a ratio of k_2/k_1 of 0.7 ± 0.4 at 1 atmosphere total pressure and at 298K. Graham et al.[4] obtained $k_2/k_1 < 0.001$ at 1 atmosphere and at temperatures from 254 to 283K. Howard[16] obtained an upper limit for k_2 of 3×10^{-15} cm^3/ molecule-second and a ratio of $k_2/k_1 < 0.15$ a 3 torr and 298K.

Scans through the regions where HONO absorbs following expansion of H_2O_2 and N_2O_5 indicated no detectable absorption by HONO with a detection sensitivity of $< 3 \times 10^{13}$ molecules/cm^3. These expansions were done at 263K and final pressures of 30 to 70 torr. From computer simulations, the upper limit for k_2 is 5×10^{-14} cm^2/molecule-second. Using the equation of Graham et al.[4] for k_1, an upper limit of $k_2/k_1 < 0.05$ is obtained for 263K and 30 torr.

CHAPTER V. The Reaction of OH + HNO_4

A. Experimental Procedures and Data

1. Reaction System for the Investigation of OH + HNO_4

Any chemical system used to investigate the reaction of OH with HNO_4 will be complicated. All useful methods of preparation of HNO_4 in the gas phase contain impurities, and not all methods are capable of generating HNO_4 concentrations large enough to be easily observed using infrared techniques. HNO_4, as well as some of the impurities, undergo heterogeneous reactions, ruling out the use of a static system for this study.

Not all of the preparation methods are capable of generating steady flows of HNO_4. The preparation used is the reaction of N_2O_5 with H_2O_2, which is primarily heterogeneous in the apparatus used. Attempts were made to use the preparative method for HNO_4 developed by the group at SRI.[23] Flowing the evolved gases into the cell yielded little or no HNO_4, as determined by infrared absorption. Any attempt to increase the amount of evolved HNO_4 from the preparation would produce violent bubbling, culminating in a pressure explosion.[97] This technique was abandoned in favor of the H_2O_2-N_2O_5 preparation method.

Stable flows of H_2O_2 and N_2O_5 were produced by passing "high dry" grade nitrogen through temperature-controlled saturators containing N_2O_5 and H_2O_2. The nitrogen was passed through a silica gel trap immersed in an isopropanol-dry ice slush bath prior to entry into the N_2O_5 saturator

N_2O_5 saturator to minimize production of HNO_3 by the heterogeneous reaction of N_2O_5 with H_2O in the carrier gas. The flows of H_2O_2 and N_2O_5 were mixed outside the cell. The combined flows were flowed through one of disperser tubes into the cell. Nitrogen was added at the mixing region to dilute the concentrations of the reactants and to generate the desired flow rate. The flow passed out of the cell through the other disperser tube and was exhausted into a fume hood. The flow rates were monitored with calibrated flow meters.

HNO_4 concentrations in excess of 2×10^{15} molecules/cm^3 were generated in this way. Higher concentrations probably could have been generated by increasing the concentrations of the reactants, although no attempt was made to do so. The HNO_4 concentrations appeared to be quite stable with time, with less than 5 percent variation over a period of several hours. The major impurities, besides the unreacted reactants, were HNO_3, H_2O and NO_2. HNO_3 is produced by the reaction of H_2O_2 and N_2O_5, as well as being an impurity in N_2O_5 and a product of the primarily heterogeneous reaction of H_2O and N_2O_5. H_2O is a product of the heterogeneous decomposition of H_2O_2. NO_2 is a decomposition product of N_2O_5 and HNO_4.

OH was generated by a multi-step process initiated by the photolysis of NO_2.

$$\begin{aligned} NO_2 + h\nu &\rightarrow NO + O \\ O + NO_2 &\rightarrow NO + O_2 \\ 2x(HNO_4 + M &\rightleftarrows HO_2 + NO_2 + M) \\ 2x(NO + HO_2 &\rightarrow OH + NO_2) \\ \text{net: } 2HNO_4 + h\nu &\rightarrow 2OH + 2NO_2 + O_2 \end{aligned} \qquad (56)$$

Black lamps were used as the light source for photolysis. The output of the lamps (Fig. 7) provides good overlap with the near UV NO_2 absorption band. The other compounds absorb only weakly in this region, minimizing the effect of interference by their photolysis products.

To minimize the effect of heterogeneous reactions on the kinetics of the system, the black lamps were turned on and off periodically to induce periodic changes in the concentrations of the intermediates such as NO, O and OH. The fluctuations in the intermediates will induce changes in the concentrations of the reactants and products which can be observed by infrared absorption. The technique of molecular modulation[98] is based on this concept.

In the absence of interfering reactions, the reactions that will occur following the reactions in (56) will depend on the competition for OH by various species in he system. If $OH + NO_2 + M$ is faster than other OH reactions and NO_2 is present in large amounts,

$$\begin{aligned} 2HNO_4 + h\nu &\rightarrow 2OH + 2NO_2 + O_2 \\ 2x(OH + NO + M &\rightarrow HNO_3 + M) \\ \text{net:}\quad 2HNO_4 + h\nu &\rightarrow 2HNO_3 + O_2 \end{aligned} \qquad (57a)$$

will occur. If almost all of the OH is consumed by reaction with HNO_4, then the following scheme will occur.

$$\begin{aligned} 2HNO_4 + h\nu &\rightarrow 2OH + 2NO_2 + O_2 \\ 2x(OH + HNO_4 &\rightarrow H_2O + NO_2 + O_2) \\ \text{net:}\quad 4HNO_4 + h\nu &\rightarrow 4NO_2 + 2H_2O + 3O_2 \end{aligned} \qquad (57b)$$

These extreme cases indicate the effect of the relative rates of reaction of OH with NO_2 and HNO_4.

If OH reacts primarily with NO_2, considerable amounts of HNO_3 should be generated. The quantum yield for HNO_4 destruction should be two, and the concentration of NO_2 should not change as the lamps are turned on and off.

If OH reacts primarily with HNO_4, no HNO_3 should be generated. The quantum yield for HNO_4 destruction should be twice as high as in the previous situation. Production of NO_2 would occur while the lamps are on, and the amount of NO_2 produced should equal the amount of HNO_4 destroyed.

The actual situation is likely to be intermediate between these two extremes. The relative amounts of HNO_3 and NO_2 produced should provide an indication of the rate of $OH + HNO_4$ relative to the rate of $OH + NO_2 + M$.

The presence of N_2O_5 and H_2O_2 will complicate the chemistry, as they can generate reaction cycles that consume NO_2 but do not involve HNO_4.

$$NO_2 + h\nu \rightarrow NO + O$$
$$O + NO_2 \rightarrow NO + O_2$$
$$2x(N_2O_5 \xrightarrow{M} NO_2 + NO_3)$$
$$2x(NO + NO_3 \rightarrow NO_2 + NO_2)$$
$$\text{net: } 2N_2O_5 + h\nu \rightarrow 4NO_2 + O_2$$

$$NO_2 + h\nu \rightarrow NO + O$$
$$O + NO_2 \rightarrow NO + O_2$$
$$2x(NO + HO_2 \rightarrow HO + NO_2)$$
$$2x(OH + H_2O_2 \rightarrow H_2O + HO_2)$$
$$\text{net: } 2H_2O_2 + h\nu \rightarrow 2H_2O + O_2$$

The chemistry of the system becomes more complicated as these cycles are taken into consideration. The important gas phase reactions for this system are listed in Table 14. The number of OH radicals produced per photon will be reduced due to the reactions competing for the consumption of oxygen atoms and NO. Once OH is produced it may react with either NO_2, HNO_4, H_2O_2 or HNO_3. The branching that occurs here will have an effect on the amplitudes of the concentration fluctuations observed as the lamps are turned on and off.

There are a number of heterogeneous reactions that occur in the system. HNO_4 and H_2O_2 decompose on the cell walls. A number of the heterogeneous reactions discussed previously and elsewhere[59-62,92]

TABLE 14

1	$OH + HNO_4 \rightarrow H_2O + NO_2 + O_2$
2	$O + NO_2 \rightarrow NO + O$
3	$O + NO \xrightarrow{M} NO_3$
4	$O + NO \xrightarrow{M} NO_2$
5	$NO + HO_2 \rightarrow HO + NO_2$
6	$NO + NO_3 \rightarrow NO_2 + NO_2$
7f,7r	$N_2O_5 \overset{M}{\rightleftharpoons} NO_2 + NO_3$
8f,8r	$HNO_4 \overset{M}{\rightleftharpoons} HO_2 + NO_2$
9	$NO_2 + NO_3 \rightarrow NO + NO_2 + O_2$
10	$HO_2 + HO_2 \rightarrow H_2O_2 + O_2$
11	$OH + NO_2 \xrightarrow{M} HNO_3$
12	$OH + HNO_4 \rightarrow H_2O + NO_2 + O_2$
13	$OH + H_2O_2 \rightarrow H_2O + HO_2$
14	$OH + HNO_3 \rightarrow H_2O + NO_3$

could occur in the system as well. With the exception of NO, the concentration of none of the species involved in the reactions varies strongly with the lamp output. The heterogeneous reaction of NO with H_2O_2 appears to be slow,[62] and consequently is unimportant in this system. The rates of the other heterogeneous reactions should not be strongly affected by presence or absence of the photolytic light. Thus, the observed fluctuations in the concentrations of the species monitored should not be influenced by heterogeneous reactions that may occur.

2. Experimental Technique

There are a number of three body reactions that are of importance in this system. The pressure regime in which the experiments are done will strongly affect the kinetics of the system. At one atmosphere pressure, reaction (3) in Table 14 will compete with reaction (2) in Table 14 for oxygen atoms and reduce the amount of NO produced, as well as generate more NO_3. The net effect will be that fewer OH radicals will be produced at one atmosphere pressure than at lower pressures. The reaction rate of reaction (11) (Table 14) is fast at one atmosphere pressure and, in most cases, will be a major loss term for OH in the system. At lower pressures, however, the equilibria between $HNO_4 \rightleftharpoons HO_2 + NO_2$ and $N_2O_5 \rightleftharpoons NO_2 + NO_3$ will be slower than they would be at one atmosphere.

It was decided to operate at one atmosphere pressure for these experiments. There is less diffusion to the walls, reducing the effect of heterogeneous reactions. The infrared cross sections of NO_2, H_2O_2 and H_2O are larger at one atmosphere, making these species

easier to monitor. The flows of the reactants and carrier gas are easier to control and stabilize at one atmosphere than at lower pressures. The HNO_4 and N_2O_5 equilibria will be faster, making the equilibria more useful for predicting HO_2 and NO_2 concentrations.

The experiments were done at 263 K, 273 K and 283 K. Limitations on the temperature range that could be studied were imposed by the black lamps and by the kinetics of the system. The output of the lamps decreases with temperature. The amplitudes of the fluctuations induced by the lamps is proportional to the lamp output, and below 263 K, the fluctuations would be difficult to detect and would require extensive averaging. At temperatures above 283 K, the ratio of NO_2 to HNO_4 becomes large enough that virtually all of the OH will react with NO_2. The NO_2 concentration must be kept low enough such that not all the OH will react by reaction (11) (Table 14). It must be large enough to generate a detectable signal when the lamps are turned on and off. The amplitude of the fluctuations induced by the lamps will be proportional to the amount of NO_2, as well as the light intensity.

The experiments were performed by producing stable flows of N_2O_5, H_2O_2, and N_2 carrier gas through the cell. The concentrations of HNO_3, HNO_4, H_2O_2, H_2O, N_2O_5 and NO_2 were monitored first without and then with the photolytic lamps turned on. If necessary, the flow rates were adjusted so there was sufficient HNO_4 present and that the NO_2/HNO_4 ratio was not too large. In addition, neither of the reactants could be in large excess because they would dominate the chemistry by the cycles mentioned above.

Once the desired flow had been obtained, the lamps were turned on and off periodically by a stable low frequency square wave source driving the lamp flasher. Early experiments were done using molecular modulation techniques to obtain phase and amplitude information for each specie observed. With lamp flashing frequencies in the range of 0.06 to 1.0 Hz, the amplitudes were too small to be observed without excessively long averaging periods, with the exception of NO_2. The technique was abandoned in favor of directly observing the optical density fluctuation of each specie as the lamps were turned on and off at a very low frequency.

These experiments were done by flowing the reactants and carrier gas through the cell with the lamps flashing with a period of 480 seconds. At this frequency, concentrations changed sufficiently to be observed by conventional infrared spectroscopy. After the concentrations had stabilized, each specie of interest was observed in sequence. The monochromator was set to a wavelength on an absorption band of the molecule to be monitored. The transmitted light intensity was converted to voltage and fed into the Fabritek signal averager for storage. The signal was monitored for eight lamp flashing cycles. The process was repeated for all the compounds to be observed. The wavelengths to monitor concentrations are as follows:

NO_2	6.258 μm	H_2O_2	7.896 μm
H_2O	6.634 μm	N_2O_5	8.040 μm
HNO_3	7.400 μm	HNO_4	12.315 μm

The transmitted light intensities are recorded before and after each experiment with the cell evacuated and filled with one atmosphere of carrier gas. These values are used to calculate the optical density at each wavelength. The wavelengths at which H_2O_2 and N_2O_5 were monitored overlapped with other absorptions. H_2O_2 was monitored on its Q branch, which overlapped with HNO_3, N_2O_5 and HNO_4. The wavelength at which N_2O_5 was monitored contains an absorption due to H_2O_2. The cross sections of N_2O_5, HNO_3 and HNO_4 at 7.896 μm were determined relative to the wavelengths at which they were monitored. The contribution due to HNO_3 and HNO_4 was subtracted from the observed optical density at 7.896 μm. The resulting curve was stored. The contribution to this curve by N_2O_5 was fairly small; so, the uncorrected 8.040 μm curve was used to subtract out the N_2O_5 contribution. The 7.896 μm curve was then used to correct the 8.040 μm curve. The corrected 8.040 μm represents only N_2O_5 and was used to make the final correction to the 7.896 μm curve which was stored earlier.

The optical density curves are summed over the eight lamp periods to reduced noise and eliminate small random fluctuations in concentrations. The optical density curves are converted into concentrations by using the cross sections determined earlier. Cross sections for the curves obtained at 273 K and 283 K were obtained by interpolating between the values obtained at 263 K and 293 K. A least squares linear regression program is used to obtain slopes of the curves for each quarter and half of the lamp period. In a few cases, the curve exhibited a net upward or downward slope due to a small increase or

decrease in concentration during the course of the run. This was corrected for by adjusting the net slope of the curve to zero. The rate of change of the curves was small, ranging from somewhat larger than 10^{11} molecules/cm^3-second to less than 10^9 molecules/cm^3-second. The concentrations of the species observed were in the range of about 10^{13} to 10^{15} molecules/cm^3.

3. Actinometry

The light intensity produced by the black lamps must be known accurately in order to analyze the observed behavior of the species in the reaction system. The light intensity will directly affect the amount of NO generated and consequently it will be related to the amount of OH produced. The emitted light will primarily photolyze NO_2, although the long wavelength tails of the UV absorptions of N_2O_5, H_2O_2, HNO_4 and HNO_3 overlap slightly with the black lamp output.

The light intensities were determined by photolyzing NO_2 in one atmosphere of N_2 at 283 K, 273 K and 263 K, and observing the decay of NO_2 at 6.258 μm. Three types of measurements were made. In the first two measurements, a bulb was filled with a measured pressure of NO_2 and then expanded into the evacuated cell. Nitrogen was added to one atmosphere pressure. In the first type of measurement, the NO_2 profile was recorded in the Fabritek signal averager while the lamps were on at a constant current. In the second type of measurement, the lamps were turned on and off with a period of 480 seconds while the NO_2 profile was recorded in the Fabritek.

The third type of measurement invoved flowing NO_2 in one atmosphere of nitrogen while the lamps were turned on and off periodically. The fluctuation in NO_2 concentration was again monitored with the Fabritek. The NO_2 profile was analyzed in the same manner as the profiles obtained from the H_2O_2-N_2O_5 flow experiments.

The observed decays were analyzed by comparing them with computer simulations with different light intensities using the CHEMK kinetics computer program. An average near-UV cross section of 4.8×10^{-19} cm^2/molecule was used for NO_2 in the simulations. This was derived from the product of the corrected lamp spectrum and the NO_2 UV absorption spectrum at one nm intervals, which were then summed for λ = 290 to 460 nm and divided by the integrated lamp spectrum. Any error in the value of the average NO_2 cross section will be compensated by the calculated light intensity, since the product of the cross section and the light intensity determines the number of molecules photolyzed.

Similar calculations were done for N_2O_5, H_2O_2, HNO_4 and HNO_3 to determine how significant the photolysis of these species was. The photolysis rates of all of these compounds were less than 0.5 percent of the photolysis rate of NO_2.

The light intensities derived from the second and third types of measurements were in good agreement, being within 10 percent of each other. The light intensity obtained from the first type of measurement was somewhat higher. This was due to the type of source activating the lamp driver. A lower current was supplied by the very low

frequency generator than that supplied for the dc experiments. Thus, the lamps had greater output during the dc runs.

There was a tendency for the lamp intensity to decrease slightly during the course of an experiment. During the four minute period for lamps were on, the drift in the output was generally less than ±3 percent of the average. The lamps do exhibit an initial output spike when first turned on.

Since the second and third types of actinometry measurements more closely simulate the experimental conditions, the light intensity values obtained from these runs were used in the analysis of the results. The light intensities at each temperature were:

263 K	0.5×10^{15}	photons/cm^2-second
273 K	1.0×10^{15}	" " "
283 K	2.5×10^{15}	" " "

B. Results and Discussion

The observed concentration profiles of NO_2, HNO_4, HNO_3, N_2O_5 and H_2O_2 provide a basis with which the rate constant for the reaction of OH with HNO_4 can be determined. The profiles can also provide information on the products of this reaction. Typical experimental profiles of the observed species are illustrated in Fig. 47 (from run F). NO_2 and HNO_4 generally had the largest fluctuations in concentration. The lamps were on during the first half of the run, and off during the second half of the run. The run shown was done at 283 K.

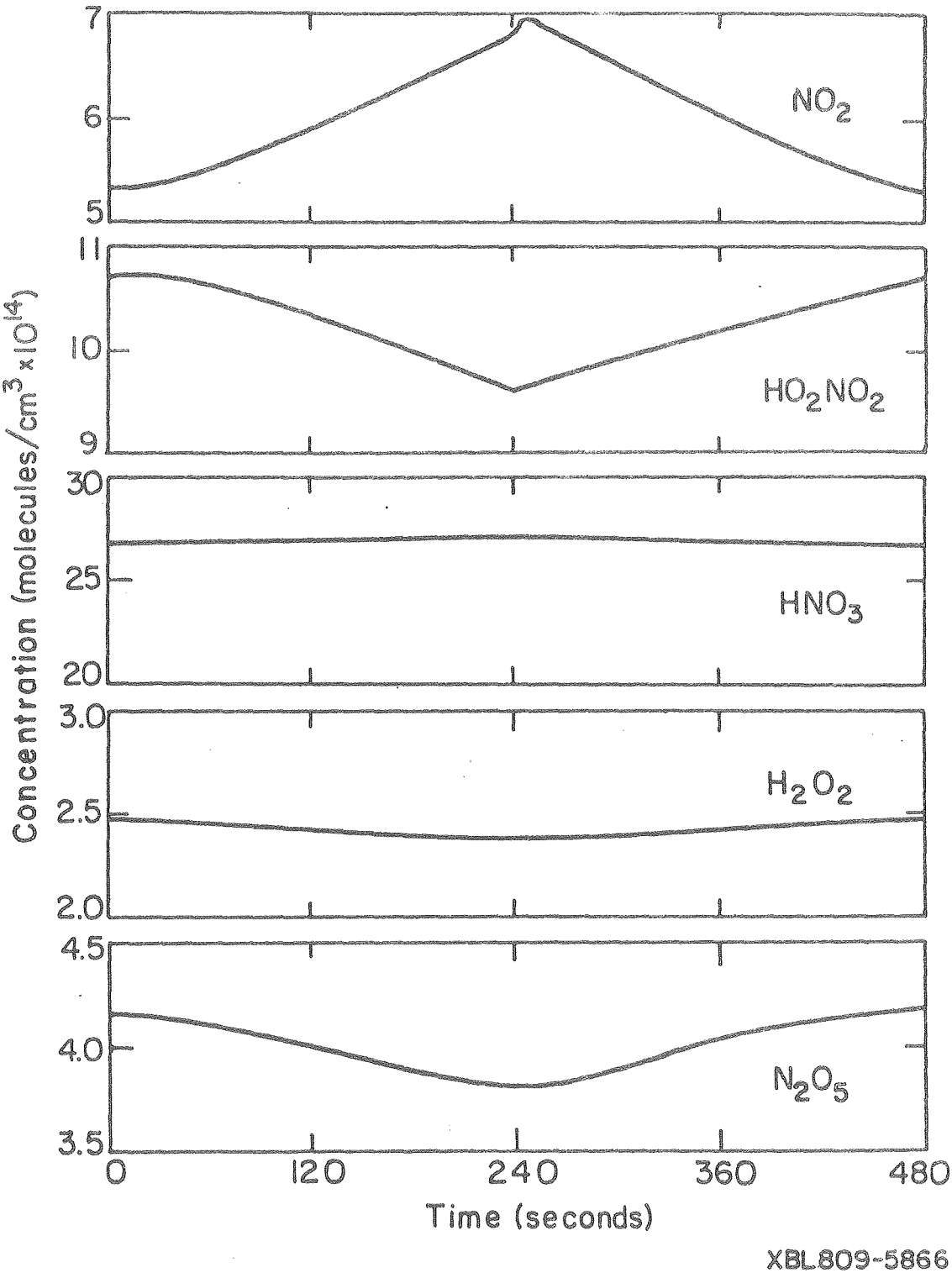

Fig. 47 Concentration profiles during one lamp cycle, starting when the lamps are turned on.

The concentrations of NO_2, HNO_4, HNO_3, H_2O_2 and N_2O_5 for the seven runs used in the analysis are listed in Table 15. The average slopes of the concentration profiles for the half cycle during which the lamps were on were obtained by a linear regression program run in the PDP-8/ℓ minicomputer interfaced to the Fabritek. The experimentally derived slopes for all the runs are listed in Table 16 with the standard deviations from the least square fit analysis. Actual uncertainties may be larger in some cases. This is due to errors in the correction for spectral overlap, and correction for drift in concentration during a run.

To be able to develop a value for the rate constant of the reaction of OH with HNO_4, a method must be devised to analyze the slopes in terms of the rate constant. Analytic expressions for the chemical system are difficult to generate because of its complexity and the large fluctuations in concentrations of the intermediates, particularly NO, O, and OH. Use of the steady-state approximation is unlikely to be valid for these three intermediates.

Another difficulty is the occurrence of heterogeneous reactions in the system. These reactions can affect the concentrations of a number of the observed species. The use of light modulated at a low frequency should reduce their influence, since the heterogeneous rates should not be influenced by the presence or absence of light. An exception to this are heterogeneous reactions involving NO, since the NO concentration is closely coupled to the light output.

TABLE 15

concentrations in molecules/cm^3

	NO_2	HNO_4	HNO_3	H_2O_2	N_2O_5
263K					
Run A	1.6×10^{14}	1.8×10^{15}	3.0×10^{15}	7.2×10^{14}	5.5×10^{13}
273K					
Run B	1.7×10^{14}	1.5×10^{15}	2.7×10^{15}	1.0×10^{15}	1.7×10^{14}
Run C	9.3×10^{13}	7.0×10^{14}	1.4×10^{15}	2.4×10^{15}	6.4×10^{13}
Run D	1.7×10^{14}	7.9×10^{14}	1.5×10^{15}	5.3×10^{14}	1.2×10^{14}
283K					
Run E	1.6×10^{14}	8.1×10^{14}	1.7×10^{15}	2.4×10^{15}	1.6×10^{14}
Run F	6.0×10^{14}	1.0×10^{15}	2.7×10^{15}	2.1×10^{14}	4.2×10^{14}
Run G	3.5×10^{14}	6.0×10^{14}	1.6×10^{15}	4.8×10^{14}	1.4×10^{14}

TABLE 16

Slopes in units of molecules/cm^3-second

	NO_2	HNO_4	HNO	H_2O_2	N_2O_5
263K					
Run A	$2.9 \pm 0.4 \times 10^{10}$	$-3.8 \pm 0.6 \times 10^{10}$	$-1.3 \pm 1.3 \times 10^{9}$	$-3.5 \pm 2.0 \times 10^{9}$	$1.5 \pm 1.0 \times 10^{9}$
273K					
Run B	$7.9 \pm 0.2 \times 10^{10}$	$-7.6 \pm 0.5 \times 10^{10}$	$1.0 \pm 1.0 \times 10^{10}$	$-2.0 \pm 0.5 \times 10^{10}$	$-0.5 \pm 4.0 \times 10^{9}$
Run C	$2.7 \pm 0.2 \times 10^{10}$	$-4.3 \pm 0.5 \times 10^{10}$	$-3.5 \pm 5.0 \times 10^{10}$	$-4.8 \pm 0.5 \times 10^{10}$	$-2.5 \pm 2.0 \times 10^{9}$
Run D	$6.5 \pm 0.6 \times 10^{10}$	$-7.6 \pm 0.8 \times 10^{10}$	$-2.2 \pm 2.0 \times 10^{10}$	$4.3 \pm 4.0 \times 10^{9}$	$-4.5 \pm 2.0 \times 10^{9}$
283K					
Run D	$1.6 \pm 0.1 \times 10^{11}$	$-1.6 \pm 0.2 \times 10^{11}$	$2.5 \pm 2.5 \times 10^{10}$	$-1.0 \pm 0.2 \times 10^{10}$	$-9.0 \pm 0.4 \times 10^{10}$
Run F	$6.6 \pm 0.2 \times 10^{11}$	$-4.7 \pm 0.2 \times 10^{11}$	$4.4 \pm 1.0 \times 10^{10}$	$-3.4 \pm 0.2 \times 10^{10}$	$-1.6 \pm 0.2 \times 10^{11}$
Run G	$3.6 \pm 0.2 \times 10^{11}$	$-3.0 \pm 0.2 \times 10^{11}$	$5.0 \pm 2.0 \times 10^{10}$	$-5.7 \pm 0.4 \times 10^{10}$	$-7.9 \pm 0.2 \times 10^{10}$

An alternative to deriving an analytic expression for the rate constant can be developed by tracing the destruction channels for intermediates after they are produced. A fairly simple mechanism can be developed, although the assumptions used to generate it may not be entirely valid.

The initial step of the system is the photolysis of NO_2, reaction 1 in Table 14. The O atom will react primarily with NO_2 to form the products NO + O_2 (reaction 2) or NO_3 (reaction 3). The relative rates of these reactions are known for one atmosphere pressure. The NO produced here will react with either HO_2 or NO_3. The HO_2 can be considered to come from the decomposition of HNO_4. The NO_3 can be considered to come from either reaction 3 or from N_2O_5 decomposition. The equilibrium constants for HNO_4 and N_2O_5 can be used to predict the relative concentrations of NO_3 and HO_2 from the observed concentrations of N_2O_5, HNO_4 and NO_2. These values, in turn can be used to calculate the relative rates of reactions (5) and (6) in Table 14, which determines the fraction of NO converted to OH.

If the assumptions made so far are valid, the number of OH radicals produced per photon absorbed can be determined, as well as the amount of formation or destruction of NO_2, HNO_4 and N_2O_5. The OH produced will be consumed by reactions (11)-(14) in Table 14. With the exception of reaction (12), the rate constants for these reactions are known. The relative rates of consumption of OH by these reactions will have an effect on the rate of change in concentration of NO_2, HNO_3, HNO_4 and H_2O_2. If the rate constant for OH + HNO_4 is small, most

of the OH will react with NO_2 and H_2O_2. NO_2 production will be small, HNO_3 production large, and HNO_4 destruction small when the lights are on. If the rate constant is large, HNO_4 can effectively compete with NO_2 and H_2O_2 for OH. This will increase NO_2 production, decrease HNO_3 production, and increase HNO_4 destruction during illumination of the system.

This simplifed mechanism ignores a number of somewhat slower reactions, the flow-in and flow-out of all the species involved and assumes that HO_2 and NO_3 remain in equilibrium with NO_2, and HNO_4 and N_2O_5, respectively. It does qualitatively illustrate the behavior of the system and its dependence on the rate constant of OH with HNO_4. The use of the equilibria of reactions (8) and (9) in Table 14 to determine HO_2 and NO_3 concentrations is not likely to be valid at low temperatures, where the forward and reverse rates will be slow. The flow out of intermediates can be an important factor in the determination of their concentration. This is particularly true for NO.

Since the observed rates of change of concentrations when the lamps are on are in the range of 10^{-4} to 10^{-6} of the total concentration per second, fairly small production or destruction terms can significantly affect the observed result. To be able to quantitatively predict the rate of change of the observed species, and consequently obtain a value of the rate constant for reaction (12) in Table 14, a method is needed to accurately determine the behavior of all of the important species in the chemical system. The CHEMK chemical kinetics computer program described previously was used for this purpose.

The list of reactions and rate constants used for modeling the chemical system used in this study is included in Appendix C. Inputs into the program included temperature, light intensity and lamp flashing period. The flow-in rates of NO_2, HNO_4, HNO_3, H_2O_2 and N_2O_5 were adjusted until the calculated concentrations agreed with the observed values. The flow-in rates help to correct for any unknown reactions not included in the reaction set. A reaction producing a species can be replaced by a flow-in term for that species if the reaction proceeds at a steady rate. A number of heterogeneous reactions may occur in this system and their occurrence can be compensated for by the flow terms. The program was run for a sufficient number of simulated lamp cycles such that there was little or no change in the concentration of any species from cycle to cycle. The final cycle of the output was used to determine the rate of change in concentrations during the period the lamps were on and the period when the lamps were off.

Programs were run to simulate each experimental run. The flow rates were adjusted using a value of 1.0×10^{-12} cm^3/molecule-second for the rate constant of reaction (12) in Table 14. Programs were then run with this rate constant assigned values ranging from 2×10^{-13} to 2×10^{-11} cm^3/molecule-second without further adjustment in the flow rates. There was some variation of the concentrations of several species with the rate constant of $OH + HNO_4$. NO_2 was the species most strongly affected by this rate constant. These changes in concentration did not significantly affect the calculated rate of change of concentrations. Concentration profiles for NO_2, HNO_4, HNO_3, H_2O_2

and N_2O_5 are shown for a typical simulation in Fig. 48. The simulation done was of the experimental run shown in Fig. 47. The rate constant for the reaction of OH + HNO_4 used was 2 x 10^{12} cm^3/molecule-second.

The rate of change, or slope, of a concentration during a half cycle was determined by calculating the slope from the concentrations computed at various times during the half cycle and averaging them. In situations where either the concentration or slope did not change by large amounts during the half cycle, the initial and final concentrations were used to determine the slope. Slopes from the simulations were obtained for NO_2, HNO_4, HNO_3, H_2O_2 and N_2O_5, which are the same species for which the experimental values of the slopes were obtained. The experimentally determined slopes and the slopes from the simulations were then compared to determine which value of the rate constant for the reaction of OH + HNO_4 used in the simulations provided the best agreement. The slopes from the computer simulation for NO_2 and HNO_4 during the half cycle when the lamps were on are plotted against the rate constant used for OH + HNO_4 in Figs. 49-55 for experimental runs A through G. The experimentally determined slopes for NO_2 and HNO_4 are superimposed on the curves. The error bars indicate one standard deviation uncertainty in the experimental values.

Typical curves for calculated slopes of HNO_3, H_2O_2 and N_2O_5 vs. OH + HNO_4 rate constant are shown in Fig. 56 along with the experimental values from run C, the run being simulated. The calculated slopes of HNO_3, H_2O_2 and N_2O_5 usually do not exhibit a very strong dependence on the rate constant of the reaction of OH with HNO_4.

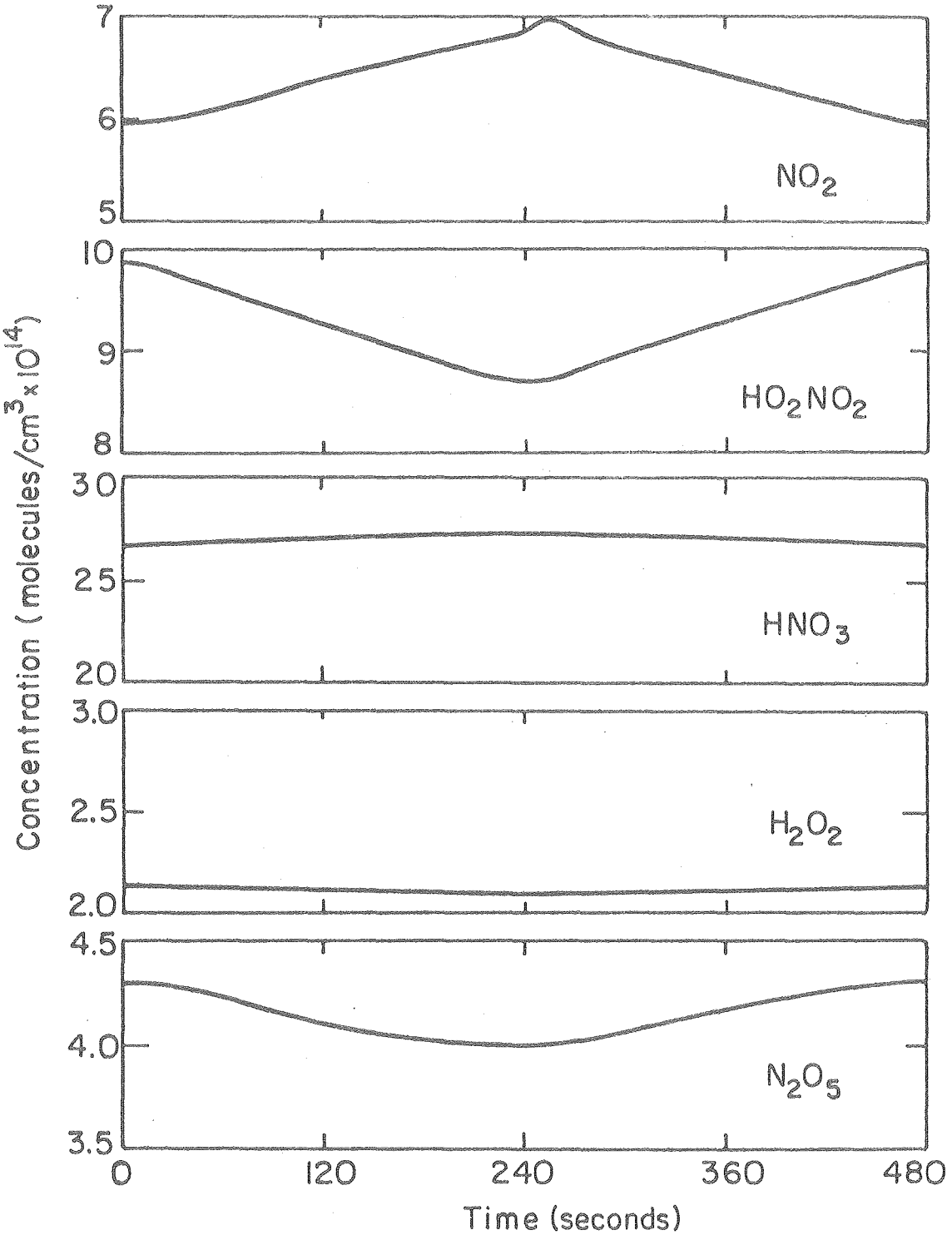

Fig. 48 Calculated concentration profiles during one cycle, starting when the lamps are turned on.

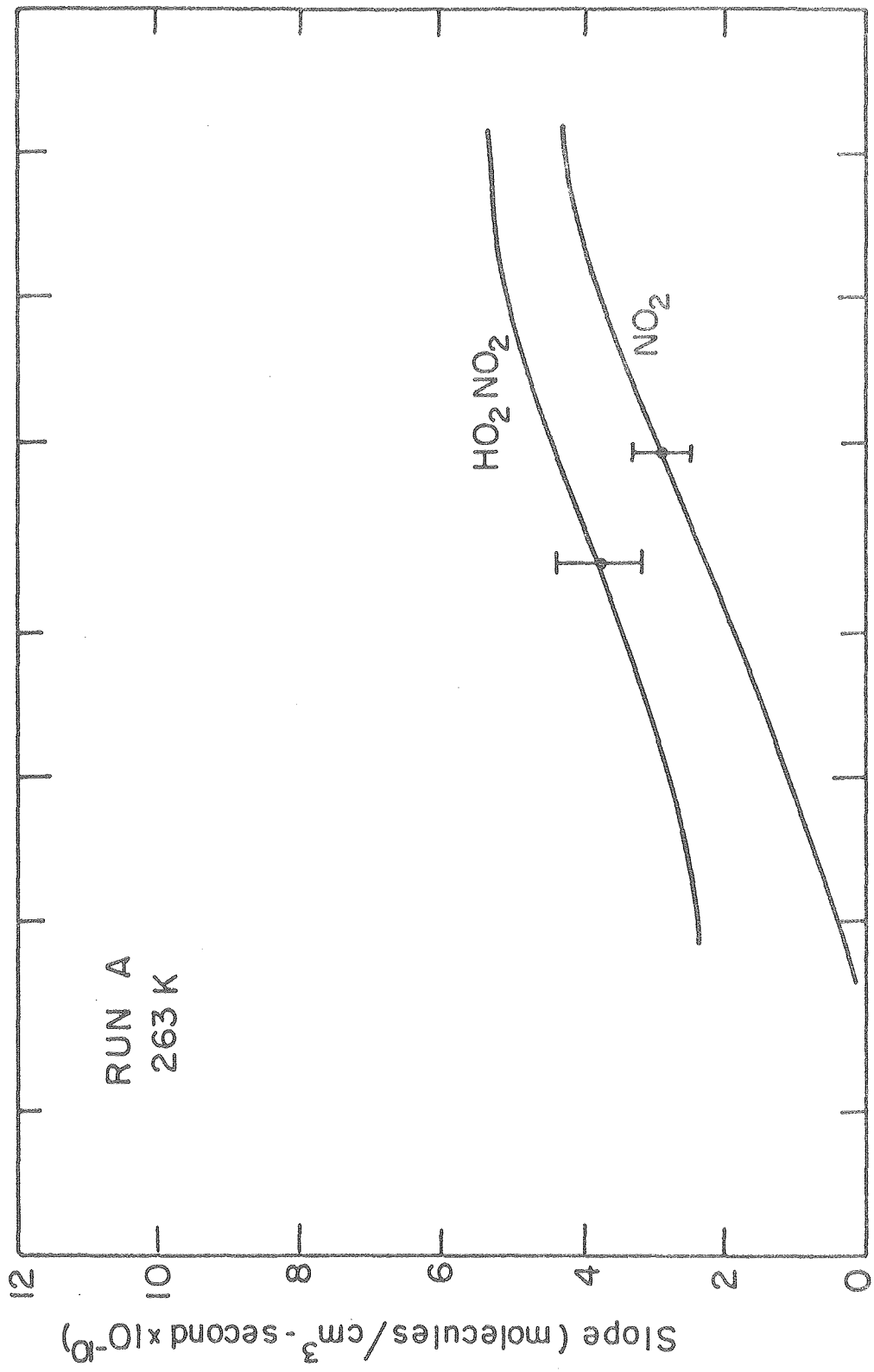

XBL809-5857

Fig. 49 Comparison of calculated and experimental slopes - Run A

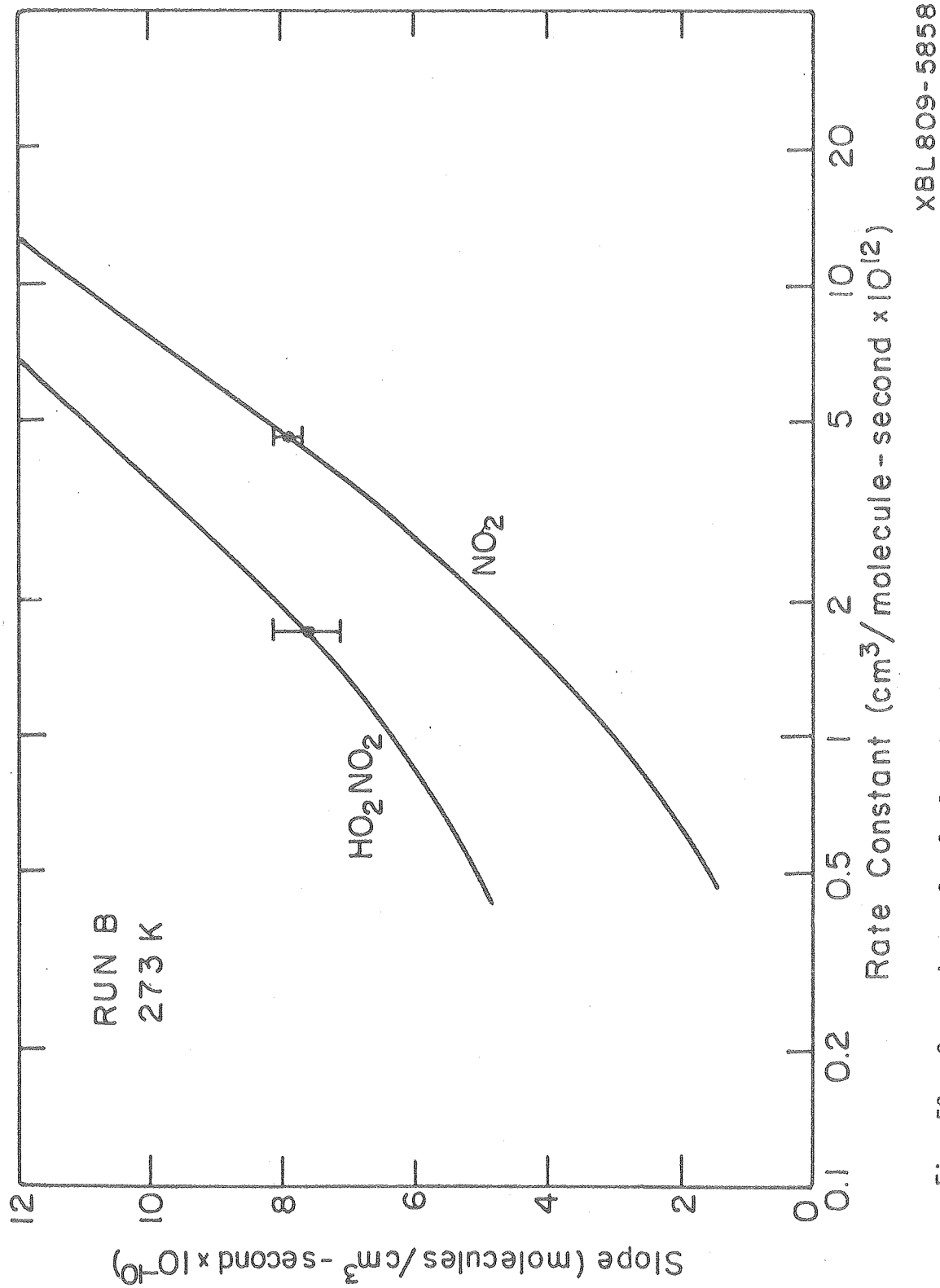

XBL809-5858

Fig. 50 Comparison of calculated and experimental slopes - Run B

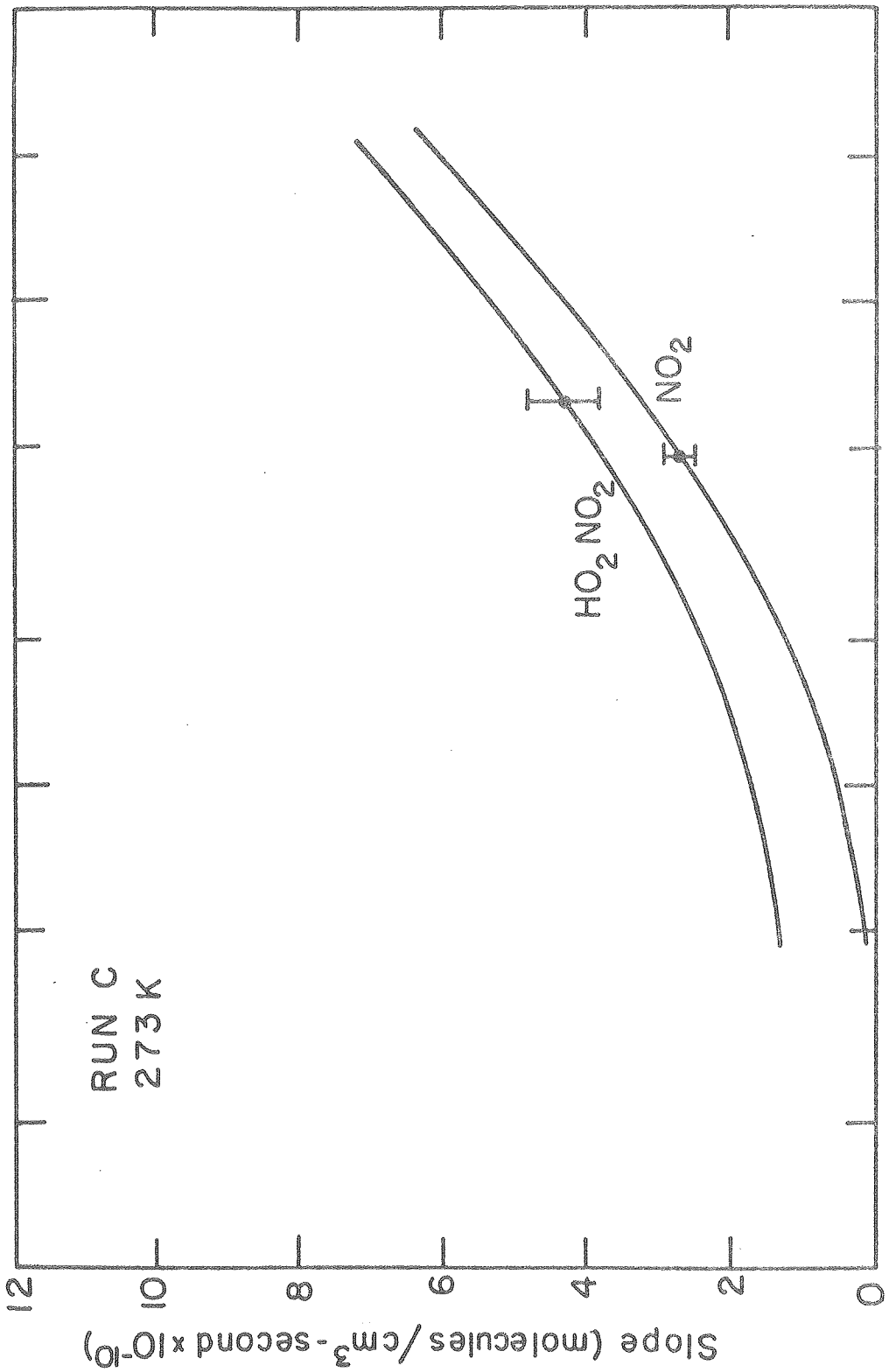

XBL809-5859

Fig. 51 Comparison of calculated and experimental slopes - Run C

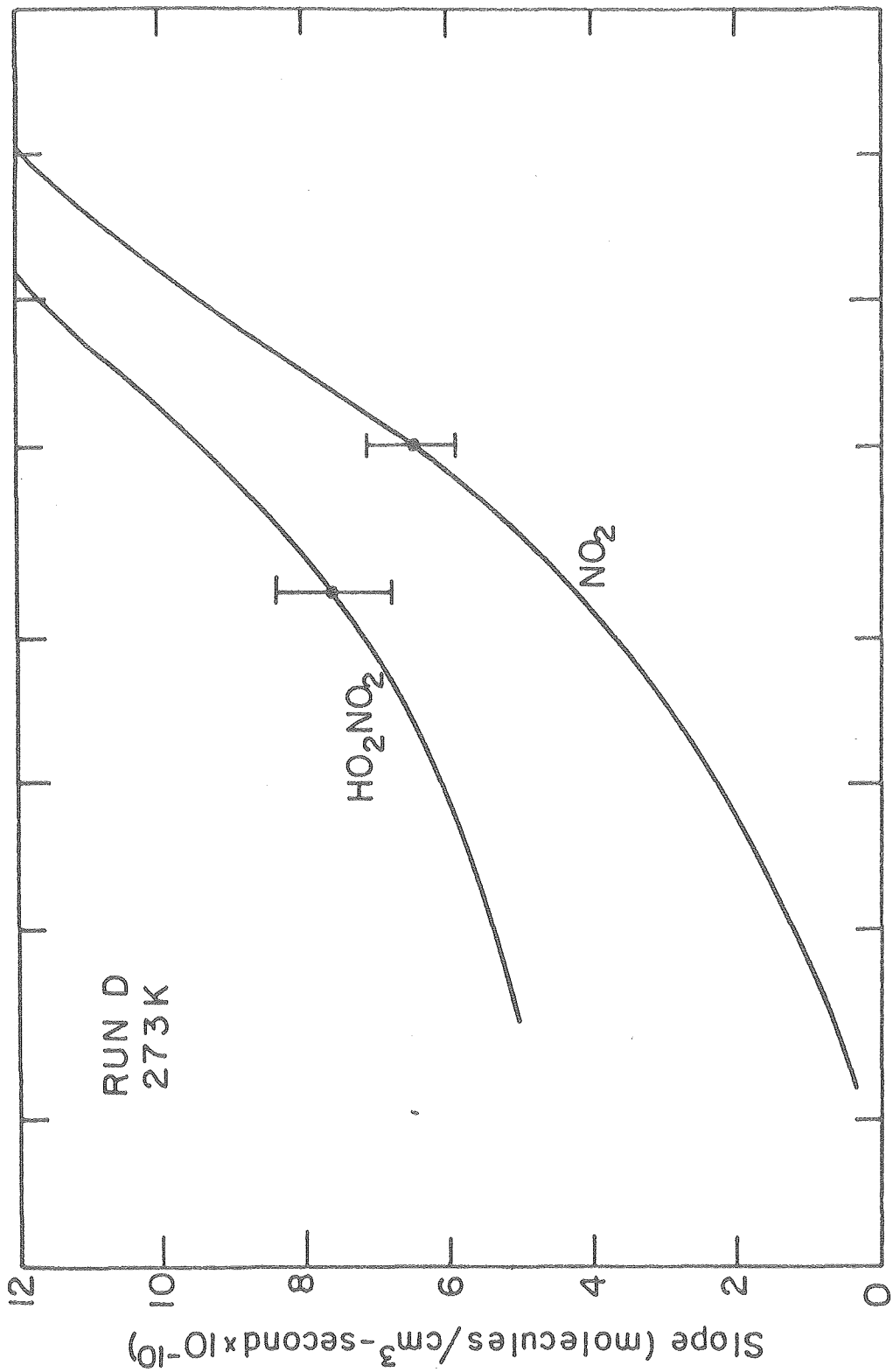

XBL 809-5860

Fig. 52 Comparison of calculated and experimental slopes - Run D

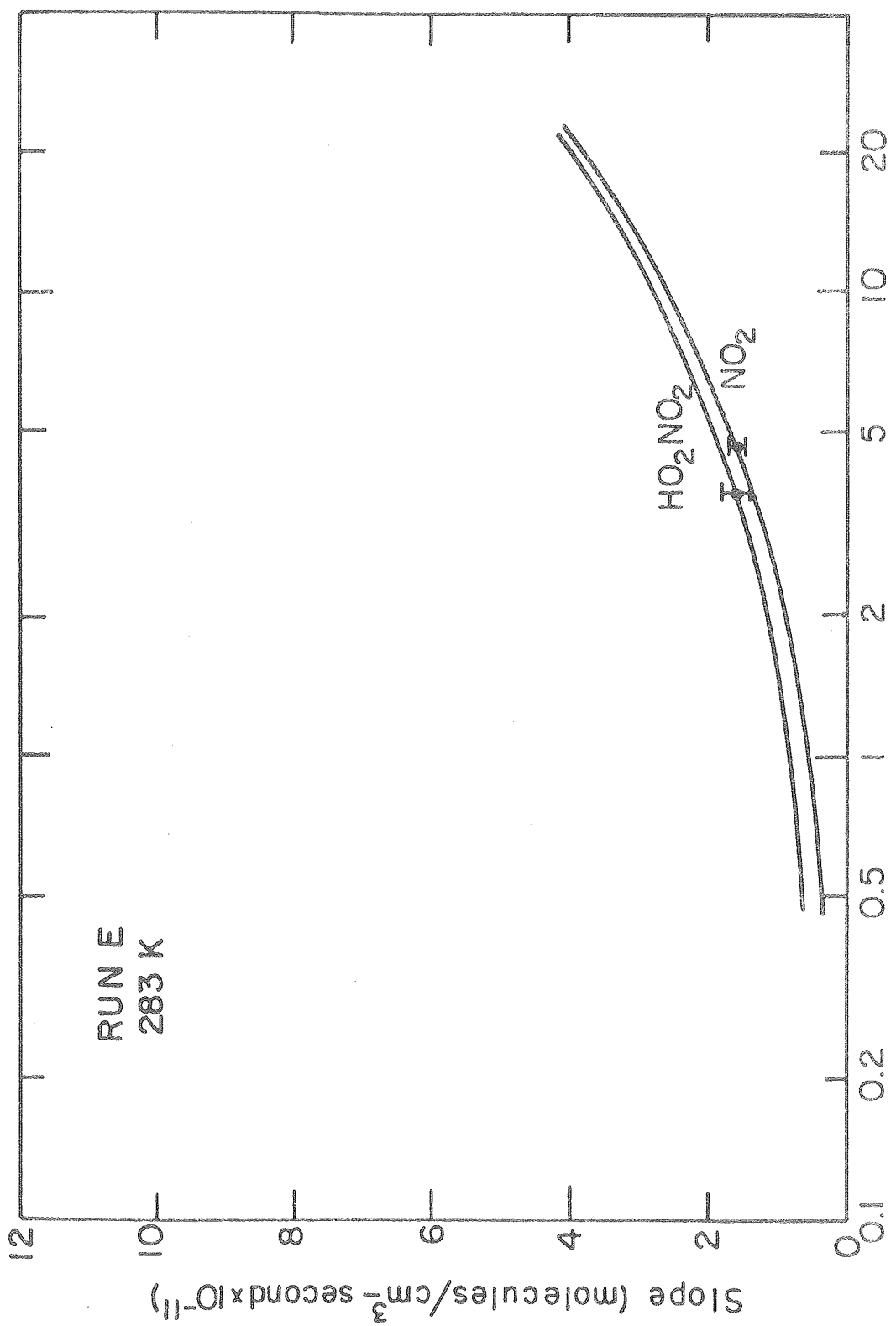

XBL809-5861

Fig. 53 Comparison of calculated and experimental slopes - Run E

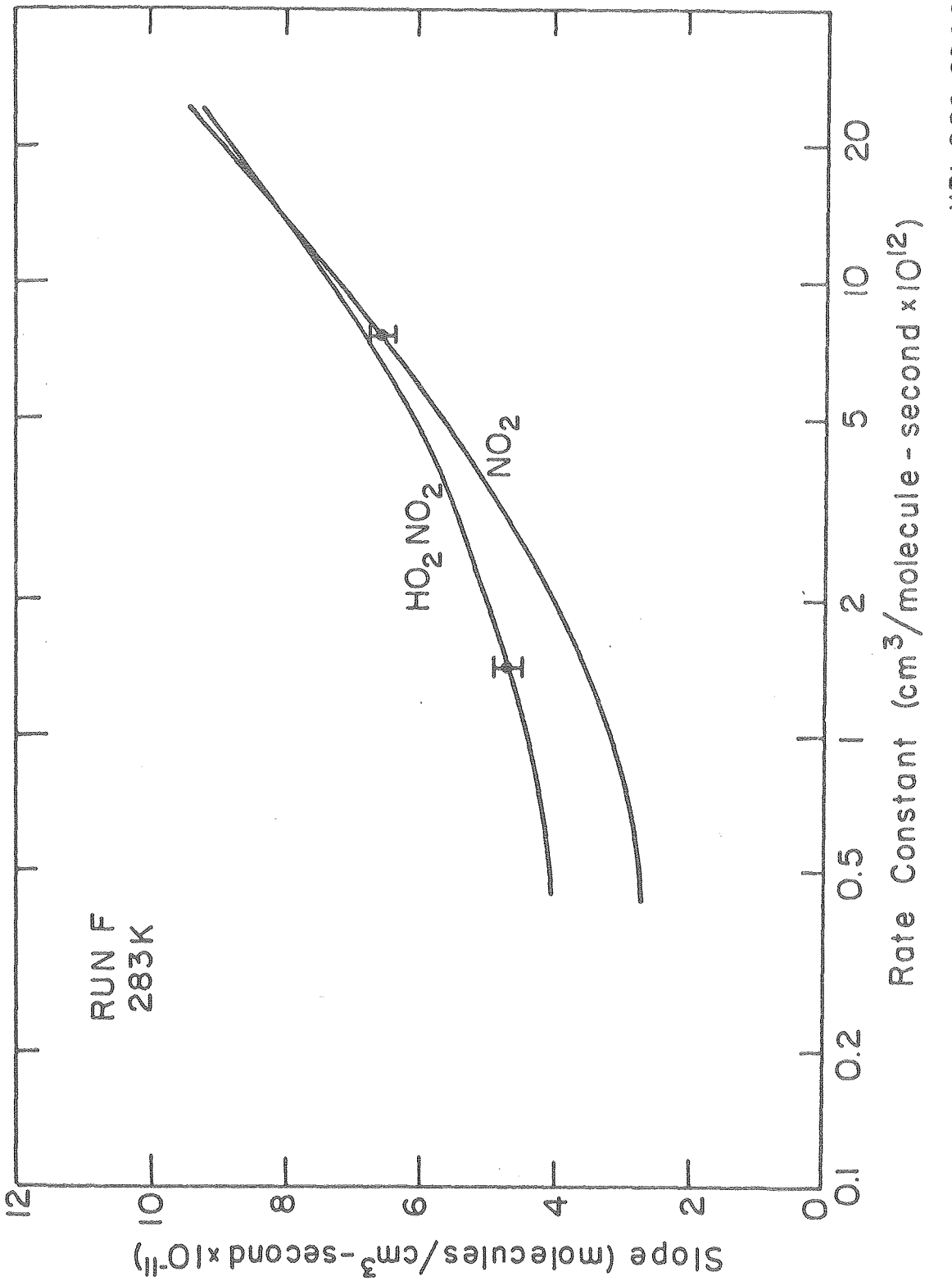

XBL 809-5862

Fig. 54 Comparison of calculated and experimental slopes - Run F

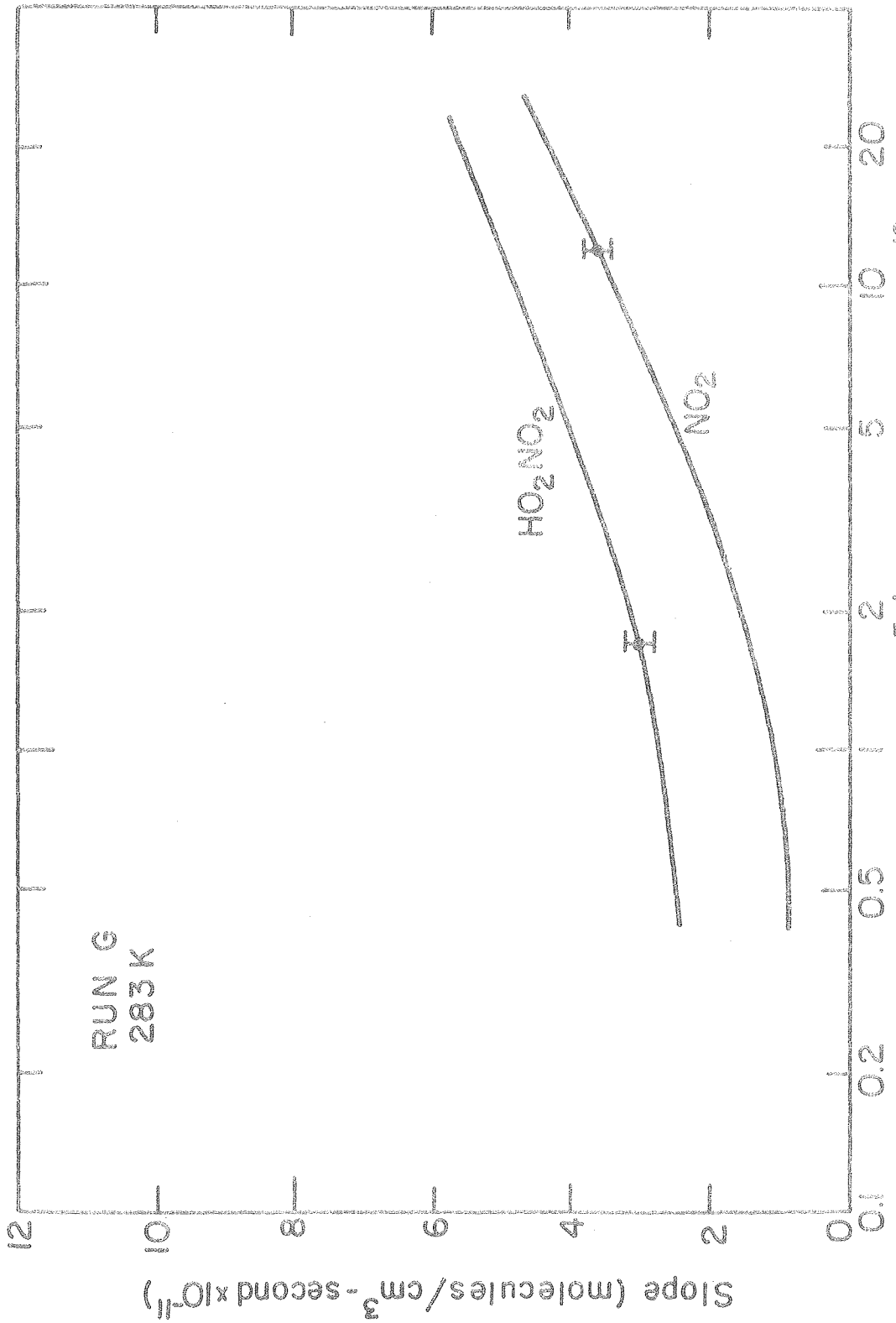

XBL 809-5863

Fig. 55 Comparison of calculated and experimental slopes - Run C

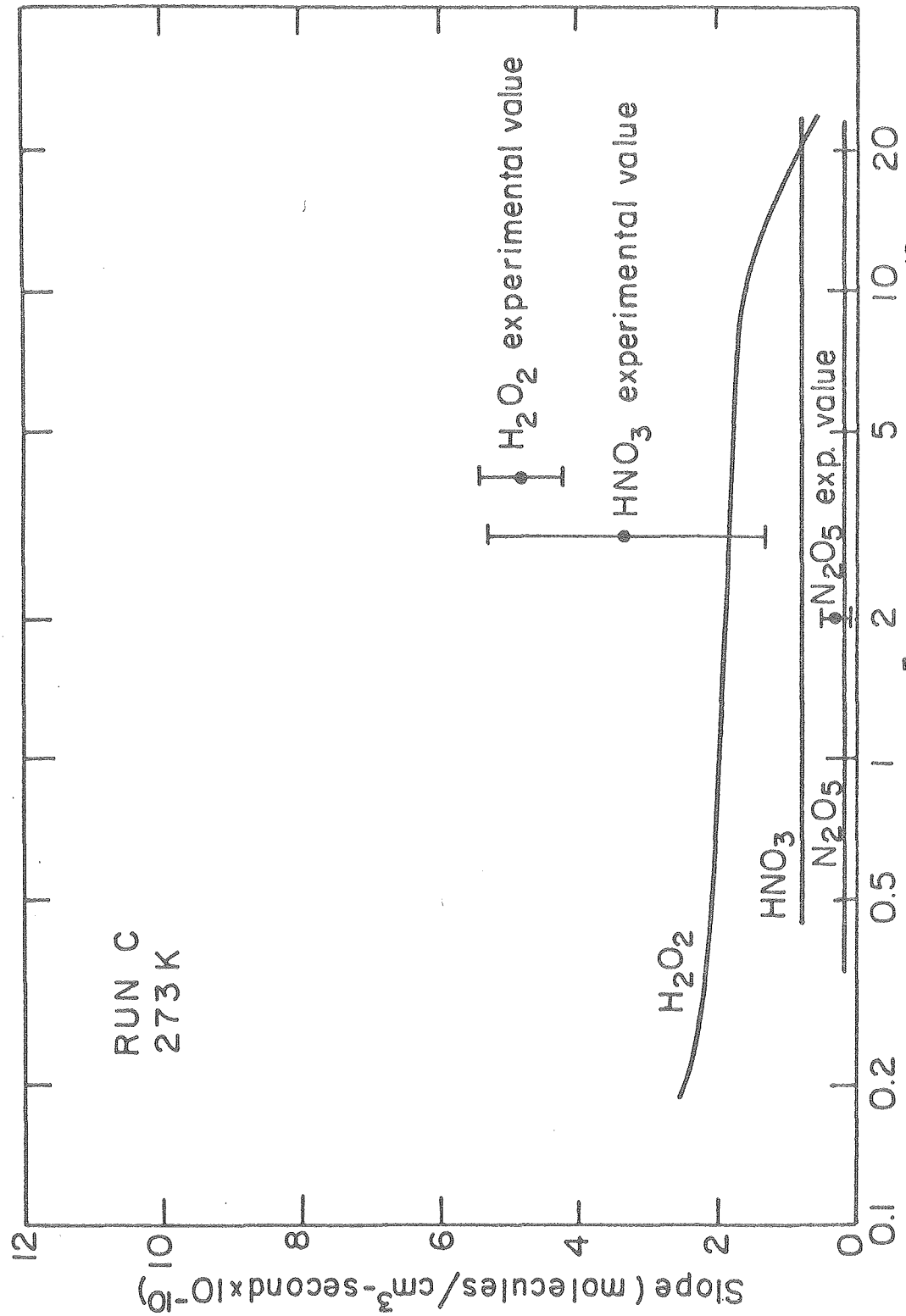

XBL 809-5864

Fig. 56 Comparison of experimental and calculated slopes for HNO_3, H_2O_2 and N_2O_5

In general, the experimentally determined values of the slopes of HNO_3, H_2O_2 and N_2O_5 did not agree well with the calculated values.

There are a number of possible causes for the discrepancies between calculated and experimental values for HNO_3, H_2O_2 and N_2O_5. The HNO_3 slopes were generally small and the total HNO_3 concentration was large. The optical system exhibits a transmission minimum in the region that HNO_3 is monitored, possibly due to the overcoating on the mirrors in the cell. This resulted in a fairly small signal with which HNO_3 was monitored. The HNO_3 profiles usually exhibited a net change in concentration, even after the cycles were averaged. As a result, most of the runs required a correction to eliminate this. The concentration of nitric acid tended to be the most variable of the species monitored. It also has a tendency to adhere to the cell walls, increasing the possibility of its involvement in heterogeneous reactions. N_2O_5 also absorbs weakly at the wavelength at which HNO_3 was monitored, and corrections had to be made when this absorption was significant. These factors created considerable undertainty in the HNO_3 profile and made it unreliable as an indicator for the rate constant for $OH + HNO_4$.

H_2O_2 and N_2O_5 are both somewhat unstable and decompose heterogeneously. Their heterogeneous decomposition rates are variable and are dependent on the conditioning of the cell surfaces. Since it was not possible to observe all the species simultaneously, the heterogeneous decomposition rates could be different at the time of observation of different species. However, these rates should not contribute significantly to the observed slopes, unless a variable intermediate such as NO is involved in the decomposition mechanism.

The wavelengths used to monitor H_2O_2 and N_2O_5 overlap with other species. Absorption bands for H_2O_2 and N_2O_5 that are free of interfering absorptions are either too weak to be of use or are outside the spectral range of the optical system. The interfering absorptions were approximately corrected for by subtracting their estimated optical density contribution from the total optical density obtained at the monitoring wavelength. For H_2O_2, this involved making corrections for HNO_4, HNO_3 and N_2O_5. The wavelength used to monitor N_2O_5 has an interfering absorption by H_2O_2. This required first correcting for the HNO_3 and HNO_4 absorptions and then making iterative corrections for N_2O_5 and H_2O_2. The accuracy of the corrections is not as high as would be desirable. The correction for HNO_3 introduces a significant amount of noise into the curves. The temperature, pressure and concentration dependence of the cross sections of the interfering species at these wavelengths is unknown, and this introduces uncertainty to the corrections.

These factors make the reliability of the data obtained for changes in H_2O_2, N_2O_5 and HNO_3 low. In a number of runs, the slopes obtained for these species are small, contributing to the uncertainty. The poor agreement between the experimental data and the simulations supports the contention that the H_2O_2, N_2O_5 and HNO_3 results are not very reliable. The uncertainty and the potential error in the experimental data and the insensitivity of the slopes from the simulations to the rate constant for $OH + HNO_4$ supported the decision not to use them in the rate constant determination.

The data obtained from the observation of NO_2 and HNO_4 should be relatively free from the problems associated with H_2O_2, N_2O_5 and HNO_3. The slopes of both NO_2 and HNO_4 were reasonably large for all the runs. The simulations indicated that both species are fairly sensitive to the OH + HNO_4 rate constant.

The values for the rate constant for the slopes of HNO_4 and NO_2 from each run were obtained from the rate constant value at which the curve from the simulations agreed with the experimental determination, as indicated in Figs. 49-55. The uncertainties for these values of the rate constant were obtained by determining at which point on the experimental slope, increased or decreased by its uncertainty, would intersect the slope. The values were averaged to give an uncertainty for each rate constant determination. The mean of the values of the rate constant was obtained by weighted averaging, where the values were weighted by the inverse of their uncertainties. Weighted means were obtained for the points from the HNO_4 slopes, the NO_2 slopes and both slopes combined. The values for the rate constant of the reaction of OH with HNO_4 are:

HNO_4 data	$1.9 \pm 0.3 \times 10^{-12}$	cm^3/molecule-second
NO_2 data	$5.0 \pm 0.3 \times 10^{-12}$	" " "
combined data	$3.4 \pm 0.2 \times 10^{-12}$	" " "

There is some discrepancy between the result from the HNO_4 data and the result of the NO_2 data. Part of this is due to the high values for the NO_2 data obtained in runs F and G.

There are several sources of error that should be considered. The photolytic light intensity must be well known to accurately simulate the experimental run. An error of 20 percent in the light intensity used in the simulation can shift the slope vs. rate constant curve sufficiently to cause as much as a 50 percent error in the value obtained for the rate constant. The lamps were monitored continuously during the experiments with a UV photodiode-Schott UG-5 filter combination. The lamps exhibited some fluctuation during each cycle, but this was less than ± 3 percent of the average value. There was a small decrease in light intensity during the course of the experiments. This was generally less than 5 pecent. Every effort was made to have identical settings for each run. The light intensity variation, as indicated by the lamp monitor, was less than 5 percent from run to run at a given temperature.

Heterogeneous reactions, particularly those involving intermediates, could influence the observed chemistry. The heterogeneous oxidation of NO into NO_2 could significantly increase the NO_2 slopes in the system. Other possibilities are heterogeneous reactions of NO with HNO_3 or H_2O_2.

$$NO + HNO_3 \rightarrow HONO + NO_2$$
$$NO + H_2O_2 \rightarrow HONO + OH$$

These reactions could have an effect on the slopes of the species observed if their rates were large enough. The most significant effect of these reactions would be to reduce the amount of NO available to form OH. NO concentrations were generally below that observable by infrared spectroscopy in the apparatus used, since very long path lengths were not obtainable. Observation of NO concentrations would provide a check of the possibility of other reactions of NO.

Errors in the computer simulation of the chemistry could come from an inadequate reaction set or incorrect rate constants. A considerably larger reaction set, which included a number of reactions considered to be of marginal importance, was tested and was found to give essentially the same resuls as the reaction set listed in Appendix C. Most of the rate constants for the reactions used in the reaction set are well known. The slopes generated by the program are not very sensitive to the flow rates, and the flow rate uncertainty is less than 10 percent. Heterogeneous or unknown reactions that have not been included in the reaction set of the simulation could be responsible for generating curves that produce an apparent discrepancy between the HNO_4 and NO_2 results.

The reactions that affect the HNO_4 profile are

$$HNO_4 \rightleftharpoons HO_2 + NO_2$$

$$OH + HNO_4 \rightarrow H_2O + NO_2 + O_2$$

The NO_2 profile is affected by a large number of reactions. Consequently, the results obtained from the HNO_4 are considered to be a better indicator of the rate constant for $OH + HNO_4$ than those obtained from NO_2. By weighting the HNO_4 data twice as much as the NO_2 data, a value of

$$k(OH + HNO_4) = 2.9 \pm 1.0 \times 10^{-12} \text{ cm}^3\text{/molecule-second}$$

is obtained. The uncertainty given is obtained from taking all known sources of error into consideration. This value is in agreement with the upper limits for the rate constant given by Graham et al.[18] and Barker et al.[23]

The value does not disagree with rate constant for other OH hydrogen abstraction reactions. A few of the reactions are listed below with the ΔH° and rate constant for each.

reaction	ΔH° (kcal/mole)	rate constant (cm^3/molecule-second)
$OH + HO_2 \rightarrow H_2O + O_2$	-67.6	3.5×10^{-11}
$OH + HNO_2 \rightarrow H_2O + NO_2$	-40.2	6.6×10^{-12}
$OH + HNO_4 \rightarrow H_2O + NO_2 + O_2$	-48.4	2.9×10^{-12}
$OH + H_2O_2 \rightarrow H_2O + HO_2$	-34.0	1.6×10^{-12}
$OH + HNO_3 \rightarrow H_2O + NO_3$	-17.8	8.5×10^{-14}

The products of the reaction OH with HNO_3 have been recently identified in this laboratory as H_2O and NO_3.[99]

This study also indicates that the products of the reaction of OH with HNO_4 are $H_2O + NO_2 + O_2$. Simulations which used a product set of either $HO_2 + HNO_3$ or $H_2O_2 + NO_3$ gave NO_2 slopes an order of magnitude below that obtained with a product set of $H_2O + NO_2 + O_2$. NO_2 slopes of such a small magnitude cannot be reconciled with the experimental results.

Several attempts were made to observe HONO in the system. HONO concentrations were below ~3 x 10^{13} molecules/cm^3, the approximate detection limit in the system. HONO concentrations were expected to be low because it would be photolyzed by the photolytic light and the reactions producing it are fairly slow. As a result, the upper limit for the rate constant for the reaction

$$HO_2 + NO_2 \rightarrow HONO + O_2$$

obtained from the experiments involving expansion of H_2O_2 and N_2O_5 could not be improved.

CHAPTER VI. THE PHOTOCHEMISTRY OF THE HO_x-NO_x-CO_x SYSTEM

A. Experimental Procedures and Data

The experiments described here were designed to simulate the ozone generation cycle shown in (21). They were performed at total pressures of 0.1 and 1.0 atmosphere at three temperatures: 263 K, 293 K and 313 K. NO_2, H_2O_2 and CO were flowed into the cell in O_2 carrier gas. When the photolytic lamps were turned on, the intermediates involved in the cycle were generated.

The gases were flowed with the photolytic lamps off. The gases were mixed outside the cell and flowed through both disperser tubes. The flow was exhausted through the large port at one end of the cell. The flows were measured and maintained at a fixed flow rate using calibrated flow meters. The flows were regulated to give reasonable optical densities of the species of interest. After flowing for 30 minutes, the signals were measured at wavelengths where the species of interest absorb. The flow was then stopped. The monochromator was set at a wavelength to observe the decay profile of a particular species and the lamps were turned on. The signal was stored in the Fabritek signal averager. The lamps were turned off after 30 minutes and the signals were again measured at wavelengths of interest. This was done to get the concentrations of the species before and after photolysis. The wavelengths and the species observed are listed below.

3.428 μm - NO_2	6.634 μm - H_2O
4.238 μm - CO_2	7.400 μm - HNO_3
4.609 μm - CO	8.040 μm - H_2O_2
5.244 μm - NO	9.477 μm - O_3

The flow was then restored at the same flow levels. This process was repeated until the decay profiles of all the species listed above had been obtained. No data were collected during the first photolysis run, because the concentrations of a number of species had not attained stable levels.

This process was varied somewhat for the experiments done at 0.1 atmosphere pressure. The flow was started and allowed to continue for 30 minutes, at the end of which the transmitted light intensity at the eight wavelengths listed was observed. The flow was then stopped and the cell was rapidly evacuated to 75 torr. Observation was begun at one wavelength, and the photolytic lamps were turned on. At the end of 30 minutes, the lamps were turned off and the transmitted light intensities at the wavelengths of interest were observed. The cell was then filled with O_2 carrier gas to one atmosphere and the flows were restarted. As with the one atmosphere experiments, the process was repeated until all desired species had been observed. The first run was not used to allow concentrations to stabilize.

The light intensities to be used as references for the observations made before, during and after photolysis were obtained before and after each set of photolysis runs. Early experiments were hampered by excessive change in the transmitted light intensity over

the course of a set of runs. This was caused by the degradation of the mirror coatings by H_2O_2 and HNO_3. A sufficiently thick (2000 Å) overcoat of MgF_2 on the mirrors prevented the occurrence of this in later experiments. The reference light intensities were obtained with the cell evacuated and at 0.1 and 1.0 atmosphere total pressure. There were generally some changes in the reference light level with pressure.

The measurements at the wavelengths of interest that were made before and after each run were used to determine the concentrations of the listed species before and after each photolysis run. The concentrations were averaged over the set of runs done to characterize the chemistry of each condition. The decay profiles obtained were adjusted to agree with the initial values of the average concentrations when necessary. The initial average concentrations were used as inputs for computer simulations of the kinetics. The averaged initial concentrations for the runs are listed in Table 17.

Separate observations were made of ozone in the system, since it was present in very low concentrations. The CaF_2 windows used in early experiments were replaced with BaF_2 windows for increased transmission in the 10 μm region. The spectrometer path length was increased to 32 meters to provide increased sensitivity. The runs were performed at 293 K and one atmosphere pressure. The techniques described previously to obtain decay profiles were also used here. The monochromator was set at 9.478 μm and data were collected by the Fabritek. The lamps were turned on 30 seconds after data collection

TABLE 17

Initial Concentrations for HO_x-NO_x-CO_x Runs

	NO_2	NO	CO_2	CO	H_2O	H_2O_2	HNO_3
313K, 1 ATM	8.6E15	7.1E12	3.4E13	9.3E15	2.9E15	1.0E15	1.7E15
313K, 0.1 ATM	7.9E14	1.8E13	2.1E13	6.7E14	7.8E14	1.3E14	1.6E14
293K, 1 ATM	6.3E15	3.7E13	5.0E13	1.1E16	9.9E15	2.9E15	6.3E15
293K, 0.1 ATM	5.2E14	6.3E12	7.1E12	9.4E14	7.9E14	2.2E14	4.5E14
263K, 1 ATM	1.1E16	1.8E13	4.2E13	1.1E16	4.8E15	4.0E14	4.9E15
263K, 0.1 ATM	6.9E14	6.2E12	3.7E13	1.3E15	4.0E14	2.0E13	3.8E14

was begun. Seventy seconds after the lamps were turned on, data collection was stopped and the spectral region from 8.96 to 10.32 μm was scanned. This procedure was repeated five times, with concentrations allowed to stabilize by flowing the reactants for 30 minutes between runs. The five 9.478 μm observations and the five scans were averaged to reduce noise.

The sum of the scans is shown in Fig. 57. The ozone absorption band from cross-section measurements is indicated by the dashed line. The noise in the trace is due to the weakness of the analytical light, caused by the large number of reflections needed to obtain the necessary path length. The optical density shown converts into an ozone concentration of about 0.5 to 2 x 10^{13} molecules/cm^3.

The sum of the observations made at 9.478 μm were analyzed using a linear regression program to obtain slopes and intercepts before and after the lamps were turned on. From the start of the scan to the time the lamps were turned on, the slope of the summed optical density was $-3.6 \pm 2.3 \times 10^{-4}$ $second^{-1}$ and the intercept was 0.020 ± 0.004. From the time the lamps were turned on to the time the scan was completed, the slope was $4.2 \pm 0.6 \times 10^{-4}$ $second^{-1}$, and the intercept was 0.006 ± 0.004.

The photolytic light source for these experiments consisted of two 30 watt germicidal lamps and two 30 watt black lamps. This combination was used to allow sufficient photolysis of both NO_2 and H_2O_2. The lamps were monitored with a UV enhanced photodiode and a Schott UG-5 filter. The monitor was more sensitive to the output from the black

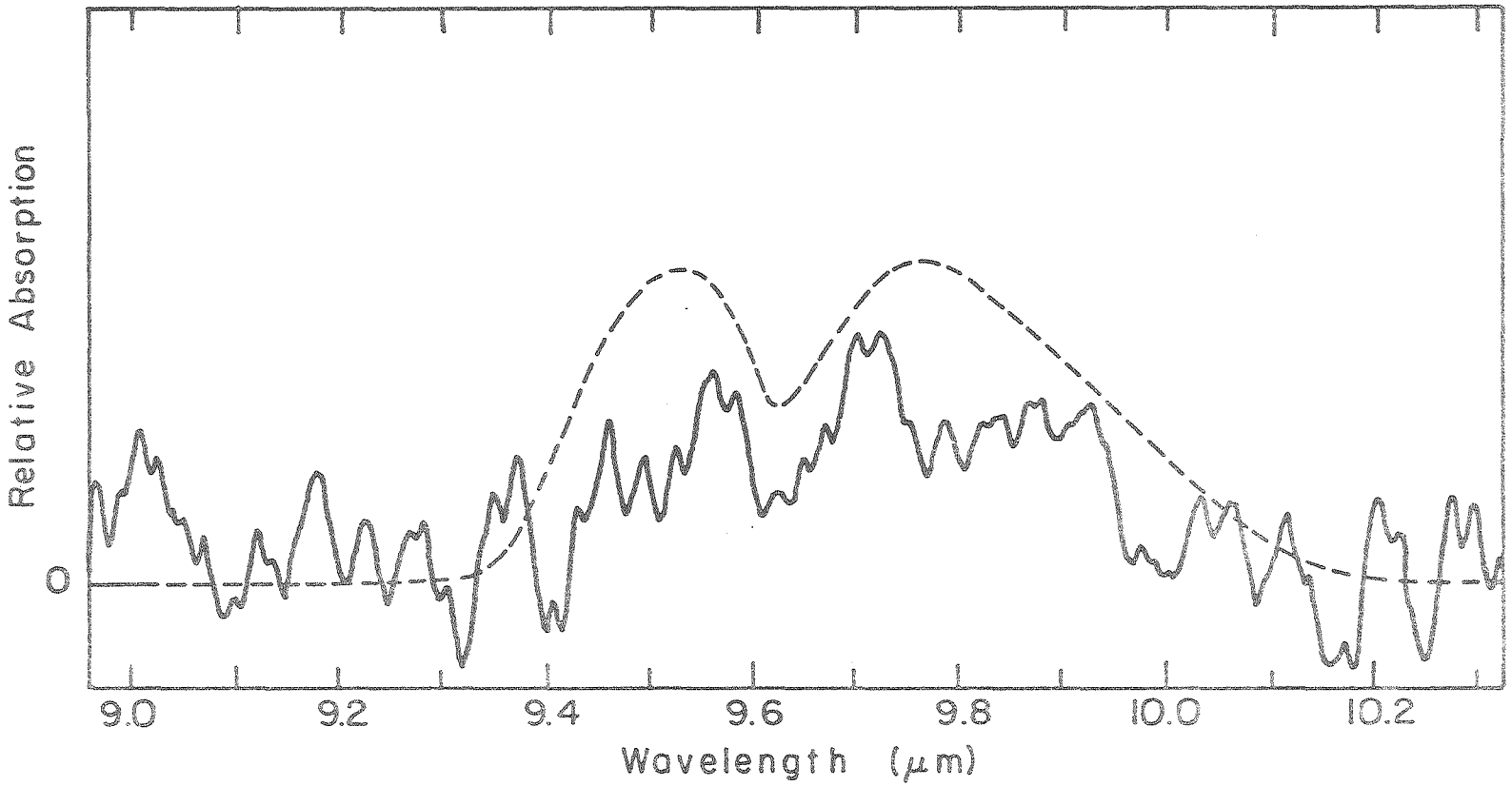

XBL809-5867

Fig. 57 Sum of scans made after activation of the photolytic lights

lamps than the 254 nm output from the germicidal lamps. The lamp behavior typically observed by the monitor is illustrated in Fig. 58. Some fluctuations, amounting to less than ±3 percent of the mean value, occurred in the first 5 minutes after the lamps were turned one. The output was stable from that time on until the end of the run.

Actinometry was performed to determine the lamp output of both the germicidal and the black lamps at the three temperatures used in the experiments. The photolysis rate of H_2O_2 by the black lamps was determined to be less than 0.5 percent of the photolysis by the germicidal lamps. Consequently, H_2O_2 photolysis was used to obtain the light intensities of the 254 nm output of the germicidal lamps.

H_2O_2 was flowed through the cell with N_2 carrier gas until the desired concentration was obtained, as observed with the 8.040 μm H_2O_2 absorption. The flow was stopped, and the decay of H_2O_2 in the dark was observed. The lamps were turned on and the decay rate of H_2O_2 was observed after the intermediates had built up to steady state concentrations. The lamps were turned off and the dark decay of H_2O_2 was again recorded. H_2O_2 has an overall quantum yield of two in this system.

$$
\begin{aligned}
H_2O_2 + h\nu &\rightarrow HO + HO \\
HO + H_2O_2 &\rightarrow H_2O + HO_2 \\
HO + HO_2 &\rightarrow H_2O + O_2 \\
\text{net} \quad 2\,H_2O_2 + h\nu &\rightarrow 2\,H_2O + O_2
\end{aligned}
\qquad (58)
$$

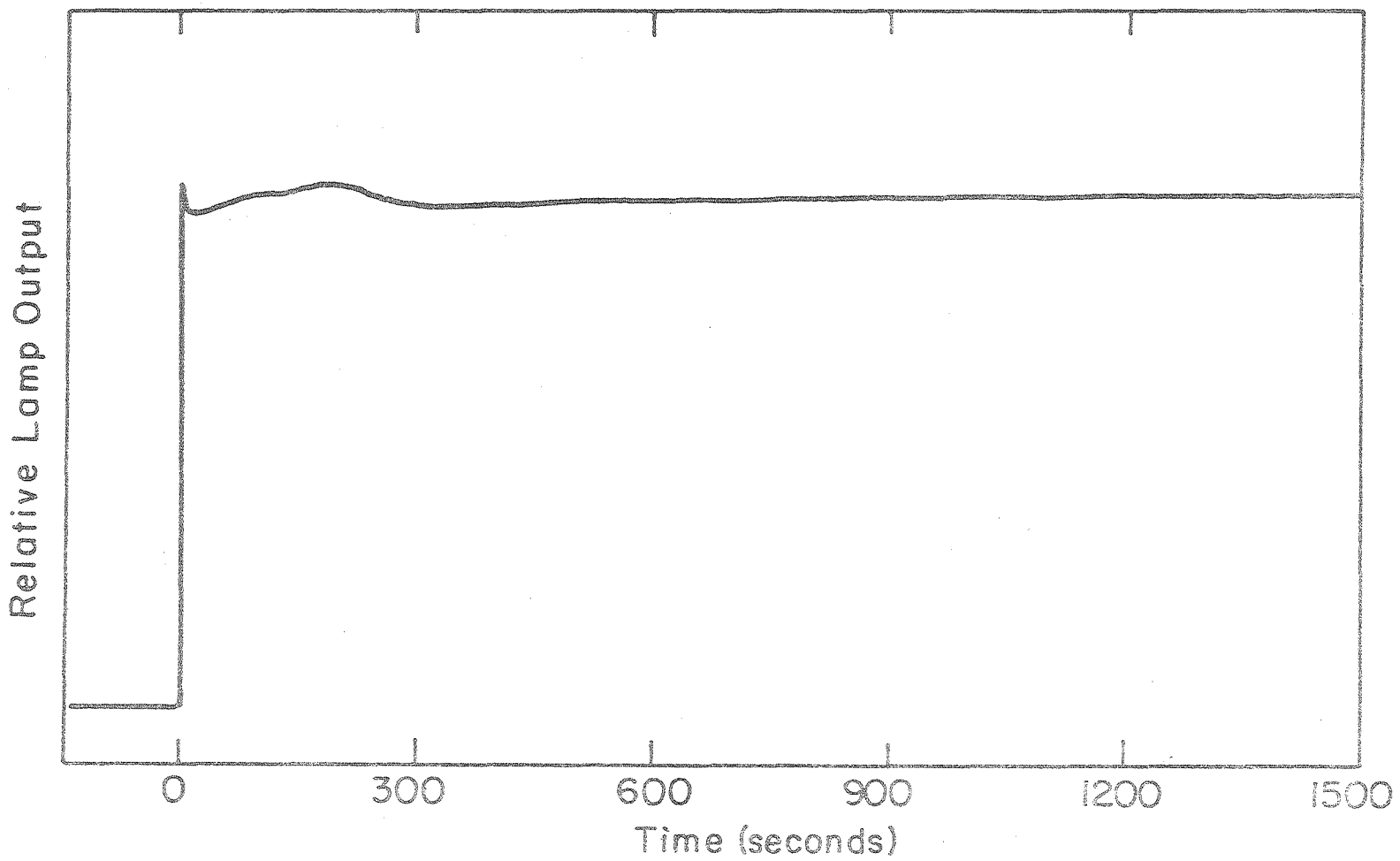

XBL809-5868

Fig. 58 Photolytic lamp output with time, as observed by the photodiode monitor

The photolysis rate was obtained by subtracting the average of the dark decays from the rate observed with the lights on. The light intensities obtained were

$$I\ (254\ nm\ ,\ 313\ K) = 4.8 \times 10^{15}\ photons/cm^2\text{-second}$$
$$I\ (254\ nm\ ,\ 293\ K) = 4.0 \times 10^{15}\ photons/cm^2\text{-second} \qquad (59)$$
$$I\ (254\ nm\ ,\ 263\ K) = 2.2 \times 10^{15}\ photons/cm^2\text{-second}$$

The light intensities for the black lamps were obtained by disconnecting the two germicidal lamps from the lamp driver and photolyzing NO_2. A 1081 cm^3 bulb was filled with a measured pressure of NO_2. This was expanded into the cell, which was then filled with one atmosphere of N_2. The black lamps were turned on and the NO_2 decay was monitored at 3.428 μm. The quantum yield for NO_2 will be between one and two under these conditions. The decays were analyzed using a quantum yield[67] of 1.67. They were also analyzed by computer simulation to take into consideration the formation of species such as NO_3 and N_2O_5. The black lamp light intensities obtained were:

$$I\ (313\ K) = 4.3 \times 10^{15}\ photons/cm^2\text{-second}$$
$$I\ (293\ K) = 3.1 \times 10^{15}\ photons/cm^2\text{-second}$$
$$I\ (263\ K) = 1.0 \times 10^{15}\ photons/cm^2\text{-second}$$

The light intensities obtained were used in the analysis of the decays and in computer simulation of the experiments.

B. Results and Discussion

The kinetics and photochemistry of the H_2O_2 - NO_2 - CO system was investigated because of their importance to the chemistry of trace species in the troposphere. Fishman and Crutzen[51] and Heicklen et al.[111] have proposed a photolytic cycle for the generation of ozone in the troposphere.

$$\begin{aligned} CO + HO &\rightarrow CO_2 + H \\ H + O_2 &\xrightarrow{M} HO_2 \\ HO_2 + NO &\rightarrow HO + NO_2 \\ NO_2 + h\nu &\rightarrow NO + O \\ O + O_2 &\xrightarrow{M} O_3 \\ \text{net:}\quad CO + 2O_2 &\rightarrow CO_2 + O_2 \end{aligned} \qquad (26)$$

For this cycle to make an important contribution to the tropospheric ozone budget, each of the reactions listed must be the dominant pathway for the reaction of the reactants involved.

The compounds used in these experiments were maintained at concentration levels in the range of 10^{13} to 10^{16} molecules/cm^3. These levels were much higher than those present in unpolluted regions of the troposphere, but were necessitated by the limited sensitivity of the spectrometer system. This factor produced considerably different kinetics than those occurring in the atmosphere. Another difference was the presence of the cell walls, on which heterogeneous reactions could occur. Heterogeneous reactions had to be considered in the

analysis of the decay profiles. This is particularly true of H_2O_2, which is known to be involved in a number of heterogeneous reactions.

The large number of species and the large number of reactions that occur make this system difficult to analyze. The CHEMK computer program, described previously, was used to simulate the kinetics of the experimental runs. The reactions and rate constants used are listed in Appendix C. The experimentally derived initial concentrations and light intensities were used as inputs for the program. The final concentrations from experiment and theory are compared in Table 18. The initial concentrations in both cases are those listed in Table 17. While there is reasonable agreement between the experimental and calculated results for the one atmosphere runs, there is generally poor agreement between the experimental and calculated results for the 0.1 atmosphere runs. This appears to be largely due to difficulties in obtaining reproducible concentrations at 0.1 atmosphere and monitoring them accurately. Experimental and calculated profiles for the one atmosphere and 0.1 atmosphere runs at 293 K are compared in Figs. 59 and 60, respectively.

The poor agreement between experimental and calculated results could be due to a number of factors. The rapid evacuation of the cell could cause cooling of the gases and condensation of species such as H_2O, H_2O_2 and HNO_3. These could slowly evaporate during the run and give misleading results. The light intensity transmitted through the cell varies slightly with cell pressure and the effect is

TABLE 18

Final Concentrations of Observed Species

	NO_2	CO_2	CO	NO	H_2O	HNO_3	H_2O_2
313K, 1 atm							
experimental	6.4E15	6.3E13	8.7E15	5.4E14	3.9E15	2.8E15	1.3E13
calculated	6.3E15	5.3E13	9.3E15	1.9E15	3.6E15	2.1E15	8.7E13
313K, 0.1 atm							
experimental	8.1E13	1.0E13	1.4E14	2.3E13	3.5E14	6.8E13	3.2E13
calculated	1.2E14	2.7E13	6.6E14	6.4E14	8.8E14	1.8E14	8.1E12
293K, 1 atm							
experimental	3.9E15	1.2E14	1.1E16	5.6E14	1.2E16	9.2E15	3.9E13
calculated	4.6E15	1.3E14	1.1E16	6.3E14	1.2E16	7.3E15	2.0E14
293K, 0.1 atm							
experimental	9.0E13	2.5E13	1.1E15	5.7E14	9.1E14	6.4E14	1.5E13
calculated	1.4E14	2.1E13	9.3E14	3.3E14	9.6E14	4.8E14	1.7E13
263K, 1 atm							
experimental	1.1E16	5.1E13	1.1E16	1.2E14	4.8E15	3.3E15	3.9E14
calculated	8.8E15	5.0E13	1.1E16	6.9E14	5.1E15	5.4E15	3.6E13
263K, 0.1 atm							
experimental	2.1E14	3.0E15	2.6E15	3.2E14	4.0E14	5.5E14	3.1E12
calculated	3.3E14	3.9E13	1.3E15	4.1E14	4.2E14	3.9E14	1.8E12

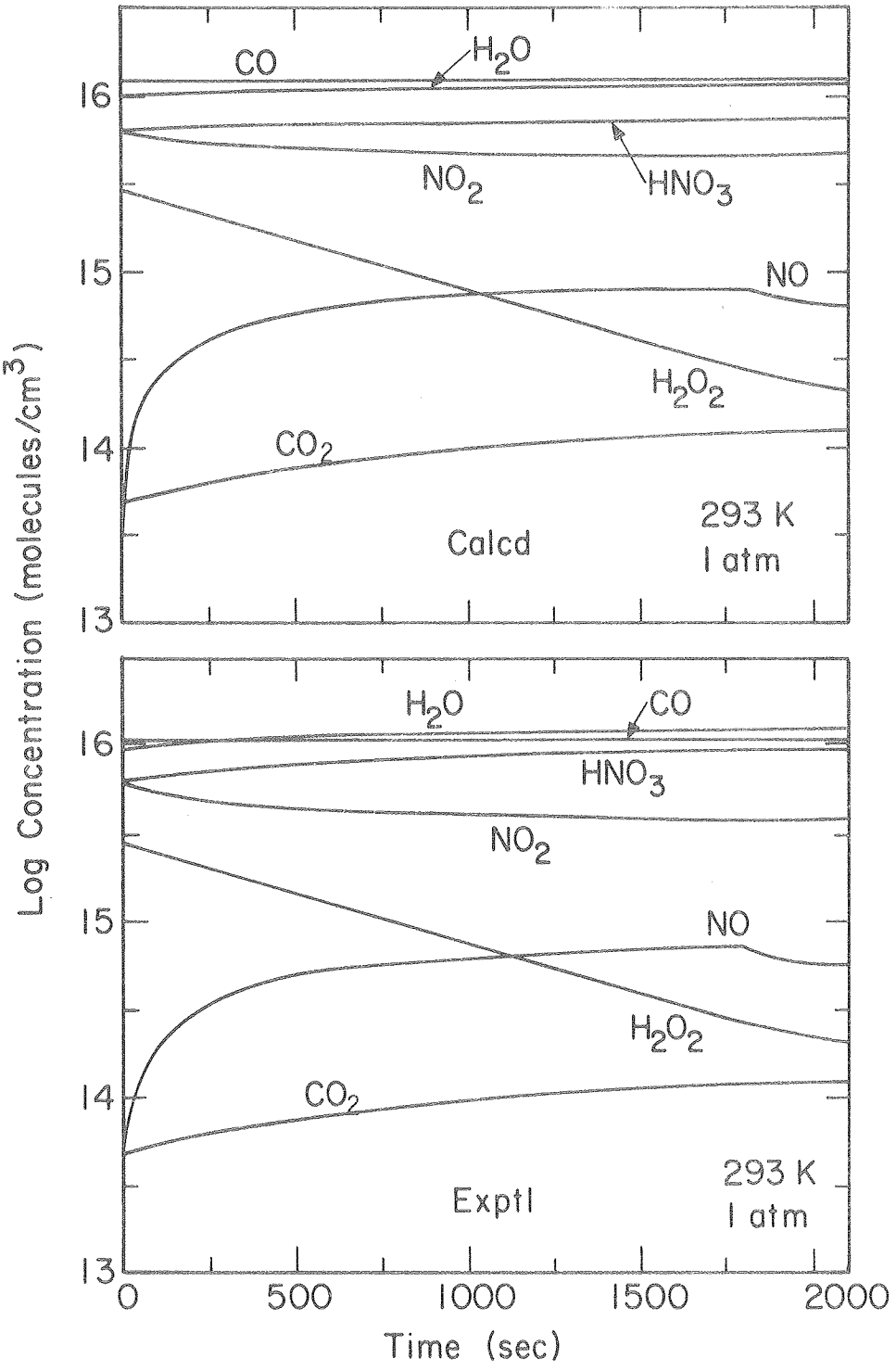

XBL 8010-12174

Fig. 59 Comparison of experimental (lower) and calculated (upper) concentration profiles at 293 K and 1.0 atmosphere pressure

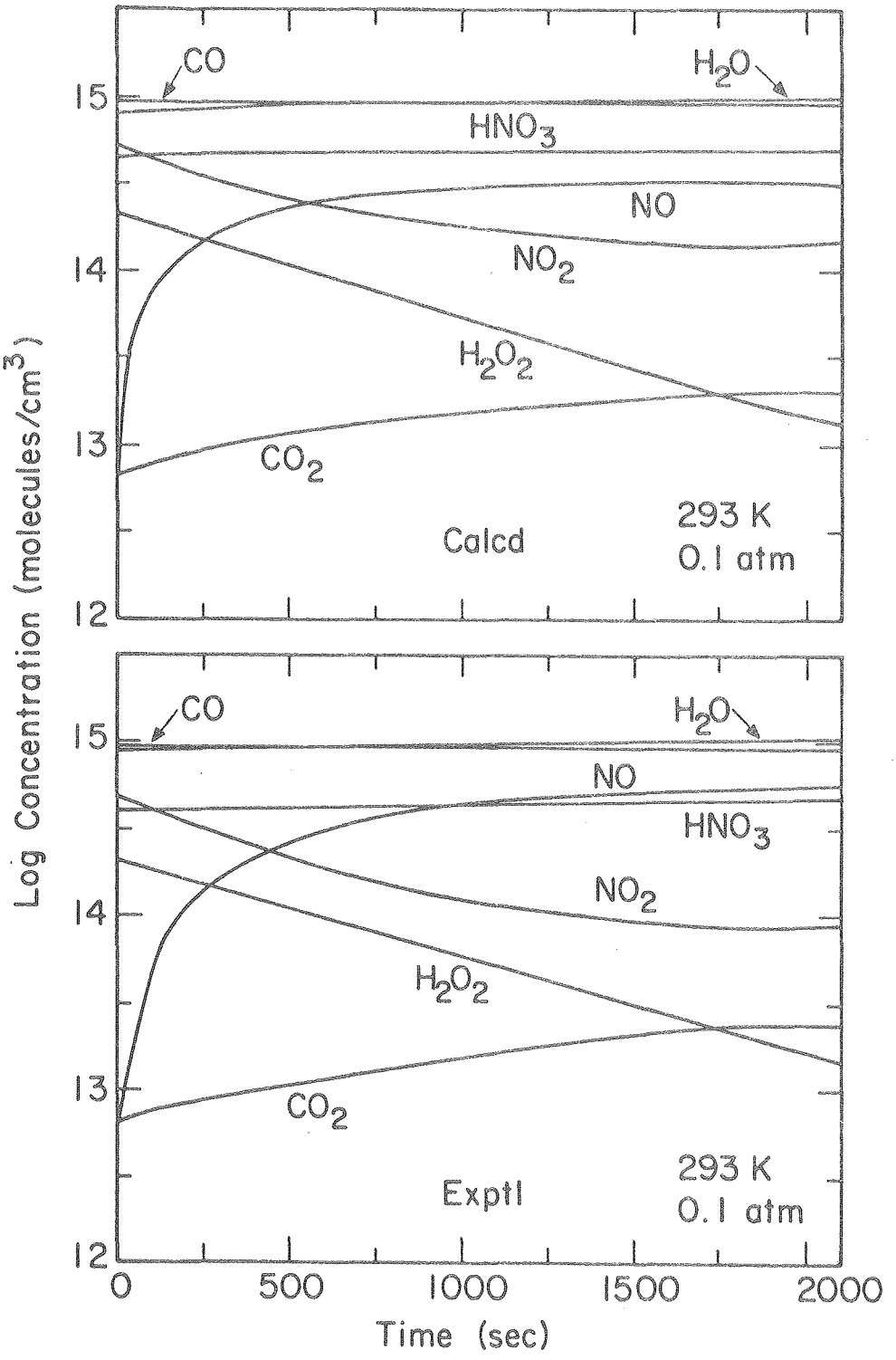

XBL 8010-12175

Fig. 60 Comparison of experimental (lower) and calculated (upper) concentration profiles at 293 K and 0.1 atmosphere pressure.

not entirely reproducible. Since the concentrations of most species and their corresponding absorptions are small under these conditions, small shifts in the baseline can have a significant effect. The cross sections at 0.1 atmosphere are generally small and somewhat uncertain at low concentrations. There was considerable run-to-run fluctuation in the concentrations of several species. This was caused in part to the difficulty in re-establishing stable flows of the reactants. It was decided not to use low pressure runs because of these difficulties.

The differences between the experimental and calculated profiles were analyzed to determine the cause of the difference. The runs at 293 K and 313 K have higher HNO_3 concentrations and lower NO and H_2O_2 concentrations than predicted by the simulations. This suggests a heterogeneous reaction of NO or NO_2 with H_2O_2 to form HNO_3. The 263 K experimental run indicates higher NO_2 and H_2O_2 concentrations and lower NO and HNO_3 concentrations than predicted by the simulations. This could be due to the lamps having lower light output than that used in the simulation.

The conversion of CO to CO_2 in the system occurs by the two reactions of CO + HO and CO + O + M. In all runs, the simulations indicate that the CO + HO reaction is much faster than the CO + O + M reaction. Considerable investigation of the CO + HO reaction has been done, but it is still imperfectly understood. The CO and CO_2 profiles agree well in the 293 K and 263 K runs. The 313 K run suggests that the OH + CO rate constant is higher at 313 K than at lower

temperatures. There have been other studies that indicate that the reaction does exhibit such a temperature dependence.[100]

The observation of the build-up of small amounts of ozone, as indicated in Fig. 57, is consistant with the results of computer simulations. The simulations predict the build-up of ozone to concentrations of ~1 x 10^{13} molecules/cm^3 about 10 seconds after the lamps are turned on, and then a slow decay to levels of ~1 x 10^{11} molecules/cm^3 at the end of the run. The experimentally observed concentrations were in the range of ~0.5-2 x 10^{13} molecules/cm^3. This was indicated by both the scans and the observations at 9.478 μm. The uncertainty arises from the noise in the optical density due to the weak signal.

The presence of HONO and HNO_4 was not confirmed. The computer simulations predict maximum concentrations that would be only marginally detectable in the system. This suggests rough agreement between the experimental results and simulated results in terms of the HONO and HNO_4 chemistry.

The experimental results, in general, appear to confirm the validity of the reaction system used to model the experiments. The major difficulties in the experiments is the occurrence of heterogeneous reactions and the need to perform repeated photolysis runs to observe all the species.

If the computer simulations are accurate models of the gas phase kinetics in the experiments, the reaction rate predictions made by the

simulations can be analyzed to determine which reactions are responsible for the ozone production and whether the CO oxidation cycle is active in the experiments performed.

The simulations indicate that the build-up of ozone is due to the initial photolysis of NO_2 to produce oxygen atoms. These combine with oxygen molecules to form ozone. As the NO produced by photolysis builds up, it reacts with ozone, reducing its concentration.

For the cycle listed in (26) to operate successfully each step in the cycle must be the dominant pathway for the consumption of the intermediates involved. The computer simulations indicate that the CO oxidation cycle was not active in the experiments performed. The reaction rate of HO with CO was small compared to the rate for $HO + NO_2 + M$ to form HNO_3. The rate of $H + O_2 + M$ was the major loss mechanism for hydrogen atoms. The reactions of $HO_2 + NO_2 + M$ and $NO + NO_3$ were more important in the balance of HO_2 and NO, respectively, than the reaction of $HO_2 + NO$. $NO_2 + h\nu$ and $O + O_2 + M$ were major destruction mechanisms for NO_2 and oxygen atoms.

In addition, the CO_2 production rate would be the same as the gross ozone production rate if the cycle were responsible for the ozone generation. The simulations of the experiments indicate that this was not the case.

The operation of the CO oxidation cycle as an ozone production mechanism will be dependent on the concentration balance of a number of trace species. In the troposphere, the concentrations of the HO_x

and NO_x species need to be critically balanced for the mechanism to operate. To be able to determine the behavior of ozone in the atmosphere, the general differential equation for ozone concentration must be analyzed in the manner presented by Johnston and Podolske[112]. The relaive importance of the terms in the differential equation will depend on the region of the atmosphere under consideration.

In conclusion, the experimental results cannot confirm the existence of a CO oxidation mechanism that is responsible for ozone production in the atmosphere. The presence of heterogeneous reactions make experimental confirmation difficult. To determine if it does occur in the troposphere, studies need to be made of the concentrations of trace species and accurate knowledge obtained of the temperature and pressure dependence of the rate constants for the reaction involved.

ACKNOWLEDGMENTS

I would like to thank Professor Harold S. Johnston for his guidance and support throughout my graduate career. While allowing a student to develop on his own, he was always available as a sounding board and a source of information and ideas.

The encouragement and assistance of my fellow graduate students has been both helpful and enjoyable. Particular thanks go to Peter Connell, Bill Marinelli, Herb Nelson and Jim Podolske, with whom I have had many stimulating and engaging discussions during my career.

The personnel of the Department of Chemistry and the Lawrence Berkeley Laboratory have been most helpful in their support of this research.

I would particularly like to thank Lisa for her emotional support and understanding.

Special thanks are due to my parents. Their support and encouragement were a source of inspiration.

This work was supported by the Materials and Molecular Research Division of the U. S. Department of Energy under contract No. W-7405-ENG-48.

APPENDIX A: PHOTOMULTIPLIER TUBE GATING

In many experimental situations, it is sometimes desirable to observe low level light signals which have been preceded by any intense pulse of light. A photomultiplier tube (PMT) is an excellent device with which to monitor low intensity light. However, it can be easily saturated or possibly damaged when exposed to high light intensity. Recovery from saturation is too slow to monitor signals immediately following the saturating pulse.

A technique that exists to circumvent this problem is that of gating the PMT off during the saturating pulse.[101-103] There are five general methods of doing this: pulsing the photocathode, pulsing the first dynode, pulsing other dynodes or groups of dynodes, pulsing the high voltage supply, or pulsing a special gating electrode that exists in a few tubes.

There are a number of problems that exist in gating PMT's. Electrical pickup, ringing, afterpulsing and excited photocathode states can make signal measurement after gating difficult. The problems are discussed in more detail elsewhere.[101-103]

The circuit discussed here has been used successfully with 1P28-class PMT's. A schematic diagram of the modified dynode chain is shown in Fig. A1. The gating technique involves temporarily shorting dynodes 6 and 7 together via Q_1 to prevent further amplification of the electron cascade initiated by the intense pulse of light.

A pulse of approximately -5 volts and pulse width between 1 and 10 microseconds from a suitable pulse generator is applied to the pulse

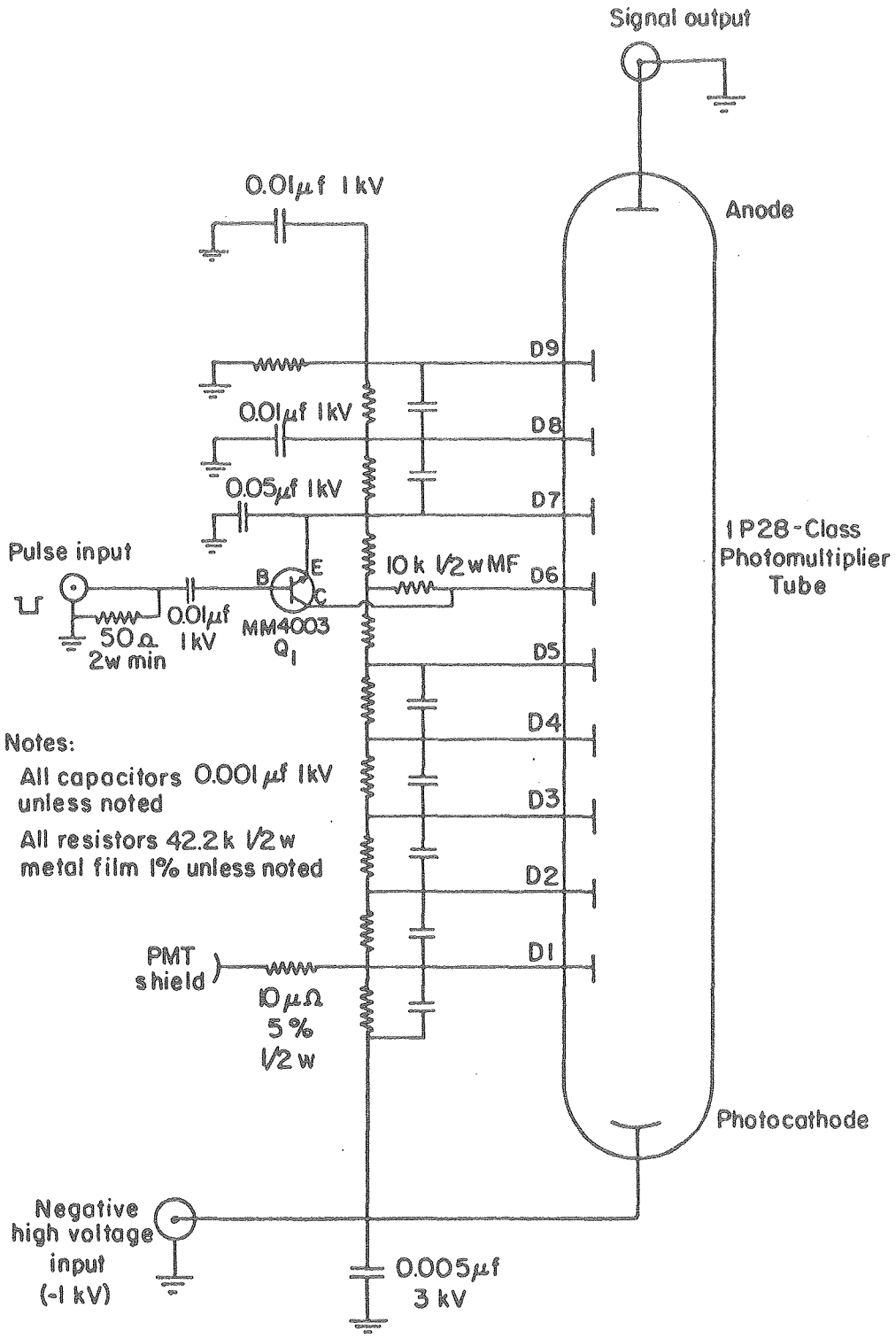

Fig. A1 Photomultiplier tube gating circuit

input immediately preceding the intense pulse of light. The circuit has rise and fall times of less than one microsecond. It has been used to gate a PMT off for periods of 1 to 10 microseconds. The circuit provides an attenuation of 1000 while the pulse is applied. The system is sensitive to the rise and fall times of the input pulse and also to the current capacity of the pulse generator. These parameters need to be optimized to provide maximum performance of the circuit.

APPENDIX B: PRESSURE BROADENING OF ROTATIONAL LINES IN INFRARED SPECTRA

There are a number of factors that must be considered when investigating the effect of broadening of spectral lines by pressure. The spectrometer transmission function, or spectral slit function, will play an important role in the observed effects. For a spectrometer with entrance and exit slit widths of equal width, the slit function will be a triangle if diffraction is neglected. If the entrance and exit slit widths are not equal, the slit function will be trapezoidal in shape.[104] Most spectrometer systems operate with equal entrance and exit slits. The slit function can then be defined as

$$f(\nu - \nu_0) = 1 - |\nu - \nu_0| / w$$

for $\nu - \nu_0 \leq w$ and $f(\nu - \nu_0) = 0$ elsewhere, where ν_0 is the center frequency and w is the spectral slit width (FWHM). This is illustrated in Fig. B1.

With an experimental apparatus scanning through a spectral region, the actual response will in general not be triangular. The detector response time and the RC time constant of the amplifier circuitry will act to round the slit function and displace the observed slit function, or instrumental response function, from the actual slit function.[105]

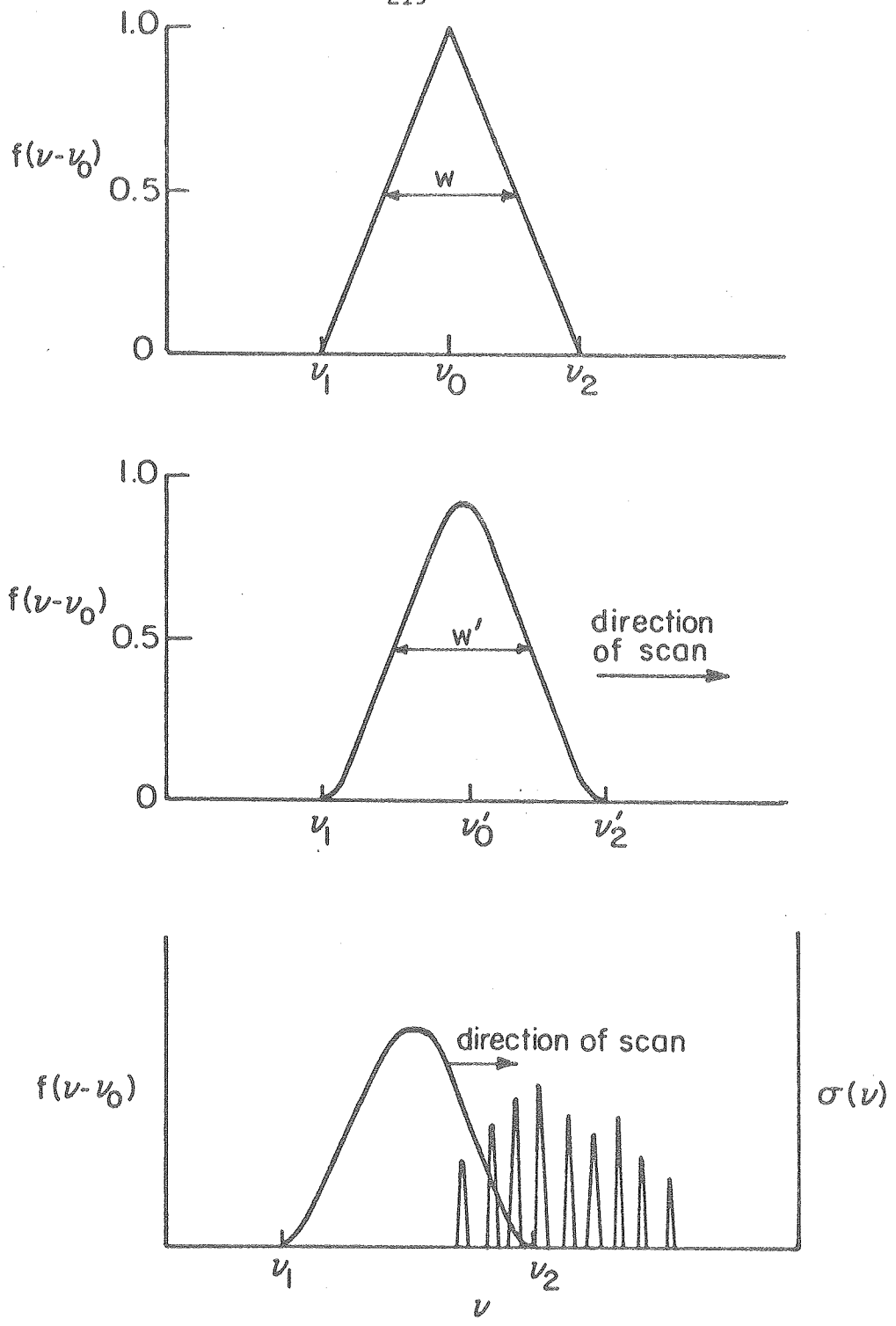

XBL 806-5355

Fig. B1 Slit functions (top) Ideal slit function
(center) experimental slit function, $\nu_0' \neq \nu_0$
(bottom) experimental slit function being scanned across a spectral feature

The overlap of the instrumental response function with the spectral features that are being scanned will determine the broadening effects observed. If the response function is much narrower than the spectral features, the broadening will be directly observable. If the response function is wider than the spectral feature, the broadening will not be directly observable. However, information can be obtained on the linewidths indirectly.[106]

The broadening of rotational lines of infrared absorption bands is largely due to Lorentz broadening. Measurements[107] have shown the rotational lines of HCl, H_2O and CO_2 infrared absorptions to have Lorentzian shape and have shown the rotational linewidth to increase in proportion to pressure. Simple Lorentz broadening theory is based on the concept of a sudden change in the radiation emitted or absorbed by an atom or molecule at the time of collision. The assumptions made are that the mean time between collisions is large compared to the collision time, and there is a change of phase or break of the radiation. This causes the radiation to be spread into a series of independent wave-trains, which causes broadening of the line. The Lorentz linewidth,[108] δ, can be written as

$$\delta = \frac{4N\rho^2 P}{\sqrt{\pi m R T}}$$

where N = Avogadro's number

ρ = optical collision diameter or cross section

p = pressure

m = molecular weight if a pure gas is involved; reduced mass if a gas mixture is involved.

R = the gas constant

T = temperature

The optical collision diameters may be greater or less than the gas kinetic collision diameters.

To obtain a measure of the transmittance or absorbance that occurs when a slit function is moved across a spectral feature, one must integrate across the frequency region transmitted by the slit.

$$T = 1 - A = \frac{\exp(-\sigma(\nu)n\ell)\ f(\nu - \nu_0)\ d\nu}{f(\nu - \nu_0)d\nu}$$

where T = transmittance

A = absorbance

$f(\nu-\nu_0)$ = slit function

ν_1, ν_2 = limits of slit function

$\sigma(\nu)$ = cross section as a function of ν

n = number of absorbers per unit volume

ℓ = path length

This integral has been analyzed for a number of situations that exist in spectroscopy,[104,109,110] although one cannot derive a general equation valid in all situations. When the simplifying assumptions used are valid or nearly so, the experimental and theoretical agreement is good.

The theoretical interpretation is useful when the absorption band structure is known. Structure from high resolution work can be applied to a lower resolution system if the slit function, or instrument response function, is known. However, without such data, most pressure broadening effects have to be determined empirically.

APPENDIX C: REACTION SETS FOR NUMERICAL MODELING OF CHEMICAL SYSTEMS

The following three tables are lists of the sets of reactions and rate constants used to model the chemistry of the three systems investigated in this research. The simulations were done with the CHEMK chemical kinetics program described in the text. The rate constant are in units of $(cm^3/molecule)^n$ $seconds^{-1}$, where n = 0 for unimolecular and heterogeneous reactions, n = 1 for bimolecular reactions and n = 2 for termolecular reactions. Activation energies are in K.

The first reaction set is that used to model the expansion of H_2O_2 and N_2O_5 into the cell and the kinetics that occur after expansion. The first six reactions are used to describe the flow-in of the reactants and the carrier gas. X is a dummy variable used to implement this process. The effective rate constant for the flow in will depend on the ultimate concentration of the species without reaction and is given by

$$k_{eff}[A]_o = \frac{1}{t_o} \frac{[A]}{[X]_o}$$

where t_o is the time constant for the flow system, $[X]_o$ is the initial concentration assigned to the dummy variable and $[A]_o$ is the ultimate concentration of the specie A. The flow-out of X is given by $k_{eff} = 1/t_o$.

The second reaction set listed below was used in simulations of very low frequency photolysis of flowing H_2O_2 and N_2O_5 in one atmosphere nitrogen carrier gas. The first five reactions are photolysis reactions. The effective cross sections for the species were determined by calculating relative j-values from the absorption spectra for the compounds and the measured emission spectrum of the black lamps. Light intensities obtained from NO_2 photolysis where used as a reference.

The rate constants used for the heterogeneous reactions were assigned values that were typically observed during experiments. The reaction products for heterogeneous HNO_4 decomposition were assumed to be HO_2 and NO_2. Supporting evidence for tnis assumption comes from experiments where H_2O_2 and N_2O_5 were expanded into the cell containing a low pressure of NO. The rates of the flow-in reactions were used to provide agreement between the observed and calculated concentrations of NO_2, H_2O_2, HNO_4, N_2O_5 and H_2O. If a species was inert, its effective flow-in rate constant would be the flow rate times the concentration in the cell divided by the cell volume. The effective flow-out rate constants are simply the flow rate divided by the cell volume. This was 1.9×10^{-3} $second^{-1}$ for all the runs that were done.

The reaction set in the third table was used to model the chemistry in the HO_x - NO_x - CO_x system. Since this was a non-flowing system, no flow reactions had to be included.

Two germicidal lamps and two black lamps were used as photolytic light sources for the system. The black lamps have broad output in the near UV and the germicidal lamps have strong output at 254 nm. NO_2 and HONO were the only species strongly photolyzed by the black lamps. Photolysis rates of other species were less than 1 percent of their respective photolysis rates at 254 nm and were not included.

The large number of reactions was needed because of the large number of species present, many of which are quite reactive. While the rates of some of the reactions are not very fast, they are important in determining the concentrations of some intermediates.

The heterogeneous reactions (46-49) were assigned values that were typical of the heterogeneous rates in the system. Other heterogeneous reaction may have been occurring in the system. They were not studied in depth and no good estimates could be obtained for them. Consequently, they were not included in the reaction set.

TABLE C-1

Reactions Used to Model Expansion Experiments

Flow Reactions

1	$x = x + M$	$k_{eff} \times [M]$
2	$x = x + N_2O_5$	$k_{eff} \times [N_2O_5]$
3	$x = x + H_2O_2$	$k_{eff} \times [H_2O_2]$
4	$x = x + HNO_3$	$k_{eff} \times [HNO_3]$
5	$x = x + H_2O$	$k_{eff} \times [H_2O]$
6	$x =$	0.23

Chemical Reactions

7	$N_2O_5 + H_2O_2$	$= HNO_3 + HNO_4$	note 1	
8	HNO_4	$= HO_2 + NO_2$	note 2	–
9	$HO_2 + NO_2$	$= HNO_4$	note 2	–
10	N_2O_5	$= NO_2 + NO_3$	note 3	–
11	$NO_2 + NO_3$	$= N_2O_5$	note 3	–
12	$NO_2 + NO_3$	$= NO + NO_2 + O_2$	2.3×10^{-13}	1000
13	$NO + NO_3$	$= NO_2 + NO_2$	1.9×10^{-11}	–
14	$HO_2 + HO_2$	$= H_2O_2 + O_2$	2.5×10^{-12}	–
15	$HO_2 + NO$	$= OH + NO_2$	8.1×10^{-12}	–
16	$OH + H_2O_2$	$= H_2O + HO_2$	1.0×10^{-12}	–
17	$OH + NO_2 + M$	$= HNO_3 + M$	2.4×10^{-30}	–
18	$OH + HO_2$	$= H_2O + O_2$	3.0×10^{-11}	–
19	$HO_2 + NO + M$	$= HNO_3 + M$	5.6×10^{-33}	–
20	H_2O_2	$= H_2O$	note 4	–

Table C-1 (continued)

21	HNO_4	$= HO_2 + NO_2$	note 4	-
22	N_2O_5	$= HNO_3$	note 4	-
23	H_2O	$= HNO_3$	note 4	-

Note 1: This was varied to provide the best fit with experimental data.

Note 2: The empirical expressions given by Ref. 18 were used to calculate the effective rate constant for each pressure and temperature.

Note 3: The expressions developed by Connell[67] were used for these rate constants.

Note 4: These reactions simulate heterogeneous reactions that occur in the cell. Reactions 22 and 23 simulate the heterogeneous reaction of N_2O_5 and H_2O to form $2HNO_3$. The effective first order rate constants were variable, depending on temperature and conditioning of the cell. They were generally in the range of 1×10^{-2} to 1×10^{-4} $second^{-1}$ in the H_2O_2-N_2O_5 system.

TABLE C-2

Reactions Used to Model Low Frequency Photolysis Experiments

	Photolysis Reactions		σ_{eff}	Q.Y.
1	$NO_2 + h\nu$	= $NO + O$	$4.8 \times 10^{-19} cm^2$	1.0
2	$N_2O_5 + h\nu$	= $NO_2 + NO_2 + O$	$2.1 \times 10^{-21} cm^2$	1.0
3	$H_2O_2 + h\nu$	= $OH + OH$	$2.9 \times 10^{-22} cm^2$	1.0
4	$HNO_4 + h\nu$	= $HO_2 + NO_2$	$2.0 \times 10^{-22} cm^2$	1.0
5	$HNO_3 + h\nu$	= $OH + NO_2$	$8.2 \times 10^{-23} cm^2$	1.0
	Chemical Reactions		A	E_a
6	$HNO_4 + M$	= $HO_2 + NO_4 + M$	note 1, note 2	
7	$HO_2 + NO_2 + M$	= $HNO_4 + M$	note 1, note 2	
8	$N_2O_5 + M$	= $NO_2 + NO_3 + M$	note 1, note 2	
9	$NO_2 + NO_3 + M$	= $N_2O_5 + M$	note 1, note 2	
10	$NO_2 + NO_3$	= $NO + NO_2 + O_2$	2.3×10^{-13}	1000
11	$NO + HO_2$	= $HO + NO_2$	8.1×10^{-12}	-
12	$NO + NO_3$	= $NO_2 + NO_2$	1.9×10^{-11}	-
13	$O + NO_2$	= $NO + O_2$	9.3×10^{-12}	-
14	$O + NO_2 + M$	= $NO_3 + M$	9.0×10^{-32}	-
15	$O + NO + M$	= $NO_2 + M$	1.55×10^{32}	-384
16	$OH + HNO_4$	= $H_2O + NO_2 + O_2$	note 3	-
17	$OH + NO_2 + M$	= $HNO_3 + M$	note 4	-
18	$OH + H_2O_2$	= $HO_2 + H_2O$	1.6×10^{-12}	-
19	$OH + HNO_3$	= $H_2O + NO_3$	8.5×10^{-14}	-
20	$HO_2 + HO_2$	= $H_2O_2 + O_2$	2.5×10^{-12}	-
21	H_2O_2	= H_2O	1×10^{-3}	-
22	HNO_4	= $HO_2 + NO_2$	1×10^{-3}	-
23a	N_2O_5	= HNO_3	1×10^{-3}	-
23b	H_2O	= HNO_3	note 5	-
	Flow Reactions			
24		= NO_2	note 6	
25		= HNO_3	"	
26		= N_2O_5	"	
27		= HNO_4	"	
28		= H_2O_2	"	
29		= H_2O	"	
30	NO_2	=	1.9×10^{-3}	
32	HNO_3	=	"	
33	HNO_4	=	"	
34	H_2O_2	=	"	
35	H_2O	=	"	
36	NO	=	"	

Table C-2 (continued)

Note 2: Values for these equations were obtained from empirical equations given by Graham et al.[18] and Connell[67].

Note 2: M dependence is included implicitly in the rate constant.

Note 3: This rate constant was varied from 2 x 10^{-13} to 2 x 10^{-11} (cm^3/molecule-second) to determine the best fit with experimental data.

Note 4: This reaction exhibits a complicated pressure and temperature dependence. The values for the conditions in which the experiments were done were obtained from JPL Publication 79-27.

Note 5: Reactions 23a and 23b are designed to simulate the heterogeneous reaction of H_2O and N_2O_5. The value for the rate constant of 23b was varied to provide unity stoichiometry for H_2O and N_2O_5.

Note 6: These effective rate constants were used to match the calculated concentrations with those observed for each run.

TABLE C-3

Reactions Used to Model HO_x-NO_x-CO_x Photochemistry

			A	E_a
1	$O + O_2 + M$	$= O_3 + M$	1.1E-34	-510
2	$O + O_3$	$= O_2 + O_2$	1.9E-11	2300
3	$O + NO + M$	$= NO_2 + M$	1.55E-32	-584
4	$O + NO_2$	$= NO + O_2$	9.3E-12	
5	$O + NO_2 + M$	$= NO_3 + M$	9.0E-32	
6	$O + NO_3$	$= NO_2 + O_2$	1.0E-11	
7	$O + HO_2$	$= HO + O_2$	3.1E-11	
8	$O + H_2O_2$	$= HO + HO_2$	2.8E-12	2125
9	$O + CO + M$	$= CO_2 + M$	6.5E-33	2180
10	$O(^1D) + O_2$	$= O_2 + O$	2.9E-11	-67
11	$O(^1D) + O_3$	$= O_2 + O_2$	1.2E-10	
12	$O(^1D) + O_3$	$= O_2 + O + O$	1.2E-10	
13	$O(^1D) + NO_2$	$= NO + O_2$	1.0E-10	
14	$O(^1D) + H_2O$	$= HO + HO$	2.3E-10	
15	$O(^1D) + H_2O_2$	$= HO + HO_2$	5.2E-10	
16	$O(^1D) + CO_2$	$= CO_2 + O$	6.8E-11	-117
17	$O_2 + NO + NO$	$= NO_2 + NO_2$	3.3E-39	-530
18	$O_2 + H + M$	$= HO_2 + M$	6.7E-33	-290
19	$O_3 + M$	$= O + O_2 + M$	7.4E-10	11430
20	$O_3 + NO$	$= NO_2 + O_2$	2.3E-12	1450
21	$O_3 + NO_2$	$= NO_3 + O_2$	1.2E-13	2450
22	$NO + NO_2 + H_2O$	$= HONO + HONO$	6.0E-38	
23	$NO + NO_3$	$= NO_2 + NO_2$	1.9E-11	
24	$NO + HO + M$	$= HONO + M$	2.0E-32	-1110
25	$NO + HO_2$	$= NO_2 + HO$	4.0E-12	-225
26	$NO_2 + NO_2 + M$	$= N_2O_4 + M$	3.0E-35	-1040
27	$NO_2 + NO_3$	$= NO_2 + NO + O_2$	2.3E-13	1000
28	$NO_2 + NO_3(+M)$	$= N_2O_5(+M)$	note 1	
29	$NO_2 + H$	$= HO + NO$	7.1E-10	505
30	$NO_2 + HO(+M)$	$= HNO_3(+M)$	note 2	
31	$NO_2 + HO_2(+M)$	$= HNO_4(+M)$	note 3	
32	$NO_3 + NO_3$	$= NO_2 + NO_2 + O_2$	8.5E-13	2450
33	$H + H_2O_2$	$= H_2 + HO_2$	2.0E-12	1400
34	$H + H_2O_2$	$= HO + H_2O$	3.0E-12	1400
35	$HO + HO_2$	$= H_2O + O_2$	3.5E-11	
36	$HO + H_2O_2$	$= H_2O + HO_2$	1.6E-12	
37	$HO + HONO$	$= H_2O + NO_2$	6.6E-12	
38	$HO + HNO_3$	$= H_2O + NO_3$	8.5E-14	
39	$HO + HNO_4$	$= H_2O + NO_2 + O_2$	note 4	
40	$HO + CO$	$= H + CO_2$	2.7E-13	
41	$HO_2 + HO_2$	$= H_2O_2 + O_2$	2.3E-12	
42	$HONO + HONO$	$= NO + NO_2 + H_2O$	9.5E-19	
43	$HNO_4(+M)$	$= HO_2 + NO_2(+M)$	note 3	
44	$N_2O_4 + M$	$= NO_2 + NO_2 + M$	4.2E-7	

45	$N_2O_5(+M)$	= $NO_2 + NO_3(+M)$		note 1
46	H_2O_2	= H_2O		note 5
47	N_2O_5	= $HNO_3 + HNO_3$		note 5
48	$H_2O + NO_2 + NO_2$	= $HONO + HNO_3$		note 5
49	$H_2O_2 + NO_2$	= $HNO_3 + HNO_3$		note 5
50	$NO_2 + h\nu$	→ $NO + O$		note 6
51	$HONO + h\nu$	→ $HO + NO$		"
52	$H_2O_2 + h\nu$	→ $HO + HO$		"
53	$N_2O_5 + h\nu$	→ $NO_2 + NO_2 + O$		"
54	$HNO_3 + h\nu$	→ $HO + NO_3$		"
55	$HNO_4 + h\nu$	→ $HO_2 + NO_2$		"
56	$O_3 + h\nu$	→ $O(^1D) + O_2$		"
57	$O_3 + h\nu$	→ $O + O_2$		"
58	$NO_2 + h\nu$	→ $NO + O$		
59	$HONO + h\nu$	→ $HO + NO$		"
60	$NO_3 + h\nu$	→ $NO_2 + O$		"

Note 1: These reactions have a complex pressure and temperature dependence. The values were obtained from formulas in Ref. 67.

Note 2: Rate constant values obtained from formula in JPL Publication 79-27.

Note 3: Rates constant values obtained from formulas in Ref. 18.

Note 4: The value for this rate constant was obtained experimentally.

Note 5: These reactions were designed to simulate heterogeneous reactions. Values used for the rate constants were those typically observed for the heterogeneous reactions involved.

Note 6: The reactions listed here represent photolysis by the black lamps and germicidal lamps. Only NO_2 and HONO are significantly photolyzed by the black lamps. The black lamp photolysis rate for all other species is less than 1 percent of their respective germicidal lamp photolysis rate and not included. Reactions 58 and 59 represent the black lamp photolysis of NO_2 and HONO, respectively. Reaction 60 represents the photolysis of NO_3 by the 546nm mercury line.

BIBLIOGRAPHY

1. P. A. Leighton, Photochemistry of Air Pollution, (Academic Press, N.Y., 1961).
2. H. S. Johnston, Science 173, 517 (1971).
3. H. Niki, P. D. Maker, C. M. Savage and L. P. Breitenbach, Chem. Phys. Lett. 45, 564 (1977).
4. R. A. Graham, A. M. Winer and J. N. Pitts, Chem. Phys. Lett. 51, 215 (1977).
5. J. Fishman and P. J. Crutzen, Nature 274, 855 (1978).
6. J. D'Ans and W. Friederich, Z. Anorg. Chem. 73, 325 (1911).
7. R. Schwarz, Z. Anorg. Chem. 258, 3 (1948).
8. R. A. Cox and R. G. Derwent, J. Photochem. 4, 139 (1975).
9. R. Simonaitis and J. Heicklen, J. Phys. Chem. 78, 653 (1974).
10. R. Simonaitis and J. Heicklen, J. Phys. Chem. 80, 1 (1976).
11. P. L. Hanst and B. W. Gay, Environ. Sci. and Tech. 11, 1105 (1977).
12. S. Z. Levine, W. M. Uselman, W. H. Chan, J. G. Calvert and J. H. Shaw, Chem. Phys. Lett. 51, 215 (1977).
13. R. Simonaitis and J. Heicklen, NASA Scientific Report No. 454 (March, 1977).
14. A. C. Baldwin, J. R. Barker, D. M. Golden and D. G. Hendry, J. Phys. Chem. 81, 2483 (1977).
15. J. P. Jesson, L. C. Glasgow, D. L. Filkin and C. Muller, Geophys. Res. Lett 4, 513 (1977).

16. C. J. Howard, J. Chem. Phys. 67, 5258 (1977).

17. A. C. Baldwin and D. M. Golden, J. Phys. Chem. 82, 644 (1978).

18. R. A. Graham, A. M. Winer and J. N. Pitts, J. Chem. Phys. 68, 4505 (1978).

19. W. M. Uselman, S. Z. Levine, W. H. Chan, J. G. Calvert and J. H. Shaw, Chem. Phys. Lett. 58, 437 (1978).

20. R. A. Graham, A. M. Winer and J. N. Pitts, Geophys. Res. Lett. 5, 909 (1978).

21. L. T. Molina and J. J. Molina, to be published (1980).

22. R. A. Cox and K. Patrick, Int. J. Chem. Kinet. 11, 635 (1979).

23. J. R. Barker, P. L. Trevor, R. A. Kenley, J-S. Chang, J. E. Davenport and B. Y. Lan, SRI Project No. PYU-7921, Final Report (1980).

24. K. L. Demerjian, J. A. Kerr and J. G. Calvert, Adv. Environ. Sci. Technol. 4, 1 (1974).

25. C. J. Howard and K. M. Evenson, Trans. Amer. Geophys. Union 58, 464 (1977).

26. D. L. Baulch, R. A. Cox, R. F. Hampson, J. A. Kerr, J. Troe and R. T. Watson, J. Phys. Chem. Ref. Data 9, 295 (1980).

27. L. F. Keyser, J. Phys. Chem. 84, 1659 (1980).

28. E. F. Danielson, J. Atmos. Sci. 25, 502 (1968).

29. L. Aldaz, J. Geophys. Res. 74, 6943 (1969).33.

30. H. U. Dutsch, Adv. Geophys. 15, 219 (1971).

31. L. A. Ripperton and F. M. Vukovich, J. Geophys. Res. 76, 7328 (1971).

32. H. Levy, Planet. Space Sci. 20, 919 (1972).

33. S. C. Wofsey, J. C. McConnell and M. B. McElroy, J. Geophys. Res. 77, 4477 (1972).

34. W. L. Chameides and J. C. G. Walker, J. Geophys. Res. 78, 8751 (1973).

35. P. J. Crutzen in Physics and Chemistry of the Upper Atmosphere, ed. B. M. MaCormac, D. Reidel, Dordrecht, Netherlands (1973).

36. P. Fabian, Pure Appl. Geophys. 106-108, 1044 (1973).

37. H. Levy, Planet. Space Sci. 21, 575 (1973).

38. W. L. Chamides and J. C. G. Walker, J. Geophys. Res. 79, 4126 (1974).

39. P. J. Crutzen, Tellus 26, 47 (1974).

40. P. Fabian, J. Geophys. Res. 79, 4124 (1974).

41. W. Seiler, Tellus, 26, 116 (1974).

42. E. R. Reiter, Rev. Geophys. Space Phys. 13, 459 (1975).

43. W. L. Chameides and D. H. Stedman, Environ. Sci. Technol. 10, 150 (1976).

44. R. Chatfield and H. Harrison, J. Geophys. Res. 81, 421 (1976).

45. W. L. Chameides and J. C. G. Walker, J. Geophys. Res. 81, 413 (1976).

46. W. L. Chameides and D. H. Stedman, J. Geophys. Res. 82, 1787 (1977).

47. R. Chatfield and H. Harrison, J. Geophys. Res. 82, 5965 (1977).

48. E. F. Danielson and V. A. Mohnen, J. Geophys. Res. 82, 5867(1977).

49. P. J. Crutzen and J. Fishman, Geophys. Res. Lett. 4, 321 (1977).

50. P. Fabian and P. G. Pruchniewicz, J. Geophys. Res. 82, 2063 (1977).

51. J. Fishman and P. J. Crutzen, J. Geophys. Res. 82, 5897 (1977).

52. V. A. Mohnen, A. Hogan and P. Coffey, J. Geophys. Res. 82, 5889 (1977).

53. R. W. Stewart, S. Hameed and J. P. Pinto, J. Geophys. Res. 82, 3134 (1977).

54. J. Fishman and P. J. Crutzen, Nature 274, 856 (1978).

55. P. R. Zimmerman, R. B. Chatfield, J. Fishman, P. J. Crutzen and P. L. Hanst, Geophys. Res. Lett. 5, 679 (1978).

56. J. Fishman, S. Soloman and P. J. Crutzen, Tellus 31, 432 (1979).

57. C. J. Howard and K. M. Evenson, Geophys. Res. Lett. 4, 437 (1977).

58. J. F. Noxon, J. Geophys. Res. 83, 3051 (1978).

59. E. D. Morris, Jr. and H. Niki, J. Phys. Chem. 77, 1929 (1973).

60. I. R. McKinnon, J. G. Mathieson and I. R. Wilson, J. Phys. Chem. 83, 779 (1979).

61. I. M. Campbell and P. E. Parkinson, J. Chem. Soc. Farad. Trans. I. 75, 2048 (1979).

62. D. Gray, E. Lissi and J. Heicklen, J. Phys. Chem. 76, 1919 (1972).

63. R. J. Gelinas, J. Comput. Phys. 9, 222 (1972).

64. C. W. Gear, Comm. A. C. M. 14, 176 (1971).

65. A. C. Hindmarsh, Lawrence Livermore Laboratory Report UCID-30001, Rev. 1 (1972).

66. G. Z. Whitten and J. P. Meyer, "CHEMK: A Computer Modeling Scheme for Chemical Kinetics," Systems Applications, Inc. Report (1979).

67. P. S. Connell, Doctoral Thesis, University of California at Berkeley, (May 1, 1979) LBL-9034.

68. G. E. Gibson and N. S. Bayliss, Phys. Rev. 44, 188 (1933).

69. J. G. Calvert and J. N. Pitts, Jr. Photochemistry (1966), p. 696.

70. G. Schott and N. Davidson, J. Am. Chem. Soc. 80, 1841 (1958).

71. F. H. Verhoek and F. Daniels, J. Am. Chem. Soc. 53, 11250 (1931).

72. P. A. Giguere, J. Chem. Phys. 18, 88 (1950).

73. D. J. McCaa and J. H. Shaw, J. Mol. Spectros. 25, 374 (1968).

74. C. L. Lin, N. K. Rohatgi and W. B. DeMore, Geophys. Res. Lett. 5, 113 (1978).

75. L. T. Molina, S. D. Schinke and M. J. Molina, Geophys. Res. Lett. 4, 580 (1977).

76. E. C. Y. Inn and Y. Tanaka, Advances in Chemistry Series No. 21, 263 (1959).

77. M. Griggs, J. Chem. Phys. 49, 857 (1968).

78. R. A. Graham, Doctoral Thesis, University of California at Berkeley (November, 1975) LBL-4147.

79. A. B. Harker, Doctoral Thesis, University of California at Berkeley (September, 1972) LBL-1114.

80. J. G. Calvert, W. H. Chan, E. Niple, R. J. Nordstrom, J. H. Shaw, W. R. Skinner and W. M. Uselman, "Applications of Fourier Transform Spectroscopy to Air Pollution Problems," Ohio State University Research Foundation R. F. Report 4221-AL (1976).

81. L. H. Jones, R. M. Badger and g. E. Moore, J. Chem. Phys 19, 1599 (1951).

82. G. E. McGraw, D. L. Bernitt and I. C. Hisatsune, J. Chem. Phys. 45, 1392 (1966).

83. R. F. Hampson and D. Garvin, Reaction Rate and Photochemical Data for Atmospheric Chemistry 1977 NBS, U.S. Dept. of Commerce, May 1978.

84. G. D. Gillispie and A. U. Khan, J. Chem. Phys. 65, 1624 (1976).

85. R. A. Graham and H. S. Johnston, J. Phys. Chem. 82, 254 (1978).

86. E. J. Jones and O. R. Wulf, J. Chem. Phys. 5, 873 (1937).

87. F. Biame, J. Photochem. 2, 139 (1973).

88. R. A. Cox and R. G. Derwent, J. Photochem. 6, 23 (1976/77).

89. I. M. Campbell and P. E. Parkinson, J. Chem. Soc. Far. Trans. I, 75, 2048 (1979).

90. W. C. Schumb, C. N. Satterfield, R. L. Wentworth, Hydrogen Peroxide (Reinhold Publishing Corp., N.Y., 1955)p. 221.

91. R. C. Weast, ed., Handbook of Chemistry and Physics (Chemical Rubber Company, 51st edition, 1970-71).

92. E. W. Kaiser and C. H. Wu, J. Phys. Chem. 81, 187 (1977).

93. R. F. Hampson, ed., J. Phys. Chem. Ref. Data 2, 267 (1973).

94. A. P. Altshuller, J. Phys. Chem. 61, 251 (1957).

95. D. M. Waldorf and E. L. Balb, J. Chem. Phys. 39, 432 (1963).

96. P. A. Akishin, L. V. Vilkov, E. Z. Zasorin, N. G. Rambini and V. P. Spiridonov, J. Phys. Soc. Japan. 17, 18 (1961).

97. H. H. Nelson, private communication.

98. H. S. Johnston, G. E. McGraw, T. T. Paukert, L. W. Richard and J. Van de Bogaerde, Proc. Nat. Acad. Sci. U. S. 57, 1146 (1967).

99. W. J. Marinelli, private communication.

100. R. F. Hampson and D. Garvin, ed. Reaction Rate and Photochemical Data for Atmospheric Chemistry 1977 NBS Special Publication 513.

101. R. Wardle, "Gating of Photomultipliers," EMI Company, R/P 061.

102. F. DeMarco and E. Penco, Rev. Sci. Inst. 40, 1158 (1969).

103. M. Rossetto and D. Mauzerall, Rev. Sci. Inst. 43, 1244 (1972).

104. J. R. Nielson, V. Thornton and E. B. Dale, Revs. Mod. Phys. 16, 307 (1944).

105. G. E. Streit, Doctoral Thesis, University of California at Berkeley (August, 1974) LBL-2795

106. A. M. Thorndike, J. Chem. Phys. 16, 311 (1948).

107. G. Kortum and H. Verleger, Proc. Phys. Soc. 63, 462 (1950).

108. H. E. White, Introduction of Atomic Spectra (McGraw-Hill, N.Y., 1934), p. 104.

109. W. M. Elsasser, Phys. Rev. 54, 126 (1938).

110. S. S. Penner and D. Weber 19, 1351 (1951).

111. J. Heicklen, K. Westberg and N. Cohen, Center for Air Environmental Studies Publication No. 115-60, University Park, PA (1969).

112. H. S. Johnston and J. R. Podolske, Rev. Geophys. Space Phys. 16, 491 (1978).

113. F. Magnotta, Doctoral Thesis, University of California at Berkeley (November, 1979) LBL-9981.